Technische Universität München

TUM School of Natural Sciences

Higher-order and Quotient group symmetry-protected topological phenomena

Julian Ferdinand Rainer Bibo

Vollständiger Abdruck der von der TUM School of Natural Sciences der Technischen Universität München zur Erlangung eines Doktors der Naturwissenschaften (Dr. rer. nat.) genehmigten Dissertation.

Vorsitz: Prof. Dr. Alexander Holleitner

Prüfer*innen der Dissertation:

1. Prof. Dr. Frank Pollmann
2. Prof. Dr. Johannes Knolle

Die Dissertation wurde am 10.11.2022 bei der Technischen Universität München eingereicht und durch die TUM School of Natural Sciences am 01.02.2023 angenommen.

Technical University of Munich

Higher-order and Quotient group symmetry-protected topological phenomena

Julian Bibo

Supervisor: Prof. Dr. Frank Pollman

Second Examiner: Prof. Dr. Johannes Knolle

Those who have the privilege to know,
have the duty to act (A. Einstein).

Thesis advisor: Prof. Dr. Frank Pollman *Julian Bibo*

Higher-order and Quotient group symmetry-protected topological phenomena

ABSTRACT

In this thesis, we study two aspects of interacting bosonic symmetry-protected topological (SPT) phases. First, we focus on the recently introduced branch of higher-order SPTs, which were so far mainly considered in non-interacting free-fermion systems. Second, we study quotient group symmetry-protected topological phenomena for one-dimensional SPTs and discuss how additional gapped degrees of freedom can endow quantum critical points, separating such states, by topological properties or keep topological signatures robust even though the actual phase is trivial.

In the first part, we investigate a concrete, strongly-interacting 2D model system that realizes a higher-order SPT phase. Thereby, using a combination of numerical methods and analytical treatments, we construct an experimentally accessible topological invariant for which we provide experimental relevant data, discover signatures of the non-trivial topology in the entanglement spectrum and establish a bulk-boundary correspondence—the Achilles' heel of topological states of matter. These findings significantly increase the understanding of these states and, in particular, allow experimentalists to verify those phases in the lab.

In the second part, we consider quotient group symmetry-protected topological phenomena for two concrete cases using a combination of numerical and analytical tools. Thereby, among other things, we contribute to the understanding of quantum phase transitions between those states. More precisely, for a particular class of one-dimensional SPTs we discover that there are more direct and stable transitions as initially expected. We explain that this is due to the fact that the global symmetry group acts as a quotient group at low-energies and, thus, leaves additional gapped degrees of freedom at quantum criticality, which can endow the latter with additional topological properties. Furthermore, by a similar mechanism, we demonstrate that topological signatures of the Haldane phase remain robust over a large parameter regime *even though* the global symmetry (in the fermionic Hilbert space) cannot protect the non-trivial SPT and, consequently, the bulk is strictly speaking in a trivial phase. As a consequence, we introduced a new branch in this field, dubbed *quotient group symmetry-protected topological phases*. This discovery opens the door for experimentalists to measure signatures of SPT phases without the necessity to realize an actual SPT.

Thesis advisor: Prof. Dr. Frank Pollman *Julian Bibo*

Quotientengruppen symmetriegeschützte topologische Phänomene und symmetriegeschützte Phasen höherer Ordnung

KURZFASSUNG

In dieser Dissertation untersuchen wir zwei Aspekte wechselwirkender bosonischer symmetriegeschützter topologischer (SGT) Phasen. Zu Beginn fokussieren wir uns auf den kürzlich entdeckten Zweig der SGT Phasen höherer Ordnung, die bisher überwiegend in nicht wechselwirkenden Systemen freier Fermionen betrachtet wurden. In der zweiten Hälfte untersuchen wir Quotientengruppen symmetriegeschützte topologische Phänomene für eindimensionale SGT Phasen und diskutieren, wie zusätzliche Freiheitsgrade quantenkritische Punkte, zwischen solchen Zuständen, mit topologischen Eigenschaften versehen oder topologische Signaturen schützen können, obwohl die zugrundeliegende Phase trivial ist.

Der erste Teil der Arbeit beginnt mit der Analyse eines konkreten, stark wechselwirkenden 2D Modellsystems, das eine SGT Phase höherer Ordnung realisiert. Dabei konstruieren wir eine experimentell zugängliche topologische Invariante, für die wir zusätzlich experimentell relevante Daten bereitstellen. Anschließend diskutieren wir nichttriviale Signaturen im Verschränkungsspektrum dieser Phasen. Des Weiteren beweisen wir mithilfe dieses Modells die Korrespondenz zweier topologischer Invarianten, die Eigenschaften des Randes und des Innern charakterisieren – ein fundamentales Merkmal topologischer Phasen. Diese Ergebnisse verbessern das Verständnis dieser Zustände erheblich und ermöglichen es insbesondere Experimentatoren, diese Phasen im Labor zu verifizieren.

Im zweiten Teil betrachten wir Quotientengruppen symmetriegeschützte topologische Phänomene für zwei konkrete Fälle mit einer Kombination aus numerischen und analytischen Methoden. Damit tragen wir unter anderem zum besseren Verständnis von Quantenphasenübergängen zwischen diesen Zuständen bei. Genauer gesagt, entdecken wir für eine bestimmte Klasse von eindimensionalen SGT Phasen, dass es weitaus mehr direkter Phasenübergänge gibt als ursprünglich erwartet. Dies ist darauf zurückzuführen, dass die globale Symmetriegruppe bei niedrigen Energien als Quotientengruppe fungiert und somit zusätzliche Freiheitsgrade mit endlicher Energielücke am quantenkritischen Punkt hinterlässt, die Letzteren mit zusätzlichen topologischen Eigenschaften ausstatten können. Des Weiteren zeigen wir, dass aufgrund desselben Mechanismus, die topologischen Eigenschaften der Haldane Phase über ein großes Parameterregime robust bleiben, *obwohl* die globale Symmetrie (im fermionischen Hilbertraum) die SGT Phase nicht schützen kann und sich der Zustand streng genommen in einer trivialen Phase befindet. Um diesem Phänomen Rechnung zu tragen, haben wir den Begriff der *Quotientengruppen symmetriegeschützten topologischen Phasen* etabliert. Diese Entdeckung eröffnet Experimentatoren die Möglichkeit, Signaturen von SGT Phasen zu messen, ohne eine tatsächliche SGT Phase realisieren zu müssen.

Contents

Chapter 1

Introduction

Condensed matter physics is the study of large assemblies of interacting, dense arrays of particles. In solids, for example, the interatomic distances are of the order of ~ 1Å, which corresponds to the size of individual atoms. Because matter is made up of atoms, studying these systems requires knowledge of atomic and molecular physics. Furthermore, depending on temperature, quantum mechanics becomes more or less important. Since particle numbers in such systems are enormous $\sim 10^{23}$, it is practically impossible to solve single equations of motion and, thus, condensed matter systems are completely characterized in terms of macroscopic properties, requiring knowledge of statistical mechanics and thermodynamics. Consequently, condensed matter physics is not only the study of many interacting particles, but also connects many branches of physics.

In (condensed matter) systems in which constituent particles are closely packed together, i.e., interparticle distances are of atomic size, physics is not governed by properties of individual atoms or molecules; instead, such systems behave fundamentally different as expected from single particle physics. A crystal, for instance, is a highly-correlated regular arrangement of atoms; thus, knowing the position of a single atom immediately tells us the position of all other atoms (up to fluctuations around the equilibrium position). Typical excitations of solid materials are lattice vibrations, a collective phenomenon in which all atoms participate. Energy scales of such excitations are commonly much smaller than energy scales set by individual atoms ($\sim 10^{-2}$ eV $\ll 13$ eV). There are many other collective phenomena such as superfluidity, superconductivity, magnetism and various quantum Hall effects that are a consequence of interacting, many particle systems that cannot be understood from the perspective of a few degrees of freedom. This fundamental principle, which occurs almost everywhere in nature, is known as *emergence*. The message is simple: even if we know the functionality of all parts of the system, the collection can behave fundamentally different [1].

Condensed matter systems can realize different phases of matter, and the task of physicists is to classify and specify their properties. For this, temperature plays an important role, namely, there are phases of matter, so-called quantum phases, which strictly only exist at zero temperature and are not stable to thermal fluctuations [2]. In this thesis, we focus exclusively on such states of matter. For the classification of phases of matter, symmetries are crucial. In fact, symmetries are the Achilles' heel for the quantum phases studied in this work—that is, without symmetries we cannot distinguish those states of matter. This also applies to spontaneous-symmetry-breaking phases, for which Lev Landau developed an enormously successful theory more than

80 years ago, the so-called "Landau theory of symmetry breaking" [3]. This theory successfully describes many phases of matter, such as crystal formation [spontaneous-symmetry-breaking of translations and rotations], (anti-)ferromagnetism [spin-rotational symmetry] or superfluidity [$U(1)$ phase rotations]. However, there are new types of orders for which this classification does not differentiate distinct phases of matter. In 2016 Kosterlitz, Thouless and Haldane were awarded the Nobel Prize for their discovery of topological phases and their transitions. Among other things, they explained why there is a (thermal) phase transition in the classical 2D XY model—although the Mermin-Wagner-Hohenberg-Coleman theorem forbids spontaneous-symmetry-breaking for two-dimensional systems at finite temperatures[1].

In fact, it is the case that topological phases lack local order parameters and long-range order that characterize these phases of matter. What are topological phases of matter? Xiao-Gang Wen summed this up very clearly in his colloquium on the "Zoo of Topological Phases of Matter" [4]. According to this, topological phases of matter are zero-temperature orders characterized by a finite bulk gap and rich patterns of many-body entanglement. There are many topological phases of matter, including the quantum Hall states [5–7], first discovered in 1980. These states are characterized by long-range entanglement—the origin of topological order. This is reflected in two intriguing properties of topologically ordered states, which are the non-trivial exchange statistics of their excitations, which in 2D can take arbitrary values and, thus, called anyons [8] and, second, the degeneracy of their ground states depends on the topology of the manifold. This is a clear-cut implication that these states are truly different from product states. Importantly, these states of matter require no symmetry protection.

For the second class of topological phases, symmetries are crucial, that is, these phases of matter exist only in the presence of symmetry; thus named symmetry-protected topological phases of matter. These states of matter have no intriguing bulk properties, but, as we shall see several times in this thesis, are characterized through anomalies at their boundaries. For instance, such anomalies can be zero-energy modes at the boundary, which are hallmarks of non-interacting free-fermion topological insulators. A well-studied example is the quantum Spin Hall effect [9–12], a time reversal symmetric topological insulator ($\mathbb{Z}_2$ classified), whose bulk is insulating, and its edge is characterized by extended-zero energy states, that are robust to symmetry-preserving perturbations—i.e., are symmetry-protected. In this thesis, however, we mainly focus on strongly-interacting bosonic systems, among which is the antiferromagnetic spin-1 Heisenberg model, whose ground state is known to be a symmetry-protected topological phase protected by spin-rotation symmetry, time reversal symmetry and bond-centered reflections [13–17]. In fact, these phases of matter occur in very different variations, and their topological properties can be protected by on-site symmetries, spatial symmetries and combinations thereof [18–20]. Recently, different orders of symmetry-protected topological phases have been introduced, which got named higher-order topological insulators—in the non-interacting case [21–23]. Thereby, higher-order characterizes the dimension on which

[1] Indeed, this transition cannot be explained by Landau's theory, since it is a topological phase transition.

anomalies occur. For example, a second-order symmetry-protected topological phase in 2D is characterized by anomalies at the corners, or hinges in three dimensions.

As already mentioned, these orders cannot be detected by methods used for symmetry breaking phases; however, there is another intriguing property of these states, and that is, the way how these phases can be transformed to a trivial state. A common way, of course, is to simply break all symmetries that are essential to protect this phase. However, for topological phases protected by symmetry, there is another way—without the necessity of symmetry breaking—that is, symmetry extension. This means that the protecting symmetry group is enlarged, which can be achieved, for example, by introducing additional degrees of freedom, thereby trivializing the state of interest. In theoretical models, for example, we very often use spin chains as an effective description, which certainly can be very successful. However, if we remember that these approximations remain true only in certain limits, then symmetry-protected topological phases can be trivialized if we take these additional degrees of freedom into account.

1.1 Motivation, Questions & Methods

This thesis is mainly concerned with the classification and characterization of symmetry-protected topological phases. First, we consider a higher-order symmetry-protected topological phase in a bosonic setup, where one of our main intentions is to propose an experimentally accessible model, whose topological nature can be probed in laboratories. However, before this is possible, we first need to argue that the system of interest literally realizes such phase and, importantly, propose measurable invariants.

Second, in the introduction, we said that symmetry-protected topological phases of matter can be trivialized by extending the symmetry group. If a symmetry group G is extended by another group H, then the inverse operation is taking the quotient group, that is $G = \tilde{G}/H$. As we shall see, a crucial step towards understanding quotient group symmetry-protected topological phenomena is a separation of energy scales. Thereby, low-energy properties are fully governed by the quotient group, while the subgroup—to which we take the quotient—acts non-trivially on high-energy degrees of freedom. In such setups, there can be additional degrees of freedom that can endow quantum criticality with non-trivial topological properties. Moreover, we will demonstrate that this gives also rise to a new phenomenon, called quotient group symmetry-protected topological phases.

1.1.1 Higher-order topological phases

When higher-order topological phases were discovered in the mid of 2018, there have already been many theoretical results [20–26], in particular, for non-interacting systems [21–24, 27], to classify these states of matter and, importantly, arguing its robustness. However, at that time, most theoretical models developed so far have been either non-interacting or consisted of complicated spin interactions [20]. After Bernevig, Benalcazar and Hughes [21, 22] found a 2D free-fermion generalization of the Su-Schrieffer–Heeger [28] model, a two-dimensional higher-order topological insulator, which, however, requires a

non-trivial gauge flux to be gapped, we asked if there is a bosonic analogue, which is easier accessible in experiments. The most promising candidate was the Bose-Hubbard model, which is experimentally well-controlled [29–32]. Moreover, in one dimension—for infinite strong on-site repulsion—it can be transformed to the Su-Schrieffer-Heeger model [28, 33], a one-dimensional fermionic symmetry-protected topological phase. Consequently, we asked if the two-dimensional Bose-Hubbard model on a square lattice with dimerization also gives rise to a higher-order symmetry-protected topological phase—and—indeed, it does. However, aside from the advantage that this model does not need gauge fluxes to be gapped, it allows physicists to study interactions and their effects on the robustness of these phases. While initially the main motivation for studying this model was to pave the way towards an experimentally accessible higher-order topological setup, we have been interested in a more profound understanding of higher-order topological phases in this particular model. To this end, we answered the following questions:

1. Does the 2D Bose-Hubbard model on square lattice with alternating hopping amplitudes realize a higher-order topological phase, and is it robust?

2. What are genuine topological invariants characterizing this phase, and how can they be accessed in experiments?

3. Can we find a relation between these topological invariants, in particular, a bulk-boundary correspondence—relating bulk topology to anomalies at the corners?

These were the questions at the beginning of the PhD, but as time proceeded, many other questions came to our mind, which we answered during the PhD.

1.1.2 Quotient group symmetry-protected topological phenomena

In 2017 Tsui et. al [34] studied quantum phase transitions among fixed-point models of one-dimensional symmetry-protected topological phases protected by a direct product of cyclic groups, $\mathbb{Z}_n \times \mathbb{Z}_n$. For each n, there are n distinct phases, and each is characterized by a fixed-point Hamiltonian. However, the authors only considered phase transitions among neighboring classes and did not consider transitions between phases whose index differ by more than one. But, the authors speculated that those transitions split into successive transition of neighboring phases, which we showed is not the case. For instance, in the case of $\mathbb{Z}_4 \times \mathbb{Z}_4$ symmetry, we found that all transitions in this symmetry group are direct (for a single parameter interpolation of fixed-point Hamiltonians). Thereby, we realized that non-neighboring transitions of this symmetry group can be fully understood by neighboring transitions of the lower-dimensional $\mathbb{Z}_2 \times \mathbb{Z}_2$ symmetry group, or said differently, the transition between the two topologically distinct phases of $\mathbb{Z}_2 \times \mathbb{Z}_2$ symmetry is embedded into a higher-dimensional Hilbert space. This was the first time we encountered that low-energy properties, in particular, quantum criticality is governed by the quotient group, and that there are additional gapped degrees of freedom

at quantum criticality. At the beginning of the PhD, this opened many ways to proceed, upon which we choose the following two: On one hand, we investigated quantum criticality of these models even further, and have been interested in:

1. How robust are these direct transitions, and if so, what causes their robustness?
2. Is it fine-tuned for this particular symmetry group, $\mathbb{Z}_4 \times \mathbb{Z}_4$, or does it hold for other n as well?
3. How generic are the observations made for this particular model?

On the other hand, it has been known that the Haldane phase, a symmetry-protected topological phase—among others protected by spin-rotation symmetry and often studied in spin chains—can be trivialized by fluctuating charges. As previously said, spin chains often arise as an effective, low-energy description of more complicated degrees of freedom, which in this particular case can be obtained from strongly-interacting fermions subjected to a bipartite lattice, the so called (Fermi-)Hubbard model [35]. The mechanism behind this trivialization process is symmetry extension, which has been known before [36–39], but what has not been studied at this point was the robustness of topological signatures. Thus, the following questions needed to be answered:

1. How robust are topological signatures if the Haldane phase is trivialized by fluctuating charges?
2. If they are robust, what causes their robustness, and how general is this?
3. How are the quotient symmetry-protected topological phenomena found previously and here are related?

This list is by no means exhaustive and many more interesting questions have been addressed during this PhD, but those are the question we started with.

1.1.3 Methods

To tackle the above questions, we used a combination of analytical and numerical tools. On the analytical side, we mostly used the standard formalism of quantum mechanics and only a very few concepts of field theory. For numerical purposes we used exact diagonalization and the overwhelming successful algorithm, the so-called density renormalization group ansatz, first introduced by Steve White in 1992 [40, 41]. This variational method is the optimal ansatz to numerically consider one-dimensional symmetry-protected topological phases because these states fulfill an area law and, thus, only a few eigenstates of the reduced density matrix contribute significantly to the entanglement. This is exactly the property on which the truncation scheme of this algorithm is build on, and that is also the reason why it is so successful. In particular, with the help of this algorithm the

excitation gap of the spin-1 Heisenberg model was found to very high precision [41]. Although for two-dimensional systems the algorithm is much less powerful[2], it nevertheless allows us to gain insight into fascinating states of matter [42].

1.2 Outline of the thesis and publications

Here we first give an overview of how this thesis is structured. A detailed outline is given at the beginning of each individual chapter. Further, we list all publications that have been obtained during this PhD. There, we briefly summarize the main contributions of individual authors.

1.2.1 Thesis overview

Below, we summarize the most important aspects of each individual chapter.

Part I: Higher-order symmetry-protected topological phenomena

Chapter 2

This chapter serves as a review of the most important concepts we are using during this thesis. Thereby, we start with reviewing two equivalent definitions when two quantum states belong to the same phase of matter, and how states can be differed according to their entanglement properties. Further, we give a rather general introduction to symmetry-protected topological phases, and name the most important characteristics. Since in this thesis we exclusively consider bosonic phases, we discuss various examples of bosonic symmetry-protected topological states of matter, and along this, we introduce many concepts used in this thesis. This chapter ends with a discussion on possible processes to trivialize symmetry-protected topological phases, which is demonstrated for a particular example.

Chapter 3

Here we introduce the 2D Bose-Hubbard model on a square lattice with alternating hopping amplitudes at half-filling. This chapter starts with a definition of the Hamiltonian and its symmetries. Further, we consider the exactly solvable cases and argue that it indeed realizes a higher-order topological phase. Afterwards we discuss its relation to models known in the literature, in particular, its relation with the aforementioned 2D generalization of the Su-Schrieffer-Heeger model. Given this, using numerical methods, we demonstrate that this model for strong enough on-site repulsion among the bosons, realizes two distinct gapped phases. After this is settled, we study the topological classification of this model. For this, we discuss a higher-order generalization of the Zak

[2] In one dimension the entanglement entropy is constant because here the area consists of two points, while in 2D the area grows proportional to the length of the boundary.

phase, and in full detail argue that fractional charges at the corners serve as a genuine topological invariant—that is experimentally accessible. To this end, we provide full counting statistics to which experimentalists can compare to. This chapter ends with a brief estimation of parameters to argue that this particular model studied here is experimentally accessible.

Chapter 4

In chapter four we study higher-order topological phases of the 2D Bose-Hubbard model on a super-lattice at various fillings from two different points of view: First, we introduce a many-body invariant that is, on one hand, accessible in experiments, and, on the other hand, related to previously introduced fractional corner charges. Moreover, we discuss in full detail that this many-body invariant is related to the Wen-Zee response—characterizing the non-trivial interplay of gravitational and electromagnetic degrees of freedom. This has been first discussed in the quantum Hall effect, and it was shown that non-trivial topology of space affects the filling of Landau Levels [43]. Later, this response was generalized to symmetry-protected topological phases protected by a direct product of an on-site symmetry and a spatial symmetry [44]. The first part ends with a numerical demonstration of this many-body invariant for small clusters of the Bose-Hubbard model at different fillings, using exact diagonalization.

In the second part, we study non-trivial signatures of the entanglement spectrum of higher-order topological phases. For this, we consider two different cases: In the first case, the anomaly at the corner is related to a Kramers degeneracy, a two-fold degeneracy protected by symmetry. Here we demonstrate that if we cut out a corner of the system that the entanglement spectrum is fully degenerate in even multiplicities, which we numerically demonstrate using the 2D super-lattice Bose-Hubbard model. Second, we introduce a new entanglement property dubbed "higher-order entanglement", that is, several (i.e., more than one) symmetric bipartitions of the system are needed to reveal the non-trivial degeneracy of the entanglement spectrum. This chapter ends with a numerical calculation of the higher-order entanglement spectrum of the half-filled super-lattice Bose-Hubbard model.

Chapter 5

This is the last chapter where we consider higher-order topological phases in the context of the 2D super-lattice Bose-Hubbard model. The main achievement here is a strict bulk-boundary correspondence of a true bulk quantity and the fractional charges at the corners. To this end, we show that full periodic boundary conditions are not the optimal choice for describing higher-order topological systems and introduce a new type of boundary conditions, so-called corner periodic boundary conditions. Further, we introduce a new variant of a higher-order Zak (Berry) phase, which opens the door for proving the aforementioned bulk-boundary correspondence. To argue this, we make use of Thouless pumps, that are, adiabatic, cyclic variations of parameters along a symmetry breaking path encircling the gapless region—separating the distinct higher-order

topological phases of the half-filled 2D Bose-Hubbard model. Along such path, we have pumped one charge through the corners of the system, which is related to a non-trivial change of the higher-order Zak (Berry) phase. This is demonstrated by various numerical calculations. To literally prove this, we use two main tools: First, we extend Resta's construction [45] of the polarization in the many-body context to higher-order systems and, second, use an adiabatic approximation to evaluate the charge transport, upon which we find a relation of the fractional corner charge and the higher-order Zak (Berry) phase. This new variant of the higher-order Zak (Berry) phase differs from the one introduced in chapter 3, namely, it is only well-defined in the limit of hardcore bosons (infinitely strong on-site repulsion); however, we demonstrate—at least numerically—that the previous version of the higher-order Zak (Berry) phase leads to identical conclusions. The chapter ends with a sketch of a possible solution to this problem.

Part II: Quotient group symmetry-protected topological phenomena

Chapter 6

Here we discuss quotient group symmetry-protected topological phenomena in $\mathbb{Z}_n \times \mathbb{Z}_n$ symmetric one-dimensional lattice models. In particular, we focus on fixed-point Hamiltonians of $\mathbb{Z}_n \times \mathbb{Z}_n$ symmetry-protected topological phases and their transitions. Thereby, we discover that there are many more direct quantum phase transitions as initially expected; however, in terms of central charges, specifying the underlying conformal field theory, there are only three different possibilities (for paths considered here). Since the low-energy properties are fully governed by the quotient group, there are remaining gapped degrees of freedom that can lead to further distinction of conformal field theories. Indeed, we demonstrate that these additional degrees of freedom can endow the critical theory with topological properties. To demonstrate this, we study the $\mathbb{Z}_4 \times \mathbb{Z}_4$ symmetric case in full detail. In particular, we show that at quantum criticality the quotient group, together with another symmetry, gives rise to an emergent anomaly, that is, it forbids a gapped, symmetric ground state. Upon perturbing this transition by another fixed-point Hamiltonian of this class ($\mathbb{Z}_4 \times \mathbb{Z}_4$), we show that quantum criticality can be gapped out, but it is parametrically stable. This we argue analytically as well as numerically by providing a full phase diagram. In the second part, we generalize these observations to transitions in higher $\mathbb{Z}_n \times \mathbb{Z}_n$ symmetry groups. Further, we argue that a Hamiltonian, which consists of an equal-weighted super position of all fixed-point models cannot have a gapped, symmetric ground state, and that the additional $\mathbb{Z}_n$ symmetry appearing there, can be enhanced to a global $U(1)$ symmetry. This chapter ends with a generalization of observations made for this concrete lattice model, in particular, when to expect additional gapped degrees of freedom on phase transitions between distinct classes of symmetry-protected topological phases.

Chapter 7

While in the previous chapter the global symmetry group, $\mathbb{Z}_n \times \mathbb{Z}_n$, is able to protect a non-trivial SPT, this is not the case for the Haldane phase in the fermionic Hilbert space and, thus, the bulk is strictly speaking in a trivial phase. Consequently, there is no bulk phase transition required to trivialize this phase, which is thus dubbed a "quotient group symmetry-protected topological phase". The name results from the observation that topological signatures remain robust as long as low-energy degrees of freedom are fully characterized in terms of the quotient group. To showcase this, we consider the Haldane phase in the bond-alternating ionic Hubbard model, a descendant of the (Fermi-)Hubbard model. At weak interactions among fermions, the Haldane phase can adiabatically be connected to its trivial phase without encountering a quantum phase transition—thereby trivializing the Haldane phase by fluctuating charges. One of the main questions of this chapter is to ask, how immediate topological signatures of the Haldane phase disappear if charges start to fluctuate. Second, we show that there is an unnecessary quantum criticality separating the Haldane phase from its trivial counterpart, which remains robust beyond the limit of perturbation theory. To argue its robustness, we introduce a quantized invariant that reflects an emergent anomaly of the quotient group with a duality symmetry—exchanging the two possible alternations of the Hamiltonian. This anomaly forbids a gapped, symmetric ground state, and is parametrically stable due to a finite gap associated with gapped degrees of freedom. With lowering interactions, the anomaly is lifted—by symmetry extension—towards a gapped, symmetric phase. To support analytical claims, we map out a full phase diagram in a two-dimensional parameter space, explicitly demonstrating that topological signatures remain robust over a large parameter regime, and that the unnecessary quantum criticality persists as long as there is an emergent anomaly. The chapter ends with a brief discussion on general emergent anomalies for other symmetry groups and dimensions.

Chapter 8

Here, we summarize for each chapter the most relevant results of this thesis, which together with the former paragraphs give already a good overview of this thesis.

1.2.2 Summary of publications

Below, we summarize all publications that have been obtained during this PhD. For this, we first list publications contained in this thesis.

Publications contained in this thesis

[P1] "Fractional corner charges in a two-dimensional superlattice Bose-Hubbard model" by **Julian Bibo**, Izabella Lovas, Yizhi You, Fabian Grusdt, and Frank Pollmann, appeared in Phys. Rev. B 102, 041126(R). Julian Bibo has written the manuscript, and did the numerical calculations as well as worked out the details together with Izabella Lovas. Yizhi You supported this work with fruitful discussions. Fabian

Grusdt initialized the project, and together with Frank Pollmann, supervised this project.

[P2] "Higher-order entanglement and many-body invariants for higher-order topological phases" by Yizhi You, **Julian Bibo**, and Frank Pollmann, appeared in Phys. Rev. Research 2, 033192. This work separates into two parts, where the first part has been worked out by Yizhi You, and the second part as well as numerical calculations have been done by Julian Bibo and Frank Pollmann.

[P3] "Thouless Pumps and Bulk-Boundary Correspondence in Higher-Order Symmetry-Protected Topological Phases" by Julian F. Wienand, Friederike Horn, Monika Aidelsburger, **Julian Bibo**, and Fabian Grusdt, appeared in Phys. Rev. Lett. 128, 246602. The project was initialized and supervised by Julian Bibo and Fabian Grusdt, which got support from Monika Aidelsburger. Julian F. Wienand, Friederike Horn and Julian Bibo have written the main text, and did the numerical calculations. The analytical arguments have mainly been developed by Julian Bibo and Fabian Grusdt.

[P4] "Quantum criticality and quotient group protected topological phenomena of quantum chains with $\mathbb{Z}_n \times \mathbb{Z}_n$ symmetry" by **Julian Bibo**, Ruben Verresen, and Frank Pollmann. The manuscript is already prepared, but this work has not been published yet. The project was initialized by Ruben Verresen, which together with Frank Pollmann supervised this work. Julian Bibo wrote the manuscript, did all numerical calculations and together with Ruben Verresen worked out the analytical arguments.

[P5] "Quotient symmetry protected topological phenomena" by Ruben Verresen, **Julian Bibo**, and Frank Pollmann, arXiv:2102.08967. This work is currently in the review process of Physical Review Letters. Julian Bibo and Ruben Verresen contributed *equally* to this work. Julian Bibo did all numerical calculations, and together with Ruben Verresen worked out the analytical arguments of this work. Ruben Verresen has written main parts of the manuscript and Frank Pollmann supervised the project.

Publications not contained in this thesis

[P6] "Skeleton of matrix-product-state-solvable models connecting topological phases of matter" by Nick G. Jones, **Julian Bibo**, Bernhard Jobst, Frank Pollmann, Adam Smith, and Ruben Verresen, appeared in Phys. Rev. Research 3, 033265. Julian Bibo contributed substantially to the analytical arguments, numerical calculations and writing of the manuscript.

[P7] "Realizing the symmetry-protected Haldane phase in Fermi–Hubbard ladders" by Pimonpan Sompet, Sarah Hirthe, Dominik Bourgund, Thomas Chalopin, **Julian Bibo**, Joannis Koepsell, Petar Bojović, Ruben Verresen, Frank Pollmann, Guillaume Salomon, Christian Gross, Timon A. Hilker and Immanuel Bloch, appeared

in Nature (2022). Julian Bibo did the numerical calculations and substantially, together with Ruben Verresen and Frank Pollmann, contributed to the theory aspects of this work.

[P8] "Fracton Critical Point in Higher-Order Topological Phase Transition " by Yizhi You, **Julian Bibo**, Frank Pollmann, Taylor L. Hughes, appeared in Phys. Rev. B 106, 235130. Yizhi You and Taylor Hughes worked out the analytical arguments, Julian Bibo and Frank Pollmann contributed with numerical calculations.

[P9] "Fractonic critical point proximate to a higher-order topological insulator: How does UV blend with IR?" by Yizhi You, **Julian Bibo**, Taylor L. Hughes, Frank Pollmann, arXiv:2101.01724. This work has substantial overlap with the previous one. Yizhi You worked out the analytical arguments, Julian Bibo and Frank Pollmann contributed with numerical calculations, and Taylor Hughes and Frank Pollmann supervised the project.

Chapter 2

Review of quantum phases and symmetry-protected topological phases

For classifying quantum phases of matter, we first need to define when two different quantum states belong to the same phase. If, according to such a definition, two states are in the same phase, they can still differ in certain aspects such as local expectation values of observables, but, nevertheless, share the same universal features that characterize the phase. This is a great advantage because it is impossible to study all variants of condensed matter systems, and secondly, to understand matter around us, it is not necessary to investigate each representative individually. From statistical mechanics, as well as from daily experiences, we know that a given phase of matter is stable if we adjust parameters such as the temperature in a suitable range. For example, if we boil water at atmospheric pressure in a temperature regime $0°\mathrm{C} < \mathrm{T} < 100°\mathrm{C}$, then although the temperature of the fluid changes, it remains water. Alternatively, in the quantum context, if we slightly tune interactions among bosons, the system remains in a superfluid state. Thus, pictorially, we can visualize phases of matter as extended islands in parameter space. In more formal language, the state of a system is described in terms of a state variable such as the free energy, which is in one-to-one correspondence with the partition function derived from microscopic degrees of freedom. A given phase of matter is stable as long as the free energy or its derivatives are changing continuously.

Phase transitions are signaled by discontinuities in the thermodynamic state variables or their derivatives [46, 47]. For quantum systems operating at zero temperature, the partition function is fully specified by the ground state associated with a given Hamiltonian and, consequently, quantum phase transitions are expected when the ground state changes discontinuously [2, 48]. Such discontinuities can be, for example, a level transition between two energy levels (first-order transition) or a gap closure to the continuum of states (second-order transition), which can be detected from jumps in the expectation value of derivatives of the Hamiltonian.

Built on these observations, Refs. [49, 50] have given a precise definition, when two quantum states belong to the same phase of matter, or said differently, are equivalent. Although the first formulation of this definition gives a conceptual understanding when two quantum states are equivalent, it is less useful for practical purposes, since this formulation is based on spectral properties and eigenstates of the Hamiltonian for which we often—due to complexity—have very limited access[1]. Nevertheless, there is a

[1]The complexity of quantum systems grows exponentially with the number of degrees of freedom. For

second—yet equivalent—definition in terms of local unitary circuits that does not require knowing spectral properties of a given Hamiltonian, and is therefore more appropriate for practical applications.

According to this formulation, quantum states can be differed by their entanglement patterns [49, 50], that is, not all wave functions describing a given state of matter can be converted into a product state with zero entanglement. For a subclass of states, which we mainly consider in this chapter, this only holds if symmetries are taken into account. In fact, symmetries play an important role in classifying phases of matter. For example, different phases of water can be distinguished based on their symmetries; while water retains continuous translations and rotations, ice does not. Here, due to the lattice structure of ice, translations, and rotations are discrete symmetries. However, with the discovery and understanding of the quantum Hall effect [5, 51], it was realized that not all phases of matter can be distinguished in this way, in fact, there are phases of matter that share the same symmetry properties—yet they are not equivalent [4]. Such phases include so-called symmetry-protected topological (SPT) phases that have a symmetric bulk, but behave anomalously if considered with boundaries.

Overview. This chapter is divided into two main parts: In the first part, we mainly focus on the equivalence relation of two states of matter, thereby reviewing the definitions given by Refs. [49, 50], and, in particular, consider its peculiarities in the thermodynamic limit. Building on the previous definition, we discuss in Sec. 2.1.1 that there are two fundamentally different quantum states in nature, which can be distinguished according to their entanglement patterns. Further, we show that symmetries play an important role in defining equivalent states of matter. In fact, as we demonstrate in Sec. 2.1.2, symmetries can lead to further differentiation of quantum states and, thus, impose additional restrictions on how parameters can be changed. After introducing symmetries, the first part ends with an alternative formulation of equivalence of states using local unitary circuits (Sec. 2.1.3).

Based on the previous formulation, we start Sec. 2.2 with a rather general definition of symmetry-protected topological phases, specify their characteristic properties, and give a brief overview of what these phases look like. Furthermore, we consider different variations of these states of matter, starting with one-dimensional bosonic SPTs, Sec. 2.2.1, and their classifications. We then consider a two-dimensional example of bosonic SPTs, Sec. 2.2.2, before introducing the notion of higher-order SPTs in Sec. 2.2.3. Similar to the previous case, we demonstrate the characteristic properties of higher-order topology on a particular example. Finally, in Sec. 2.2.4 we briefly consider different mechanisms how SPT phases can be trivialized and demonstrate this explicitly using the former example of a 2D bosonic SPT (A more detailed overview can be found at the beginning of Sec. 2.2.).

example, for a spin-1/2 chain with L sites, the number of states is given by 2^L.

2.1 Two equivalent states of matter

Very often in this thesis we will come across the question when a pair of two quantum states $|\Psi\rangle$ and $|\Phi\rangle$, which we assume to be the ground states of a local, gapped Hamiltonian, belongs to the same phase of matter. According to Refs. [49, 50] two quantum states are a representative of a common quantum phase if they can be smoothly (continuously) connected.

(I) Equivalence of states: Two quantum states $|\Psi\rangle$ and $|\Phi\rangle$ are said to be in the same phase of matter if and only if there is a path of local, gapped Hamiltonians $\hat{H}(g)$ with $g \in [0, 1]$ and ground states $|\psi(g)\rangle$ such that $|\psi(0)\rangle = |\Psi\rangle$ and $|\psi(1)\rangle = |\Phi\rangle$.

Such a definition defines an equivalent relation among two quantum states $|\Psi\rangle \sim |\Phi\rangle$. It is said that the corresponding Hamiltonians belong to the same universality class. Before we proceed, let us briefly elaborate on the following question: *Why is this a sensible definition?* As stated in the introduction, at zero temperature the partition function—fully characterizing the thermodynamic properties of the system—is given by the ground state of the Hamiltonian. Thus, a phase transition is signaled by a non-analytic behavior of the ground state and its expectation values. However, as long as the gap is finite, observables, and, in particular, the expectation values of the Hamiltonian and its derivatives are an analytic function of all of its parameters and, thus, change smoothly [2, 52]. With this definition, a given phase of matter corresponds to a finite region in parameter space (see, for example, Fig. 2.1).

Furthermore, such a definition allows us to study simple representatives of a given phase, often denoted as *fixed-point* models. These models are exactly soluble and, hence, give us the possibility to investigate specific properties of a phase of matter[2]. In addition to that, we are not always interested in particular values of observables. For example, to characterize spontaneous-symmetry-breaking (SSB) phases it is sufficient to know if the corresponding order parameter has a finite expectation value in the thermodynamic limit[3]. For topological phases, a similar argument holds. As we will see, such phases are commonly classified in terms of discrete quantum numbers that remain unchanged if the Hamiltonian is continuously deformed, i.e., only perturbations are added that respect the symmetry and keep the bulk gap finite.

Thermodynamic limit

For the above definition to be meaningful, another aspect is important, namely, it must be well-defined in the thermodynamic limit, where particle number (or number of spins) and volume tend to infinity, $N \to \infty$, $V \to \infty$, but the density $n = N/V$ is fixed.

[2] In Chap. 6 we study fixed-point models of a particular class of symmetry-protected topological phases in one dimension.

[3] Sometimes the expectation value vanishes, although there is SSB. Then, SSB can be detected from the two-point correlation function, which approaches a finite value even if distances extend to infinity.

Why is this important? The bulk gap of a generic quantum system, whose spectrum becomes gapless in the thermodynamic limit, is always finite if the system is considered on a finite size geometry [2, 52]. Thus, at finite sizes, the above definition of equivalence is always satisfied. If this were allowed, this would lead to wrong physical conclusions. For example, a quantum system whose thermodynamic limit state exhibits spontaneous-symmetry-breaking has always a symmetric ground state at finite size, i.e., $V < \infty$ [53]. Consequently, for any finite system we would expect the state to be equivalent to its symmetric companion, which is clearly not the case. A paradigmatic example of such a case is the one-dimensional transverse field Ising model, governed by the Hamiltonian [2],

$$\hat{H}_{\text{Ising}}(g, J) = -g \sum_n \hat{X}_n - J \sum_n \hat{Z}_n \hat{Z}_{n+1}, \quad g \geq 0, \quad J \geq 0. \tag{2.1}$$

This Hamiltonian has a $\mathbb{Z}_2$ symmetry generated by $\prod_n \hat{X}_n$. For large $g/J \to \infty$, the ground state is a symmetric product state given by $|\Psi\rangle = \prod_n |{\rightarrow}\rangle_n$, where $|{\rightarrow}\rangle_n$ denotes the eigenstate of $\hat{X}_n$ with eigenvalue $+1$. This state remains symmetric—even in the thermodynamic limit. On the other hand, if $g/J \to 0$ there are two degenerate ground states $|\Psi\rangle_\uparrow = \prod_n |{\uparrow}\rangle_n$ and $|\Psi\rangle_\downarrow = \prod_n |{\downarrow}\rangle_n$. Here $|{\uparrow}\,({\downarrow})\rangle_n$ denotes the eigenstate of $\hat{Z}_n$ with eigenvalue $+(-)1$. Clearly, none of these states are symmetric. However, for any finite size system we always find a symmetric ground state, independent of g/J. For $g/J \to 0$, there are two symmetric states that are exponentially close in energy. If $L \to \infty$ the ground state spontaneously breaks the $\mathbb{Z}_2$ symmetry [2, 53], and the order parameter gains a non-zero expectation value $\langle \hat{Z}_n \rangle \neq 0$. Moreover, from the exact solution it is known that at $J = g$ the bulk gap scales as $\Delta \sim 1/L$ [54][4]. Consequently, for any finite L we would conclude that, according to the definition above, both states are in the same phase, which is clearly not the case. In summary, this example clearly illustrates that for the definition above to be meaningful, we have to require that the bulk gap along the path must be finite and system size independent as we approach the thermodynamic limit.

2.1.1 Short-ranged versus long-ranged entangled states

According to classifications of quantum phases of matter [49, 50], there are two fundamentally different quantum states, which can be distinguished based on their entanglement properties. A quantum state that hosts no correlations and entanglement is called a *product state* [52]. A d-dimensional product state, upon blocking of sites, is characterized by the fact that its density matrix can be written as a tensor product $\hat{\rho} = \bigotimes_{\boldsymbol{x}} \hat{\rho}_{\boldsymbol{x}}$ over building blocks labelled by $\boldsymbol{x}$[5]. Building on this definition, there are two separate classes of quantum states: On one hand, there are quantum states for which exist

[4] If one solves the transverse field Ising model for finite L with PBC, then there is a subtlety if we apply the Jordan-Wigner transformation. Indeed, the Hamiltonian becomes block diagonal with sectors labeled by fermion parity. The ground state is then found in the sector with even number of fermions and anti-PBC. From this, we find that $\Delta \sim 1/L$.

[5] For example, for a system having a two-site translation symmetry, the unit cell consists of two-sites and the building blocks are unit cells and not individual sites.

no path of local, gapped Hamiltonians such that they can be connected to a product state. Quantum states falling into this category are called *long-ranged entangled* (LRE) states [4, 49]. Examples of such states are *intrinsically topologically ordered* states, such as the fractional quantum Hall states [7, 55, 56] or the toric code [57]. A hallmark of such states is that the ground state degeneracy of these states depends on the topology of the underlying geometry. The toric code, for example, considered on a torus has four degenerate ground states, while on a cube, the ground state is unique. Such a feature—the topology dependent ground state degeneracy—is a sufficient condition for the ground state not being connectable with a product state[6].

Contrary, a quantum state $|\Psi\rangle$ is called short-ranged entangled (SRE) if it can be, according to definition (I), transformed into a product state [4, 49, 50]. Typical representatives of such states are phases of matter that exhibit spontaneous-symmetry-breaking. As we will discuss next, symmetries can distinguish different SRE entangled states—even forbid that states can be converted into product states. However, up to this point, we have not yet considered symmetries. Hence, the two ground states of the foregoing introduced quantum Ising model are two examples of SRE states that can be continuously transformed into a product state (without symmetry).

2.1.2 Symmetries and restrictions of paths

So far, the only requirement was that the bulk gap is finite as the thermodynamic limit is approached; however, if paths are further restricted by symmetry, then not all SRE states belong to the same phase anymore, and can be transformed into a product state. For example, the two different states of the one-dimensional transverse field Ising model become distinct only in the presence of $\mathbb{Z}_2$ symmetry. If this symmetry is explicitly conserved along a path connecting the two different states, then unavoidably the bulk gap has to close. Thus, in the presence of symmetries the definition gains further constraints:

(II) Equivalence of states with symmetries: Two quantum states $|\Psi\rangle$ and $|\Phi\rangle$ are said to be in the same phase of matter if and only if there is a path of local, gapped and symmetric Hamiltonians $\hat{H}(g)$ with $g \in [0, 1]$ and ground states $|\psi(g)\rangle$ such that $|\psi(0)\rangle = |\Psi\rangle$ and $|\psi(1)\rangle = |\Phi\rangle$.

In a given parameter space, symmetries lead to further differentiation of SRE entangled states, see Fig. 2.1, which give rise to isolated regions that cannot be adiabatically connected. For SRE states such phases are SSB phases or symmetry-protected topological phases, which, unlike SSB phases, cannot be captured by local order parameters or long-range correlations associated to it. Although LRE states are distinct—even in the absence of symmetry—symmetries can also enrich phase diagrams including LRE states called symmetry-enriched topological order [4, 49].

[6] The topology dependent degeneracy of ground states exhibiting intrinsic topological order gives a non-trivial contribution to the entanglement entropy [4]. By construction, the entanglement entropy of a product state—independent of the geometry—is always zero and, thus, a product state can never have a topology dependent degeneracy.

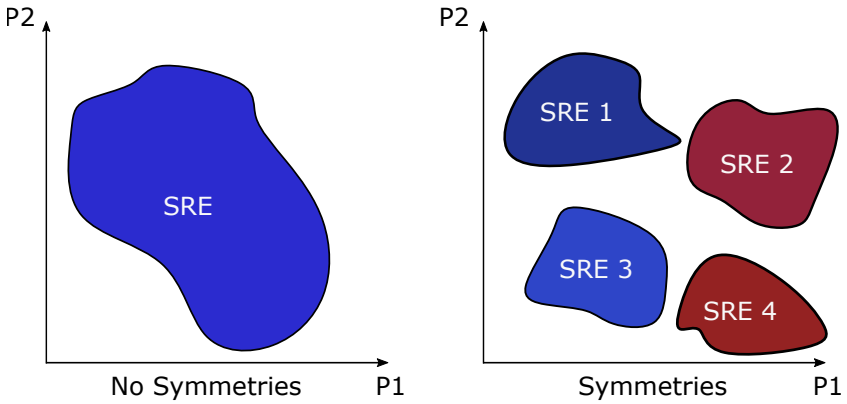

Figure 2.1: **SRE phases and symmetries.** If no symmetries are considered all SRE states, for a given set of parameters $\{\mathrm{P1}, \mathrm{P2}\}$, belong to the same phase (left). On the other hand, in the presence of symmetries formerly equivalent states become different (right).

2.1.3 Local unitary circuits

Up to this point, we argued that two states of matter belong to the same phase if there is a path of local, gapped (and symmetric) Hamiltonians that connects these states. However, in practice it is difficult to find such paths and—in particular—prove that its bulk gap stays finite as we approach the thermodynamic limit. Therefore, Chen and co-workers [49, 58] came up with an alternative—yet equivalent—definition when two quantum states belong to the same phase of matter:

(III) Local unitaries: Two quantum states $|\Psi\rangle$ and $|\Phi\rangle$ are said to be in the same phase of matter if and only if there is a local (symmetric) unitary transformation such that: $|\Phi\rangle = \hat{U}\,|\Psi\rangle$, where $\hat{U}$ is parametrized as follows:

$$\hat{U} = \hat{\mathcal{P}} \exp\left(-i \int_0^1 \mathrm{d}g\, \hat{H}(g)\right). \tag{2.2}$$

The operator $\hat{\mathcal{P}}$ denotes path ordering and $\hat{H}(g)$ is a local, gapped (symmetric) Hamiltonian.

The definition of local unitary operations is reminiscent of time evolution of quantum states in quantum mechanics [59]. The former requirement of a system size independent, finite bulk gap translates here to a finite evolution time in the thermodynamic limit that does not grow with system size. Upon using the Suzuki-Trotter[7] decomposition, the local

[7] Given an exponential of operators, the formally exact Suzuki-Trotter decomposition is defined as $\exp(\hat{A}+\hat{B}) = \lim_{N\to\infty}\left(\exp(\hat{A}/N)\exp(\hat{B}/N)\right)^N$. For any practical purpose, N is large but finite, which cause an approximation error depending on the order of the decomposition [60].

unitary operation can be transformed into a finite-depth quantum circuit [52] given by,

$$\hat{U}_M = \prod_{l=1}^{M} \hat{U}^{(l)}, \quad \hat{U}^{(l)} = \prod_{\boldsymbol{x}} \hat{U}^{(l)}_{\boldsymbol{x}}, \tag{2.3}$$

where $\hat{U}^{(l)}_{\boldsymbol{x}}$ acts on finite, non-overlapping regions labelled by $\boldsymbol{x}$ and $M < \infty$ is the finite number of layers (see Fig. 2.2). On-site symmetries, for instance, are represented as finite-depth quantum circuits with $M = 1$, and $\boldsymbol{x}$ labels actual building blocks.

Note the local unitary operator defined in Eq. (2.2) has an important property: It can be *continuously* connected to identity, and in the presence of symmetry, it is symmetric at each step. Thus, if such a unitary operation is represented by a quantum circuit, only those quantum circuits are allowed for which this property is satisfied. This constraint is important, and without it, actual distinct states would be equivalent. To illustrate this, let us consider the following $\mathbb{Z}_2 \times \mathbb{Z}_2$ symmetric Hamiltonian with PBC [52, 61][8]:

$$\hat{H}_{\text{cluster}}(g, J) = -g \sum_n \hat{X}_n + J \sum_n \hat{Z}_{n-1} \hat{X}_n \hat{Z}_{n+1}, \quad g \geq 0, \quad J \geq 0, \tag{2.4}$$

where the symmetry is generated by $\prod_n \hat{X}_{2n-1}$ and $\prod_n \hat{X}_{2n}$. The non-trivial Hamiltonian $\sim \hat{Z}_{n-1} \hat{X}_n \hat{Z}_{n+1}$ can be obtained from the paramagnet by a two-site gate, two-layer quantum circuit,

$$\hat{U} = \prod_n \exp\left(i \frac{\pi}{4} \hat{Z}_n \hat{Z}_{n+1} \right), \quad \hat{U}^\dagger \hat{X}_n \hat{U} = \hat{Z}_{n-1} \hat{X}_n \hat{Z}_{n+1}, \tag{2.5}$$

that is symmetric with respect to $\mathbb{Z}_2 \times \mathbb{Z}_2$ symmetry. As we will show later, the ground state for $g/J \to 0$ is a non-trivial SPT and, thus, cannot be transformed into a product state via a symmetric path of local, gapped Hamiltonians. Without the constraint that a quantum circuit—connecting two quantum states of the same phase—must be continuously and symmetrically connectable to identity, we falsely would conclude that both states of $\hat{H}_{\text{cluster}}$ can be connected by a finite-depth quantum circuit. However, the caveat is that this circuit *cannot* be continuously connected to identity if we require it to be symmetric at each step of the transformation.

If a local unitary transformation is represented as a quantum circuit, then an evolution with finite time corresponds to a finite-depth quantum circuit. From Fig. 2.2 we see that if the number of layers becomes of the order of system size, then correlations spread all over the system and states are certainly no longer short-ranged entangled. Indeed, it was shown that if the number of layers reaches system size, that SRE state can be transformed into LRE states [62]. Without restrictions due to symmetry, *all* SRE states can be transformed into each other using local unitary operations.

[8] Note the relative sign is not relevant here, it can be changed by the following unitary $\hat{V} = \prod_n \hat{X}_{4n-3} \hat{X}_{4n-2}$.

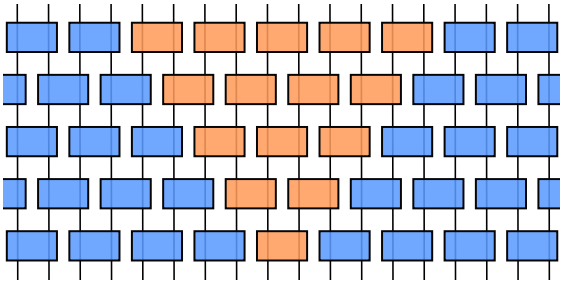

Figure 2.2: **Finite-depth quantum circuit with causal cone.** A finite-depth quantum circuit with a two-site gate $x = 2$ is shown. The number of layers is finite, which thus results in a finite causal cone. Outside the causal cone, quantum correlations are negligible.

2.2 Symmetry-protected topological phases

In the previous section, we discussed when two quantum states of matter can be considered as equivalent. Thereby, we argued that in practice it is often very hard to prove that a given path of local, gapped Hamiltonians has a finite bulk gap in the thermodynamic limit. However, we demonstrated that this is not necessary if we use local unitary circuits. Based on this formulation, we can give a rather general definition of SPT phases, another class of SRE states. These states can be defined as follows [49, 50, 58]:

Symmetry-protected topological states. A short-ranged entangled quantum state $|\Psi\rangle$ that is symmetric with respect to a given symmetry S, is called an SPT state if it cannot be connected to a product state via a symmetric, local unitary transformation defined in Eq. (2.2).

Given this rather general definition of SPT states, how do we in practice know that there is no such unitary circuit? Since SPT states are symmetric, we cannot make use of local order parameters to distinguish different SPTs; thus Landau's theory of symmetry breaking [3, 63] fails to classify such phases of matter. Instead, we will show that distinct classes of SPTs can be differed by invariants that are quantized by symmetries:

Distinction of SPT phases. For a given symmetry S that protects distinct classes of non-trivial SPTs, we can associate a discrete set of quantized invariants $Q = \{q_1, ..., q_n\}$ with $|Q| > 1$ and $n < \infty$ that assigns a label to each class of SPTs. The values of the quantized invariants are unchanged by continuous deformations of the Hamiltonians (see definition (II)). Each set of quantized invariants characterizes a universality class.

For example, if we consider Fig. 2.1, then each bubble can be a different SPT to which we can assign a quantum number. Note, there can also be more symmetries that protect

a given phase. Thus, in general, we need to consider a set of symmetries denoted as $\mathcal{S} = \{S_1, S_2, S_3, ..., \}$, where to each symmetry we define a set of quantized invariants. If we add or remove certain symmetries, then formerly two equivalent states become distinct or vice versa. In practice: To be able to assign labels to SPT phases, we first have to define the set of protecting symmetries and their representations.

SPT phases—an overview

SPT phases of matter appear in various ways and can be protected by different kinds of symmetries such as on-site symmetries (time reversal, spin rotations), spatial symmetries (bond-centered inversion, C_n-rotations) or combinations thereof [19, 20, 26, 64–66]. For bosons, SPTs exist only in the presence of strong interactions because weakly-interacting bosons have the tendency to cluster—thereby forming a Bose-Einstein condensate [67, 68]. For fermions, however, SPTs exist irrespective of interactions, which is a consequence of Pauli blocking, but note that interactions can non-trivially change the classifications of fermionic SPTs [69, 70]. SPTs in non-interacting, free-fermion systems usually appear in the context of *topological insulators* [71–75]. However, not every topological insulator is an SPT, but every free-fermion SPT is a topological insulator. For example, Chern insulators are topological insulators but not an SPT. Indeed, these phases of matter do not require any symmetry to be topologically non-trivial.

SPTs and boundaries

If SPT phases are considered on closed manifolds, then the ground state is unique, gapped, and symmetric. Since SPTs are SRE states, the bulk has featureless excitations [4, 52]. This contrasts with LRE states that exhibit topological order. For example, for the formerly introduced toric code model, a $\mathbb{Z}_2$ topologically ordered state, excitations are so-called Abelian anyons that are particles that have non-trivial exchange statistics[9], which can even be fractional [76–78] or non-Abelian [77–79], that is, the exchange of two particles does not simply result in a phase factor; instead, corresponds to a linear transformation of the state. It appears that the bulk of SPTs is by no means different from that of a trivially disordered product state. However, this is not the full story. If an SPT is coupled to gauge fields, then the resulting model can have excitations that have non-trivial exchange statistics, revealing its non-trivial nature [80, 81].

The situation is different if SPTs are subjected to a manifold with edges because then its non-trivial nature does not require further manipulations. This can be seen from the argument given in Ref. [82]. Considering an SPT with boundary is equivalent to an interface of a non-trivial SPT with the vacuum, which we denote as trivial phase. Since on either side of the interface, phases are gapped and symmetric, we can continuously tune parameters inside each phase without crossing a discontinuity. However, by assumption both phases have been different such that there must be a gap closing once we cross the interface. If this was not the case, then according to our definition,

[9] For Abelian anyons, the two particle wave function picks up an arbitrary phase factor under exchanging two particles, $\Psi(\boldsymbol{x}_2, \boldsymbol{x}_1) = e^{i\theta}\Psi(\boldsymbol{x}_1, \boldsymbol{x}_2)$, $\theta \in \mathbb{R}$.

both phases must be equivalent. Since the gap closing is spatially confined, this signals a zero-energy mode[10]. In general, SPT phases are characterized by anomalies at the boundary of the system, which can be gapless zero-energy modes, SSB, or even topological order[11] [18, 71, 72, 82, 85–91].

Stacking property

Previously, we argued that to each class of an SPT, we can associate a quantized invariant. As it turns out, the sets of quantized invariants form groups [64, 74]. From this, we can deduce a so-called *stacking property* of SPTs, that is, forming a tensor product of two SPTs, labeled by invariants q_A and q_B, results in a third SPT phase, which has a label $q_A \oplus q_B$[12]. For example, if there are only two different quantum numbers ± 1, then stacking a non-trivial SPT with itself results in a trivial phase. For a non-trivial SPT, we cannot remove the anomaly at the edges by adding symmetric perturbations; however, if we stack SPTs such that the quantized invariant becomes trivial, then we can find symmetric perturbations coupling the two SPTs such that the anomaly along the boundary is removed.

Section overview

Up to this point, we have considered SPT phases from a general perspective. In the following, however, we will demonstrate the general definitions along various examples of bosonic SPTs in different dimensions and variations. Thereby, in Sec. 2.2.1, we start with bosonic SPTs in one dimension, reviewing the former introduced cluster model and show that its ground state is actually a non-trivial SPT. Afterwards we give a summary of the general classification of these phases, and show how the Berry phase can serve as a label for such states. This part is followed by two-dimensional bosonic SPTs, Sec. 2.2.2, whose properties are discussed along an exactly solvable model of a 2D SPT. After these two subsections, where we give an introduction to conventional bosonic SPTs, that have nowadays been well-understood, we introduce in Sec. 2.2.3 the notion of higher-order topology, that is, anomalies can not only appear at the one-dimensional boundary of a 2D SPT, but also on its 0D corners, while the 1D edge remains gapped. This section starts with a concrete lattice example, and is then followed by a brief summary of a general classification of these higher-order topological phases. Finally, in Sec. 2.2.4 we discuss a particular mechanism of trivializing SPTs without breaking the symmetry or using its stacking property, and illustrate this, using the former discussed 2D SPT example.

[10] Detailed examples of such interfaces are discussed in Refs. [83, 84]

[11] Note for bosonic systems the boundary must at least have dimension two since there is no topological order for bosonic systems in one dimension [39, 49].

[12] Here "$\oplus$" denotes the addition of group elements.

2.2.1 Bosonic SPTs in one dimension

After the seminal works of Haldane [13, 14], who showed that integer spin antiferromagnetic Heisenberg models behave fundamentally different from their half-integer counterparts, namely, in contrast to the former, integer spin chains have a bulk gap and exponentially decaying correlation functions, Affleck, Kennedy, Lieb and Tasaki (AKLT) constructed an exactly solvable spin-1 model [15, 92], whose symmetric ground state has zero-energy, spin-1/2 excitations exponentially confined to the boundary. Later, Gu, Wen, Pollmann and others [16, 17, 93] uncovered the topological properties of these phases, which, among other things, have been the aforementioned fractional zero-energy excitations at the boundaries and degeneracies in the entanglement spectrum. The SPT phase associated with the AKLT model, or the spin-1 Heisenberg model, is known as Haldane phase, an SPT protected by spin rotations $SO(3)$[13], time reversal symmetry and bond-centered inversion symmetry. A few years later, it turned out that one-dimensional bosonic SPTs can be fully classified in terms of projective representations [94], whose labels are given by the second cohomology group denoted as $H^2(G, U(1))$. A systematic classification and construction of such phases was given by Ref. [50, 64].

In this section we start with a concrete example, the $\mathbb{Z}_2 \times \mathbb{Z}_2$ cluster model, and consider the model for different boundary conditions—illustrating that its ground state is actually a non-trivial SPT. Afterwards, we give the general classification in terms of projective representations and summarize implications on ground states characterized by non-trivial projective representations.

The $\mathbb{Z}_2 \times \mathbb{Z}_2$ cluster model

The previously introduced cluster model, Eq. (2.4), is an exactly solvable bosonic SPT protected, among others, by $\mathbb{Z}_2 \times \mathbb{Z}_2$ symmetry[14]. For illustrating the characterizing properties, we focus on the limit $g = 0,\ J > 0$. In this limit, the Hamiltonian reduce to

$$\hat{H}_{\text{cluster}} = \sum_n \hat{Z}_{n-1}\hat{X}_n\hat{Z}_{n+1}, \quad \mathbb{Z}_2 \times \mathbb{Z}_2 : \quad \prod_n \hat{X}_{2n-1}, \quad \prod_n \hat{X}_{2n}. \tag{2.6}$$

Note each term inside the Hamiltonian commutes and squares to identity.

Closed boundaries. For a closed manifold consisting of L sites, there are exactly L terms in the Hamiltonian. Consequently, the ground state is obtained from the condition that:

$$\hat{Z}_{n-1}\hat{X}_n\hat{Z}_{n+1} \left|\Psi_{\text{cluster}}\right\rangle = - \left|\Psi_{\text{cluster}}\right\rangle, \quad \forall n. \tag{2.7}$$

Since there is only a single ground state, it must be symmetric. The first excited state is obtained by flipping a sign of a single term, which results in a finite energy gap. Thus, as stated, for a closed manifold the ground state is gapped, unique and symmetric.

Open boundaries. On the other hand, if the system is considered with edges, then there is a two-fold degeneracy on each edge. Although at first sight this degeneracy looks fine-tuned, it is actually not. To illustrate this, consider the action of symmetry generators

[13] Actually, the $\mathbb{Z}_2 \times \mathbb{Z}_2$ subgroup is sufficient to protect this phase.
[14] For an extended discussion of this model and its protecting symmetries see, for example, Ref. [38].

on the ground state of a finite size system. Upon using that $\hat{Z}_{n-1}\hat{X}_n\hat{Z}_{n+1} = -1$, we obtain (up to a sign):

$$\prod_n \hat{X}_{2n-1}\,|\Psi^{OBC}_{\text{cluster}}\rangle \sim \hat{X}_1\hat{Z}_2\hat{Z}_L\,|\Psi^{OBC}_{\text{cluster}}\rangle\,, \quad \prod_n \hat{X}_{2n}\,|\Psi^{OBC}_{\text{cluster}}\rangle \sim \hat{Z}_1\hat{Z}_{L-1}\hat{X}_L\,|\Psi^{OBC}_{\text{cluster}}\rangle\,. \tag{2.8}$$

This clearly shows that for SPTs symmetry acts only non-trivially near the edges of the system, which is known as symmetry fractionalization [95] (for a brief review see App. C). If we focus on the left edge of the system, then we see from the Hamiltonian and the former result, that we can freely choose the $\hat{Z}$ eigenvalue on the first site, which results in a two-fold degeneracy. Upon applying the $\mathbb{Z}_2$ symmetry on odd sites, the two states are transformed into each other.

Projective transformations. Although globally symmetries commute, this is no longer true if its action is considered in the ground state subspace (gs) restricted to a single edge:

$$\begin{aligned}\mathbb{1} &= \left(\prod_n \hat{X}_{2n-1}\right)\left(\prod_n \hat{X}_{2n}\right)\left(\prod_n \hat{X}_{2n-1}\right)^\dagger\left(\prod_n \hat{X}_{2n}\right)^\dagger \\ &\overset{gs}{=} \left[\left(\hat{X}_1\hat{Z}_2\right)\hat{Z}_L\right]\left[\hat{Z}_1\left(\hat{Z}_{L-1}\hat{X}_L\right)\right]\left[\left(\hat{X}_1\hat{Z}_2\right)\hat{Z}_L\right]^\dagger\left[\hat{Z}_1\left(\hat{Z}_{L-1}\hat{X}_L\right)\right]^\dagger \\ &= \left(\hat{X}_1\hat{Z}_1\hat{X}_1^\dagger\hat{Z}_1^\dagger\right)\left(\hat{Z}_L\hat{X}_L\hat{Z}_L^\dagger\hat{X}_L^\dagger\right),\end{aligned} \tag{2.9}$$

where we used that bosonic operators defined on disjoint regions commute. Hence, on a single edge, the low-energy representation of the global symmetry anticommutes. If a representation has such a property, then it is called a projective representation [50, 94]. Let us emphasize an important point: This property is not fine-tuned and is protected by the finite gap of this Hamiltonian. If the Hamiltonian is perturbed, then the effective low-energy representations of the symmetry operators remain no longer on-site, but stay exponentially close to the edge region [94, 95].

Zero-energy modes. The anticommutation relations found on a single edge imply the existence of zero-energy modes, which we mentioned earlier. For two matrices to anticommute, their dimension must be at least two,

$$\det\left(\hat{X}_1\hat{Z}_1\hat{X}_1^\dagger\hat{Z}_1^\dagger\right) = (-1)^D = \det\left(\hat{X}_1\hat{X}^\dagger\right)\det\left(\hat{Z}_1\hat{Z}_1^\dagger\right) = 1, \tag{2.10}$$

which implies $D > 1$ and even. This property causes a two-fold degeneracy on each edge of the system.

Entanglement spectrum. If we consider the ground state on a half-infinite chain, then the anticommutation relation on the remaining edge is responsible for even degeneracies in the entanglement spectrum. To illustrate this, we need two ingredients: First, the two ground states are transformed into each other by an operator that is localized near the edge, and leaves the bulk unchanged. Second, we need to bipartite the systems into two parts; an edge region $\mathcal{E}$ and a bulk region $\mathcal{B}$, with the condition that the size of the edge region is much larger than the localization length associated to the edge mode.

Then, from the Schmidt decomposition of the ground states

$$|\Psi^1_{\text{cluster}}\rangle = \sum_\alpha \Lambda_\alpha |\alpha^1_{\mathcal{E}}\rangle |\alpha^1_{\mathcal{B}}\rangle , \quad |\Psi^2_{\text{cluster}}\rangle = \sum_\alpha \Lambda_\alpha |\alpha^2_{\mathcal{E}}\rangle |\alpha^2_{\mathcal{B}}\rangle , \tag{2.11}$$

upon using that $|\alpha^1_{\mathcal{B}}\rangle = |\alpha^2_{\mathcal{B}}\rangle$ for each α, we conclude that for each Schmidt state in the bulk, there are two Schmidt states associated with the edge region. Since the two states are orthogonal, each Schmidt value is at least two-fold degenerate, implying an even degeneracy of the entanglement spectrum[15].

Paramagnetic phase

If we repeat the above analysis for the paramagnetic phase defined in Eq. (2.4), then we find that there is a unique, gapped and symmetric ground state for closed and open boundary conditions. This implies that symmetries have a trivial projective representation in the low-energy subspace, or said differently, form a faithful representation of the symmetry. Thus, according to our definition of SPTs, we find two quantized invariants $\mathbb{Z}_2 = \{1, -1, \}$ for the $\mathbb{Z}_2 \times \mathbb{Z}_2$ symmetry defined above.

Classification in terms of group cohomology

In the previous example, we showed that all non-trivial properties followed from the low-energy representation of the global symmetry, which were denoted as projective representations. Indeed, one-dimensional bosonic SPTs were fully classified in terms of projective representations [50, 64, 85, 94, 96]. Different classes of projective representations are labeled by the second cohomology group, denoted as $H^2(G, U(1))$. For the cluster model and the paramagnet, we argued that projective representations can either commute or anticommute. Thus, we find that $H^2(\mathbb{Z}_2 \times \mathbb{Z}_2, U(1)) = \mathbb{Z}_2$ [64].

For the general classification, let us consider a local, gapped and symmetric Hamiltonian and a representation $\hat{U}^g$ of the corresponding (Abelian) symmetry group G. Thereby, $\hat{U}^g$ is a faithful representation, that is, they obey the group multiplication law

$$\hat{U}^g \hat{U}^h = \hat{U}^{gh}, \quad \forall g, h \in G. \tag{2.12}$$

Similar to the previous example, the low-energy representation of the symmetry is obtained from the action of $\hat{U}^g$ on the ground state, for which we thus write $\hat{U}^g = \hat{\mathcal{U}}^g_L \hat{\mathcal{U}}^g_R$. For projective representations such as $\hat{\mathcal{U}}^g_L$, the group multiplication law is obeyed only up to a $U(1)$ phase factor

$$\hat{\mathcal{U}}^g_L \hat{\mathcal{U}}^h_L = \omega(g,h) \hat{\mathcal{U}}^{gh}_L, \quad \hat{\mathcal{U}}^g_R \hat{\mathcal{U}}^h_R = \bar{\omega}(g,h) \hat{\mathcal{U}}^{gh}_R, \tag{2.13}$$

where the complex conjugate results from the condition that: $\hat{U}^{gh} = \hat{\mathcal{U}}^{gh}_L \hat{\mathcal{U}}^{gh}_R$ and $\hat{U}^{gh} = \hat{U}^g \hat{U}^h = \hat{\mathcal{U}}^g_L \hat{\mathcal{U}}^h_L \hat{\mathcal{U}}^g_R \hat{\mathcal{U}}^h_R$. Hence, knowing the projective representations on a single edge is sufficient; thus, we drop the subscript $L(R)$ in the following and denote the low-energy

[15] The eigenvalues of the reduced density matrix are given by the square of the Schmidt values.

representation of the symmetry as $\hat{\mathcal{U}}^g$. From the definition of $\omega(g,h)$, we see that it is not invariant under rephasing, i.e., $\hat{\mathcal{U}}^g \to \beta(g)\hat{\mathcal{U}}^g$, which thus defines an equivalence relation. Two phase factors, related by,

$$\omega'(g,h) = \omega(g,h)\frac{\beta(g)\beta(h)}{\beta(gh)}, \tag{2.14}$$

are considered to be the same element in $H^2(G,U(1))$ [64, 85]. The phase factors (or equivalence classes) $\{\omega(g,h)\}$ are denoted as 2-cocycles. Moreover, if it is possible to find a set of phase factors $\{\beta(g)\}$ such that $\omega(g,h)' = 1$, then it is called a 2-coboundary[16].

Topological invariant: To define a proper topological invariant, we have to find an expression that is invariant under gauge transformations (here rephasing). For Abelian symmetry groups, such a gauge-invariant phase factor can be obtained from the quotient of two 2-cocycles [94],

$$q(g,h) = \frac{\omega(g,h)}{\omega(h,g)} = \hat{\mathcal{U}}^g\hat{\mathcal{U}}^h[\hat{\mathcal{U}}^g]^\dagger[\hat{\mathcal{U}}^h]^\dagger, \tag{2.15}$$

which is nothing else than the commutator previously used to classify the SPT of the cluster model. Note, it is possible to find gauge-invariant phase factors for more complicated groups as well, which has been discussed in Ref. [94].

Implications of non-trivial projective representations

For the concrete example of the cluster model, we proved that all non-trivial properties such as zero-energy modes and degeneracies in the entanglement spectrum can be obtained from the projective representations. Here, we will show that this is generically the case.

Zero-energy modes. If we assume that the quantized invariant $q(g,h)$ has a $\mathbb{Z}_n$ classification, then the number of zero-energy modes on each edge is determined by the irreducible dimension of the projective representations. The irreducible dimension can be deduced by taking the determinant of the commutator:

$$\begin{aligned}\det\left(\hat{\mathcal{U}}^g\hat{\mathcal{U}}^h[\hat{\mathcal{U}}^g]^\dagger[\hat{\mathcal{U}}^h]^\dagger\right) =& [q(g,h)]^D \\ =& \det\left(\hat{\mathcal{U}}^g[\hat{\mathcal{U}}^g]^\dagger\right)\det\left(\hat{\mathcal{U}}^h[\hat{\mathcal{U}}^h]^\dagger\right) \\ =& 1.\end{aligned} \tag{2.16}$$

which implies that $D \leq n$. If $q(g,h)$ is an element of a subgroup of $\mathbb{Z}_n$, then the dimension can be less than n. Hence, for such classification, the number of edge modes is bounded by the dimension of the irreducible representation.

Entanglement spectrum. Pollmann and co-workers [93] showed that the entanglement spectrum of non-trivial SPTs have degeneracies in multiples of the irreducible dimension of projective representations. A crucial point for this to hold is that projective representations are exponentially localized near the edge of the system. Then, using a Schmidt

[16] For a detailed introduction to this, see, for example, Ref. [64].

decomposition of a half-infinite chain with an edge region much larger than the localization length, proves, similar to the cluster model, the degeneracy of the entanglement spectrum. This property remains even if we consider the entanglement spectrum of an infinite chain and, consequently, the degeneracy of the entanglement spectrum is a true bulk property. Thus, this proves a bulk-boundary correspondence: The number of edge modes determines the degeneracy of the entanglement spectrum.

Stacking property. Since projective representations are labeled by group elements, the stacking property naturally follows. Indeed, if we consider a $\mathbb{Z}_2$ label, similar to the cluster model, then the SPT is trivialized[17] by tacking two copies of the same Hamiltonian. Such Hamiltonian can be written as:

$$\hat{H}_{\text{stack}} = \hat{H}_A \otimes \mathbb{1}_B + \mathbb{1}_A \otimes \hat{H}_B, \tag{2.17}$$

where A, B label the two copies of the same Hamiltonian. With this, the projective representations have been lifted to a linear one. By adding symmetric perturbations, coupling these two Hamiltonians, the edge modes disappear and, thus, the ground state is in a trivial phase.

In practice. Since SPT states are ground states of local, gapped Hamiltonians, these states can be well approximated by tensor networks [97–99]. Once the tensor network representation is found, either analytically or numerically, we can use the methods developed by Ref. [94] to obtain the projective representations and evaluate their commutation relations.

Zak (Berry) phase

Another way of classifying certain bosonic SPT phases is to make use of the many-body generalization of the Zak phase. In 1984 Berry [100] discovered that a quantum mechanical wave function picks up a non-trivial, measurable geometric phase factor if we adiabatically[18] tune a parameter $\lambda \in \mathbb{R}$ of the Hamiltonian on a closed contour. The phase depends solely on the path in parameter space and is defined as follows:

$$\gamma(C) = i \oint_C \mathrm{d}\lambda \, \langle \Psi(\lambda) | \partial_\lambda | \Psi(\lambda) \rangle \in \mathbb{R}. \tag{2.18}$$

Whenever we talk about the Berry phase, we actually mean $e^{i\gamma}$, which is the physical relevant quantity since, unlike γ, it is invariant under gauge transformations, i.e., $|\Psi(\lambda)\rangle \to e^{i\Omega(\lambda)} |\Psi(\lambda)\rangle$. In free-fermion systems, the Berry phase is known as Zak phase [102]. There it was shown that if evaluated in the one-dimensional Brillouin zone, it is quantized due to symmetry properties of the Bloch functions. Later, Hatsugai [103] generalized this to the many-body context. Here, we will demonstrate its usefulness for a relative of the paramagnet and the cluster model.

[17] Here we assume that there is no other symmetry that might protect a non-trivial SPT.

[18] A change of parameters is adiabatically if the rate at which the parameter is changed is much slower than the characteristic frequency of a quantum system $\Delta E/\hbar$, where ΔE is the energy gap [101].

Quantum XY model. Upon a unitary transformation, given in App. B.5, Hamiltonian (2.4) map onto a dimerized quantum XY chain denoted by

$$\hat{H}_{\mathrm{XY}}(\lambda) = \sum_{n=1}^{L-1} f_n(\lambda) \left(\hat{S}_n^+ \hat{S}_{n+1}^- + \hat{S}_n^- \hat{S}_{n+1}^+ \right) + (1+\lambda) \left(\hat{S}_L^+ \hat{S}_1^- + \hat{S}_L^- \hat{S}_1^+ \right), \tag{2.19}$$

where we introduced $f_n(\lambda) = (1+(-1)^n\lambda)$ and consider PBC. For $-1 \leq \lambda < 0$ the trivial phase dominates, while for $0 < \lambda \leq 1$ the ground state is a non-trivial SPT[19]. In this representation, the global $U(1)$ symmetry is more apparent, namely, this Hamiltonian conserves the total magnetization. The remaining $\mathbb{Z}_2$ symmetry is generated by $\prod_n \hat{X}_n$. To probe the topology of the system, we have to introduce a symmetry twist, which inserts non-trivial flux into the ring on which the Hamiltonian is defined. The resulting Hamiltonian is given as follows:

$$\hat{H}_{\mathrm{XY}}(\lambda, \phi) = \sum_{n=1}^{L-1} f_n(\lambda) \left(\hat{S}_n^+ \hat{S}_{n+1}^- + \hat{S}_n^- \hat{S}_{n+1}^+ \right) + (1+\lambda) \left(e^{i\phi} \hat{S}_L^+ \hat{S}_1^- + e^{-i\phi} \hat{S}_L^- \hat{S}_1^+ \right), \tag{2.20}$$

where $\phi \in [0, 2\pi)$. The total flux is, according to Peierls substitution [104], given by the sum of all phases, which here is ϕ. The corresponding Zak (Berry) phase reads:

$$\gamma(\lambda) = i \int_0^{2\pi} \mathrm{d}\phi \, \langle \Psi(\lambda, \phi) | \partial_\phi | \Psi(\lambda, \phi) \rangle \, . \tag{2.21}$$

In the presence of the $\mathbb{Z}_2$ symmetry this phase is quantized, i.e., $e^{i\gamma(\lambda)} = \pm 1$—independent of λ. To see this, note that under the action of this symmetry the twisted Hamiltonian change as:

$$\prod_n \hat{X}_n : \ \hat{H}_{\mathrm{XY}}(\phi) \to \hat{H}_{XY}(-\phi) \Rightarrow \prod_n \hat{X}_n : \ |\Psi(\phi)\rangle \to e^{i\Omega(\phi)} \, |\Psi(-\phi)\rangle \, , \tag{2.22}$$

which implies that $\gamma = -\gamma + 2\pi\mathbb{Z}$. In the topological phase $\gamma = \pi \bmod 2\pi$, while in the trivial phase $\gamma = 0 \bmod 2\pi$, which gives another $\mathbb{Z}_2$ label.

Gauge transformations. There is a subtlety with this phase, namely, only its difference is well-defined. To illustrate this, note that there are many possibilities to introduce the flux ϕ into the ring on which the model is defined. To this end, let us consider the following gauge transformation:

$$\hat{V}(\phi) = \exp \left[i \frac{\phi}{L} \sum_n n \left(\hat{Z}_n - \frac{1}{2} \right) \right] . \tag{2.23}$$

If we apply this transformation on the Hamiltonian $\hat{H}_{\mathrm{XY}}(\lambda, \phi)$, then the resulting model is given by,

$$\hat{V}^\dagger(\phi) \hat{H}_{\mathrm{XY}}(\lambda, \phi) \hat{V}(\phi) = \sum_{n=1}^{L} f_n(\lambda) \left(e^{i\frac{\phi}{L}} \hat{S}_n^+ \hat{S}_{n+1}^- + e^{-i\frac{\phi}{L}} \hat{S}_n^- \hat{S}_{n+1}^+ \right) . \tag{2.24}$$

[19] For $\lambda = 0$ the model has quantum critical point, see App. B.5.

Under this transformation the Zak (Berry) phase, obtained from the new Hamiltonian, is non-trivially shifted

$$\gamma(\lambda) \to \gamma(\lambda) + \sum_n \frac{n}{L} \int_0^{2\pi} \mathrm{d}\phi \, \langle \Psi(\lambda,\phi)| \left(\hat{Z}_n - \frac{1}{2} \right) |\Psi(\lambda,\phi)\rangle \,. \tag{2.25}$$

In the presence of the $\mathbb{Z}_2$ symmetry this shift is quantized and independent of λ. In fact, we find:

$$\sum_n \frac{n}{L} \int_0^{2\pi} \mathrm{d}\phi \, \langle \Psi(\lambda,\phi)| \left(\hat{Z}_n - \frac{1}{2} \right) |\Psi(\lambda,\phi)\rangle = -\frac{\pi}{2} (L+1) \,. \tag{2.26}$$

Since L is even, which we here assume to be a multiple of four, we finally obtain that the Zak (Berry) phase is non-trivially shifted to $\gamma(\lambda) \to (\gamma(\lambda) - \pi/2) \mod 2\pi$ for all λ, but the difference, $\gamma(1) - \gamma(0) = \pi$, remains unchanged.

2.2.2 Two-dimensional bosonic SPTs

In the previous section, we showed that one-dimensional bosonic SPTs protected by on-site symmetries are completely classified in terms of the second cohomology group. For higher-dimensional SPTs a similar classification exists[20] and was systematically developed by Ref. [64]. In the case of two-dimensional interacting bosonic SPTs protected by an on-site symmetry G, the classification is given in terms of the third cohomology group $H^3(G, U(1))$ and its elements are called 3-cocycles $\omega(g,h,k)$ depending on three elements $g,h,k \in G$. A way to evaluate these 3-cocycles, knowing the low-energy representation, has been developed by Else and Nayak [85]. The quintessence of this approach is based on dimensional reduction. Thereby, the 3-cocycle is obtained from the low-energy representation of the symmetry on the edge of a finite subsystem of the boundary of the 2D SPT. In App. B.4 we review this approach in the context of gauge anomalies. Another way to detect the 3-cocycle has been introduced in Refs. [18, 107] using tensor network methods. In this section, however, we do not consider the general classification; instead, we will study a concrete example of a 2D SPT known as the CZX model [18] protected by $\mathbb{Z}_2$ symmetry.

CZX model

In the consideration of this model, we follow closely the discussion of Ref. [39]. The CZX model is defined on a square lattice with a four-site unit cell. Each site is made of a spin-1/2 degree of freedom. The Hamiltonian for this model is a sum of commuting terms,

$$\begin{aligned} \hat{H}_{\mathrm{CZX}} &= \sum_p \hat{H}_p \otimes \left(\hat{P}_l^r \otimes P_p^u \otimes \hat{P}_p^l \otimes \hat{P}_p^d \right) \\ \hat{H}_p &= -\left(|\uparrow\uparrow\uparrow\uparrow\rangle \langle\downarrow\downarrow\downarrow\downarrow| + |\uparrow\uparrow\uparrow\uparrow\rangle \langle\downarrow\downarrow\downarrow\downarrow| \right)_p , \quad \hat{P}_p^\alpha = \left(|\uparrow\uparrow\rangle \langle\uparrow\uparrow| + |\downarrow\downarrow\rangle \langle\downarrow\downarrow| \right)_p^\alpha , \end{aligned} \tag{2.27}$$

[20] However, for higher-dimensional SPTs there are cases beyond the group cohomology classification [105, 106].

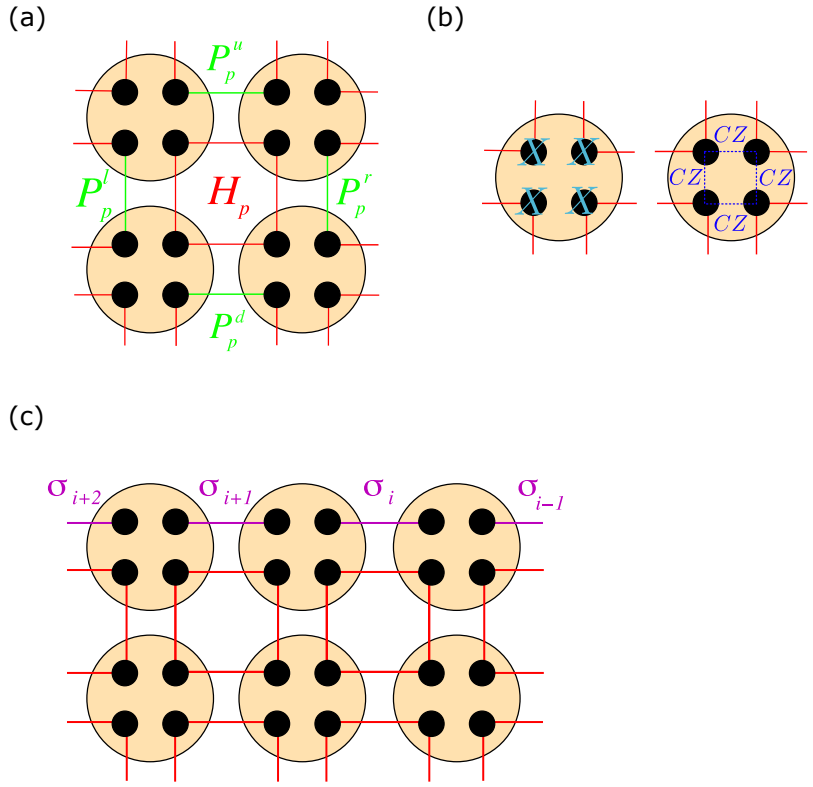

Figure 2.3: **CZX model.** Panel (a) illustrates the action of the Hamiltonian on a single plaquette. Each plaquette is surrounded by four projection operators (green links) to ensure that the Hamiltonian is symmetric. Fig. (b) displays the action of the global $\mathbb{Z}_2$ symmetry on a given site, which consists of an on-site part $\sim \hat{X}_s$ and a two-site operation $\sim \hat{U}_{\mathrm{CZ}}$. In panel (c) a possible boundary of the CZX model is shown, where effective degrees of freedom are labeled by $\{\sigma_i\}$. The figure is adapted from Refs. [18, 39].

whose action is illustrated in Fig. 2.3. The $\mathbb{Z}_2$ symmetry of this model consists of an on-site term that acts on each individual spin separately and a two-body term. The symmetry operator inside each unit cell (uc) is defined as follows [18]:

$$\begin{aligned}\hat{U}_{\mathrm{CZX,uc}} &= \left(\prod_{s=1}^{4}\hat{X}_s\prod_{s=1}^{3}\hat{U}_{\mathrm{CZ},ss+1}\right)_{\mathrm{uc}}\\ \hat{U}_{\mathrm{CZ},ss+1} &= \left(|\uparrow\uparrow\rangle\langle\uparrow\uparrow| + |\uparrow\downarrow\rangle\langle\uparrow\downarrow| + |\downarrow\uparrow\rangle\langle\downarrow\uparrow| - |\downarrow\downarrow\rangle\langle\downarrow\downarrow|\right)_{ss+1}\end{aligned} \tag{2.28}$$

Individual components of $\hat{U}_{\mathrm{CZX,uc}}$ commute and square to identity. Finally, the global symmetry is then defined as a product over all unit cells,

$$\hat{U}_{\mathrm{CZX}} = \prod_{\mathrm{uc}} \hat{U}_{\mathrm{CZX,uc}}, \quad \hat{U}^2_{\mathrm{CZX}} = \mathbb{1}. \tag{2.29}$$

The first term of the symmetry operator $\sim \prod_x \hat{X}_s$ flips all spins simultaneously and, thus, commutes with the Hamiltonian. For the second transformation, the situation is a bit more complicated. If there was no the minus sign in the last term of $\hat{U}_{\mathrm{CZ},ss+1}$, then this transformation would commute with the plaquette term. But since this not the case, we have to introduce additional projectors $\hat{P}^{\alpha}_p$, surrounding the plaquette, to ensure that the symmetry commutes with the Hamiltonian. The projectors make sure that neighboring spins are equal and, thus, there are always at least two terms that come with a minus sign canceling each other (see also Fig. 2.4).

Closed manifold. On a closed manifold, the number of constraints is equal to the number of unit cells. Since plaquette terms act on four spins simultaneously, all degrees of freedom are fixed by the condition that:

$$\hat{H}_p \otimes \left(\hat{P}^r_l \otimes P^u_p \otimes \hat{P}^l_p \otimes \hat{P}^d_p\right) |\Psi_{CZX}\rangle = -|\Psi_{CZX}\rangle \tag{2.30}$$

The unique ground state is given by,

$$|\Psi_{\mathrm{CZX}}\rangle = \prod_p \frac{1}{\sqrt{2}} \left(|\uparrow\uparrow\uparrow\uparrow\rangle + |\downarrow\downarrow\downarrow\downarrow\rangle\right)_p . \tag{2.31}$$

Since the ground state is unique, it must be symmetric. Clearly, if we flip all spins

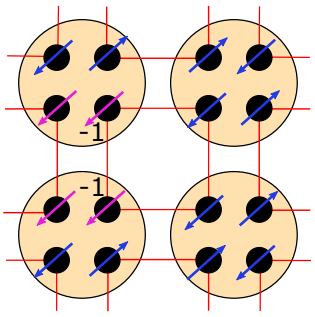

Figure 2.4: **Symmetry action.** The action of the $\mathbb{Z}_2$ symmetry on a particular configuration. Since the signs of two neighboring plaquettes cancel each other, the ground state is left invariant. Similarly, this holds for the Hamiltonian of the 2D CZX model.

simultaneously of this state, then it is left invariant. For the other term to leave the

state invariant, we use the same argument as above. Whenever there is a minus sign, it always comes twice, see Fig. 2.4, which thus leaves the state invariant. The first excited state is obtained if one of the constraints in Eq. (2.30) is violated. Hence, on a closed manifold, there is a unique, gapped and symmetric ground state.

Open boundary conditions. If we consider the same model on a manifold with edges, then the boundary is either gapless or SSB. To see this, let us consider the configuration shown in Fig. 2.3c. The spins at the boundary (marked in purple) are not contained in any plaquette, but their configuration is not arbitrary due to the action of the projectors. For minimizing the energy, two neighboring spin-1/2 degrees of freedom either point up $|\uparrow\uparrow\rangle$ or down $|\downarrow\downarrow\rangle$. Thus, in the ground state subspace two spin-1/2 degrees of freedom give rise to an effective spin-1/2 degree of freedom, denoted by $\{\sigma_i\}$ in this figure. Consequently, the edge of the CZX model can be considered as an effective one-dimensional chain of spin-1/2 degrees of freedom. To proceed, we need to find the effective symmetry action for the composite spins, which is given by,

$$\hat{U}_{\text{eff}} = \prod_i \hat{x}_i \prod_i \hat{u}_{\text{CZ},ii+1}, \quad \hat{U}_{\text{eff}}^2 = \mathbb{1}, \tag{2.32}$$

where we used different symbols to emphasize that these operators act on effective degrees of freedom. In the following we consider the edge as an effective one-dimensional system and argue that there exists no gapped, symmetric ground state $\Rightarrow$ it must be either gapless or SSB. Before we move on, let us shortly evaluate the following expression:

$$\left(\hat{u}_{\text{CZ},i-1i}\right)\left(\hat{u}_{\text{CZ},ii+1}\right)\hat{x}_i\left(\hat{u}_{\text{CZ},i-1i}\right)\left(\hat{u}_{\text{CZ},ii+1}\right) = \hat{z}_{i-1}\hat{x}_i\hat{z}_{i+1}. \tag{2.33}$$

Thus, the two-site unitary transformation acts, up to a sign, exactly the same way as the unitary circuit defined in Eq. (2.5)—mapping the paramagnet to the cluster model. Hence, a possible Hamiltonian defined on the boundary degrees of freedom can be written as:

$$\hat{H}_{\text{edge}} = -\sum_i \left(\hat{x}_i + \hat{z}_{i-1}\hat{x}_i\hat{z}_{i+1}\right). \tag{2.34}$$

However, as previously mentioned, this one-dimensional model is gapless if both Hamiltonians have the same weight[21] (see also Sec. 6.1.3). Another Hamiltonian that is compatible with $\hat{U}_{\text{eff}}$ is given by the Ising model,

$$\hat{H}_{\text{edge}} = -\sum_i \hat{z}_i\hat{z}_{i+1}, \tag{2.35}$$

which, however, has SSB with respect to $\hat{U}_{\text{eff}}$. Indeed, Chen and others [18, 108] have shown that for a symmetry that corresponds to a non-trivial 3-cocycle there cannot be a gapped, symmetric ground state in one dimension—implying SSB or gaplessness. In App. B.4 we explicitly evaluate the 3-cocycle of this symmetry using the approach of Else and Nayak [85], and demonstrate that it is indeed non-trivial. In fact, for this symmetry group there are only two different SPTs, i.e., $H^3(\mathbb{Z}_2, U(1)) = \mathbb{Z}_2$ [18].

[21] The relative sign among the two terms in the Hamiltonian is not relevant.

2.2.3 Higher-order bosonic SPT phases

In the language of higher-order topological phases, which we will introduce soon, all examples considered so far have been first-order SPTs, that is, the anomaly of the d-dimensional SPT occurred on the $(d-1)$-dimensional boundary. However, recent studies have refined the classification of SPT phases to also include crystalline symmetries, leading to anomalies on the $(d-k)$-dimensional submanifold, thus the naming of a k-th order SPT. For example, instead of having gapless modes on the one-dimensional boundary of a 2D SPT, there can be symmetry-protected gapless corners modes or hinge states in the three-dimensional case. In one dimension, there is only one order of SPTs, while in two dimensions, there is a first-order and a second-order SPT. The latter is characterized by anomalies at the corners, which can be gapless modes and/or fractional charges (e.g., see Chap. 3).

Higher-order topological phases of matter have been extensively explored in non-interacting fermionic systems, referred to as higher order topological insulators (HOTI) [21–24, 109–111] or fragile phases [112–114], and their classification is well-understood, which, however, is based on momentum state representation, where non-interacting fermions are exactly solvable. In the interacting setup, those phases are known as higher-order symmetry-protected topological (HOSPT) phases [19, 20, 25, 26, 65, 115–117]. Similar to conventional SPTs (first-order SPTs), interacting bosonic HOSPT phases are partially classified in terms of group cohomology, based on the interplay of global and crystalline symmetries [26, 65]. Let us emphasize that for further discussions we focus solely on second-order SPTs in two dimensions, where the global symmetry group of interest is given by a direct product $G = G_0 \times G_c$. Thereby, G_0 is an on-site symmetry and G_c the spatial symmetry such as C_n rotations.

In the following section we first consider a concrete example of a bosonic HOSPT phase, the so-called 2D dimerized quantum XY model, first introduced by Ref. [25] in this context. Thereby, following this reference, we show that it has typical signatures of ordinary SPTs, but the anomalies are at the corners and require spatial symmetry to be robust. Finally, we give a brief introduction to the classification of these phases.

2D dimerized quantum XY-model

The higher-order topological nature of the 2D dimerized quantum XY model was first discussed by Ref. [25]. This model is defined on a square lattice, where, similar to the CZX model, each unit cell consists of four spin-1/2 degrees of freedom and individual terms of the Hamiltonian act on plaquettes, as shown in Fig. 2.5. Thus, the Hamiltonian is given by,

$$\hat{H}_{\mathrm{XY}} = \sum_p \hat{H}_p, \quad \hat{H}_p = \sum_{s=1}^{4} \left(\hat{X}_{p,s}\hat{X}_{p,s+1} + \hat{Y}_{p,s}\hat{Y}_{p,s+1} \right). \tag{2.36}$$

This model is symmetric with respect to a global $\mathbb{Z}_2 \times \mathbb{Z}_2$ symmetry generated by,

$$\mathbb{Z}_2 \times \mathbb{Z}_2 : \quad \prod_s \hat{X}_s, \quad \prod_s \hat{Z}_s, \tag{2.37}$$

where the product is over all sites of the lattice. In addition, the Hamiltonian preserves a global C_4 symmetry around the center of the lattice (see Fig. 2.5).

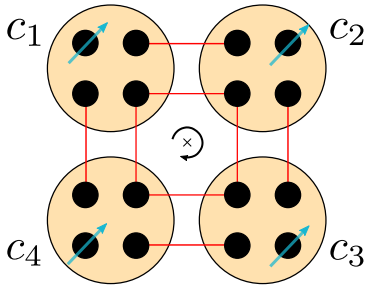

Figure 2.5: **2D dimerized quantum XY-model.** Hamiltonian (2.36) defined on a square lattice with open boundary conditions. The C_4 symmetry center (cross) is defined with respect to the center of the model, and C_4 rotations are clockwise. The corners, labeled by $\{c_i\}$, are completely decoupled; thus spins can be freely chosen, which, however, in the presence of C_4 symmetry have to be in a spatially symmetric configuration.

Closed Manifold. On a closed manifold, the ground state is unique: each spin is part of a plaquette, i.e., there are as many constraints as sites. The ground state is given by [25],

$$|\Psi_{\mathrm{XY}}\rangle = \prod_p \left[\frac{1}{2\sqrt{2}}\left(|\uparrow\uparrow\downarrow\downarrow\rangle + |\downarrow\downarrow\uparrow\uparrow\rangle + |\uparrow\downarrow\downarrow\uparrow\rangle + |\downarrow\uparrow\uparrow\downarrow\rangle\right) - \frac{1}{2}\left(|\uparrow\downarrow\uparrow\downarrow\rangle + |\downarrow\uparrow\downarrow\uparrow\rangle\right)\right]_p . \quad (2.38)$$

This state is clearly invariant if we flip all spins simultaneously, which is the case for the $\mathbb{Z}_2$ symmetry generated by $\prod_s \hat{X}_s$. On the other hand, since down spins always appear twice, the ground state is also invariant under $\prod_s \hat{Z}_s$ and, consequently, $\mathbb{Z}_2 \times \mathbb{Z}_2$ symmetric. The spatial symmetry maps different plaquettes to each other, and given that all plaquettes look the same, the state is left invariant under such transformation. For the plaquettes containing the symmetry center, we recognize that the Hamiltonian here is equivalent to a one-dimensional XY model with PBC and, thus, translation symmetric. Indeed, for these plaquettes C_4 acts as a single-site translation. The first excited state is obtained if a single plaquette is not in its ground state. The energy gap evaluated by Ref. [25] is given by $\Delta_p = 4(\sqrt{2}-1)$. Hence, as expected, the ground state considered on a closed manifold is unique, gapped, and symmetric.

Open boundary conditions. If the system is considered with edges and corners, then on the boundary the two spins, as shown in Fig. 2.5, form a singlet state, which is the

ground state to a perfectly dimerized one-dimensional quantum XY model,

$$\hat{H}_{\mathrm{XY}}^{\mathrm{boundary}} = \sum_b \hat{H}_{\mathrm{XY}}^b, \quad \hat{H}_{\mathrm{XY}}^b = \sum_{s=1}^{2} \left(\hat{X}_{b,s}\hat{X}_{b,s+1} + \hat{Y}_{b,s}\hat{Y}_{b,s+1} \right), \tag{2.39}$$

where $|\Psi_{\mathrm{XY}}^b\rangle = \sqrt{2}^{-1} \left(|\uparrow\downarrow\rangle - |\downarrow\uparrow\rangle\right)_b$. Thus, in contrast to first-order SPTs, edges of second-order SPTs are gapped and symmetric. The corners of this model are completely decoupled and can be chosen at will. However, for a C_4 symmetric configuration, all spins at the corners must be in the same state; either point up (as shown in Fig. 2.5) or point down. Since we can change between both configurations without any energy cost, there are zero-energy modes at the corners.

Projective transformations. Similar to the one-dimensional cluster model, the ground state on a geometry with edges and corners is not symmetric. Indeed, we find:

$$\prod_s \hat{X}_s \left|\Psi_{\mathrm{XY}}^{\mathrm{OBC}}\right\rangle = \hat{X}_{c_1}\hat{X}_{c_2}\hat{X}_{c_3}\hat{X}_{c_4} \left|\Psi_{\mathrm{XY}}^{\mathrm{OBC}}\right\rangle, \quad \prod_s \hat{Z}_s \left|\Psi_{\mathrm{XY}}^{\mathrm{OBC}}\right\rangle = \hat{Z}_{c_1}\hat{Z}_{c_2}\hat{Z}_{c_3}\hat{Z}_{c_4} \left|\Psi_{\mathrm{XY}}^{\mathrm{OBC}}\right\rangle. \tag{2.40}$$

Hence, analogously to the one-dimensional case, symmetry fractionalize and acts only non-trivially near the corners of the systems. While globally symmetry commutes, that is not the case at a single corner; instead, we find:

$$\hat{X}_{c_i}\hat{Z}_{c_i}\hat{X}_{c_i}\hat{Z}_{c_i} = -\mathbb{1}. \tag{2.41}$$

This leads to a two-fold degeneracy at the corner of the system and a sixteen-fold degeneracy in total, which is reduced to a two-fold degeneracy if we require C_4 symmetry. As we will discuss in Chap. 4, projective representations at the corners cause non-trivial, symmetry-protected degeneracies of the entanglement spectrum of the reduced density matrix of a single corner.

Zero-energy modes/stability of the phase. Since the corners are completely decoupled, we can choose the corner spins at will, as long as the final configuration is compatible with the spatial symmetry. In the following we will argue that C_4 symmetry is essential to the keep phase, and—in particular—the corner modes robust. The authors of Ref. [20] argued that corner modes require C_4 symmetry because otherwise we can attach one-dimensional systems along the boundaries to gap out the corners. For the current model, we could for example add another one-dimensional dimerized quantum XY model along a single edge, and then couple boundary spins[22]. However, in the presence of C_4 symmetry we need to add one-dimensional chains along each boundary and, consequently, there are three spin-1/2 degrees of freedom meeting at each corner, which thus remain half-integer.

There is also another argument, which does not require adding degrees of freedom to the boundary. So far, we argued that two phases remain separate if there is no gapped, symmetric path of local Hamiltonians. In this definition, we require the bulk gap to stay finite along the transformation. Here we will show that HOSPTs without spatial protection can be trivialized by a gap closing along the one-dimensional edge of the system. Such a procedure is shown in Fig 2.6, where we transformed the state, upon an edge gap

[22] Recall that the one-dimensional XY model has a $\mathbb{Z}_2$ classification and, thus, a stack of two of them can be trivialized.

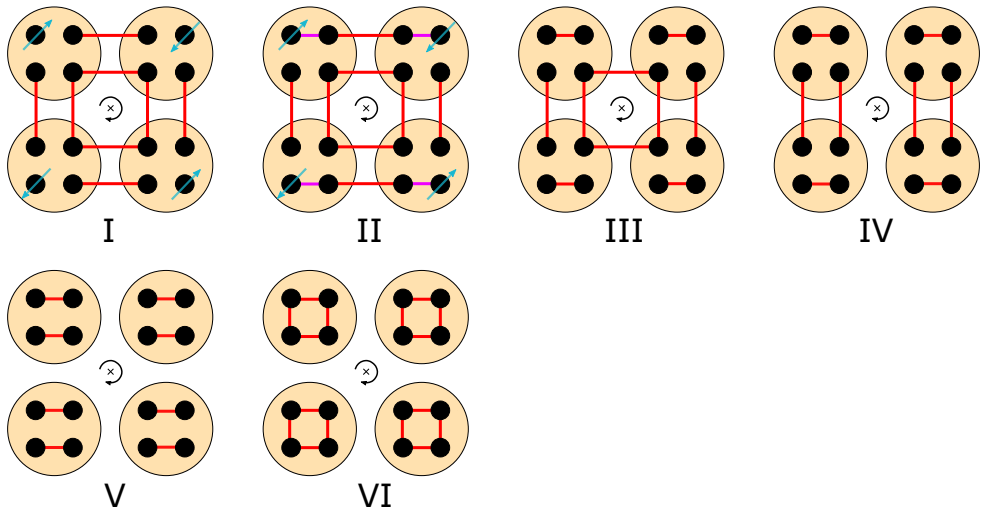

Figure 2.6: **Trivialization of the 2D XY model.** Panels I-VI show a trivialization process of the 2D XY model into a product state. Such process exists if we allow for a gap closing along the edge, which happens in step II. The bulk gap stays finite along the transformation.

closing, into a trivial product state. An essential point for this procedure to work is that in the *absence* of C_4 symmetry we can deform the central plaquette, as shown in the figure. The ground state inside the unit cell is identical to Eq. (2.38). If we, on the other hand, enforce C_4 symmetry, then the hole boundary must be gapless, but since two edges share a single corner (see also Ref. [22]), the corner mode cannot be removed regardless of how we couple sites along the boundary, while respecting symmetry. Moreover, C_4 symmetry also forbids any deformation of the central plaquette. Thus, if we in addition preserve C_4 rotations, the two phases remain separate. In Chap. 3 we consider this in more detail for a related model, which in a specific limit is identical to the 2D dimerized quantum XY model discussed here.

Thus, unlike first-order SPTs, higher-order SPTs require in addition spatial symmetries to be well-defined, although there are exceptions, namely, if there are subsystem symmetries, that are, symmetries that are conserved along one-dimensional subsystems [118]. For example, such symmetry could be particle number conservation along each row and column of the system.

Group cohomology classification of bosonic HOSPTs and beyond

As briefly mentioned in the introduction, strongly-interacting bosonic HOSPTs protected by a symmetry group $G = G_c \times G_0$ are classified in terms of cohomology groups. Here, we exclusively focus on two-dimensional second-order SPTs, where spatial symmetry is given by $G_c = C_n$ rotations. Then, according to Ref. [26] the classification of these

phases is in terms of the first cohomology group $H^1(\mathbb{Z}_n, H^2(G_0, U(1))$[23] with coefficients taken from the second cohomology group of the on-site symmetry. For the example above, the global symmetry is $G = C_4 \times \mathbb{Z}_2 \times \mathbb{Z}_2$, which results in $H^1(\mathbb{Z}_4, \mathbb{Z}_2) = \mathbb{Z}_2$ [26], where we used that $H^2(\mathbb{Z}_2 \times \mathbb{Z}_2, U(1)) = \mathbb{Z}_2$. Thus, there are two distinct HOSPTs associated to this symmetry. Hence, according to our definition of SPTs, there are two different quantized invariants $\{-1, 1\}$ distinguishing these two phases. In general, the classification with $H^2(G, U(1)) = \mathbb{Z}_m$ is given by [26]

$$H^1(\mathbb{Z}_n, \mathbb{Z}_m) = \mathbb{Z}_{\gcd(n,m)}, \quad n, m \in \mathbb{N}. \tag{2.42}$$

Physically, the classification is understood using the domain wall picture [26]: To this

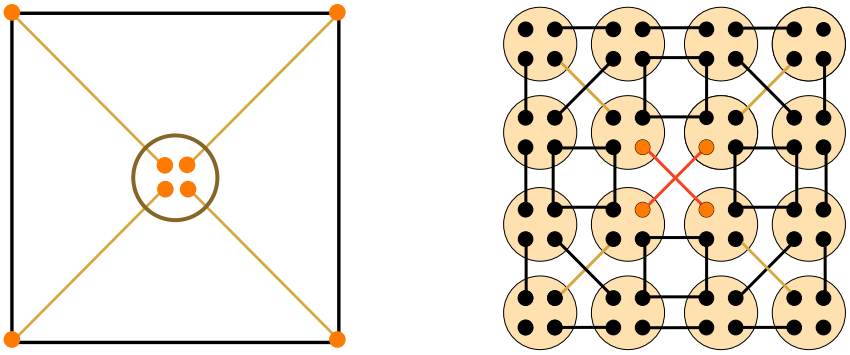

Figure 2.7: **Construction of HOSPTs.** The classification of HOSPTs can be understood in terms of the domain wall picture. Left: Each C_n domain wall (beige line) is decorated with a one-dimensional SPT such that in the center projective representations combine to a linear representation, which guarantees a gapped, symmetric bulk. At the corners, there remain projective representations. Right: The 2D XY model can be adiabatically transformed into the shape shown here. Along the diagonals (beige and red) there are one-dimensional topological XY chains that are symmetrically coupled in the center of the chain.

end, we imagine that each C_n domain wall is decorated with a one-dimensional SPT, whose topological index is an element of $H^2(G, U(1))$. However, the SPTs cannot be chosen at will. There is a compatibility condition, namely, the projective representations in the center of the chain have to become a linear representation such that the bulk is gapped and symmetric. What remains is a projective representation at the corners. This is schematically shown in Fig. 2.7. In the same figure, we show how this construction is realized in a concrete lattice model, the 2D dimerized quantum XY model. Upon an

[23] In the classification, spatial C_n rotations become an internal $\mathbb{Z}_n$ symmetry [65].

adiabatic transformation, the diagonals carry two topologically non-trivial 1D dimerized quantum XY models, which are symmetrically coupled in the center to ensure a symmetric, gapped bulk.

HOSPTs falling into this category of classifications have zero-energy excitations, which are exponentially localized near the corners. The reasoning is similar to the one-dimensional case discussed above. In addition, the projective representation at the corners will cause a non-trivial degeneracy in the entanglement spectrum of these phases, which we discuss in more detail in Chap. 4.

HOSPTs beyond this classification. In the next three chapters we will demonstrate that there are HOSPT phases beyond this classification, which, however, do *not* have protected zero-energy modes. Nevertheless, these phases show non-trivial topological signatures, such as fractional charges at the corners. For these cases, we consider only a global $G_0 = U(1)$ symmetry, which cannot protect one-dimensional SPTs, i.e., $H^2(U(1), U(1)) = \mathbb{Z}_1$ [64]. According to the classification of Ref. [26], we obtain: $H^1(\mathbb{Z}_n, \mathbb{Z}_1) = \mathbb{Z}_1$ and, thus, do not expect non-trivial HOSPTs, which, however, is not the case. In this sense, the classification given by Ref. [26] characterizes strong HOSPTs—having zero-energy excitations exponentially localized near the corners.

2.2.4 Symmetry extension and trivialization of SPT phases

Symmetry-protected topological phases are only different in the presence of symmetries. If the protecting symmetry is explicitly broken, then formerly distinct states become equivalent. Consequently, such phases of matter can be transformed to a product state by symmetry breaking. Alternatively, SPTs can be trivialized using their stacking property. For instance, if a given class of SPTs has a $\mathbb{Z}_n$ classification, we need to form a tensor product of n copies (or stack with its inverse) such that we can trivialize the state by introducing symmetric couplings. However, there is a third option how SPTs can be trivialized, namely, by symmetry extension, which has been first discussed by Refs. [36–38] in the context of the Haldane phase, and then systematically analyzed by Ref. [39]. Symmetry extension means that instead of considering a symmetry group G, we focus on its extension $\tilde{G}$ such that $G = \tilde{G}/H$ is the quotient group of $\tilde{G}$ by a normal subgroup[24] H. A paradigmatic example of such case, which is also discussed in Chap. 7, is the Haldane phase, protected, among others, by spin-rotation symmetry $SO(3)$. This phase is often discussed in terms of spin chains, such as the bond-alternating antiferromagnetic spin-1/2 Heisenberg model. In fact, this particular model results as an effective low-energy description of fermions in terms of the Hubbard model[25]. In the fermionic Hilbert space, the actual symmetry is $SU(2)$ and not $SO(3)$. For $SU(2)$, however, it is known that it cannot protect one-dimensional SPTs [64]. Thus, the Haldane phase can be trivialized by fluctuating charges, which has been discussed in Refs. [36–38]. However, as shown by Ref. [39] it is actually not necessary that the extended symmetry group *cannot* protect non-trivial SPTs. The authors argued that in the extended symmetry group $\tilde{G}$ a non-trivial cocycle associated to a group G, with $G = \tilde{G}/H$, becomes a coboundary—meaning

[24] A normal subgroup is a group such that for any $\tilde{g} \in \tilde{G}$ and $h \in H$ the following holds: $(\tilde{g})^{-1} h \tilde{g} \in H$.
[25] See Refs. [35, 119] for a derivation of the low-energy description.

it can be transformed to identity upon a gauge transformation (cf. Eq. (2.14) for the one-dimensional case).

Although the Haldane phase is a paradigmatic example to study this phenomenon, we will not do this at this point because it investigated later in this thesis, Chap. 7, where we reconsider such trivialization process from a different perspective, namely, asking how immediate topological signatures disappear if we allow for fluctuating charges in the low-energy description. Thereby, we introduce a new kind of SPT phases, so-called quotient group symmetry-protected topological phases, that unlike conventional SPTs, do not require a bulk phase transition to be trivialized—yet topological signatures such as edge modes and degeneracies in the entanglement spectrum remain parametrically stable (for more details see Chap. 7).

In this section, we will reconsider the 2D CZX model, following closely Ref. [39], and show that for a different lattice termination, the boundary can get symmetric and gapped, but this has as a consequence that the $\mathbb{Z}_2$ symmetry near the boundary acts as a $\mathbb{Z}_4$ symmetry. In this way, we have trivialized the SPT by symmetry extensions.

CZX model with a symmetric boundary

If we consider a different boundary termination of the 2D CZX model such that boundary spins are fully contained in a plaquette, defined in Eq. (2.27) (see also Fig. 2.8), then the boundary is gapped and symmetric. To achieve this, we have to modify the lattice as follows: Previously, we argued that our building blocks are unit cells consisting of four sites. However, very often the concept of unit cells is associated with translation symmetry. The idea is to group sites such that the full lattice can be built from translating these building blocks. If we now terminate the system, then commonly it is terminated such that we do not divide unit cells, as it is the case in Fig. 2.3c. However, in principle there is no need to consider unit cells if translations symmetry is not relevant or not a symmetry at all. Since the only constraint is that the lattice is square, we can choose our individual building blocks to be single spin-1/2 degrees of freedom. With that choice, the boundary in Fig. 2.8 is well-defined. To this end, we can define bulk cells and edge cells, where the former contain four and the latter two spin-1/2 degrees of freedom, respectively. To be consistent with the former discussion, Sec. 2.2.2, we still use the wording of unit cells, but keep the discussion above in mind. Given this, we also have to slightly modify the Hamiltonian near the edge, namely, whenever we consider a boundary plaquette, then such plaquette is only surrounded by three projectors $\hat{P}_p^\alpha$ instead of four. Finally, the ground state of this Hamiltonian—including its boundary—is symmetric and gapped,

$$|\Psi_{\mathrm{CZX}}\rangle = \prod_p \frac{1}{\sqrt{2}} \left(|\uparrow\uparrow\uparrow\uparrow\rangle + |\downarrow\downarrow\downarrow\downarrow\rangle\right)_p . \tag{2.43}$$

Hence, by choosing a different boundary of the 2D CZX model, the anomaly at the one-dimensional edge of the system disappears—resulting in an overall trivial phase.

Symmetry action. So far, we have seen that with a different boundary termination, the edge is symmetric and gapped. However, this also changes the action of symmetry

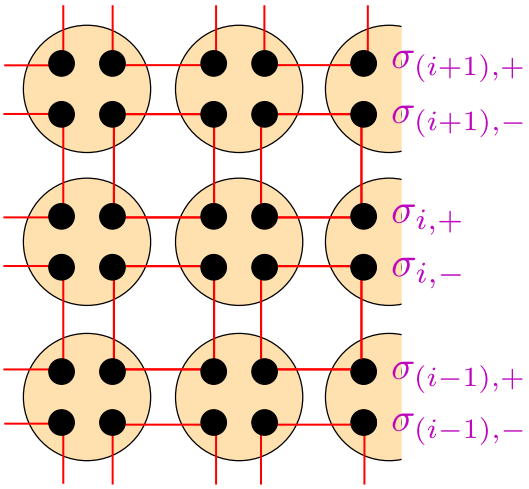

Figure 2.8: **CZX model with a symmetric boundary.** A possible boundary of the CZX model is shown. In contrast to Fig. 2.3c, the "unit cell" along the boundary consists of only two spins instead of four (for an explanation, see text). This way, the boundary spins are fully contained in a plaquette term of the Hamiltonian. Thus, unlike the case shown in Fig. 2.3c, this boundary is symmetric and gapped. However, as a consequence, symmetry acts in an extended way, i.e., it becomes a $\mathbb{Z}_4$ symmetry along the boundary. The spin-1/2 degrees of freedom inside a unit cell i have additional labels, where "+" denotes the upper and "−" the lower spin, respectively. The figure is adapted from Ref. [39].

along the boundary. To this end, let us consider the symmetry representation inside a half unit cell denoted by i, where the two spin degrees of freedom are labeled by "+" and "−", respectively (following the notation of Ref. [39]). Then, the symmetry is given as follows [39]:

$$\hat{U}_{CZX,i} = \hat{X}_{i,+}\hat{X}_{i,-}\hat{U}_{CZ,i+i-}. \tag{2.44}$$

If we evaluate the square of this operator, then it does not square to identity; instead, we obtain [39]:

$$\left(\hat{X}_{i,+}\hat{X}_{i,-}\hat{U}_{CZ,i+i-}\right)^2 = -\hat{Z}_{i,+}\hat{Z}_{i,-}, \tag{2.45}$$

i.e., the symmetry on the boundary does no longer act as $\mathbb{Z}_2$; instead, it becomes a $\mathbb{Z}_4$ symmetry. However, note that in the bulk, the symmetry still squares to identity. Nonetheless, choosing this termination of the lattice, the global symmetry is extended from $\mathbb{Z}_2 \to \mathbb{Z}_4$. Given that a non-trivial SPT does not admit a gapped, symmetric boundary, this state must be in a trivial phase and, consequently, the SPT is trivialized.

Symmetric, gapped ground state. In the previous analysis of the CZX model, Sec. 2.2.2, we argued that the effective representation of symmetry along the boundary, Eq. (2.32), is associated to a non-trivial 3-cocycle and, thus, forbids a gapped, symmetric ground

state. Here we will do the converse, namely, by showing that there exists a gapped, symmetric state, we prove that the 3-cocycle associated to this representation must be trivial[26]. Indeed, using that $\hat{U}_{\mathrm{CZ},i+i-} = (|\uparrow\uparrow\rangle\langle\uparrow\uparrow| + |\uparrow\downarrow\rangle\langle\uparrow\downarrow| + |\downarrow\uparrow\rangle\langle\downarrow\uparrow| - |\downarrow\downarrow\rangle\langle\downarrow\downarrow|)_{i+i-}$, it is easily shown that the following state:

$$|\Psi_{i+i-}\rangle = \frac{1}{\sqrt{2}}\left(|\uparrow\downarrow\rangle + |\downarrow\uparrow\rangle\right)_{i+,i-}, \tag{2.46}$$

is symmetric with respect to the symmetry defined in Eq. (2.44), A possible symmetric Hamiltonian to which this state is the unique ground state is given by,

$$\hat{H} = -\sum_i \left(\hat{X}_{i+}\hat{X}_{i-} + \hat{Y}_{i+}\hat{Y}_{i-} - \hat{Z}_{i+}\hat{Z}_{i-}\right), \quad |\Psi\rangle = \prod_i |\Psi_{i+i-}\rangle\,. \tag{2.47}$$

Hence, we constructed a Hamiltonian that is invariant under this symmetry, and its ground state is unique, gapped, and symmetric, which thus implies that the current representation of symmetry is associated to a trivial 3-cocycle of $\mathbb{Z}_4$. Thus, this is an example how a 3-cocycle of $\mathbb{Z}_2$ has been trivialized in the extended symmetry group[27].

2.3 Summary & Outlook

In summary, we reviewed two equivalent definitions when two quantum states, being the ground states of a local and gapped Hamiltonian, belong to the same phase. First, we argued this is the case if there exists a path of local and gapped Hamiltonians that connect these states. Second, a more practical definition was given in terms of local unitary circuits. While for the first formulation we required that the bulk gap must be system size independent, in the second version, this translates into a finite evolution time or depth, if the local unitary transformation is given by a quantum circuit. Moreover, only those quantum circuits were allowed that can be continuously transformed to identity, which was crucial in the presence of symmetry. Indeed, we argued that symmetries can lead to further restriction of paths/local unitary transformations and, thus, formerly equivalent states can become distinct. From these definitions, we argued that there are two fundamentally different quantum states. All states that can be connected to a product state via such local unitary circuit are short-ranged entangled states, and otherwise named long-ranged entangled states. Without symmetries, all SRE belong to the same phase. In contrast, LRE states do not require any symmetries to be topological non-trivial, but symmetries can also enrich these phases.

After a discussion of equivalent states of matter, we discussed a particular class of SRE states, so-called SPT phases that have a symmetric bulk and, consequently, cannot be detected using Landau's theory of symmetry breaking; however, if we consider such phases with boundaries, there can be zero-energy modes, SSB, or even topological order. While for first-order SPTs such anomalies occur on the $(d-1)$-dimensional boundary, for

[26] In the proofs of Refs. [18, 108] it was shown that for any gapped symmetric state, the 3-cocycle associated to the representation of symmetry must be trivial.

[27] Note this last discussion is not part of Ref. [39].

k-th order SPTs, also named higher-order SPTs, anomalies are on the $(d-k)$-dimensional boundary, which can be corners in 2D, or hinges in 3D.

To demonstrate the properties of SPT phases, we studied various examples of bosonic SPTs. We started from the one-dimensional cluster model, a bosonic SPT phase protected by $\mathbb{Z}_2 \times \mathbb{Z}_2$ symmetry. Thereby, we showed that for one-dimensional bosonic SPTs all characteristic properties such as edge modes or degeneracies in the entanglement spectrum follow from projective representations labeled by the second cohomology group $H^2(G, U(1))$.

Further, we argued that related groups also classify SPTs in higher dimensions: Indeed, many first-order, d-dimensional bosonic SPTs are classified by the $(d+1)$-th cohomology group $H^{d+1}(G, U(1))$, which for two dimensions result in the third cohomology group. This we explicitly demonstrated for an exactly solvable 2D SPT phase, the CZX model, an SPT protected by $\mathbb{Z}_2$ symmetry, whose boundary is either gapless or SSB because the low-energy representation of the symmetry at the boundary is associated to a non-trivial 3-cocycle. A similar classification exists for higher-order bosonic SPTs protected by a direct product of a spatial symmetry and an on-site symmetry. In contrast to conventional SPTs, these phases are classified by the first cohomology group, which in the case of C_n rotations is given by $H^1(\mathbb{Z}_n, H^2(G, U(1))$. The coefficients are taken from the second cohomology group of the on-site symmetry. The intuition is that one-dimensional SPTs are aligned on domains walls of the spatial symmetry such that in the bulk, projective representations trivialize each other. To demonstrate this explicitly, we studied the 2D dimerized quantum XY model on a square lattice, thereby exploring its non-trivial HOSPT phase. In particular, we showed that these phases are only robust in combination with spatial symmetries because otherwise they can be trivialized by aligning one-dimensional systems at the boundary or by an edge gap closing.

In the final part, we considered different possibilities to trivialize SPTs. Since SPTs are only different from product states in the presence of symmetries, one way to make them trivial is to break the protecting symmetry. Alternatively, we can use the stacking property of SPTs. However, there is another method of trivializing SPTs, namely, by symmetry extension. This we demonstrated along the previously introduced 2D CZX model. Here, we showed that the SPT can be trivialized by choosing a different boundary termination, which naturally leads to an extension from $\mathbb{Z}_2$ to $\mathbb{Z}_4$. Thereby, the non-trivial 3-cocycle of $\mathbb{Z}_2$ symmetry has been trivialized in $\mathbb{Z}_4$ (Note since we have already cited the corresponding references in individual sections, we did not do it here again.).

Outlook. In the following three chapters we focus on higher-order SPTs, which are not captured by the aforementioned classification of these phases; however, share many properties, in particular, the degeneracy of the entanglement spectrum and anomalies at the corners. In the second part of this thesis, we study how symmetry extension can change the low-energy properties of underlying systems. On one hand, we consider cases where the extended symmetry group itself protects non-trivial SPTs. Thereby, we study, among other things, how the process of symmetry extension change low-energy properties, in particular, at quantum criticality. On the other hand, we study the trivialization of the Haldane phase, and ask, how immediate topological signatures disappear.

Part I

Higher-order symmetry-protected topological phenomena

Chapter 3

The super-lattice Bose-Hubbard model—an experimentally accessible HOSPT phase

In this chapter, we investigate higher-order topology in a strongly-interacting system. We propose an experimentally accessible, two-dimensional ultracold atomic system, a super-lattice Bose-Hubbard model (SL-BHM), supporting an HOSPT phase protected by a combination of a $U(1)$ charge conservation and C_4 lattice symmetry. This model is the strongly-interacting counterpart of the non-interacting Benalcazar-Bernevig-Hughes model (BBH) [21]—a generalization of the one-dimensional Su-Schrieffer–Heeger (SSH) [28] model. The BBH model is a non-interacting higher-order topological insulator (HOTI) protected, among others, by C_4 and chiral symmetry—hosting gapless modes on its corners. However, unlike in one dimension, where there is an exact mapping between the SSH model and the 1D SL-BHM at infinitely strong on-site repulsion [33], the 2D SL-BHM and the BBH model are only related at two, very fine-tuned points. Thus, it is initially not clear to which extent the signatures of the non-interacting model survive in the presence of interactions. For instance, the integer classification of topological free-fermion systems reduce to a $\mathbb{Z}_8$ classification in the presence of interactions [69].

Another important aspect is the experimental verification of theoretical concepts. Thus, it is crucial for theorists to construct models and observables that can be measured in experiments. Unfortunately, the experimental realization of the BBH model is challenging, as it requires a non-trivial gauge flux per plaquette to guarantee a finite bulk gap. This is not the case for the 2D SL-BHM. Another advantage of the latter is that it directly allows studying the influence of interactions on higher-order topological phases. To this end, we construct a genuine topological invariant—a fractional corner charge—which is experimentally accessible. Moreover, we provide a full counting statistics (FCS) to which experimentalists, using ultracold atomic setups [30–32], can compare to.

This chapter is based on [P1] and structured as follows: In Sec. 3.1 we introduce the Hamiltonian and the relevant symmetries of the 2D SL-BHM. Thereby, we briefly discuss its limiting cases and its connection to the two-dimensional dimerized quantum XY model, introduced in Sec. 2.2.3, and the BBH model. Afterwards, in Sec. 3.2 we consider the phase diagram of the 2D SL-BHM obtained using the density matrix renormalization group (DMRG) and give a short summary of the main ideas of the algorithm. Then, in Sec. 3.3 we classify the two distinct topological phases of the 2D SL-BHM using a higher-order Zak (Berry) phase and a fractional corner charge and discuss their relation.

Finally, in Sec. 3.4 we show the FCS for both the 1D SL-BHM and the 2D SL-BHM, supporting our claim that the fractional corner charge is a genuine topological invariant. In addition, we argue that the parameters used in our considerations are experimentally accessible.

3.1 Introduction of the two-dimensional SL-BHM

As initially pointed out, the non-interacting BBH model has severe drawbacks. On one hand, it requires a gauge flux to have a gapped bulk and, second, it does not allow studying interactions and their consequences for higher-order topological phases. These problems can be solved if we instead consider the two-dimensional SL-BHM, a stronlgy-interacting model. To argue this, we first need to introduce the Hamiltonian and its symmetries. Moreover, we will briefly talk about its relation to other models realizing a higher-order topological phase.

3.1.1 The SL-BHM on a square lattice

We consider the following SL-BHM on a two-dimensional square lattice of size $L \times L$ with L even,

$$\begin{aligned}\hat{H} = &- \left[\sum_{x=1}^{L-1}\sum_{y=1}^{L}\left(t(x)\hat{a}^\dagger_{x,y}\hat{a}_{x+1,y} + \text{h.c.}\right) + x \leftrightarrow y\right] \\ &+ \frac{U}{2}\sum_{x,y=1}^{L}\hat{n}_{x,y}\left(\hat{n}_{x,y}-1\right) - \mu\sum_{x,y=1}^{L}\hat{n}_{x,y},\end{aligned} \tag{3.1}$$

where $\hat{a}^\dagger_{x,y}$ ($\hat{a}_{x,y}$) is the creation (annihilation) operator at site (x, y), and $\hat{n}_{x,y} = \hat{a}^\dagger_{x,y}\hat{a}_{x,y}$. The particles can tunnel between neighboring sites with modulated hopping amplitudes $t(\zeta)$, $\zeta \in \{x, y\}$,

$$t(\zeta) = \begin{cases} t, & \text{for } \zeta \in \{1, 3, ..., L-1\} \\ 1-t, & \text{for } \zeta \in \{2, 4, ..., L-2\} \end{cases} \tag{3.2}$$

where $t \in [0, 1]$, while the parameter $U \geq 0$ controls the on-site repulsion between the particles and μ is the chemical potential (see Fig. 3.1a). If the on-site interaction is infinitely strong, i.e., $U \to \infty$, then the Hamiltonian describes the physics of *hardcore bosons* characterized by $\hat{n}^2_{x,y} = \hat{n}_{x,y}$. Whenever we consider hardcore bosons, we denote local operators as follows: $\hat{a}_{x,y} \to \hat{b}_{x,y}$ and $\hat{a}^\dagger_{x,y} \to \hat{b}^\dagger_{x,y}$ with commutation relations:

$$\left\{\hat{b}^\dagger_{x,y}, \hat{b}_{x,y}\right\} = \mathbb{1}_{x,y}, \quad \left[\hat{b}^\dagger_{x,y}, \hat{b}_{x',y'}\right] = 0, \; x \neq x' \vee y \neq y'. \tag{3.3}$$

Thus, locally hardcore bosons fulfill fermionic commutation relations; however, globally bosonic commutation relations are preserved.

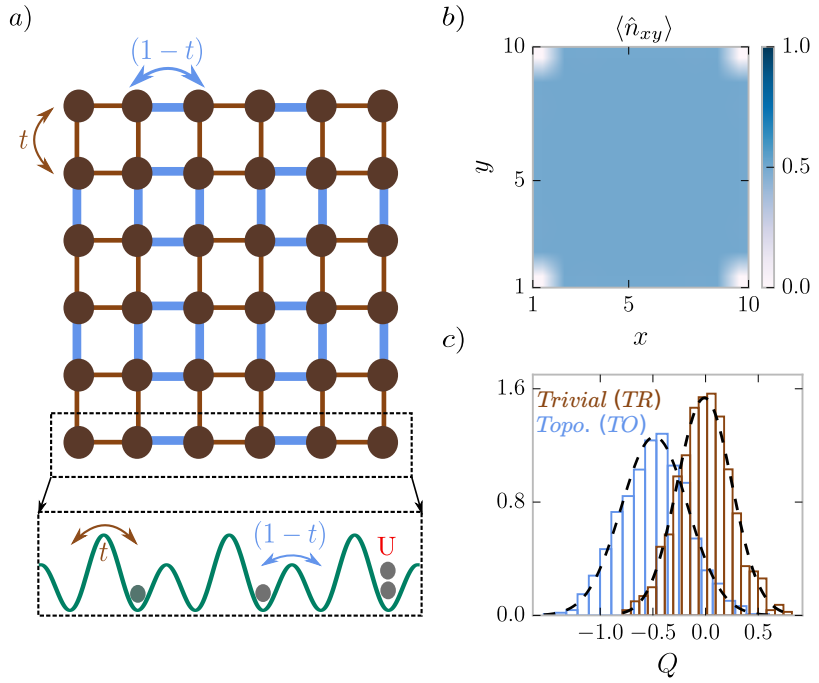

Figure 3.1: **2D SL-BHM showing an HOSPT phase with quantized fractional corner charges. a**) The SL-BHM has a 2×2 unit cell, with two different hopping amplitudes inside and between unit cells, t and $1-t$, respectively. The ground state is topological trivial (non-trivial) for $t = 1\,(t = 0)$. **b**) Average occupation number of lattice sites in the topological phase with particle number $N = L^2/2-2$, displaying four holes localized around the corners, giving rise to fractional charges $Q_{\text{corner}} = 1/2$. **c**) The full distribution function of corner charges for the trivial (topological) phase, peaked around a quantized fractional part $0\,(1/2)$. We used the parameters $N = L^2/2\,(L^2/2-2)$, $t = 0.9\,(0.1)$, $U = 32$ and $\xi_{\text{env}} = 3.2\,(3.08)$.

3.1.2 Symmetries of the SL-BHM

Hamiltonian (3.1) is C_4 symmetric with respect to the center of the lattice and preserves the total particle number $\hat{N} = \sum_{x,y} \hat{n}_{x,y}$, which gives rise to a global $U(1) \times C_4$ symmetry. In the case of hardcore bosons, $U \to \infty$, the system has two additional antiunitary $\mathbb{Z}_2^T$ symmetries denoted by $\hat{\mathcal{S}} = \prod_{x,y} \left(\hat{b}_{x,y} + \hat{b}_{x,y}^\dagger\right) K$ and $\hat{\mathcal{C}} = \prod_{x,y} \left(\hat{b}_{x,y}^\dagger - \hat{b}_{x,y}\right) K$, where K is the operator of complex conjugation. Under these transformations, local operators change as follows:

$$\hat{\mathcal{S}} : \hat{b}_{x,y}^\dagger \leftrightarrow \hat{b}_{x,y}, \quad \hat{\mathcal{C}} : \hat{b}_{x,y} \to -\hat{b}_{x,y}^\dagger, \quad \hat{\mathcal{C}} : \hat{b}_{x,y}^\dagger \to -\hat{b}_{x,y} \tag{3.4}$$

Note on-site $\hat{\mathcal{S}}$ squares to identity $\hat{\mathcal{S}}_{x,y}^2 = \mathbb{1}_{x,y}$, while $\hat{\mathcal{C}}$ squares to minus identity $\hat{\mathcal{C}}_{x,y}^2 = -\mathbb{1}_{x,y}$

3.1.3 Fixed-point phases and relation to others

Here we briefly discuss the exactly solvable cases of the 2D SL-BHM and consider its relation with other models discussed in literature. Thereby, we mainly focus on the sector at half-filling and set the chemical potential $\mu = 0$.

Fixed-point phases

To get a feeling for the two topological distinct phases of the 2D SL-BHM at half-filling, we briefly discuss the exactly solvable limits $t = 0$ and $t = 1$, respectively. In both cases, there is a finite bulk gap; for strong interactions $U \gg \max(t, 1-t)$, the bulk gap is of order $\Delta \sim \mathcal{O}(\max(t, 1-t))$.

In the *trivial phase* (TR) with $t = 1$, the ground state at half-filling is unique and C_4-symmetric (see Fig. 3.3a). In the *topological phase* (TO) with $t = 0$, the four corners are decoupled and each of them can be either filled or empty (see Fig. 3.3b). To obtain a C_4-symmetric ground state with bulk and edges at half-filling, the total particle number has to deviate from exact half-filling $N = N_0$, as $N = N_0 \pm 2$ with $N_0 = L^2/2$.

This filling anomaly[1], giving rise to quantized fractional corner charges (see Fig. 3.1), was already discussed in the context of non-interacting higher-order topological phases [27]. For hardcore bosons, the antiunitary symmetry $\hat{\mathcal{C}}$ protects in addition a two-fold degeneracy at each corner, which is a consequence of the property that $\hat{\mathcal{C}}^2_{x,y} = -\mathbb{1}_{x,y}$ on-site. This implies that corners can be occupied or empty, i.e., the particle sectors $N = N_0 \pm k$ with $k \in \{-2, ..., 2\}$ are degenerate. However, note that not all configurations are compatible with the spatial symmetry. Once U is lowered, this degeneracy is lifted, but the filling anomaly remains. Comparing the charge distributions of the two phases, we find a fractional charge $Q_{\text{corner}} = 1/2$ localized around the corners in the topological phase, Fig. 3.1, measured with respect to the average bulk filling n_0 (for a rigorous definition of Q_{corner} see Eq. (3.20) below).

Quantum XY model

The SL-BHM considered in the limit of hardcore bosons is equivalent[2] to the two-dimensional spin-1/2 quantum XY model, which was studied in Ref. [25] and reviewed in Sec. 2.2.3. The identification of operators read:

$$2\hat{S}^x_{x,y} = \hat{b}^\dagger_{x,y} + \hat{b}_{x,y}, \quad 2\hat{S}^y_{x,y} = i\left(\hat{b}^\dagger_{x,y} - \hat{b}_{x,y}\right) \quad 2\hat{S}^z_{x,y} = \mathbb{1}_{x,y} - 2\hat{n}_{x,y}. \tag{3.5}$$

The chemical potential introduced in Eq. (3.1) corresponds (up to a constant shift) to an external magnetic field in the XY model. In Ref. [25] it was argued that for $t \gg 1-t$ the ground state realizes a HOSPT phase protected by $\mathbb{Z}_2 \times \mathbb{Z}_2 \times C_4$ symmetry (see also Sec. 2.2.3). The protecting on-site symmetries are generated by $\prod_{x,y} e^{i\pi \hat{S}^x_{x,y}}$ and

[1] The filling anomaly is a consequence of open boundary conditions. For periodic boundary conditions, both phases have a unique, C_4-symmetric ground state at the same filling $n_0 = 1/2$.

[2] It is actually the same. The Hilbert space of hardcore bosons and spin-1/2 degrees of freedom is identical.

$\prod_{x,y} e^{i\pi \hat{S}^y_{x,y}}$. In the same reference, it was argued that these symmetries protect a tow-fold degeneracy at each corner, which is robust as long as in addition C_4 symmetry is preserved. Such a two-fold degeneracy is also protected by a combination of $\mathbb{Z}_2^T \times C_4$ which, in the case of spin-1/2 degrees of freedom, corresponds to time reversal symmetry $\hat{\mathcal{C}} \to \hat{\mathcal{T}} = \prod_{x,y} e^{i\pi \hat{S}^y_{x,y}} K$. As showed previously, on a single site, this symmetry squares to minus identity leading to a Kramers degeneracy—a twofold degeneracy of half-integer spin states. Note, the other representation of the antiunitary symmetry cannot protect a Kramers degeneracy.

Benalcazar-Bernevig-Hughes model

The BBH model is a free-fermion model, which is the two-dimensional generalization of the famous one-dimensional SSH model. The BBH model was first introduced in Ref. [21] and is one of the first examples of higher-order topological systems protected, among others, by a combination of chiral symmetry and C_4 rotations. Similar to the 2D SL-BHM, the BBH model is a collection of plaquette Hamiltonians defined as follows:

$$\begin{aligned} \hat{H}_{\mathrm{P}}^{\mathrm{F}} &= \sum_{j=1}^{3} \left(\hat{c}_j^\dagger \hat{c}_{j+1} + \mathrm{h.c.} \right) - \left(\hat{c}_4^\dagger \hat{c}_1 + \hat{c}_1^\dagger \hat{c}_4 \right) \\ \hat{H}_{\mathrm{P}}^{\mathrm{B}} &= \sum_{j=1}^{4} \left(\hat{b}_j^\dagger \hat{b}_{j+1} + \mathrm{h.c.} \right), \quad \hat{b}_5 \equiv \hat{b}_1, \end{aligned} \tag{3.6}$$

where we introduced the superscripts "F" for fermions and "B" for bosons, respectively. Graphically, the plaquette Hamiltonians are illustrated in Fig. 3.2. The edges can be written in a similar way. In the perfect dimerized limits, i.e., $t = 0$ or $t = 1$ and $U \to \infty$ (hardcore bosons) there is an exact mapping between the 2D SL-BHM and the BBH model. The mapping is given by the Jordan-Wigner transformation (JW) relating bosonic and fermionic operators in the following way:

$$\hat{b}_j^\dagger = e^{i\pi \sum_{i<j} \hat{n}_i} \hat{c}_j^\dagger, \quad \hat{b}_j = \hat{c}_j e^{-i\pi \sum_{i<j} \hat{n}_i}. \tag{3.7}$$

Inserting this transformation in $\hat{H}_{\mathrm{P}}^{\mathrm{B}}$ we arrive at $\hat{H}_{\mathrm{P}}^{\mathrm{F}}$ (here we explicitly used that the systems are at half-filling). We note that the plaquette Hamiltonian of the BBH model contains a π-flux per plaquette, since it can be written as

$$\hat{H}_P^F = \sum_{j=1}^{4} \left(e^{i\phi_j} \hat{c}_j^\dagger \hat{c}_{j+1} + \mathrm{h.c.} \right), \tag{3.8}$$

with $\phi_1 = \phi_2 = \phi_3 = 0$ and $\phi_4 = \pi$. According to Peierls substitution [104], the total magnetic flux per plaquette is the sum of all phase factors $\Phi = \sum_j \phi_j = \pi$. Indeed, for the two-dimensional SSH model to have a finite bulk gap, plaquettes must contain a π-flux [21, 120], which naturally arise if obtained from the bosonic model at half-filling.

The bosonic antiunitary symmetry $\hat{\mathcal{S}}_B = \prod_P \prod_j \left(\hat{b}_j^\dagger + \hat{b}_j \right) K$ (formerly called $\hat{\mathcal{S}}$) with plaquettes defined as shown in the trivial cases $t = 1$, Fig. 3.2, maps to the fermionic

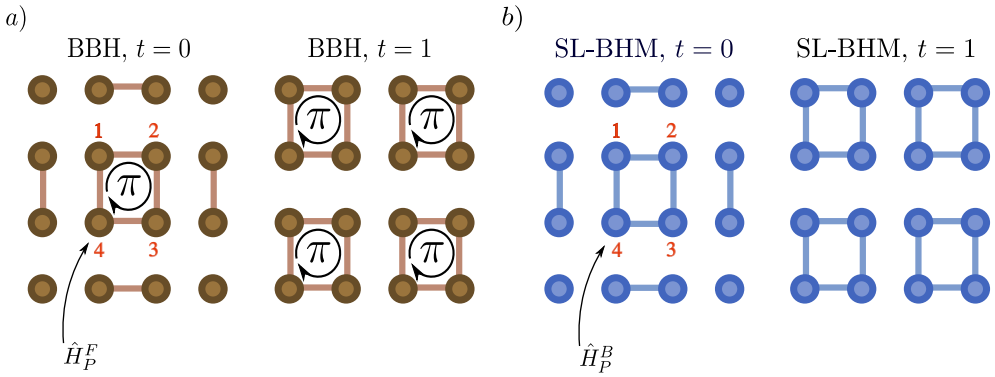

Figure 3.2: **2D lattice models. a)** 2D BBH model with a π-flux insertion per plaquette for $t = 0$ (topological) and $t = 1$ (trivial). **b)** 2D SL-BHM at infinite interaction strength $U \to \infty$ for $t = 0$ (topological) and $t = 1$ (trivial). For the limits $t = 0\,(t = 1)$, both models are in one-to-one correspondence. They can be mapped to each other using the Jordan-Wigner transformation applied to each plaquette and edge Hamiltonian individually.

chiral symmetry $\hat{\mathcal{S}}_F = \prod_P \prod_j \left(\hat{c}_j^\dagger + (-1)^j \hat{c}_j\right) K$, which together with C_4 symmetry protects the non-trivial topology of the BBH model [21]. It is important to note that the exact relationship only holds for the perfect dimerized limits at $U \to \infty$. There have been attempts to apply the JW transformation away from the dimerized limits (using hardcore bosons) [25], but after the transformation one obtains the BBH model in an external gauge field. To circumvent this problem, the authors used a mean-field treatment, which is, nevertheless, not an exact relation.

3.2 A numerical study: Robustness of gapped phases at half-filling

Before we discuss the numerical results obtained using DMRG, we briefly give an insight into the main idea of this algorithm.

DMRG in a nutshell

DMRG, which was first introduced by S. White [40, 41], has shown to be a powerful tool to study ground states of one-dimensional gapped and local Hamiltonians. The success of this algorithm is based on the fact that ground states of such systems fulfill an area law [97, 121], that is, the entanglement entropy of a subsystem grows with the size of the boundary, which in one dimension is a point and, thus, constant. Consequently, if a wave function is written in a Schmidt decomposition[3] only a few eigenvalues of the reduced

[3] A Schmidt decomposition of a state $|\Psi\rangle$ can be written as $|\Psi\rangle = \sum_\alpha \Lambda_\alpha |\alpha_A\rangle |\alpha_B\rangle$, where $\{\Lambda_\alpha\}$ are the Schmidt values and $\{|\alpha_{A(B)}\rangle\}$ the Schmidt states of the region $A(B)$.

density matrix contribute significantly to the entanglement [98, 122]. This is precisely the property on which the truncation scheme of DMRG is built on, namely, in the algorithm we keep only those states that contribute most to the weight of the spectrum of the reduced density matrix. As many other algorithms, the DMRG method is a variational Ansatz for finding the lowest energy eigenstate of a given Hamiltonian[4]. Commonly, this algorithm is formulated in terms of matrix product states (MPSs) [98, 122], a particular class of tensor network states [99, 123, 124], which have turned out to approximate true ground states of one-dimensional many-body systems extremely well. The reason is that those states inherently fulfill the area law (as we shall see soon). For a generic quantum system, the complexity grows exponentially with the number of degrees of freedom; however, the number of states contributing to ground states of one-dimensional local and gapped systems is very little [99, 124]. This is where MPSs become so powerful; the idea of MPSs is to approximate the coefficient of the wave functions by a matrix product $c_{\sigma_1,\ldots,\sigma_L} = \mathrm{tr}\,(A^{\sigma_1}\ldots A^{\sigma_L})$[5], with L sites and $A^{\sigma_i} \in \mathbb{C}^{\chi\times\chi}$, which reduces the number of parameters drastically, namely, this way the number of parameters grows only polynomially instead of exponentially as L is increased [99, 124]. The maximal entanglement captured by MPSs is $S \sim \log\chi$, which is indeed a constant for a given χ. Hence, MPSs inherently fulfill the area law. The bond dimension χ controls the quality of the approximation in DMRG calculations. For gapless systems, however, the entanglement entropy grows indefinitely and, thus, the MPS bond dimension.

DMRG in two dimensions. DMRG has been successfully generalized to two-dimensional systems [125], but it is much less powerful as the computational costs scale exponentially with the system width (along y)[6]. Nevertheless, DMRG is a good starting point, and it gives first insight into the nature of a two-dimensional system[7]—in particular—if Quantum Monte Carlo suffers from a sign problem [125]. For calculating bulk properties, the two-dimensional system is considered on a cylinder with infinite extension along x and finite circumference along y. Numerical results can then be extrapolated in bond dimension χ and circumference L_y. If correlations of a two-dimensional system are short-ranged and the correlation length is much less than the circumference of the cylinder, then this a faithful approximation.

Phase diagram

In the previous section, we argued that the 2D SL-BHM in the limit of $U \to \infty$ and strongly anisotropic hopping amplitudes realizes two distinct quantum phases. To study the robustness of the gapped phases, we mainly focus on a parameter regime $(t, U, \mu = 0)$ where the bulk is incompressible[8] and the average filling in the bulk is $n_0 = 1/2$. Thereby,

[4] One wishes to minimize the functional $E[\Psi] = \frac{\langle\Psi|\hat{H}|\Psi\rangle}{\langle\Psi|\Psi\rangle}$.

[5] Here we assumed the simplest case of a translation invariant MPS.

[6] All the information of neighboring stripes is contained in a single MPS bond. For two-dimensional systems, the area law predicts that the entropy scales with the length of the boundary $S \sim l$, which implies $\chi \sim e^l$.

[7] In 2011 Yan et al. [42] uncovered a gapped spin-liquid state of the antiferromagnetic spin-1/2 Heisenberg model on a kagome lattice using DMRG in two dimensions.

[8] This means that the density is insensitive to small changes of the chemical potential $\kappa = \frac{\partial n}{\partial \mu} = 0$ [30].

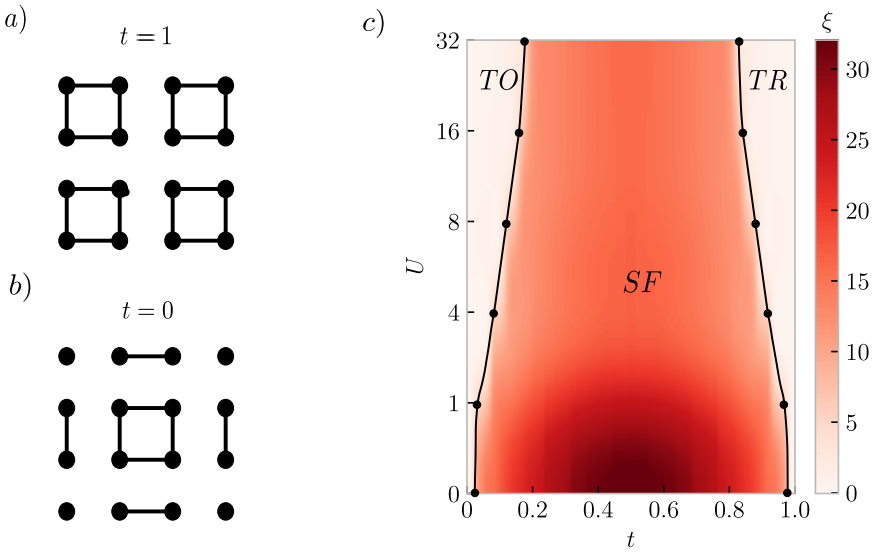

Figure 3.3: **Phase diagram and fixed-point states.** Exactly solvable limits of both phases are shown for the trivial (TR) and topological phase (TO) in **a)** and **b)**, respectively. In the topological phase, the corner of the lattice is completely decoupled from the rest of the system. Panel **c**) shows the bulk correlation length ξ against the interpolation parameter t obtained from DMRG on an infinite cylinder with circumference $L_y = 6$. The diverging correlation length is characteristic for the superfluid (SF) phase. The Hilbert space was truncated to maximal four bosons per site, and we kept $\chi = 500$ states for the simulations.

we want to answer the question to which extent the gapped phases remain as we decrease U and the anisotropy of hopping amplitudes, such that they become of the same order $t \sim (1-t)$. Therefore, we applied the infinite DMRG method [40, 122, 126, 127] to the 2D SL-BHM and considered the system on an infinite cylinder $L_x \to \infty$ with circumference $L_y = 6$ and evaluated the bulk correlation length ξ[9] shown in Fig. 3.3c. To uncover the gapped regions, we evaluated the bulk correlation length for various values of the bond dimension χ (for more details, see App. A). The phase diagram, Fig. 3.3c, clearly shows that the 2D SL-BHM has two extended gapped phases denoted as topological and trivial, respectively. The gapped regions are separated by a gapless superfluid (SF) regime.

[9]Similar to the entanglement entropy of a subsystem, the bulk correlation length diverges for gapless systems.

3.3 Topological classification of the 2D SL-BHM

This section is at the heart of this chapter, as it contains the topological classification of the 2D SL-BHM. We briefly argue why concepts of non-interacting systems cannot be used to classify the topology of the 2D SL-BHM and explain why higher multipole moments such as a quadrupole operator is not a faithful quantity to distinguish different phases of the 2D SL-BHM. Afterwards, we consider the higher-order Zak (Berry) phase, first introduced by Araki et al. [128], and then the fractional corner charge. Thereby, we argue that it serves as a genuine topological invariant.

3.3.1 Failure of non-interacting classifications and higher multipole moments

Concepts of non-interacting HOTIs [21–24, 109–111] very often rely on the momentum state representation at which non-interacting fermionic systems become exactly solvable. In the case of strongly-interacting systems there is no advantage of transforming the system to momentum space as it does not simplify the problem—it remains not solvable. Thus, many concepts developed in the non-interacting setup cannot be used for strongly-interacting systems.

Quadrupole operator. There have been other attempts to classify higher-order topology by generalizing the many-body polarization introduced by Resta [45] to a many-body quadrupole operator [129, 130]. However, it was shown that for $U(1)$ conserving systems, such an operator is not well-defined in the presence of periodic boundary conditions [131]. Any state of a given Hilbert space on which such operator acts, must obey the same boundary conditions, which is not the case if the system does not conserve the dipole moments along x and y. Nevertheless, if a system conserves the total charge and dipole moments, a quadrupole operator can be meaningfully defined [132]. In Sec. 5.2.3 we review this discussion from a more physical point of view using Thouless pumps, which clearly demonstrates that a quadrupole operator is indeed not sufficient to characterize the HOSPTs of the 2D SL-BHM.

3.3.2 Higher-order Zak (Berry) phase

The higher-order Zak (Berry) phase, classifying HOSPTs, was first introduced in Ref. [128] and is a proper topological invariant if the ground state is non-degenerate[10]. In the presence of C_4 symmetry, it is quantized. To this end, we consider the 2D SL-BHM with PBC. The higher-order Zak (Berry) phase is defined with respect to a local twist of the central plaquette, Fig. 3.2 at $t = 0$, see also Fig. 3.4, while the remaining part of the Hamiltonian, Eq. (3.1), is unchanged. The local twist is introduced via a product of three unitary operations

$$\hat{U} = \prod_{j=1}^{3} \hat{U}_j, \quad \hat{U}_j = e^{-i\hat{n}_j\phi_j}, \tag{3.9}$$

[10] We will elaborate more on this in Sec. 5.1

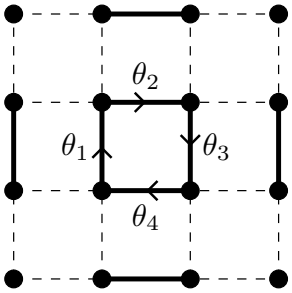

Figure 3.4: **Local twist.** The resulting Hamiltonian after inserting the local twist in the central plaquette. The hopping terms responsible for PBC are not shown. Although four variables are displayed, only three of them are independent. One of the variables is fixed by the zero flux condition $\sum_j \theta_j = 0$.

such that the central plaquette transforms as follows:

$$\hat{U}^\dagger \hat{H}_\mathrm{P} \hat{U} = e^{i(\phi_2-\phi_1)}\hat{a}_2^\dagger \hat{a}_1 + e^{i(\phi_3-\phi_2)}\hat{a}_3^\dagger \hat{a}_2 + e^{-i\phi_3}\hat{a}_4^\dagger \hat{a}_3 + e^{i\phi_1}\hat{a}_1^\dagger \hat{a}_4 + \text{h.c.}. \tag{3.10}$$

Finally, we define $\phi_j = \sum_{i=1}^{j} \theta_i$ together with a *zero flux condition*, i.e., $\sum_j \theta_j = 0$. The resulting Hamiltonian is shown in Fig. 3.4. After inserting the local twist, the ground state, $|\Psi(\theta_1, \theta_2, \theta_3, \theta_4)\rangle$, depends on four variables; however, only three of them are independent, with $(\theta_1, \theta_2, \theta_3) \in \mathbb{R}^3$.

Paths in parameter space

Although we have introduced three independent variables, it turns out that for the particular paths we choose a single parameter $l \in [0, 1)$ is sufficient. To this end, we consider four C_4 symmetry related paths, $\mathcal{L}_1, ..., \mathcal{L}_4$, which are defined as follows:

$$\begin{aligned} \mathcal{L}_1 &= \boldsymbol{O} \to \boldsymbol{G}_0 \to 2\pi \boldsymbol{e}_1, \qquad \mathcal{L}_2 = 2\pi \boldsymbol{e}_1 \to \boldsymbol{G}_0 \to 2\pi \boldsymbol{e}_2 \\ \mathcal{L}_3 &= 2\pi \boldsymbol{e}_2 \to \boldsymbol{G}_0 \to 2\pi \boldsymbol{e}_3, \quad \mathcal{L}_4 = 2\pi \boldsymbol{e}_3 \to \boldsymbol{G}_0 \to \boldsymbol{O}, \end{aligned} \tag{3.11}$$

where $\{\boldsymbol{e}_i\}$ denotes the standard basis of $\mathbb{R}^3$, $\boldsymbol{G_0} = \frac{\pi}{2}\sum_i \boldsymbol{e}_i$ and $\boldsymbol{O}$ is the origin. Along each path, the higher-order Zak (Berry) phase reads[11]:

$$\gamma_j = i \oint_{\mathcal{L}_j(l)} \mathrm{d}l \, \langle \Psi(l) | \partial_l | \Psi(l) \rangle \mod 2\pi, \quad l \in [0, 1). \tag{3.12}$$

To obtain γ_1, for example, the parametrization is as follows:

$$\mathcal{L}_1 := \begin{cases} \theta_1 = \theta_2 = \theta_3 = 2\pi l, \ \theta_4 = -6\pi l, \ 0 \le l \le \frac{1}{4} \\ \theta_1 = 2\pi l, \ \theta_2 = \theta_3 = \frac{2}{3}\pi(1-l), \ \theta_4 = -\frac{2}{3}\pi(l+2), \ \frac{1}{4} < l < 1 \end{cases}, \tag{3.13}$$

and similarly for the other trajectories.

[11] This phase is well-defined modulo 2π, which is a consequence of the fact that wave functions are only defined up to a $U(1)$ phase factor.

Quantization of the higher-order Zak (Berry) phase

A first step towards a quantization of the higher-order Zak (Berry) phase is to note that the sum over all paths vanishes,

$$\sum_i \mathcal{L}_i = \boldsymbol{O} \Rightarrow \sum_i \gamma_i = 0 \bmod 2\pi. \tag{3.14}$$

Second, C_4 symmetry maps individual paths to each other $C_4 : \mathcal{L}_i \to \mathcal{L}_{i+1}$. From this, we obtain that all four higher-order Zak (Berry) phases are identical (modulo 2π),

$$\gamma_1 = \gamma_2 = \gamma_3 = \gamma_4 \bmod 2\pi. \tag{3.15}$$

This property, together with Eq. (3.14), implies quantization of the higher-order Zak (Berry) phase,

$$\sum_i \gamma_i \equiv 4\gamma = 0 \bmod 2\pi \Rightarrow \gamma = \pi\frac{\mathbb{Z}}{4}. \tag{3.16}$$

For the 2D SL-BHM at half-filling the higher-order Zak (Berry) phase is given by $\gamma = \{0, \pi\}$, which can be deduced from the non-degenerate ground states at the exactly solvable limits $t = 0$ and $t = 1$, respectively. Note that the difference $\Delta\gamma = \gamma(t = 0) - \gamma(t = 1)$ is invariant under continuous, symmetric deformations of the Hamiltonian[12]. To numerically evaluate the higher-order Zak (Berry) phase, we considered the 2D SL-BHM on a 4×4 torus with fixed-particle number $N = 8$. The numerical results are shown in Fig. 3.5b, clearly indicating that the gapped phases realizes two distinct HOSPT phases. The quantized plateaus of the higher-order Zak (Berry) phase in Fig. 3.5b persist in the SF phase purely due to finite size effects.

3.3.3 Fractional corner charges

The higher-order Zak (Berry) can distinguish the two distinct topological phases realized by the 2D SL-BHM at half-filling. However, for an actual experiment to measure this topological invariant is a very challenging task, since artificial gauge fields at arbitrary values are required. In this part, we show that the fractional corner charge distinguishes the two gapped phases of the 2D SL-BHM and is a genuine topological invariant that is experimentally accessible.

Filling anomaly

In Sec. 3.1.3 we argued that in the topological phase, $t = 0$, the system suffers from a filling anomaly if the model is considered with open boundary conditions. Namely, the C_4-symmetric ground states have particle numbers $N = N_0 \pm 2$, where N_0 is the particle number at half-filling. For hardcore bosons, the ground states of these particle sectors have the same energy; however, once $U < \infty$ the degeneracy is lifted, but the

[12] Continuous symmetric deformations are defined such that the bulk gap of a given Hamiltonian does not close (see also Sec. 2.2.1).

filling anomaly remains. This is also the reason the 2D SL-BHM at finite U cannot be captured by the group cohomology classification discussed in Sec. 2.2.3. For a C_4-symmetric state, the average particle number in each quadrant must be the same

$$\langle \hat{N}_{q_1} \rangle = \langle \hat{N}_{q_2} \rangle = \langle \hat{N}_{q_3} \rangle = \langle \hat{N}_{q_4} \rangle \,, \tag{3.17}$$

from which we obtain $\langle \hat{N}_{q_i} \rangle = N/4$, where $\{q_i\}$ labels different quadrants. Note here we used that the Hamiltonian, Eq. (3.1), conserves the total particle number and, thus, replaced the operator $\hat{N} \to N$ by its quantum number. From the trivial phase, we know that $N_0 \mod 4 = 0$, which implies that each quadrant in the topological phase with $N = N_0 \pm 2$ carries on average a fractional charge $\sim 1/2 \pmod 1$.

Corner charge

If bulk and edges are at half-filling $n_0 = 1/2$, then fractional charges must sit near the corners. If we define individual charges with respect to the average filling $\sim \langle \hat{n}_{x,y} - n_0 \rangle$, then the following holds[13]:

$$4Q_{\text{corner}} + 4Q_{\text{edges}} + Q_{\text{bulk}} = 2, \tag{3.18}$$

where C_4 symmetry ensures that edges and corners must have the same total charge. By assumption, bulk, and edges are at half-filling, i.e., $Q_{\text{bulk}} = Q_{\text{edge}} = 0$, which implies

$$Q_{\text{corner}} = 1/2 \mod 1. \tag{3.19}$$

For the exactly solvable case at $t = 0$, we find that $Q_{\text{corner}} = \langle \hat{n}_{\text{corner}} - n_0 \rangle = 1/2$ with zero fluctuations $(\Delta Q_{\text{corner}})^2 = \langle \hat{Q}^2_{\text{corner}} \rangle - \langle \hat{Q}_{\text{corner}} \rangle^2 = 0$. If $t > 0$, then the fractional charge is no longer on-site and starts to penetrate into bulk and edge regions—resulting in non-trivial quantum fluctuations. For the fractional corner charge to be a well-defined invariant, its quantum fluctuations in the thermodynamic limit must vanish. To keep track of this, we equip the operator of the fractional corner charge $\hat{Q}_{\text{corner}}$ with an exponentially decaying envelope function[14]

$$\hat{Q}_{\text{corner}} = \sum_{x,y} e^{-\boldsymbol{r}^2/\xi^2_{\text{env}}} \left(\hat{n}_{x,y} - n_0 \right), \tag{3.20}$$

where $\boldsymbol{r} = (x, y)^T$ gives the position on the lattice. The width of the Gaussian envelope function is determined by ξ_{env}, which has to be much larger than the localization length $\xi_{\text{p,h}}$ of a particle or hole state pinned at the corner $\xi_{\text{p,h}} \ll \xi_{\text{env}}$ and much smaller than the system size $\xi_{\text{env}} \ll L$. The first constraint is needed because within a region of $\sim \xi^2_{\text{loc}}$ particle number fluctuations are of order one $(\Delta n)^2 \sim \mathcal{O}(1)$—destroying the quantization

[13] Since the system is insulating with a finite correlation length, there is a clear notion of how to divide such a system using envelope functions [133, 134]. However, for the argument the precise definitions are not necessary.

[14] This way we ensure a smooth cut-off, which would be not the case if we were using a Heaviside step function. A hard cut-off would cause particle number fluctuations of order one at the end of the cut.

of the corner charge. The second constraint ensures that we do not pick up contributions from other corners. For sufficiently large system sizes, ξ_{env} becomes independent of L—rendering the fractional corner charge as a genuine topological invariant as $L \to \infty$. The localization length is defined through the participation ratio [135],

$$\xi^2_{\text{p,h}} = \left(\sum_{x,y} \Delta n_{x,y}\right)^2 / \sum_{x,y} (\Delta n_{x,y})^2, \tag{3.21}$$

where $\Delta n_{x,y} = |\langle \hat{n}_{x,y} \rangle - n_0| \times \Theta\left(\pm(\langle \hat{n}_{x,y} \rangle - n_0)\right)$, with "+(−)" for $\xi_{\text{p(h)}}$ and with Θ denoting the Heaviside step function. Similar to the higher-order Zak (Berry) phase, the fractional corner charge distinguishes the two distinct HOSPT phases of the 2D SL-BHM with $Q_{\text{corner}} = 0(1/2)$ mod 1 in the trivial (topological) phase. The numerical results are shown in Fig. 3.5a.

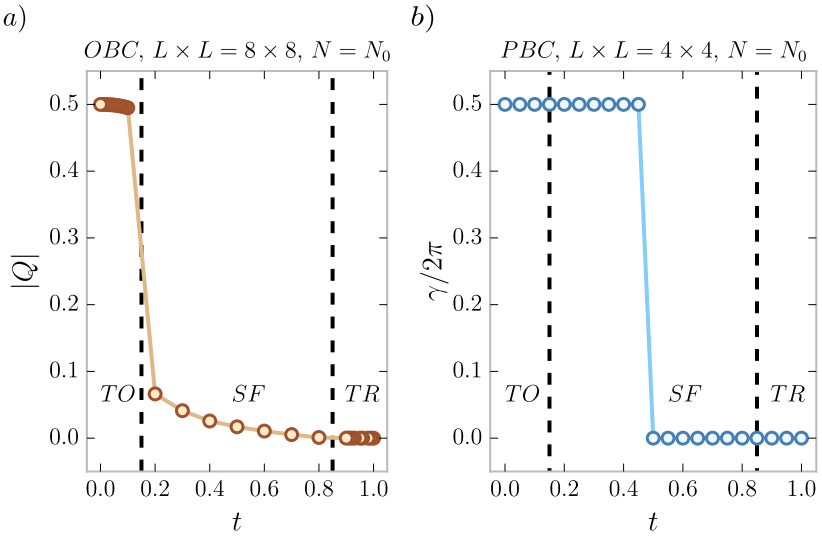

Figure 3.5: **Topological invariants. a)** Corner charge Q_{corner} as a function of hopping t at half-filling $N = N_0$, quantized to $Q_{\text{corner}} = 0\,(1/2)$ in the gapped trivial (topological) phase. We used DMRG on an 8×8 square lattice, taking $U = 32$, $\xi_{\text{env}} = 2.8$. **b)** Higher-order Zak (Berry) phase γ as a function of the hopping parameter, quantized around $\gamma = 0\,(\pi)$ in the gapped trivial (topological) phase. The result is obtained for a 4×4 square lattice with periodic boundary conditions at half-filling ($N_0 = 8$).

Stability of the fractional corner charge

To be a proper topological invariant, the fractional corner charge must be immune to continuous deformations of the Hamiltonian, i.e., any symmetric perturbations that do not close the bulk gap. Note, this does not forbid terms that lead to an edge gap closing (which we partly discussed in Sec. 2.2.3). Indeed, even if the edge gap closes,

the fractional part of the corner charge cannot change. To demonstrate this, we define polarizations denoted by P^{edge} for each edge[15]. Concentrating on a single corner, the change of the corner charge ΔQ_{corner}, due to arbitrary edge manipulations, is directly related to the change of the polarizations of the two edges meeting at this corner, ΔP_x^{edge} and ΔP_y^{edge}, by the King-Smith-Vanderbilt relation [134]

$$\Delta Q_{\text{corner}} = \sum_{\zeta \in \{x,y\}} \Delta P_\zeta^{\text{edge}} \bmod 1. \tag{3.22}$$

Due to C_4 symmetry, the contributions of the edge polarizations ΔP_x^{edge} and ΔP_y^{edge} cancel each other, confirming that Q_{corner} is robust against edge manipulations, even if the edge gap closes and, thus, reflects the properties of the bulk. This argument again emphasizes the need of spatial protections for higher-order topological phases.

3.3.4 Relation of topological invariants

In the previous discussions we argued that both the higher-order Zak (Berry) phase and the fractional corner charge classify the gapped phases of the 2D SL-BHM; however, unlike in one dimension, where the fractional charge at the edge and the many-body generalization of the Zak (Berry) phase are related by a bulk-boundary correspondence, this relation is not yet clear in higher dimensions and is part of Chap. 5. Nevertheless, it is worthwhile to briefly repeat the argument of the one-dimensional SL-BHM because it also manifests that the fluctuations of the fractional charge in the thermodynamic limit must vanish.

One-dimensional SL-BHM

The gapped phases of the 1D SL-BHM with a bulk at half-filling[16] also realize two distinct topological phases, labelled by the bulk polarization $P_{\text{1D,bulk}}$, proven to be quantized to $P_{\text{1D,bulk}} = 0\,(1/2) \bmod 1$ for a system with periodic boundary conditions [33]. This quantization relies on inversion symmetry only and $P_{\text{1D,bulk}}$ is directly related to a Zak (Berry) phase picked up by the interacting many-body wave function for twisted boundary conditions [45, 103], similar to what we discussed in Sec. 3.3.2. In a system with sharp edges, bulk-boundary correspondence manifests in a charge localized around the edge, $Q_{\text{1D,edge}}$, such that the changes of $Q_{\text{1D,edge}}$ are related to changes of the bulk polarization through $\Delta Q_{\text{1D,edge}} = \Delta P_{\text{1D,bulk}}$ [134]. Since the latter is quantized and directly related to a topological invariant (the many-body Zak (Berry) phase [33, 45]), the quantum fluctuations of $\Delta Q_{\text{1D,edge}}$ have to vanish in the thermodynamic limit $L \to \infty$.

[15] From the limiting case $t = 0$, we observe that the edges itself form a one-dimensional SL-BHM, which has extensively discussed in Ref. [33].

[16] The 1D SL-BHM also shows a filling anomaly; for the same chemical potential the two phases differ in their total particle number, with $N = N_0\,(N_0 - 1)$ in the TR (TO) phase. (See Fig. 1 of Ref. [33]).

3.4 Fractional corner charges in the context of experiments

The final part of this chapter considers the measurement of the fractional corner charge and briefly discusses the experimental realization of the 2D SL-BHM. Thereby, we explicitly provide data that can be measured in ultracold atomic setups using single-site resolution of quantum gas microscopes [30–32].

3.4.1 Measurement of fractional corner charges

For the fractional corner charge to be a proper topological invariant, we argued that its quantum fluctuations must vanish in the thermodynamic limit. To demonstrate this, we evaluated the full counting statistics of the edge and corner charges for both phases of the 1D and 2D SL-BHM, respectively. We obtained the ground state of the system using DMRG, and then generated single snapshots according to the probability distribution given by the wave function using perfect sampling [136]. Figs. 3.6a and 3.6b display the FCS of the 1D system in both phases for two different system sizes L, clearly demonstrating that the distributions centered around $Q_{1D,edge} = 0\,(1/2)$ get sharper as L increases. Figs. 3.6c and 3.6d show the 2D FCS in the TR and TO phases, respectively. Here the accessible system size L is more limited and the FCS still shows significant finite size effects, in contrast to the 1D case. This results in a broader distribution that is, however, clearly centered around $Q_{\text{corner}} = 0\,(1/2)$.

Let us emphasize, that the data shown in Fig. 3.6 could have taken from an actual experiment, where after each state preparation a single snapshot is made, and the data are drawn in a histogram [32]. This makes the fractional corner charge such a powerful topological invariant. It is experimentally accessible and allows for a direct confirmation of theoretical predictions.

3.4.2 Discussion of experimental realizations

Here, we argue that the parameter ratios used in the numerical calculations are in an experimentally accessible regime. Since the 2D SL-BHM is considered in the strongly-interacting regime, i.e., $U \gg \max(t, (1-t)) \equiv \tau$ the relevant ratio is given by τ/U. From Ref. [30], page 905, we see that this ratio for the SL-BHM can be estimated to be

$$\frac{\tau}{U} \sim \frac{d}{a} \exp -2\sqrt{\frac{V_0}{E_r}}, \tag{3.23}$$

where d is the lattice spacing, a the $s-wave$ scattering length, V_0 the lattice depth and E_r the recoil energy. In the same reference [30], page 900, it is mentioned that typical values of these parameters are $a \sim 5nm$ and $d \sim 0.5\mu m$. Thus, the ratio d/a is of order $\mathcal{O}(d/a) \sim 10^4$. For the 2D SL-BHM, the ratio of τ/U is of order $\mathcal{O}(\tau/U) \sim 10^{-2} - 10^{-3}$, and therefore, the ratio of V_0/E_r is of magnitude,

$$\mathcal{O}\left(\frac{V_0}{E_r}\right) \sim 50, \tag{3.24}$$

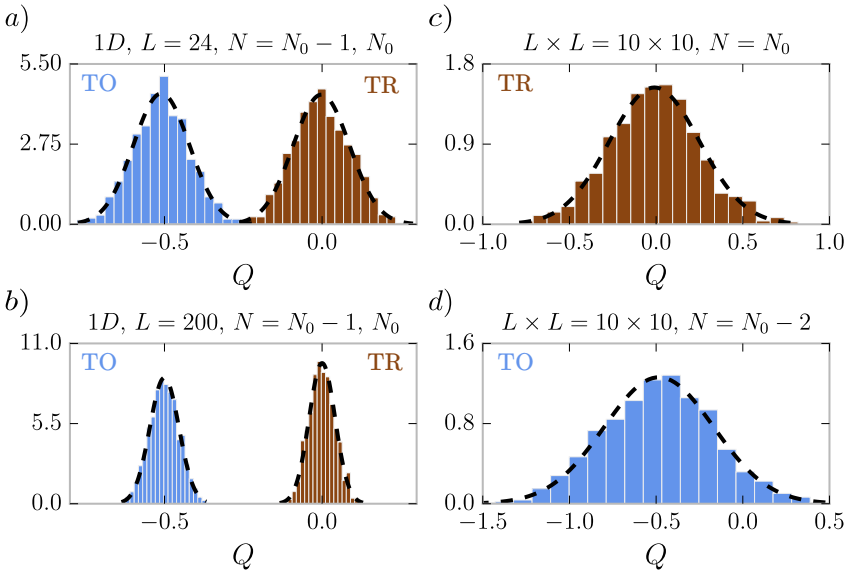

Figure 3.6: **Full counting statistics of edge and corner charges. a)** and **b)** FCS of fractional edge charge Q_{edge} of the 1D SL-BHM (defined in Ref. [33]) in the TR and TO phases, for two different system sizes $L = 24$ and $L = 200$. The distribution is peaked around the quantized value $0\,(1/2)$ in the TR (TO) phase and gets sharper with increasing L, confirming that Q_{edge} is a good quantum number in the thermodynamic limit. Parameters for the TR (TO) phase: $N = N_0\,(N_0 - 1)$, $t_1 = 0.2\,(1)$, $t_2 = 1\,(0.2)$, $U = 10$. The envelopes are $\xi_{\text{env}} = 12\,(12)$ for $L = 24$ and $\xi_{\text{env}} = 53\,(45)$ for $L = 200$, respectively. **c)** and **d)** FCS of fractional corner charge Q_{corner}, measured in the TR (TO) phase of the 2D SL-BHM for system size 10×10, peaked around $0\,(1/2)$. The width of the distribution should approach to zero in the thermodynamic limit, similar to the 1D case. Results were obtained for $N = N_0\,(N_0 - 2)$, $t = 0.9\,(0.1)$, $U = 32$ and $\xi_{\text{env}} = 3.2\,(3.08)$.

which is in a regime of experimental accessibility, see, for example, Ref. [137], where the ratio was even three times higher than the estimate in Eq. (3.24).

3.5 Summary & Outlook

In summary, we have proposed an experimentally accessible ultracold atomic system, a 2D SL-BHM around half-filling, with alternating hopping amplitudes t and $1 - t$ realizing an interacting HOSPT phase protected by charge conservation and C_4 lattice symmetry. We identified the hardcore boson model with the dimerized spin-1/2 quantum XY model and discussed its connection with a non-interacting HOTI—the BBH model—and showed that these two models are only equivalent at two points, namely, for hardcore bosons, $U \to \infty$, and $t = 0$ or $t = 1$. Further, relying on DMRG simula-

tions, we explored the phase diagram of the 2D SL-BHM and showed that it hosts two gapped topological phases[17], separated by a gapless superfluid region. Concentrating on the gapped phases, we argued that they are topologically distinct and differ in terms of a quantized fractional charge localized around the corners, intimately connected to a quantized higher-order Zak (Berry) phase. This fractional charge is robust against edge manipulations and reflects the properties of the bulk. By sampling snapshots of the ground state wave function in the Fock basis, we have demonstrated that the full distribution of the corner charge is peaked around the fractionally quantized value $0\,(1/2)$ in the trivial (topological) phase. A similar sampling can be experimentally realized in ultracold atomic settings by using state-of-the-art quantum gas microscopes [31, 32].

Outlook. Although we showed that the fractional corner charge and the higher-order Zak (Berry) phase give the same results, a precise connection as in the one-dimensional case is missing. This is puzzle is partially solved in Chap. 5 of this thesis. Furthermore, for one-dimensional SPTs, there are non-trivial signatures of topology reflected in the entanglement spectrum. Namely, it was shown that a non-trivial SPT exhibit degeneracies in the spectrum of the reduced density matrix [93] (see also Sec. 2.2.1). Naturally, the question arises if such signatures extend to higher-order topological systems, which will be part of a discussion of the next chapter.

[17] The trivial phase is a topological phase with vanishing higher-order Zak (Berry) phase and fractional corner charge, respectively, which are protected by symmetry.

Chapter 4

Higher-order entanglement and many-body invariant

In this chapter, we extend the discussion on higher-order topological systems and consider it from two different points of view: On one hand, we still lack an experimentally accessible many-body invariant that recognizes higher-order topology in a strongly-interacting setup, that captures bulk properties and is related to the fractional corner charges discussed earlier. On the other hand—a more theoretical point of view—is the study of the many-body entanglement spectrum, which has been shown to contain characteristic information on topological properties of quantum phases of matter [17, 138–144].

To this end, using the 2D SL-BHM as toy model, we first introduce a many-body invariant that differentiates non-trivial HOSPT phases from trivial ones, based on the fact, that the corresponding flux insertion operator does not commute with C_n rotation symmetry—resulting in a non-trivial shift of angular momentum. This non-commutative algebra uniquely characterizes HOSPT phases with fractional charges at the corners. One can further relate this many-body invariant to the discrete Wen-Zee [43, 44, 145] response, which intertwines the $U(1)$ gauge field and spin-connection. The Wen-Zee response can be probed either by tracking the angular momentum shift under a 2π gauge flux insertion or via measuring the charge density distribution in the presence of disclinations [20, 44, 114, 145, 146]. Remarkably, such topological response could potentially be probed and simulated in ultracold atom systems with synthetic gauge fields created by laser-assisted tunneling or rotating traps.

Second, we propose a general recipe to detect HOSPT phases from a new higher-order entanglement perspective. Different from conventional one-dimensional symmetry-protected topological phases, where the entanglement spectrum displays gapless (or degenerate) modes akin to the edge spectrum [17, 93], some HOSPT phases might exhibit gappable (non-degenerate) and featureless entanglement spectra under any arbitrary, symmetry allowed spatial cut. More precisely, if we merely cut out a C_n-wedge or perform a C_n-symmetric bipartition, the entanglement spectrum could display a unique ground state *even though* the state is in a non-trivial HOSPT phase. This implies that the conventional diagnosis of entanglement spectra fails to detect many HOSPT phases. Thus, naturally, the question arises whether we can still reveal fingerprints of HOSPT phases using entanglement spectroscopy. To this end, we introduce a new type of entanglement property, dubbed "higher-order entanglement" as a fingerprint to differentiate topological

distinct HOSPT phases. The entanglement branching structure refers to a hierarchical sequence of entanglement spectra instead of a single spectrum. By symmetrically bipartitioning a C_n-symmetric wave function, we initially obtain the first-order entanglement spectrum, which might contain non-degenerate eigenstates. Each non-degenerate eigenstate, upon further bipartitions, should then eventually at some order exhibit a fully degenerate spectrum with respect to each C_n-wedge. Consequently, the entanglement of HOSPT phases manifests a branching structure, where any non-degenerate eigenvector of the initial entanglement spectrum contains a degenerate entanglement spectrum upon further cuts.

Overview. This chapter is based on [P2] and divided into three main sections: First, in Sec. 4.1 we demonstrate using iDMRG that the 2D SL-BHM realizes, aside from the half-filled case, stable and gapped phases of matter for filling factors $n_0 \in \{1/4, 3/4\}$. Moreover, we shortly discuss the exactly solvable ground states of different fillings and review their topological classifications.

Second, in Sec. 4.2 we introduce the previously mentioned many-body invariant and discuss its relation to the generalized Wen-Zee response. To this end, we start with showing that the higher-order Zak (Berry) phase measures the C_4 eigenvalue after a 2π flux insertion. From this observation, we then construct a $U(1)$ flux insertion operator. Further, from the non-trivial commutation relations of the symmetry operators, we deduce that the same flux can be introduced via a symmetry twist related to a $\mathbb{Z}_4$ subgroup. This implies that the $\mathbb{Z}_4 \times C_4$ subgroup is sufficient to protect the HOSPT phases.

In the second half of this section, we study the response of the system to topological defects such as disclinations—starting from a lattice perspective—and reveal the connection to curvature. Afterwards, we briefly review how disclinations are treated in a continuum approximation and discuss their relation to the spin-connection. Based on this, we can study the discrete Wen-Zee response from a field theory point of view. This section ends with a numerical study of small clusters of the 2D SL-BHM, where we evaluate the many-body invariant for various fillings. Moreover, we briefly discuss how the many-body invariant can be implemented in experimental setups.

Lastly, in Sec. 4.3 we consider entanglement properties of HOSPT phases. To this end, we start with the case, where the SL-BHM has an additional antiunitary particle-hole symmetry that has projective representations at the corners.

Second, focusing solely on cases with $U(1) \times C_4$ symmetry, we show that, upon a bipartition of the system into two C_4-symmetric related regions, certain fillings have exact degeneracies in their entanglement spectrum, while for others we find both; degenerate and non-degenerate Schmidt states. At this point, we introduce the notion of higher-order entanglement, where we explicitly show that further bipartitions of non-degenerate Schmidt states result in a fully degenerate entanglement spectrum.

4.1 HOSPTs in plateaus of the SL-BHM

In the previous chapter, Chap. 3, we showed that the 2D SL-BHM has two extended gapped phases at half-filling. In this first part, we show that it also has stable, gapped phases for fillings $n_0 = \{1/4, 3/4\}$.

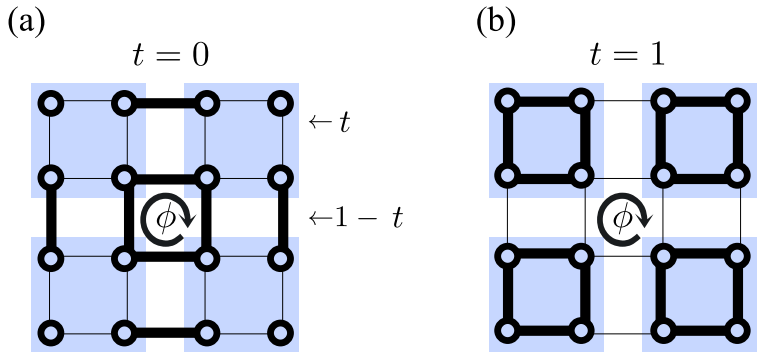

Figure 4.1: **Lattice with flux insertion.** Super-lattice hardcore boson model on a square lattice with a 2×2 unit cell with couplings t within and $1-t$ between unit cells, respectively. Gapped HOSPT phases occurring at commensurate bulk fillings factors $n_0 = \{1/4, 1/2, 3/4\}$ exhibiting different HOSPT orders (a) $t = 0$ and (b) $t = 1$. A flux insertion of ϕ at the central plaquette is used to define a many-body invariant (see text for details).

4.1.1 Gapped phases of the SL-BHM at different fillings

To detect possible gapped phases of the 2D SL-BHM at different fillings n_0, we evaluated the ground state of Hamiltonian (3.1) (see also Fig. 4.1) using hardcore bosons on an infinite cylinder along x and finite circumference along y with $L_y = 6$. For this, we fixed the hopping amplitudes to $t = 0.1$ and tuned the chemical potential μ. The results are shown in Fig. 4.2, where we see that there are indeed extended plateaus for fillings $n_0 = \{1/4, 1/2, 3/4\}$—separated by a superfluid gapless region, as expected. While we show here the case $t = 0.1$, an identical structure shows up for $t = 0.9$ (more generally, exchanging $t \leftrightarrow 1 - t$ leaves the spectral bulk properties unchanged).

Exactly solvable cases

The ground states in the plateaus are adiabatically connected to the zero-correlation length limits at $t = 0$ and $t = 1$, respectively. In these limiting cases, both ground states can be represented as a plaquette product state $|\psi_0\rangle = \prod_{\{\square\}} |\psi_{n_0}^{\square}\rangle$ (assuming PBC), where the product is over all plaquettes with strong bonds and n_0 is the average bulk

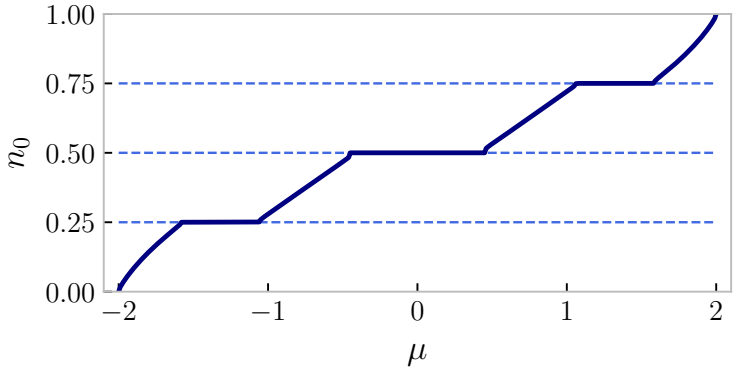

Figure 4.2: **Gapped phases.** Particle density n_0 as function of the chemical potential μ for the 2D SL-BHM obtained from DMRG simulations on an infinite cylinder with circumference $L_y = 6$ and $t = 0.1$. Extended plateaus occur at commensurate bulk particle densities $n_0 = \{1/4, 1/2, 3/4\}$.

filling,

$$|\psi^{\square}_{1/4}\rangle = \frac{1}{2}\left(|1000\rangle + |0100\rangle + |0010\rangle + |0001\rangle\right) \tag{4.1}$$

$$|\psi^{\square}_{1/2}\rangle = \frac{1}{2\sqrt{2}}\left(|1100\rangle + |0110\rangle + |0011\rangle + |1001\rangle\right) + \frac{1}{2}\left(|1010\rangle + |0101\rangle\right) \tag{4.2}$$

$$|\psi^{\square}_{3/4}\rangle = \frac{1}{2}\left(|0111\rangle + |1011\rangle + |1101\rangle + |1110\rangle\right). \tag{4.3}$$

Topological classification

According to Sec. 3.3.2 each of these states is characterized by a non-trivial higher-order Zak (Berry) phase $\gamma = \{\frac{\pi}{2}, \pi, \frac{3}{2}\pi\}$, clearly distinguishing these phases from the trivial case, $t = 1$, which itself has a vanishing higher-order Zak (Berry) phase. Equivalently, as claimed in Sec. 3.3.3, if HOSPT phases at fillings $n_0 \in \{1/4, 1/2, 3/4\}$ are considered with open boundary conditions, then the non-trivial topology is reflected by fractional corner charges $Q_{\text{corner}} = \{1/4, 1/2, 3/4\}$. As in the half-filled case, the fractional corner charges are a consequence of the filling anomalies ± 1 and ± 3, respectively. Note that, unlike in the half-filled case, we have to add additional, symmetry preserving terms to the Hamiltonian to guarantee gapped edges with appropriate filling factors. Despite the existence of fractional corner charges, the gapless modes at the corners can be symmetrically gapped out by turning on a chemical potential at each corner to pin the particle configurations. Subsequently, the degeneracy at the corner is merely a consequence of the filling anomaly and is not protected by symmetry.

4.2 Many-body invariant for HOSPT phases

Although the mathematical structure and classification of interacting HOSPT phases (or topological crystalline phases, broadly defined) is now well understood [19, 20, 26, 65, 115, 116, 147, 148], experimentally accessible bulk many-body invariants [128–130] for the characterization of such phases are still lacking. The obstacle lies in the fact that the associated topological or entanglement structure cannot be measured by any local operator. To tackle this problem, we introduce in this section a many-body invariant for HOSPT phases, which is closely related to the discrete Wen-Zee response [43, 44, 145], where a flux insertion changes the angular momentum in specific ways, and leverage its relationship with the fractional corner charge.

The section is structured as follows: We first prove, Sec. 4.2.1, that the previously introduced higher-order Zak (Berry) phase measures the C_4 eigenvalue after a 2π flux insertion. Based on this, we define in Sec. 4.2.2 an experimentally accessible many-body invariant, a $U(1)$ flux insertion operator, and after a short excursion on disclinations and their relation to differential geometry, we discuss the connection of the many-body invariant to the discrete Wen-Zee response. This section ends with numerical calculations, demonstrating that the new invariant indeed distinguishes different HOSPTs and a brief discussion on its experimental realization (see Sec. 4.2.3).

4.2.1 Higher-order Zak (Berry) phase and its relation to the C_4 eigenvalue

We demonstrate now that the higher-order Zak (Berry) phase measures the C_4 eigenvalue of the ground state of the non-trivially twisted Hamiltonian. To see this, let us recall from Sec. 3.3.2 that the higher-order Zak (Berry) phase is obtained from a local twist of the central plaquette equipped with a zero flux condition $\sum_j \theta_j = 0$ (which, e.g., fixes θ_4). The twisted plaquette Hamiltonian reads (see also Fig. 3.2)[1]:

$$\hat{H}_P(\boldsymbol{\Theta}) = \sum_{j=1}^{4} e^{i\theta_{j+1}} \hat{b}_{j+1}^\dagger \hat{b}_j + \text{h.c.}, \quad \boldsymbol{\Theta} = (\theta_1, \theta_2, \theta_3, \theta_4)^T. \tag{4.4}$$

Note that the central plaquette contains the C_4 symmetry center. From the paths defined in Eq. (3.11), we conclude that the central plaquette Hamiltonian is invariant under C_4 rotations at initial and final points of each path, and at $\boldsymbol{G}_0$[2]. At this point, the phases are given by $\boldsymbol{\Theta}(\boldsymbol{G}_0) = (\frac{\pi}{2}, \frac{\pi}{2}, \frac{\pi}{2}, -\frac{3\pi}{2})^T$.

C_4 eigenvalue

Here, we prove that the higher-order Zak (Berry) phase measures the C_4 eigenvalue of the ground state at $\boldsymbol{\Theta}(\boldsymbol{G}_0)$. For this, we use that the higher-order Zak (Berry) phase

[1] Although this is written for hardcore bosons, this equally well holds for finite $U < \infty$.
[2] This vector is defined by $\boldsymbol{G}_0 = \frac{\pi}{2}(1,1,1)^T$.

can be evaluated by the following discretized formula [101, 149]:

$$\gamma_i = -\lim_{M\to\infty} \operatorname{Im}\log \prod_{p=1}^{M} \langle \Psi(\boldsymbol{\Theta}_p^i)|\Psi(\boldsymbol{\Theta}_{p+1}^i)\rangle\,, \quad \boldsymbol{\Theta}^i = \left(\theta_1^i, \theta_2^i, \theta_3^i, \theta_4^i\right)^T \tag{4.5}$$

where θ_j^i corresponds to the path $\mathcal{L}_i$, Eq. (3.11), which itself is divided into M little pieces. Moreover, we identify $|\Psi(\boldsymbol{\Theta}_{M+1}^i)\rangle \equiv |\Psi(\boldsymbol{\Theta}_1^i)\rangle$ since individual paths $\mathcal{L}_i$ form closed loops; thus initial and final states are identical. As each state in Eq. (4.5) appears twice, this expression is inherently gauge invariant, which is also the reason it is used for numerical purposes. Using a particular gauge, called *parallel-transport gauge*[3] [101], the expression of the higher-order Zak (Berry) phase reduce to (for clarity, we choose $\gamma_i = \gamma_1$):

$$\begin{aligned}\gamma_1 &= -\lim_{M\to\infty} \operatorname{Im}\log \langle \tilde{\Psi}(\boldsymbol{\Theta}_M^1)|\tilde{\Psi}(\boldsymbol{\Theta}_1^1)\rangle \\ &= -\operatorname{Im}\log \langle \tilde{\Psi}(2\pi,0,0,-2\pi)|\tilde{\Psi}(0,0,0,0)\rangle\end{aligned} \tag{4.6}$$

where $|\tilde{\Psi}(\boldsymbol{\Theta}_p^1\rangle$ denotes the state defined with respect to the parallel transport gauge. To arrive at the conclusion, we make use of the fact that we are free to shift all phases by a constant term. Hence, we obtain ($\varphi \equiv \frac{\pi}{2}$),

$$\begin{aligned}\boxed{\gamma_1} &= -\operatorname{Im}\log \langle \tilde{\Psi}(2\pi-\varphi,-\varphi,-\varphi,-2\pi+3\varphi)|\tilde{\Psi}(-\varphi,-\varphi,-\varphi,3\varphi)\rangle \\ &= -\operatorname{Im}\log \langle \tilde{\Psi}(3\varphi,-\varphi,-\varphi,-\varphi)|\tilde{\Psi}(-\varphi,-\varphi,-\varphi,3\varphi)\rangle \\ &= -\operatorname{Im}\log \langle \tilde{\Psi}(-\varphi,-\varphi,-\varphi,3\varphi)|C_4^{-1}|\tilde{\Psi}(-\varphi,-\varphi,-\varphi,3\varphi)\rangle \\ &= \boxed{-\operatorname{Im}\log \langle \tilde{\Psi}(\boldsymbol{\Theta}(\boldsymbol{G}_0))|C_4|\tilde{\Psi}(\boldsymbol{\Theta}(\boldsymbol{G}_0))\rangle}\end{aligned} \tag{4.7}$$

where in the last step we used that $K\,|\tilde{\Psi}(\boldsymbol{\Theta}\rangle = |\tilde{\Psi}(-\boldsymbol{\Theta})\rangle$[4]. Given that formula (4.5) is inherently gauge invariant and all higher-order Zak (Berry) phases—in the presence of C_4 symmetry—are equal, we proved that γ_i measures indeed the C_4 eigenvalue of the ground state at $\boldsymbol{\Theta}(\boldsymbol{G}_0)$.

4.2.2 Constructing a many-body invariant and Wen-Zee response

In the last section, we proved that the higher-order Zak (Berry) phase, introduced by Araki et al. [128], measures the C_4 eigenvalue of the ground state of the twisted Hamiltonian. However, to study the interplay between the $U(1)$ symmetry and the spatial C_4 symmetry, the higher-order Zak (Berry) phase is not the optimal choice. Instead, we will introduce a many-body invariant that reveals the non-trivial interplay of those

[3] The main idea is to choose a gauge such that $\forall p < M$: $\operatorname{Im}\log \langle \tilde{\Psi}(\boldsymbol{\Theta}_p^i)|\tilde{\Psi}(\boldsymbol{\Theta}_{p+1}^i)\rangle = 0$. However, choosing such a gauge introduces a phase difference between the initial and final state, which is exactly the higher-order Zak (Berry) phase.

[4] There is another subtlety, namely, if we act with C_4 on a particular state, the transformed state can in general pickup a phase. However, using the gauge degree of freedom, we can choose an initial gauge such that this phase is trivial, and the last step is justified.

symmetries based on symmetry twists of the global $U(1)$ and C_4 symmetry. Thereby, we show that the subgroup $\mathbb{Z}_4 \times C_4$ is sufficient to protect the phase. Finally, considering topological defects such as disclinations in a continuum approximation, we study the generalized Wen-Zee response using topological field theory.

$U(1)$ flux insertion

At the C_4-symmetric point $\boldsymbol{\Theta}(\boldsymbol{G}_0)$, the Hamiltonian is unchanged if we choose all four phases to be equal, i.e., $\theta_1 = \theta_2 = \theta_3 = \theta_4 = \frac{\pi}{2}$ (instead of $\theta_4 = -\frac{3}{2}\pi$). If we do this, then we have introduced a 2π flux into the central plaquette, schematically shown in Fig. 4.1. Bosons hopping around the central plaquette pick up a phase. If we label the lattice sites by polar coordinates (r_j, ϕ_j), with the origin in the C_4 symmetry center, then the 2π flux can be introduced via the following unitary operator:

$$\hat{U}_{2\pi} = \exp\left[i \sum_{j \in \, sites} \phi_j \hat{n}(r_j, \phi_j) \right], \tag{4.8}$$

while there is no net flux in any other plaquette. To insert this 2π flux into the central plaquette, we first need to separate the hoppings that lead to PBC. Therefore, we write the Hamiltonian as follows:

$$\hat{H} = \hat{H}_{OBC} + \delta \hat{H}_{PBC}, \tag{4.9}$$

where $\hat{H}_{OBC}$ contains all hoppings shown in Fig. 4.1 and $\delta \hat{H}_{PBC}$ leads to PBC. Finally, the 2π flux is inserted by acting with $\hat{U}_{2\pi}$ on the Hamiltonian with open boundary conditions,

$$\hat{H}_{2\pi} = \hat{U}_{2\pi}^{\dagger} \hat{H}_{OBC} \hat{U}_{2\pi} + \delta \hat{H}_{PBC}. \tag{4.10}$$

This is important because if we acted on the full Hamiltonian, then we would introduce the 2π flux in two plaquettes. For what follows, we consider the Hamiltonian with open boundary conditions; however, for numerical purposes it is more suitable to take PBC because then, we do not have to consider edge effects.

Commutation relations and angular momentum shift

At this point, we can study the interplay between flux insertion and C_4 symmetry. To this end, we define the action of the spatial symmetry on local operators as follows:

$$C_4 \hat{n}(r_j, \phi_j) C_4^{-1} := \hat{n}(r_j, \phi_j - \pi/2), \tag{4.11}$$

rotating each site clockwise by an angle of $\frac{\pi}{2}$. Hence, the commutation relation of the flux insertion operator and C_4 reads:

$$\hat{U}_{2\pi}^{\dagger} C_4 \hat{U}_{2\pi} = \exp\left(i \frac{\pi}{2} \hat{N} \right) C_4, \tag{4.12}$$

which depends on the total particle number modulo four. Thus, for HOSPTs suffering from a filling anomaly, the angular moment is shifted. To demonstrate this explicitly,

let us act with the gauged spatial symmetry on the exactly solvable plaquette states defined in Eqs. (4.1, 4.2, 4.3). Before flux insertion, all plaquette states have zero angular momentum; however, after flux insertion the angular momentum is shifted:

$$\begin{aligned}
\exp\left(i\frac{\pi}{2}\hat{N}\right) C_4|\psi^{\square}_{1/4}\rangle &= e^{i\frac{\pi}{2}}|\psi^{\square}_{1/4}\rangle \\
\exp\left(i\frac{\pi}{2}\hat{N}\right) C_4|\psi^{\square}_{1/2}\rangle &= e^{i\pi}|\psi^{\square}_{1/2}\rangle \\
\exp\left(i\frac{\pi}{2}\hat{N}\right) C_4|\psi^{\square}_{3/4}\rangle &= e^{i\frac{3\pi}{2}}|\psi^{\square}_{3/4}\rangle.
\end{aligned} \tag{4.13}$$

Thus, the $U(1)$ flux insertion leads to a shift of the angular momentum[5] $J \to J + \frac{l}{4}$ with $l \in \mathbb{Z}_4$. Note this property remains true even away from the exactly solvable limits since the symmetry eigenvalue cannot change unless the bulk gap closes.

A discrete gauge flux

From the commutation relation with the flux insertion operator, Eq. (4.12), we see that it is the particle number modulo four which plays an important role. Indeed, if we insert the 2π flux in the central plaquette via the $\mathbb{Z}_4$ subgroup generated by $\hat{P}_4 = \exp i\frac{\pi}{2}\hat{N}$, then the previous results, i.e., the commutation relation Eq. (4.12) and the non-trivial angular momentum shift remain. The symmetry twist, generated by the $\mathbb{Z}_4$ subgroup, is defined by (using polar coordinates),

$$\hat{V}_{2\pi} = \exp\left(i\frac{\pi}{2}\hat{N}_{\frac{\pi}{4}}\right)\exp\left(i\pi\hat{N}_{\frac{3\pi}{4}}\right)\exp\left(i\frac{3\pi}{2}\hat{N}_{\frac{5\pi}{4}}\right)\exp\left(2\pi i\hat{N}_{\frac{7\pi}{4}}\right), \tag{4.14}$$

where introduced a particle number operator for each quadrant. This also shows that the $\mathbb{Z}_4 \times C_4$ symmetry is sufficient to protect the four distinct HOSPT phases of the 2D SL-BHM. This is in agreement with the result of the previous chapter, Chap. 3, where we saw that it is the fractional part of the charge per quadrant that distinguished different HOSPT phases. Since we enforced a global $U(1)$ symmetry, together with a second condition, namely, that edges and bulk have on average a filling $n_0 \in \{1/4, 1/2, 3/4\}$—the fractional charge was found at the corner of the system[6].

Disclinations and charge

So far, we studied the response of the system after flux insertion associated to the internal $U(1)$ symmetry. In this part, we want to consider the response of the HOSPT phases by introducing flux associated to the spatial symmetry. A symmetry twist associated to a spatial symmetry is equivalent to a topological defect in the lattice [20, 65], which for the model considered here means to introduce disclinations. Physically, this corresponds to remove a part of the system and recombine the remaining sites. For C_4 symmetry, we

[5] The eigenvalues of C_4 are given by $e^{2\pi i J}$.

[6] Without the global $U(1)$ symmetry we can in principle remove all particles in a C_4-symmetric manner, except the particles in the central plaquette, see Fig. 4.4.

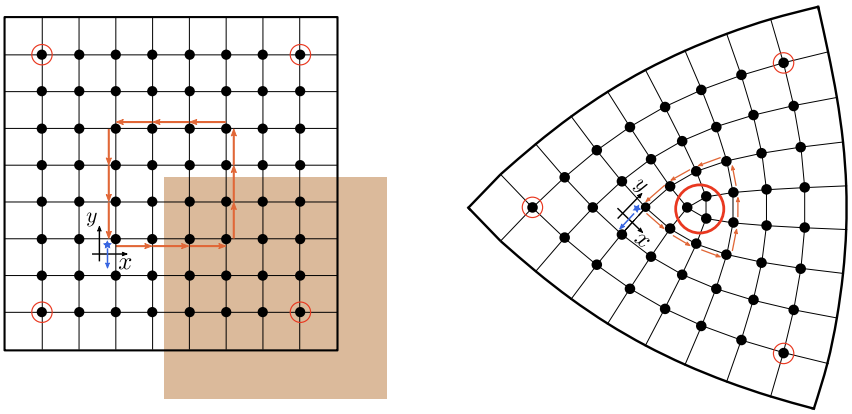

Figure 4.3: **A $\frac{\pi}{2}$-disclination after removing one quadrant.** The remaining sites are reconnected, introducing a topological defect in the lattice. The red circles highlight the corners and the disclination core. The blue star denotes the observer and the blue arrow his/her view at the beginning of the cycle. The observer is following the path marked with orange arrows. To perform the closed loop, the observer has to be rotated by 90° as a first step. The figure is adapted from Ref. [150].

can remove one, two, three, or four quadrants (see Fig 4.3). Each of these procedures corresponds to a $\frac{2\pi}{4}n,\ n \in \mathbb{Z}_4$ disclination flux[7]. For HOSPT phases with filling anomaly, the disclination core binds a fractional charge. Before we argue this explicitly, let us emphasize that there is a sum rule (see also Ref. [151]). From the previous chapter, Chap. 3, we know that the sum over all corner charges modulo integer is zero. Thus, this must remain true before and after we removed a quadrant of the system. Recall for a system with total particle number $N = 4k \pm l$, upon subtracting the average filling, the corner charge takes values $\pm l/4$ with $l \in \mathbb{Z}_4$ labeling different HOSPTs[8]. Thus, the sum of the corner charges is equal to l (or vanishes modulo an integer).

Trivial phase: To understand the physics of the trivial phase, it is sufficient to study its fixed-point limit, shown in Fig. 4.1b. If we remove a quadrant[9] of this phase, displayed in Fig. 4.4, then we simply obtain a copy of the total system with just one quarter of the total particle number. Since there was not any corner charge before, there is no charge bound to the disclination core. This result is consistent with previous discussion, where the trivial phase did not experience an angular momentum shift after flux insertion.

Topological phase: For the topological fixed-point limit, Fig. 4.1a, the situation is a bit more complicated. However, as sketched in Fig. 4.4, we can first symmetrically localize all particles—except the one in the central plaquette—and then remove one quadrant. From the same figure, we see that the upper-left corner, arising from the central plaquette,

[7] Below, we will explicitly show that a disclination corresponds to a curvature flux.
[8] In the following we do not differentiate between positive and negative corner charges; what is important is the fractional part.
[9] We assume that the size of this quadrant is much larger than ξ^2 where ξ denotes the correlation length.

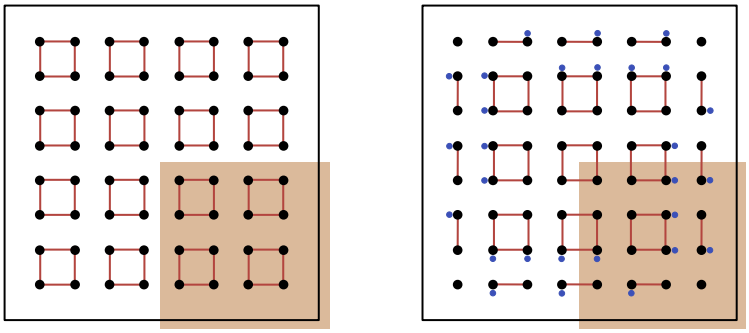

Figure 4.4: **Disclinations of fixed-point phases.** Left: Removing a quadrant of the trivial fixed-point limit. The removed subsystem is a copy of the total system. Right: Removing a quadrant of the topological fixed-point limit at half-filling. In addition, the blue points label particles, which can be C_4 symmetrically localized, demonstrating that the removed subsystem is again a copy of the total system with vanishing total fractional charge.

can have different occupations depending on the overall filling. Nevertheless, the total fractional charge of the removed quadrant is zero[10], which implies that there must be a fractional charge $l/4$ bound to the disclination core. This is a consequence of the fact that initially each quadrant carries a fractional charge, whose total sum is equal to l (or vanishes modulo an integer). The fractional charge bound to the disclination core exactly agrees with the angular moment shift discussed previously.

From Fig. 4.4 we see once more that if we give up the global $U(1)$ symmetry and only preserve its $\mathbb{Z}_4$ subgroup that we can symmetrically remove all particles in the trivial case, and all particles, surrounding the central plaquette, in the topological case. However, what remains is the fractional charge inside each quadrant!

Disclinations and differential geometry

To develop a field theoretical argument, describing the previous interplay of electromagnetic and gravitational degrees of freedom, we need to understand how one deals with disclinations in the framework of differential geometry, using a continuum approximation of crystals, where the crystalline background is considered as a continuous medium [152–154].

Lattice. As a starting point, however, we first study this connection from a lattice point of view, following closely Ref. [155]. To this end, we imagine an observer inside the lattice, performing closed loops in either configuration, i.e., in the ideal crystal or the crystal containing a disclination. Thereby, he/she is able to run along the lines, shown in Fig. 4.3, whenever his/her view is oriented along the lines. In the ideal crystal, the observer encircles the central plaquette, while in the second case the disclination core.

[10]Note, we assumed that the removed system can be considered as a copy of the large system.

The amount of rotation and translation he/she gathered, while performing the closed loop counter-clockwise, defines the holonomy of the path. If the observer starts facing south, then the holonomy of the closed loop shown in Fig. 4.3 is given by[11],

$$\hat{r}_4 \cdot \hat{T}_{3\boldsymbol{e}_x} \cdot \hat{r}_4 \cdot \hat{T}_{3\boldsymbol{e}_x} \cdot \hat{r}_4 \cdot \hat{T}_{3\boldsymbol{e}_x} \cdot \hat{r}_4 \cdot \hat{T}_{3\boldsymbol{e}_x} = \hat{T}_{\boldsymbol{0}} \cdot \hat{r}_4^4 = 1, \tag{4.15}$$

where $\hat{r}_4$ rotates the observer by $\pi/2$, $\hat{T}_{\boldsymbol{e}_x}$ is a translation along x and we used that $\hat{r}_4 \cdot \hat{T}_{\boldsymbol{e}_x} = \hat{T}_{\boldsymbol{e}_y} \cdot \hat{r}_4$. If we consider the view of the observer as a vector, then we have parallel transported a vector around a closed loop. Since the observer did neither pick up translations nor rotations, the holonomy of this path is trivial, which is generically the case for flat spaces such as the Euclidean space[12]. Instead, in the presence of a disclination, the path has non-trivial holonomy,

$$\hat{r}_4 \cdot \hat{T}_{2\boldsymbol{e}_x} \cdot \hat{r}_4 \cdot \hat{T}_{2\boldsymbol{e}_x} \cdot \hat{r}_4 \cdot \hat{T}_{2\boldsymbol{e}_x} = \hat{T}_{-2\boldsymbol{e}_x} \hat{r}_4^3. \tag{4.16}$$

Indeed, a non-trivial holonomy implies a non-trivial curvature of space. This is the connection to differential geometry we want ⇒ *disclinations are a source of curvature*[13].

For what follows, we consider only the amount of rotation picked up when encircling the disclination core. The angle Ω accumulated during the path is called the Frank angle and uniquely determines the disclination. For the given example here, we find that $\Omega = -\pi/2$ ($\hat{r}_4^3$ is a rotation counter-clockwise by $3\pi/2$). The negative sign tells us that material has been removed; however, the sign is not consistently used in literature. Very often a positive sign is associated with removing material, while adding additional material is associated with a negative sign (see, for example, Ref. [47]).

Continuum approximation. In this second part, we follow the sign conventions that whenever material is removed, the Frank angle Ω is positive. As said in the beginning, topological defects such as disclinations can be treated within the framework of differential geometry if we assume that the crystalline background can be considered as a continuous medium [152–154]. In this setup, a perfect crystal is characterized by a flat Riemannian manifold with Euclidean metric $\delta_{ij} = \mathrm{diag}(+,+,+)$ (considering three dimensions), i.e., there is neither curvature nor torsion, which implies the absence of disclinations and/or dislocations. A crystal with disclinations, however, corresponds to a Riemannian manifold with non-trivial curvature [152, 156], i.e., the metric describing space is no longer flat[14]. If on such manifold, a vector is parallel transported around a closed loop, then the initial and final vector differ. How these vectors differ is determined by the Riemann curvature tensor. Indeed, if a vector with components v^p is

[11] On each corner the local xy frame is rotated by 90°.

[12] We already learned in school how to parallel transport a vector in Euclidean space. After performing a closed loop, initial and final vector are identical.

[13] An intuitive approach to disclinations: Imagine the following situation: Take a piece of paper and scissors. First, we cut the paper such that all its sides have the same lengths. Afterwards, we remove one quadrant, and then try to reconnect the remaining edges. If we do this, then unavoidably the paper near the disclination core starts to curve.

[14] The 2-sphere is an example of a curved Riemannian manifold. The metric tensor is given by $g_{\theta\theta} = 1$ and $g_{\phi\phi} = \sin^2\theta$. All other components are zero.

parallel transported around a closed loop, on an infinitesimal square, on a manifold with sides $\mathrm{d}x$ and $\mathrm{d}y$, we obtain [157][15]:

$$v'^p - v^p = \mathrm{d}x^m \mathrm{d}y^n R_{mn}{}^p{}_q v^q, \tag{4.17}$$

where the indices m, n, p, q label coordinates of an arbitrary curvilinear coordinate system[16] and $R_{mn}{}^p{}_q$ is the Riemann curvature tensor[17]. For a flat manifold, the Riemann curvature tensor is identically zero. Moreover, in two dimensions it is completely specified by the Levi-Cevita tensor and the Gaussian curvature [157][18]:

$$R_{mnpq} = K \epsilon_{mn} \epsilon_{pq}, \quad \epsilon_{mn} = \sqrt{g} \tilde{\epsilon}_{mn}, \quad \epsilon_{pq} = \sqrt{g} \tilde{\epsilon}_{pq} \tag{4.18}$$

where $\tilde{\epsilon}_{mn}$ denotes the Levi-Cevita symbol with $\tilde{\epsilon}_{12} = 1$ and $\sqrt{g}$ the square root of the determinant of the metric tensor.

Alternatively, the Riemann curvature tensor can be fully expressed in terms of the spin-connection denoted by ω_{mpq}[19], which in two dimensions reduce to [157]

$$R_{mnpq} = \left(\partial_m \omega_n - \partial_n \omega_m\right) \epsilon_{pq}. \tag{4.19}$$

Comparing the results of Eq. (4.18) and Eq. (4.19), we obtain:

$$\left(\partial_m \omega_n - \partial_n \omega_m\right) = K \sqrt{g} \tilde{\epsilon}_{mn}. \tag{4.20}$$

Finally, we can make the connection to the Frank angle characterizing disclinations. For a two-dimensional system, the Frank angle Ω is defined through the following integral [44, 152]:

$$\Omega = \oint_{C(x^m)} \mathrm{d}x^m \omega_m = \frac{1}{2} \int_{S(x^m)} \mathrm{d}x^m \wedge \mathrm{d}x^n \left(\partial_m \omega_n - \partial_n \omega_m\right), \tag{4.21}$$

where the curve encircles the disclination core[20]. For this, we used the generalized Stokes theorem. Using Eq. (4.20), we arrive at the final result

$$\Omega = \int_S \mathrm{d}^2 x \sqrt{g} K, \quad \mathrm{d}^2 x = \mathrm{d}x_1 \wedge \mathrm{d}x_2. \tag{4.22}$$

This definition is reminiscent of electromagnetism, where Φ is the flux of the magnetic flux density through a surface $\Phi = \int_S B$, associated to some closed curve C [44, 158]. Consequently, as stated previously, a disclination is a non-trivial source of curvature.

[15] Here we used a symmetry property of the Riemann curvature tensor, namely, that $R^k{}_{lij} = R_{ij}{}^k{}_l$.
[16] An example of such coordinates is given by polar coordinates where $\{x^1, x^2\} = \{r, \phi\}$.
[17] Indices can be raised and lowered using the metric tensor g_{mn}.
[18] For the sphere, with $\det(g) = R^2 \sin^2\theta$ and $K = R^{-2}$, we find $R_{\theta\phi\theta\phi} = \sin^2\theta$.
[19] In two dimensions this can be written as $\omega_{mpq} = \omega_m \epsilon_{pq}$ [157].
[20] The integration is on a manifold with non-trivial curvature and the wedge product is defined as follows: $\mathrm{d}x \wedge \mathrm{d}y = -\mathrm{d}y \wedge \mathrm{d}x$.

Wen-Zee response

Now we have set the stage to study the interplay of electromagnetic and gravitational degrees of freedom using topological field theory. Thereby, we demonstrate from the field theory point of view that a magnetic flux carries fractional angular momentum and a disclination (≡ curvature flux) carries fractional charge. This is exactly described by the discrete Wen-Zee response. The Wen-Zee response has been first discovered in the context of the quantum Hall effect (QHE) [43], which is shortly reviewed in the box below.

Wen-Zee response and QHE

For the integer QHE effect on a plane, the electron number N_e and the number of magnetic flux quanta N_ϕ are related by an integer ν, the filling factor, $N_e = \nu N_\phi$ [159, 160]. Moreover, a longitudinal electric field along x causes a current density along y, $j_y = \sigma_{xy} E_x$ where $\sigma_{xy} = \frac{\nu}{2\pi}$ [a] is the quantized Hall conductivity. The response of the Hall states to an external electromagnetic field in curved space-time can be described by an effective topological field theory (≡ independent of the metric); the Chern-Simons theory in (2+1)D [159–162]

$$S_{CS} = \frac{\nu}{4\pi} \int \mathrm{d}^3x \; \tilde{\epsilon}^{\mu\rho\lambda} A_\mu \partial_\rho A_\lambda - \int \mathrm{d}^3x \sqrt{g} \; j^\mu A_\mu + \int \mathrm{d}^3x \sqrt{g} \; \rho_0 A_0 \tag{4.23}$$

where A_μ is the external electromagnetic U(1) gauge potential, $\sqrt{g}$ the square root of the determinant of the metric tensor and $\tilde{\epsilon}^{\mu\rho\lambda}$ is the Levi-Cevita symbol. The current density of the system can be obtained from the principle of least action with respect to A_μ [161, 162],

$$0 = \frac{1}{\sqrt{g}} \frac{\delta S_{CS}}{\delta A_\mu} \Rightarrow \rho = \frac{\nu}{2\pi} \frac{B_0 + \delta B}{\sqrt{g}}, \quad j^i = \frac{\nu}{2\pi} \epsilon^{ij} \frac{E_j}{\sqrt{g}}, \tag{4.24}$$

where $j^0 = \rho$ and ρ_0 is the ground state density of the unperturbed system. For a system on a two-dimensional plane, we find that $\sqrt{g} = 1$. Thus, integrating the zeroth component over the two-dimensional space, we obtain: $N_e = \nu N_\phi$. So far, we considered the QHE on a two-dimensional plane; however, if considered on a compact manifold such as a 2-sphere, the relation between the electron number and magnetic flux quanta experiences a non-trivial shift: $N_e = \nu N_\phi \to N_e = \nu N_\phi + \nu^2$ [43, 159]. This shift is solely a consequence of the non-trivial topology of the sphere and related to its curvature. Indeed, Wen and Zee showed that if the QHE is considered on a compact manifold, there is another topological term that needs to be included into the effective field theoretic description [43] (following the conventions of Ref. [163]):

$$S_{CS} \to S_{CS} + S_{WZ} = S_{CS} + \frac{\kappa}{2\pi} \int \mathrm{d}^3x \; \tilde{\epsilon}^{\mu\rho\lambda} \omega_\mu \partial_\rho A_\lambda \tag{4.25}$$

The second field ω_μ, behaving like a $U(1)$ gauge field, is the spin-connection and is related to the Gaussian curvature K as follows [162, 163] (see also Eq. (4.19)):

$$\partial_1\omega_2 - \partial_2\omega_1 = K\sqrt{g} \tag{4.26}$$

Again, from the principle of least action we obtain the particle number density,

$$\rho = \frac{\nu}{2\pi}\mathcal{B} + \frac{\kappa}{2\pi}K, \quad \mathcal{B} = \frac{B_0 + \delta B}{\sqrt{g}}, \tag{4.27}$$

which is non-trivially shifted. Integrating this over the 2-sphere, using the Gauss-Bonnet theorem, we get the total particle number,

$$N_e = \nu N_\phi + \frac{\kappa}{2\pi}\int_{S^2} \mathrm{d}^2x\sqrt{g}\, K = \nu N_\phi + \kappa\chi(S^2) = \nu N_\phi + 2\kappa, \tag{4.28}$$

which implies $\kappa = \nu^2/2$. Note for a torus there is no shift, since $\chi(T^2) = 0$. Replacing $\omega_i \to A_i$ and $K \to \mathcal{B}$, we see that the curl of ω is a source of flux. Given this analogy, let us recall that a charged particle moving in a magnetic field acquires an Aharanov-Bohm phase $\exp(iq\oint A)$, thus similarly we can define a quantum number s, which was called spin (not the spin of electrons) such that a particle with spin s, moving on a manifold with curvature acquires a phase $\exp(is\oint\omega)$ [43]. Wen and Zee interpreted this spin semiclassically as angular momentum of the Larmor orbits, for which they found that $s_n = (n - 1/2)$ for the n-th Landau level [43].

[a] Here we choose units such that $\hbar = c = e = 1$.

Recently, the ideas of the Wen-Zee response have been generalized to classify SPTs protected by a combination of spatial and internal symmetries such as $C_4 \times \mathbb{Z}_4$ [44], which is a generalization of Ref. [164]. There the authors have classified SPTs protected by a direct product of cyclic groups using topological field theories such as Chern-Simons or Dijkgraaf-Witten field theories. In the generalization of the Wen-Zee response, the authors of Ref. [44] studied only those field theories that are irreducible in the sense that any non-trivial subgroup of the total symmetry group contributes to the protection of the SPT. Indeed, the authors concluded that in 2+1D the symmetry group $C_4 \times \mathbb{Z}_4$ is sufficient to protect bosonic SPT phases, which agrees perfectly with our previous results, namely, that the HOSPT phases of the 2D SL-BHM are protected by $C_4 \times \mathbb{Z}_4$ symmetry[21]. To arrive at this conclusion, the authors of Ref. [44] considered the following topological field theory on a compact manifold $\mathcal{M}_3$ (using the notation of differential forms):

$$S_{WZ} = \frac{l}{2\pi}\int_{\mathcal{M}_3} \omega \wedge \mathrm{d}A, \quad l \in \mathbb{Z}_4, \tag{4.29}$$

where l labels the level of the field theory. As we will see soon, this integer characterizes

[21] However, for the fractional corner charges to be meaningful we need to enforce $U(1) \times \mathbb{C}_4$.

the fractional charge as well as the fractional angular momentum. The fields ω[22] and A are non-dynamical $\mathbb{Z}_4$ gauge fields associated to gravitational and electromagnetic degrees of freedom, respectively. To study the classification, there have been three conditions: (i) the large gauge transformations of the fields have periodicity of 2π,

$$\oint \delta A = 0 \mod 2\pi, \quad \oint \delta\omega = 0 \mod 2\pi, \tag{4.30}$$

(ii) the fields have $\mathbb{Z}_4$ gauge symmetry,

$$\oint A = n_A \frac{2\pi}{4}, \quad \oint \omega = n_\omega \frac{2\pi}{4}, \quad (n_A, n_\omega) \in \mathbb{Z}_4 \times \mathbb{Z}_4, \tag{4.31}$$

and (iii) a Dirac quantization condition ($\equiv$ the total flux is multiple of 2π)

$$\int_{\mathcal{M}_2} \mathrm{d}A = 0 \bmod 2\pi, \quad \int_{\mathcal{M}_2} \mathrm{d}\omega = 0 \bmod 2\pi. \tag{4.32}$$

For the partition function $\sim e^{iS_{WZ}}$ to be invariant under large gauge transformations, we must require that $l \in \mathbb{Z}$. The second constraint, i.e., the level identification, $l \sim l+4$ can be obtained from flux identification [164]. Although globally the total flux must be multiple of 2π, locally we can allow for fractional fluxes so called *monodromy defects*, which can be viewed as external flux insertions or symmetry twists [44, 164]. On the lattice, for example, such an isolated defect corresponds to a disclination. From Eq. (4.31) we see that if a given region contains exactly four defects, then this is equivalent to no defect (modulo 2π)[23]. Again, from the lattice point of view, this is consistent with the fact that only the fractional charge is relevant.

Response. To study the response of the system, we need to evaluate the variation of the action with respect to the fields ω_μ and A_μ, from which we obtain the associated currents. From the integral over the zeroth component of the currents, we obtain the fractional values of the charge and angular momentum [44]:

$$Q = \frac{1}{4}\int_{\mathcal{M}_2} \mathrm{d}^2x\sqrt{g}\,\frac{\delta S_{WZ}}{\sqrt{g}\delta\omega_0} = \frac{l}{4}, \quad J = \frac{1}{4}\int_{\mathcal{M}_2} \mathrm{d}^2x\sqrt{g}\,\frac{\delta S_{WZ}}{\sqrt{g}\delta A_0} = \frac{l}{4}. \tag{4.33}$$

Note that the charge is associated with respect to a variation of ω_0 (the gauge field belonging to gravitational degrees of freedom), while the fractional angular momentum is the response of a variation with respect to A_0 (the gauge field linked to electromagnetic degrees of freedom). This result agrees perfectly with what we found in the previous discussion. A 2π flux insertion leads to an angular momentum shift[24] $J \to J + \frac{l}{4}$ and a disclination binds a fractional charge $\frac{l}{4}$.

4.2.3 Numerical measurement of the Wen-Zee response

We now numerically compute the previously introduced many-body invariant, using exact diagonalization of small clusters (see Fig. 4.5). For this, we calculate the shift of

[22] The field ω corresponds to the previously defined spin-connection (cf. Eq. (4.19)).
[23] If the fields had different gauge symmetries, say $\mathbb{Z}_{N_1}$ and $\mathbb{Z}_{N_2}$, then flux identification would give $l \sim l + N_{12}$, where $N_{12} = \gcd(N_1, N_2)$ is the greatest common divisor.
[24] Recall, the eigenvalues associated to C_4 symmetry are defined by $e^{2\pi i J}$.

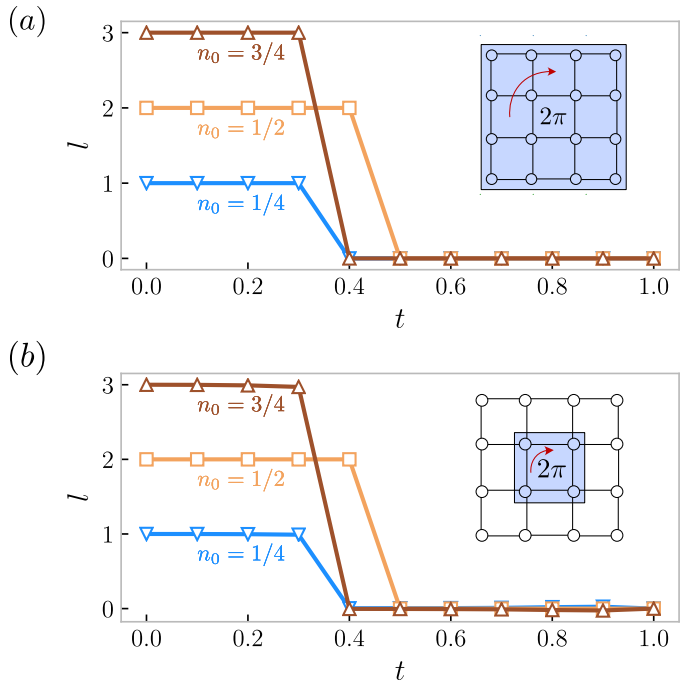

Figure 4.5: **Numerical data of Wen-Zee response.** Angular momentum shift of Hamiltonian (3.1) after inserting a 2π flux through the central plaquette. The numerical data is shown for 4×4 clusters at different commensurate filling factors $n_0 = \{1/4, 1/2, 3/4\}$ with gapped corners. Panel (a) shows the response for a $\pi/2$ rotation of the full lattice and (b) for a partial rotation that only involves the central plaquette.

the angular momentum quantum number modulo four defined by:

$$l = \frac{2}{\pi} \left(\arg \langle C_4 \rangle_{2\pi} - \arg \langle C_4 \rangle_0 \right) \bmod 4, \tag{4.34}$$

where $l = 1, 2, 3$ and the expectation values are taken with respect to the ground states with $|\psi\rangle_{2\pi}$ and without flux insertion $|\psi\rangle_0$, respectively. Thereby, the former state is the ground state of Hamiltonian (4.10) and $|\psi\rangle_0$ is the ground state of Hamiltonian without flux (4.9). We expect that there is only a non-zero shift if the ground state has non-trivial topology, or more precisely, describes one out of three different HOSPT phases with non-zero fractional corner charges. To illustrate the results, let us consider the case $t = 0$, at filling $n_0 = 1/2$ with $|\psi^{\square}_{1/2}\rangle_0$ defined in Eq. (4.2) and

$$\begin{aligned} |\psi^{\square}_{1/2}\rangle_{2\pi} = &\frac{1}{2\sqrt{2}}(-|1100\rangle + |0110\rangle - |0011\rangle + |1001\rangle) \\ &- \frac{i}{2}(|1010\rangle - |0101\rangle). \end{aligned} \tag{4.35}$$

Using Eq. (4.34), we find a non-trivial shift $l = 2$ and, hence, the ground state is topological non-trivial. Analogously, we can understand the response for filling factors $n_0 = 1/4$ and $n_0 = 3/4$. As the quantized Wen-Zee response $\frac{l}{2\pi}\omega \wedge \mathrm{d}A$ is local, a 2π flux insertion changes the configuration of the wave function only within an area spanned by the correlation length around the center. Moreover, the non-trivial topology can already be detected by a partial rotation of a symmetric block of sites around the center (e.g., the central plaquette $\equiv \tilde{C}_4$). Since $\tilde{C}_4$ does generally not commute with the Hamiltonian, except in the limits $t = 0$ and $t = 1$, we find $\langle \tilde{C}_4 \rangle_{2\pi} \sim e^{-\alpha \tilde{\ell}_B} e^{il\frac{\pi}{2}}$, where $\tilde{\ell}_B$ is the linear size of the rotated block and $\alpha > 0$ some constant. The angular momentum shift l extracted from this quantity can still be used to characterize the phases, as shown in Fig. 4.5b. Furthermore, let us emphasize that the partial rotation serves as a bulk invariant as long as the ground state is locally C_4-symmetric. Importantly, it does not depend on a symmetric termination of the lattice.

Experimental realization

We expect that the invariant can be probed in cold atom or ion trap experiments by introducing an artificial U(1) gauge flux created by rotating traps or coherent light–matter interaction and measuring the angular momentum shift implemented by local random unitaries [165–167].

4.3 Entanglement diagnosis for HOSPT phases

The study of many-body entanglement, as obtained from the reduced density matrix $\hat{\rho}_A$ for a bipartition of the system into two disjoint parts A and B, has been shown to be a very useful tool for the characterization of quantum phases of matter [168]. Moreover, the relation between the topological structure and the entanglement spectrum, i.e., the spectrum of the reduced density matrix $\hat{\rho}_A$, has been widely explored [17, 138–144]. Remarkably, most salient topological properties including quasi particle statistics, edge excitations, central charge and topological Berry phase can be readily reached by scrutinizing the entanglement spectrum.

In Ref. [169] it has been proposed that certain HOSPT phases can be characterized by the entanglement spectrum, more precisely, it was suggested that the low-lying eigenvalues e_α of the entanglement Hamiltonian $\hat{\mathcal{H}}$[25] (i.e., the logarithm of the reduced density matrix) reflects the energy spectrum of the in-gap states and, hence, can be treated as a fingerprint of topological phases. However, such straightforward correspondence between bulk topology and entanglement spectrum might not apply to strongly-interacting HOSPT states. First and foremost, some interacting HOSPT states contain a featureless gapped entanglement spectrum, equivalently to their trivial phase counterparts. In addition, the correspondence between the low-lying part of the entanglement spectrum and the bulk topology cannot be taken too literally [143]. Since the reduced density

[25] For free-fermion systems, the spectrum e_α is given by $e_\alpha = -\log \frac{\xi_p}{1-\xi_p}$ where ξ_p are the eigenvalues of the reduced density matrix [170].

matrix is the partition function of the entanglement Hamiltonian (EH) at finite temperatures, the high-energy modes in the entanglement spectrum (ES) also contribute to the intertwined features of the ground state. In particular, the low-lying states of the ES may undergo a phase transition, while the bulk phase remains unchanged [143].

In this section, we analyze the universal features of the many-body EH in various interacting HOSPT phases. It is worthy to emphasize that both the low-lying states and the highly excited part of the ES are responsible for the ground state pattern of HOSPT phases, so there is no reason to overlook the excited states in the EH. To set the stage, we will first establish a Kramers theorem for the EH in HOSPT phases:
If the symmetry operator acting on each C_n corner is projective, then the reduced density matrix with respect to each C_n corner cut exhibits level degeneracies for the whole entanglement spectrum.
However, for generic $C_n \times U(1)$ symmetric HOSPT phases, which do not render a projective symmetry at the corner, the ES upon spatial bipartition might be non-degenerate and, hence, cannot be treated as a fingerprint for HOSPT states. To conquer this obstacle, we introduce a new entanglement property—*higher-order entanglement,* as illustrated in Fig. 4.6b. The basic idea is that we implement further bipartitions for the

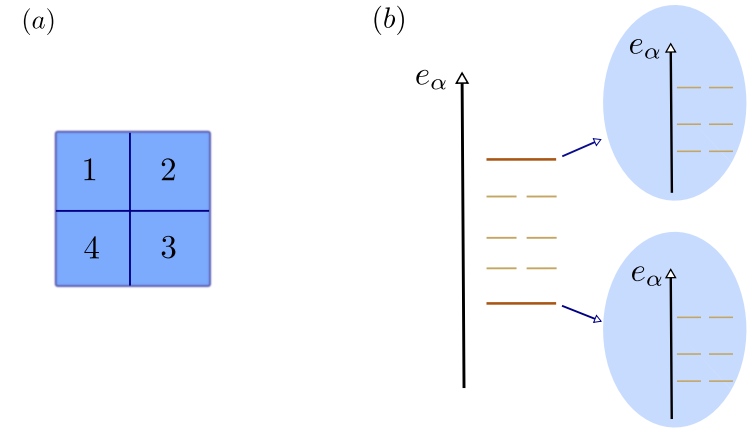

Figure 4.6: **Higher-order entanglement branching structure.** In panel (a) the ground state is divided into four symmetric regions and in (b) the hierarchical sequencing of the entanglement spectrum is shown. First, we trace out region (2-4) to obtain the reduced density matrix for region (1-3). Second, for any single-valued eigenvector of the entanglement Hamiltonian the entanglement spectrum between regions 1 and 3 is calculated, showing a two-fold degeneracy for the full spectrum.

non-degenerate part of the spectrum, which in turn shows degeneracies. This higher-order entanglement branching phenomena is a unique feature of HOSPT phases, and is closely connected to the fractional corner charge and Wen-Zee response. In particular, the higher-order entanglement indicates that the traditional ES is inadequate for characterizing the topological feature of the ground state. A complete viewpoint of the ground state structure requires a hierarchical sequence of the entanglement branch.

4.3.1 Entanglement spectrum for HOSPTs with projective symmetry at the corner

In this part, we explore the ES of HOSPT phases protected by $C_n \times G$ symmetry, in which G renders a projective representation at the C_n corner. For example, the HOSPT phase in the SL-BHM with $\mu = 0$ and $n_0 = 1/2$ has particle (hole) states localized at the corners, which are protected by $\hat{\mathcal{C}}$ (with $\hat{\mathcal{C}}_{xy}^2 = -\mathbb{1}_{xy}$), Eq. (3.4), and C_4 symmetry, respectively. We denote this as the generalized *Kramers theorem* of the entanglement Hamiltonian.

To this end, let us consider a Schmidt decomposition, with Schmidt values $\{\Lambda_\alpha\}$, that cuts out one quadrant of the ground state $|\psi_0\rangle$,

$$|\psi_0\rangle = \sum_\alpha \Lambda_\alpha |A_\alpha\rangle_1 |B_\alpha\rangle_{234}, \tag{4.36}$$

where the regions (1) and (2-3-4) are defined as in Fig. 4.6a. The Schmidt states $\{|A_\alpha\rangle_1\}$ and $\{|B_\alpha\rangle_{234}\}$ form an orthogonal basis of the two parts, respectively (see Fig 4.7). The

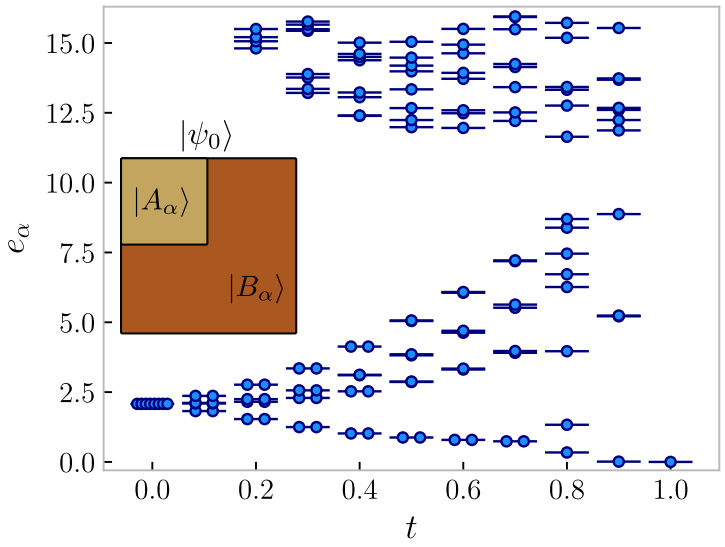

Figure 4.7: **Entanglement spectrum of a corner.** Corner entanglement spectrum for the particle-hole symmetric case ($\mu = 0$) with even degeneracies of the low-energy part in the HOSPT phase with half-charge corner states. The weak symmetry breaking potential at the corners, which we use to obtain a unique ground state, leads to a breaking of degeneracies at higher entanglement energies. In the trivial phase, we obtain a gapped featureless entanglement spectrum.

reduced density matrix $\hat{\rho}_1$ is diagonal in the Schmidt basis $\hat{\rho}_1 = \sum_\alpha \Lambda_\alpha^2 |A_\alpha\rangle_{11}\langle A_\alpha|$ and

the entanglement spectrum is given by $e_\alpha = -2\log\Lambda_\alpha$. We first demonstrate that the Schmidt spectrum is block diagonal in the G basis, provided G is a symmetry of the ground state. Let us act with the symmetry operation G on the ground state such that,

$$G|\psi_0\rangle = \sum_\alpha \Lambda_\alpha G|A_\alpha\rangle_1 G|B_\alpha\rangle_{234}. \tag{4.37}$$

As G is an internal on-site symmetry, it acts on the two regions independently. We then set $G|A_\alpha\rangle_1$ as the new basis for the Schmidt decomposition and by doing so, the reduced density matrix for region (1) is,

$$\hat{\rho}_1 = \sum_\alpha G\Lambda_\alpha^2|A_\alpha\rangle_{11}\langle A_\alpha|G^{-1} = G\hat{\rho}_1 G^{-1}. \tag{4.38}$$

This implies that G commutes with the reduced density matrix $\hat{\rho}_1$ and the Schmidt spectrum is block diagonal with blocks labelled by the symmetry eigenvalues. Now assume G has a projective representation at the corners. We start with a simple example where $G = \hat{\mathcal{C}}$. This is precisely the case in Eq. (3.1) at $\mu = 0$ and $U \to \infty$ ($\equiv$ hardcore bosons). As the reduced density matrix $\hat{\rho}_1$ commutes with $\hat{\mathcal{C}}$, we can regard the EH $\hat{\rho}_1 = e^{-\hat{\mathcal{H}}_1}$ as a many-body system with $\hat{\mathcal{C}}$ symmetry. Since $\hat{\mathcal{C}}$ is projective for each corner, we have $\hat{\mathcal{C}}^2 = -\mathbb{1}$ for $\hat{\rho}_1$, which indicates $\hat{\mathcal{C}}$ is projective when acting on the reduced density matrix with respect to the corner region. Consequently, all eigenstates in the EH come in Kramer pairs. For the last statement to be true, it is crucial that $\hat{\mathcal{C}}$ is antiunitary[26].

Numerical evaluation

To demonstrate the previous result, we take the model in Eq. (3.1) at the $\hat{\mathcal{C}}$ symmetric point $\mu = 0, U \to \infty$, i.e., hardcore bosons at half-filling. In the HOSPT state ($t \to 0$), the corner is decoupled—resulting in a two-fold level degeneracy and in a projective representation of $\hat{\mathcal{C}}$ symmetry at the corner. In numerical simulations, these zero energy states at the corner would unavoidably couple with each other due to finite size effects. To avoid such long-range entanglement from the corner zero modes, we apply a weak local chemical potential at each corner to pin the corner configurations without affecting the bulk. Although $\hat{\mathcal{C}}$ symmetry is weakly broken near the corners, the two-fold degeneracy of the low-lying states in the ES, contributed from the local entanglement near the cut-center, still persists. However, the degeneracy of the highly excited spectrum is slightly lifted as a consequence of the weak symmetry breaking near the corners. In Fig. 4.7 we plot the ES with respect to the relative hopping amplitude t. In the HOSPT phase, the low-lying part of the ES exhibits a robust two level degeneracy. As already mentioned, the high-energy part displays level splitting due to $\hat{\mathcal{C}}$ symmetry breaking at the corners. In the trivial phase, the ES is featureless with a unique ground state.

[26] The antiunitary part is crucial for the proof of Kramers theorem. Assume there is a unique ground state such that $\mathcal{C}|\Psi\rangle = c|\Psi\rangle$. Applying $\mathcal{C}$ twice on this state gives: $\mathcal{C}^2|\Psi\rangle = |c|^2|\Psi\rangle$; however, with $\mathcal{C}^2 = -\mathbb{1}$ this implies $|c|^2 = -1$, which is a contradiction. Hence, there cannot be a unique state.

4.3.2 Higher-order entanglement in HOSPT phases

We will now explore the properties of the entanglement spectrum of HOSPT phases that do not exhibit projective representations at the corners. We begin by demonstrating that the HOSPT model in Eq. (3.1) with $C_4 \times U(1)$ symmetry can host featureless entanglement spectra for any spatial cut away from $\mu = 0$ (i.e., broken particle-hole symmetry). Let us again focus on the reduced density matrix $\hat{\rho}_1$ with respect to the C_4-symmetric quadrant cut in Figs. 4.6a and 4.7. For HOSPT phases with corner charge $Q_{\text{corner}} = 1/4\,(3/4)$, away from the points with fine-tuned t, the ES for region (1) has a unique ground state. This non-degenerate spectrum is a consequence of the broken $\hat{\mathcal{C}}$ symmetry[27]. Thus, the configurations with even or odd number of charges in each quadrant have different weights. Let us consider a typical fixed-point wave function of the HOSPT phases with 1/4 charge at the corner, which can be written as a product of plaquette entangled states, analogously to Eq. (4.1). If we trace out a corner site from the plaquette, the reduced density matrix has unique eigenvalues 1/4 and 3/4, respectively. Meanwhile, if we make a C_4-symmetric cut as shown in Fig. 4.6a by tracing out the

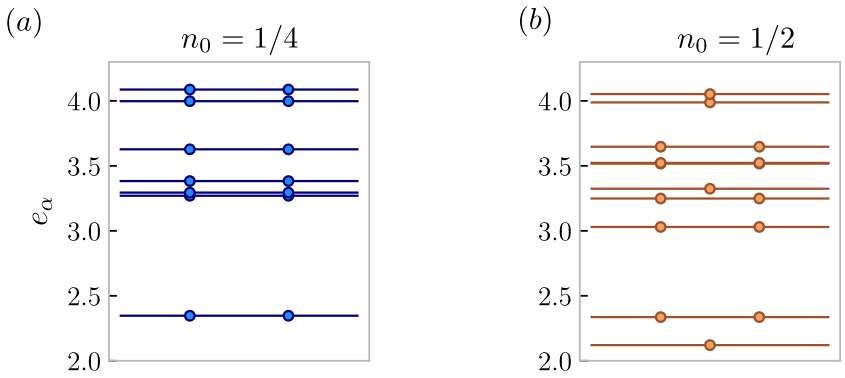

Figure 4.8: **Higher-order entanglement.** Higher-order entanglement spectrum for a C_4-symmetric bipartition (1-3)-(2-4) (see Fig. 4.6a) of the ground state of Hamiltonian (3.1) ($\mu = 0$, $U \to \infty$) by tracing out the two diagonal corners. The simulation is made for $t = 0.1$ with corner charges 1/4 (a) and 1/2 (b), respectively. The latter case shows a featureless entanglement spectrum with a unique ground state.

region (2-4), we find a robust degeneracy and all eigenvalues appear in pairs as shown in Fig. 4.8a. If we, however, consider a HOSPT phase with corner charge $Q_{\text{corner}} = 1/2$, the ES for region (1-3) has unique and degenerate low-lying states (see Fig. 4.8b). To summarize, the traditional ES is insufficient for recognizing generic HOSPT phases, since it provides only limited information about the ground state topology. We therefore introduce a new entanglement property—*higher-order entanglement* with a hierarchical sequence of the ES to categorize distinct HOSPT phases.

[27] Note, such a state can never be particle-hole symmetric since the number of holes and particles is different.

$C_4 \times U(1)$ symmetry

We now elaborate the power of higher-order entanglement branching for HOSPT phases with $C_4 \times U(1)$ symmetry, but the argument can be generalized to any C_{2^n} symmetry. As a starting point, we bipartite the system into two C_4 symmetry related regions (1-3) and (2-4), respectively (see Figs. 4.6a and 4.9a). The Schmidt decomposition for the two regions is given by,

$$|\psi_0\rangle = \sum_\alpha \Lambda_\alpha |A_\alpha\rangle_{13} |B_\alpha\rangle_{24}. \tag{4.39}$$

The two halves are related by symmetry, and thus the Schmidt states are transformed into each other $|A_\alpha\rangle_{13} \leftrightarrow C_4|B_\beta\rangle_{24}$. Since the ground state $|\psi_0\rangle$ is C_4-symmetric, no matrix elements connecting states with different Schmidt eigenvalues Λ_α can occur. A unique Schmidt value Λ_α implies that $|A_\alpha\rangle_{13} = C_4|B_\alpha\rangle_{24}$ with two equal configurations. When $|A_\alpha\rangle_{13} \neq C_4|B_\alpha\rangle_{24}$, the Schmidt spectrum has to be degenerate to ensure that the state is C_4-symmetric. Moreover, as the theory is $U(1)$ symmetric, each Schmidt state has a well-defined charge number. When the HOSPT phase contains fractional corner charges $Q_{\text{corner}} = 1/4\,(3/4)$, the total charge number of the ground state is odd $4N+1\,(4N+3)$. Under this circumstance, the Schmidt states $|A_\alpha\rangle_{13}$ and $|B_\alpha\rangle_{24}$ must have different $U(1)$ charges to ensure that the total charge number is odd. This in turn implies that $|A_\alpha\rangle_{13} \neq C_4|B_\alpha\rangle_{24}$ and, consequently, all Schmidt values Λ_α must be degenerate for a C_4-symmetric ground state $|\psi_0\rangle$.

Higher-order entanglement

When the HOSPT phase contains fractional corner charges $Q_{\text{corner}} = 1/2$, with the total charge being even $4N+2$, it is possible to have unique Schmidt values. For this specific case, the ground state wave function of the $C_4 \times U(1)$ symmetry-protected HOSPT phase is adiabatically connected to two, in the C_4 symmetry center crossing, one-dimensional SL-BHMs along the diagonal and off-diagonal direction, respectively (see also Fig. 2.7). Although the corner still carries fractional charge, there is no entanglement between regions (1-3) and (2-4) resulting in a single-valued ES.

This is where the higher-order entanglement becomes crucial: We first separate the Schmidt spectrum into a degenerate part (with $|A_\alpha\rangle_{13} \neq C_4|B_\alpha\rangle_{24}$) and a unique part (with $|A_\alpha\rangle_{13} = C_4|B_\alpha\rangle_{24}$), as shown in Fig. 4.9a. Let us further bipartite each unique Schmidt state to obtain a hierarchical sequence of the higher-order ES (see Fig. 4.9b),

$$|A_\alpha\rangle_{13} = \sum_\gamma \Lambda_\gamma |C_\gamma\rangle_1 |D_\gamma\rangle_3. \tag{4.40}$$

Note that equivalently we could have considered the corresponding state $|B_\alpha\rangle_{24}$. The two halves are related by $C_2 = C_4^2$ symmetry and, consequently, the Schmidt states are transformed into each other $|C_\gamma\rangle_1 \leftrightarrow C_2|D_\delta\rangle_3$ with $\Lambda_\gamma = \Lambda_\delta$. Moreover, all unique Schmidt states $|A_\alpha\rangle_{13}$ must have charge number $2N+1$ to guarantee the total charge of the ground state is $4N+2$. Thus, we can use a similar argument to show that all Schmidt

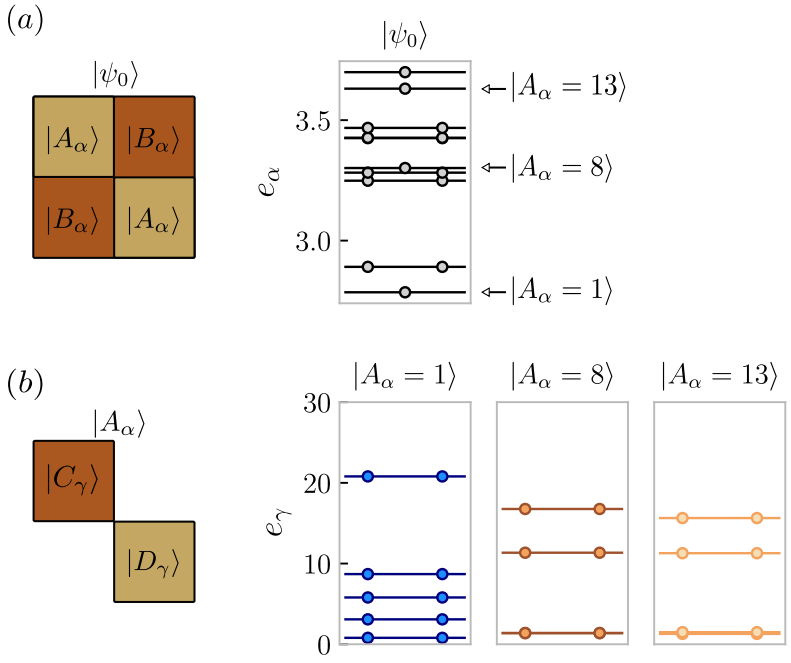

Figure 4.9: **Higher-order entanglement spectrum.** Entanglement spectra of the HOSPT phase with half-corner charge at $t = 0.1$. (a) Entanglement spectrum for a bipartition in which the two parts are related by the C_4 symmetry. (b) Higher-order entanglement branches of the unique Schmidt states with exact degeneracies.

values must come in degenerate pairs. In particular, there cannot be a single state in the decomposition with $|C_\gamma\rangle_1 = C_2|D_\gamma\rangle_3$ and, thus, the entire spectrum must be degenerate. The argument flows as follows: If there is a single state with $|C_\gamma\rangle_1 = C_2|D_\gamma\rangle_3$, then $|C_\gamma\rangle_1$ should carry 1/2 charge number to guarantee the total charge for $|A_\alpha\rangle_{13}$ being odd. However, as the elementary charge is an integer, half charges only appear as a cat state $|0\rangle + |1\rangle$ and, consequently, breaking $U(1)$ symmetry. Numerically, as shown in Fig 4.9, we confirmed the expected higher-order entanglement branching structure for the SL-BHM defined in Eq. (3.1).

Generalizations to C_{2^n}

A similar argument holds for C_{2^n} symmetric HOSPT phases: The entanglement branching structure is similar, but we just need to duplicate the bipartition step further as the initial Schmidt spectrum might contain a series of non-degenerate eigenstates. If we take such state out and redo the bipartition $n-1$ times, the resultant n-th order spectrum should always contain two-fold degeneracies. In particular, it is worth emphasizing that if we merely make a C_{2^n} symmetric corner cut and calculate the ES of that region, the ES may not display any robust degeneracy. This is obvious for the plaquette entangled state $|\psi^{\square}_{3/4}\rangle$ defined in Eq. (4.3) with ES eigenvalues 1/4 and 3/4, respectively.

4.4 Summary & Outlook

In this chapter, we took two different routes to characterize higher-order topology in strongly-interacting models, such as the two-dimensional SL-BHM. Thereby, starting from the higher-order Zak (Berry) phase, we derived a topological many-body invariant that characterizes HOSPTs by revealing a non-commutative algebra with C_n rotations that is closely related to fractional corner charges found in the previous chapter (Chap. 3). The interplay of electromagnetic and gravitational degrees of freedom is described by the discrete Wen-Zee response. To study the corresponding topological field theory, we first argued that lattice defects such as disclinations are a source of curvature and in a continuum description are closely related to the spin-connection[28]. Finally, using exact diagonalization of small clusters, we demonstrated the practical relevance of the many-body invariant.

Second, we studied the entanglement spectrum of HOSPT phases and revealed its non-trivial relation to fractional corner charges as well as the discrete Wen-Zee response. To this end, we first considered the entanglement spectrum of HOSPTs that have an additional symmetry rendering projective representations at the corners and established a generalized Kramers theorem. Further, we introduced a new concept called higher-order entanglement, to scrutinize and differentiate various higher-order topological phases from a hierarchical sequence of the entanglement structure. Namely, certain HOSPTs, upon a C_n-symmetric bipartition, have at first-order a featureless entanglement spectrum, that is, the spectrum contains both; degenerate and non-degenerate Schmidt states. However, if a HOSPT phase is non-trivial, we showed that if we further bipartite non-degenerate Schmidt states, we finally obtain a fully degenerate entanglement spectrum.

Outlook. So far, we studied the discrete Wen-Zee response only for a particular model; however, as several times said, we believe that the Ansatz is true in general and holds for all $U(1) \times C_n$ symmetric HOSPTs. To this end, it might be useful to study another concrete example. Alternatively, another route we could take is to study HOSPTs in higher dimensions and ask, to which extent those ideas can be generalized. Definitely, all of those are certainly valid questions/thoughts; however, at this stage we are mostly interested in another point: Although we made a significant step forward in finding a bulk-boundary correspondence, we have not yet found a relation that equates changes of the fractional corner charge and the higher-order Zak (Berry) phase, similar to the one-dimensional case (see Sec. 3.3.4). A first step towards such a relation is shown in the next chapter.

[28] Recall, the spin-connection forms the second gauge field in the field theory description of the Wen-Zee response.

Chapter 5

Thouless pumps and bulk-boundary correspondence in higher-order symmetry-protected topological phases

Protected (gapless) modes on submanifolds of topological phases of matter are a characteristic phenomenon of such states. For one-dimensional systems such as the SSH model, charge accumulation at the 0D boundary results from a non-trivial bulk polarization, which, discovered by King-Smith and Vanderbilt [171], was shown to be a manifestation of the Zak (Berry) phase of the underlying Bloch bands [102, 172]. Resta generalized this soon to interacting many-body systems with periodic boundaries by relating the polarization to the many-body position operator and the generalized Zak (phase) [45] (see also Sec. 3.3.4). Intuitively, the bulk-boundary correspondence for such systems can be understood as follows: Changing the bulk polarization is intimately linked to changes of the charges residing at the boundary. Such quantized charge transport is exactly described by topological Thouless pumps [29, 173–177].

As we have seen in Chap. 3 the one-dimensional SL-BHM at half-filling is characterized by a filling anomaly resulting in fractional edge charges, which are in one-to-one correspondence with a bulk polarization [29, 177]. Since the construction of the 1D and 2D system is closely connected, it is tempting to believe that such bulk-boundary correspondence can be straightforwardly generalized. As partially discussed in Chap. 3, there were proposals by recent works [129, 130] that tried to generalize the many-body polarization of Resta to a many-body quadrupole operator; however, these approaches have sparked controversy for $U(1)$ conserving systems [131] because the definition of such operator has led to inconsistent results.

Although we saw that the C_4 higher-order Zak (Berry) phase and the fractional corner charge signal non-trivial topology of the 2D SL-BHM, there has been no exact correspondence between those two invariants so far. As a first step towards such relation, we introduce a simplified version of a higher-order Zak (Berry) phase that, however, is only well-defined for HOSPTs with hardcore bosons at half-filling. Nevertheless, by extending the ideas of Resta's seminal work [45] to higher-order topology, upon using Thouless pumps and quantized charge transports, we can find an exact correspondence between a topological bulk invariant and fractional corner charges—obtaining a *bulk-boundary correspondence* for strongly-interacting higher-order topological systems.

Overview. This chapter is based on [P3] and divided into four main sections: In the

first part, Sec. 5.1, we reconsider the C_4 higher-order Zak (Berry) phase introduced by Ref. [128] and consider peculiarities of the invariant as we approach the thermodynamic limit. To resolve these, we introduce a new kind of boundary conditions so-called *Corner Periodic Boundary Conditions* (CPBC), upon which we construct a simplified $\mathbb{Z}_2$ quantized higher-order Zak (Berry) phase.

Further, in Sec. 5.2 we consider two different Thouless pumps connecting topologically distinct HOSPT phases and characterize the charge transport in terms of four Chern numbers that are directly linked to the windings of the $\mathbb{Z}_2$ higher-order Zak (Berry) phases, defined for each corner. Thereby, the Chern numbers have to fulfill a sum rule to guarantee net charge conservation. Moreover, we briefly argue that the $\mathbb{Z}_2$ higher-order Zak (Berry) phase can characterize Thouless pumps even at finite interaction strength, although its quantizing symmetry is broken. This section ends with a numerical case study of Thouless pumps of the SL-BHM and a brief discussion on quadrupole operators, based on insights we obtained from the Thouless pumps.

Section 5.3 is at the heart of this chapter, since it proves the bulk-boundary correspondence by extending Resta's idea [45] to higher-order topological systems. Moreover, using an adiabatic expansion, we can relate the change of the corner charge during one cycle to a current through the corner, which is sensed by the $\mathbb{Z}_2$ higher-order Zak (Berry) phase introduced at this corner. Moreover, to build on this, using a half-Thouless pump cycle, we can directly relate a non-trivial, quantized change of the $\mathbb{Z}_2$ higher-order Zak (Berry) phase to the emergence of quantized fractional corner charges.

Lastly, in Sec. 5.4 we shortly discuss a possible extension of the bulk-boundary correspondence for the C_4 higher-order Zak (Berry) phase, which we extensively discussed in Chap. 3. Thereby, we shed light on aspects that directly generalize and sketch a possible way how the bulk-boundary correspondence remains true for this invariant—although we have not worked out the details yet.

5.1 The higher-order Zak (Berry) phase revised

In the previous chapters we have seen that the higher-order Zak (Berry) phase introduced by Ref. [128] distinguishes the topologically distinct HOSPT phases of the 2D SL-BHM at different fillings. However, up to this point, we have not yet justified that this invariant is actually well-defined if we approach the thermodynamic limit. To this end, we start in this section with discussing certain difficulties of the higher-order Zak (Berry) phase as we approach $L \to \infty$. Then, we present a possible solution to overcome these problems by defining new boundary conditions, and finally we introduce a simplified higher-order Zak (Berry) phase quantized for HOSPTs with $U(1) \times \mathbb{Z}_2 \times C_4$ symmetry using two different gauge choices.

5.1.1 Deficiencies of the higher-order Zak (Berry) phase

In Chap. 3 we showed that the higher-order Zak (Berry) phase can be obtained from twisting the central plaquette of the many-body Hamiltonian (see Fig. 3.4). Although there is a zero flux condition for the central plaquette, there is, however, non-zero flux

in the neighboring plaquettes, which can be seen from Fig. 3.4. For finite systems, this is not problematic because there is always a finite gap[1]; however, for infinite systems, $L \to \infty$, we are not guaranteed that the bulk gap under flux insertion remains finite. If the bulk gap was not finite in the thermodynamic limit, that would imply that the higher-order Zak (Berry) phase is not a genuine topological invariant. One solution to this problem would be to find a gauge transformation that distributes the local twists over many links such that locally the flux is proportional to $\sim 1/L$ and, hence, locally the flux vanish as we approach the thermodynamic limit. However, here we will present another solution, namely, introducing new boundary conditions.

5.1.2 Corner periodic boundary conditions

To circumvent the previous problem of inserting finite flux in the bulk, we introduce new boundary conditions so-called *Corner Periodic Boundary Conditions* (CPBC) connecting only the links at the corners, as displayed in Fig. 5.1. Compared to PBC, such a

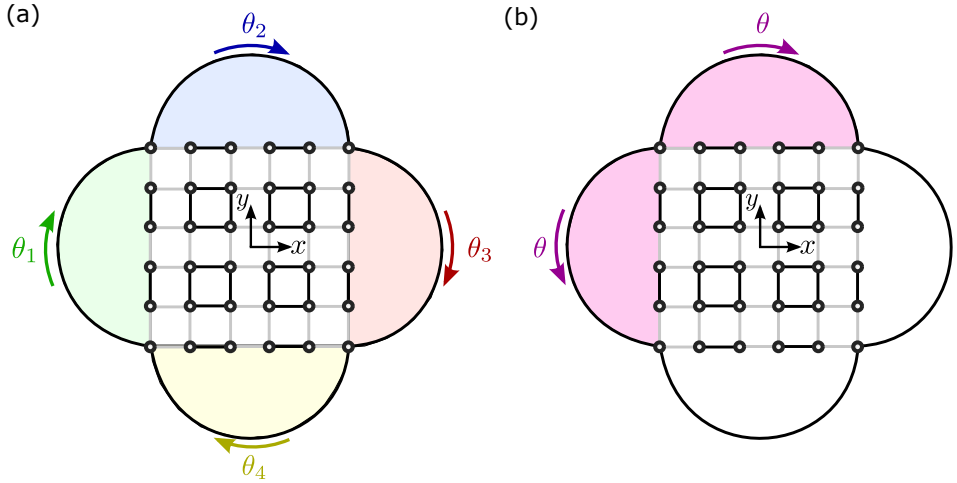

Figure 5.1: **CPBC and higher-order Zak (Berry) phases.** Corner periodic boundary conditions for the 2D SL-BHM, with fluxes (shaded regions) at the corner-connecting links. Compared to PBC, such a system has edges. (a) If we apply the construction of the higher-order Zak (Berry) phase of Ref. [128] to the corner-connecting links, then we are guaranteed to not introduce flux in the bulk of the system. Panel (b) shows the $\mathbb{Z}_2$ higher-order Zak (Berry) phase. Only two out of our links are twisted, and there is only a single parameter θ.

system has edges and, consequently, we can clearly distinguish bulk and edge properties. Moreover, this allows us to move the Ansatz of Ref. [128] to the outside of the system, which guarantees that there is no flux in the bulk of the system and renders the higher-

[1] Clearly, there are exceptions. In particular, there might be level crossings due to changes of quantum numbers.

order Zak (Berry) phase to be a well-defined, genuine topological invariant as $L \to \infty$. However, this Ansatz has also drawbacks, in particular, for fillings $n_0 \in \{1/4, 3/4\}$. While for the half-filled case the edges in the thermodynamic limit are well-defined, the situation is different for other fillings. Here we must add terms to the boundary that, on one hand, ensure the correct filling, and, on the other hand, keep edges gapped as $L \to \infty$.

5.1.3 A $\mathbb{Z}_2$ quantized higher-order Zak (Berry) phase

For studying a bulk-boundary correspondence, we first introduce a simplified higher-order Zak (Berry) phase that distinguishes the HOSPTs of the SL-BHM for hardcore bosons at half-filling. In Sec. 3.1 we showed that the SL-BHM in this limit has two additional antiunitary symmetries. One of those we denoted by $\hat{\mathcal{S}}$, Eq. (3.4), which has the property that $\hat{\mathcal{S}}^2_{x,y} = \mathbb{1}$. For what follows, we redefine this operator, namely, we remove the operation of complex conjugation in the definition and consider it as a unitary $\mathbb{Z}_2$ symmetry, i.e., $\hat{\mathcal{S}}^{-1} i \hat{\mathcal{S}} = i$. However, the action on local operators is unchanged and given as follows: $\hat{b}^\dagger_{x,y} \leftrightarrow \hat{b}_{x,y}$[2].

Construction of the $\mathbb{Z}_2$ higher-order Zak (Berry) phase

The construction is similar to the higher-order Zak (Berry) phase introduced in Sec. 3.3.2. To this end, we decompose the Hamiltonian into two parts $\hat{H}^{CPBC} = \hat{H}^{OBC} + \hat{H}^{C}$, where $\hat{H}^{C}$ contains the corner-connecting links and $\hat{H}^{OBC}$ is defined in Eq. (3.1). If we label the corners counter-clockwise, starting from the upper-left corner, then this Hamiltonian is given by[3]

$$\hat{H}^{\mathrm{C}} = -t \left(\hat{a}^\dagger_{c_1} \hat{a}_{c_2} + \hat{a}^\dagger_{c_2} \hat{a}_{c_3} + \hat{a}^\dagger_{c_3} \hat{a}_{c_4} + \hat{a}^\dagger_{c_4} \hat{a}_{c_1} + \mathrm{h.c.} \right). \tag{5.1}$$

The phase twist is then introduced by applying the gauge transformations $\hat{U}_i$, $i \in \{1, 2, 3, 4\}$ on $\hat{H}^{C}$ *only*:

$$\hat{H}^{\mathrm{C}}_i(\theta) = \hat{U}^\dagger_i(\theta) \hat{H}^{\mathrm{C}} \hat{U}_i(\theta), \tag{5.2}$$

with $\hat{U}_i(\theta) = e^{i\theta \hat{n}_{c_i}}$. Here $\hat{n}_{c_i}$ is the particle number operator at the i-th corner. Since there are four corners, there are four possible ways to introduce the phase twist, as shown in Fig. 5.2. Although C_4 is not crucial for the quantization of this phase, it, nevertheless, relates different gauge choices $C_4 : \hat{U}_i \to \hat{U}_{i+1}$, where rotations are defined counter-clockwise. Compared to the C_4-quantized higher-order Zak (Berry) phase, this simplified version depends entirely on a single parameter. Again, we have a zero flux condition, namely, summing up all phase factors along the corner-connecting links results in zero total flux. Finally, the $\mathbb{Z}_2$ higher-order Zak (Berry) phase is evaluated via the following formula:

$$\gamma_i = i \int_0^{2\pi} \mathrm{d}\theta \, \langle \psi_i(\theta) | \partial_\theta | \psi_i(\theta) \rangle \, . \tag{5.3}$$

[2] Recall that for hardcore bosons we use a different notation.
[3] Since this is true for any value of U we use the general notation of bosonic operators.

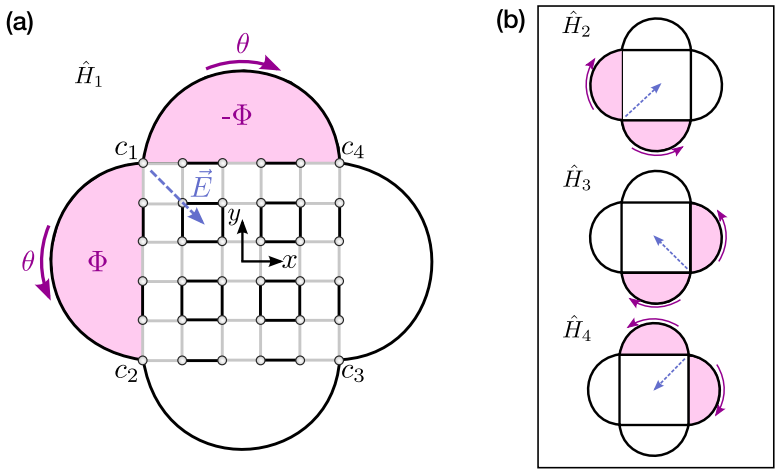

Figure 5.2: **Direction-dependent sensing of charge flow.** Model with corner-periodic boundary conditions (CPBC). We propose four gauge choices $\hat{U}_1$ (a), $\hat{U}_2$, $\hat{U}_3$, $\hat{U}_4$ (b) that are connected by C_4-symmetry, Eq. (5.2). The higher-order Zak (Berry) phases defined on these choices act as sensors of charge flow. They are only sensitive in the direction of the electric field (blue) that is induced when the flux in the outer super-cells becomes time-dependent.

Quantization of the $\mathbb{Z}_2$ higher-order Zak (Berry) phase

To show quantization of the $\mathbb{Z}_2$ higher-order Zak (Berry) phase, we assume $U \to \infty$ and use that the twisted Hamiltonians transforms under $\hat{\mathcal{S}}$ as follows[4]:

$$\hat{\mathcal{S}}\hat{H}_i^{CPBC}(\theta)\hat{\mathcal{S}} = \hat{H}_i^{CPBC}(-\theta), \tag{5.4}$$

which implies that $\hat{\mathcal{S}}\,|\psi_i(\theta)\rangle = e^{i\varphi(\theta)}\,|\psi_i(-\theta)\rangle$. Using this, we obtain:

$$\begin{aligned}\gamma_i =& i\int_0^{2\pi} \mathrm{d}\theta\, \langle\psi_i(\theta)|\hat{\mathcal{S}}^2\partial_\theta|\psi_i(\theta)\rangle \\ =& i\int_0^{2\pi} \mathrm{d}\theta\, \langle\psi_i(-\theta)|\partial_\theta|\psi_i(-\theta)\rangle - \int_0^{2\pi} \mathrm{d}\theta\, \partial_\theta\varphi(\theta) \\ =& -\gamma_i + 2\pi\mathbb{Z},\end{aligned} \tag{5.5}$$

which implies that $2\gamma_i = 0 \mod 2\pi$ and consequently $\gamma_i \in \{0, \pi\}$[5]. Indeed, as shown in Fig. 5.3, we see that the $\mathbb{Z}_2$ higher-order Zak (Berry) phase distinguishes the two topologically inequivalent phases of the SL-BHM at half-filling and $U \to \infty$. Thereby,

[4] Note that $\hat{\mathcal{S}}^2 = \mathbb{1}$.
[5] In the last step of the derivation we used that $|\psi_i(\theta + 2\pi)\rangle = |\psi_i(\theta)\rangle$.

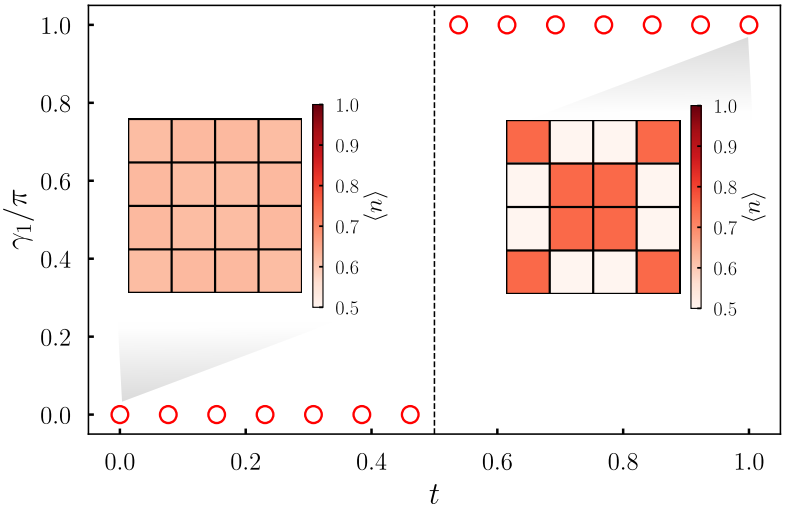

Figure 5.3: **Quantized $\mathbb{Z}_2$ higher-order Zak (Berry) phase.** We show γ_1 (γ_2,γ_3 and γ_4 look identical) as a function of the tunneling parameter t at half-filling ($N = L^2/2$) and with CPBC for $L = 4$. The insets show the density expectation values of a 4×4 system at filling $N = L^2/2+2$. Even though the non-trivial phase ($t > 0.5$) does not exhibit any corner states due to CPBC, the two extra particles above half-filling lead to an occupation imbalance between edge doublets and bulk plaquettes that is unique to the non-trivial phase.

C_4 symmetry ensures that the $\mathbb{Z}_2$ higher-order Zak (Berry) phases on each corner are the same, i.e., $\gamma_1 = ... = \gamma_4 \bmod 2\pi$.

A different gauge choice

Later, in Sec. 5.3 we prove a rigorous bulk-boundary correspondence for the $\mathbb{Z}_2$ higher-order Zak (Berry) phase. However, this necessitates that we are able to apply perturbation theory, which requires the phase twists locally to be of order $\sim 1/L$. To this end, we use the degree of freedom that there are many ways of how we can introduce the phase twists into the system (cf. Sec. 2.2.1). Up to this point, we chose to twist the corner-connecting links; however, choosing another gauge transformation $\hat{V}_i(\theta)$—defined with respect to each corner—we can distribute the phase twists over all hoppings in a triangle T_i spanned by the corners $c_{i-1} \leftarrow c_i \rightarrow c_{i+1}$. This is graphically shown in Fig. 5.4 (for $i = 1$). Thereby, as desired, each phase twist is of order $\sim 1/L$. For the triangle T_1, for example, the gauge transformation is given by

$$\hat{V}_1(\theta) = \exp\left(i\frac{\theta}{L}\hat{X}_1\right), \quad \hat{X}_1 = \sum_{x,y\in T_1} f_{x,y;1}\hat{n}_{x,y}, \quad f_{x,y;1} = (y-x). \tag{5.6}$$

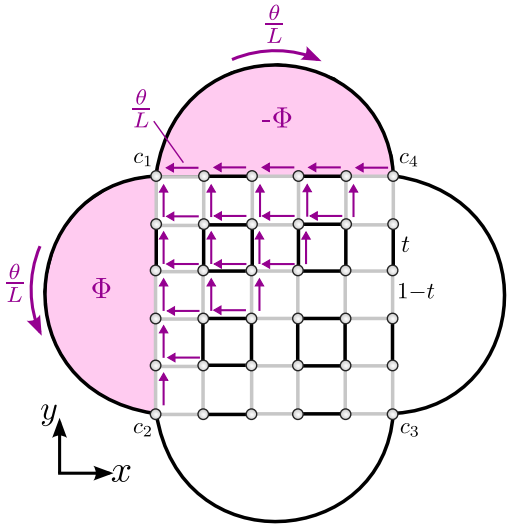

Figure 5.4: **A different gauge choice.** In the new gauge, the phase twist is distributed over all hoppings contained in the upper triangle T_1 spanned by the corners $c_2 \leftarrow c_1 \rightarrow c_4$. Each hopping is modulated by a phase factor with angle θ/L. The direction is such that a particle hopping from right (bottom) to left (top) acquires a phase factor $e^{i\theta/L}$. Inside the bulk there is no flux, but there is a flux $\Phi = \theta$ in the outer rings formed by CPBC. The gauge transformations for the other triangles can be obtained by applying C_4 symmetry on this configuration.

Other triangles and gauge choices can be obtained from applying C_4 rotations counter-clockwise. The new Hamiltonian, obtained from this gauge choice, reads:

$$\hat{H}_{i;V}^{CPBC}(\theta) = \hat{V}_i(\theta)\hat{H}_i^{CPBC}(\theta)\hat{V}_i^{\dagger}(\theta). \tag{5.7}$$

Note, unlike $\hat{H}_i^{CPBC}(\theta)$, this Hamiltonian is not invariant under a shift of 2π, instead: $\hat{H}_{i;V}^{CPBC}(\theta + 2\pi) = \hat{V}_i(2\pi)\hat{H}_{i;V}^{CPBC}(\theta)\hat{V}_i^{\dagger}(2\pi)$. After applying the gauge transformation to the Hamiltonian, the resulting $\mathbb{Z}_2$ higher-order Zak (Berry) phase experiences a non-trivial shift:

$$\gamma_{i;V} = \gamma_i - \int_0^{2\pi} \mathrm{d}\theta \, \langle\psi_i(\theta)|\frac{\hat{X}_i}{L}|\psi_i(\theta)\rangle \, . \tag{5.8}$$

However, by applying the same trick as shown in Eq. (5.5), it is easily derived that the shift, in the presence of $\hat{\mathcal{S}}$ symmetry, is quantized and given by,

$$\int_0^{2\pi} \mathrm{d}\theta \, \langle\psi_i(\theta)|\frac{\hat{X}_i}{L}|\psi_i(\theta)\rangle = \frac{\pi}{L}\sum_{x,y\in T_i} f_{x,y;i}. \tag{5.9}$$

Although individual values of the $\mathbb{Z}_2$ higher-order Zak (Berry) phase are shifted, the difference is unchanged, i.e., $\Delta\gamma_i = \Delta\gamma_{i;V} \bmod 2\pi$, which is sufficient because in actual experiments only differences are accessible [172].

5.2 Introduction to Thouless pumps and their application

A *Thouless pump* is a cyclic adiabatic variation of external parameters along a symmetry breaking path. If the path encircles a gapless point (or region) separating two topologically distinct quantum phases, then it leads to quantized charge transport that characterizes the topology of the bulk [29, 173–177]. Before we proceed, let us briefly explain the keywords: The path must be *cyclic* because to characterize the topology of the path, using Chern numbers, we need to have a two-dimensional compact manifold such as a torus, which is defined by the corresponding parameters. For example, for non-interacting systems, the parameter space is usually given by the 2D Brillouin zone [71, 178]. Further, the path must be *adiabatic*[6] since we want to relate changes of ground state properties to Chern numbers. Moreover, by definition, such a path only exists if we explicitly *break those symmetries* that distinguish the two topologically distinct phases (see Sec. 2.1.2). Lastly, it is important that the path *encircles* the gapless point/region. From a physical standpoint, we can interpret this as a source of flux, which is quantized, if integrated over a compact manifold. Otherwise, the Chern number can be rewritten as a winding number of the $\mathbb{Z}_2$ higher-order Zak (Berry) phase. A curve not encircling the gapless point/region can be continuously shrunk to a point. Clearly, such a path cannot have a non-trivial winding number.

For the 2D SL-BHM, the pumping cycle consists of a closed trajectory in a Δ-t parameter space characterized by a single parameter λ. The path crosses two $\mathbb{Z}_2$-symmetric (as well as C_4-symmetric) points and avoids—by explicit symmetry breaking—closing the bulk gap, see Fig. 5.5b. Here, Δ controls the strength of additional on-site potentials. The arrangement of the local density terms dictates the direction of the charge transport, while the $\mathbb{Z}_2$ higher-order Zak (Berry) phases serve as direction dependent sensors of charge flow (see Fig. 5.2).

In this section, we first introduce the pumping procedures, which are used to investigate the quantized charge transport in the 2D SL-BHM. Second, we discuss how to characterize Thouless pumps using Chern numbers and their relation to the $\mathbb{Z}_2$ higher-order Zak (Berry) phase and charge transport. Lastly, we consider a concrete case study of the 2D SL-BHM on small clusters using exact diagonalization. From these results, we briefly argue why a quadrupole operator cannot characterize the HOSPTs of the 2D SL-BHM.

5.2.1 Pumping procedures

In this part, we introduce two different pumping procedures, from which we gain inside into the topology of the 2D SL-BHM at half-filling and $U \to \infty$.

[6] i.e., at each point along the path the system is in its instantaneous ground state and there is a finite gap to the excited states.

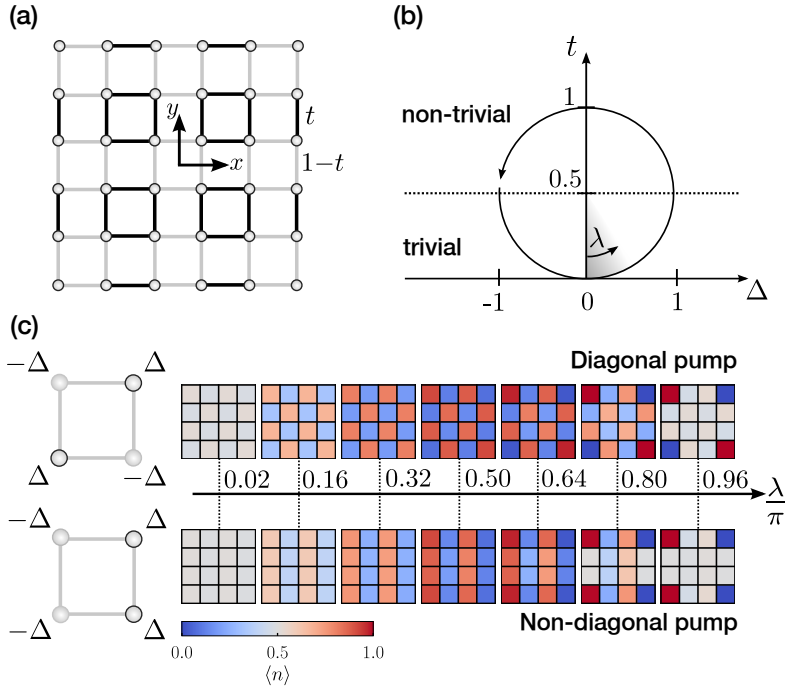

Figure 5.5: **Thouless pumps in the 2D SL-BHM.** (a) Interacting bosons on a square lattice with staggered tunneling (strengths t and $1-t$, respectively) and OBC. (b) Thouless pump parametrized by $\lambda \in [0, 2\pi)$, as defined in the text, with Δ controlling additional on-site potentials shown in (c). (c) Density evolution during a diagonal (upper panel) and a non-diagonal (lower panel) half-Thouless pump cycle, ending in a quadrupole and a dipole configuration, respectively. On the left, the corresponding arrangements of the additional on-site potentials are sketched: For creating a diagonal Thouless pump, we add in each plaquette shifts of equal sign on diagonally opposite sites. For creating a non-diagonal Thouless pump, we add shifts of the same sign on the same side.

Diagonal Charge transport (diagonal pump)

For the diagonal pump, each plaquette is decorated with on-site potentials in a cross-diagonal arrangement, Fig. 5.5c top left. The corresponding Hamiltonian is defined as follows:

$$\hat{H}^{CPBC}_{i;\mathrm{diag}}(\lambda,\theta) = \hat{H}^{OBC}(\lambda) + \hat{H}^{C}_{i}(\lambda,\theta) + \Delta(\lambda) \sum_{x,y=-D}^{D} (-1)^{[(x+D)+(y+D)]} \hat{n}_{x,y}, \qquad (5.10)$$

where $D = (L-1)/2$[7]. The parameter θ is associated to the $\mathbb{Z}_2$ higher-order Zak (Berry) phase, while λ controls the pump procedure. The subscript "i" tells us on which corner

[7]These coordinates are measured from the C_4 symmetry center placed in the center of the lattice.

we introduce the phase twist, as shown in Fig. 5.2. The trajectory in Δ-t parameter space is a shifted circle with $t(\lambda) = (1+\cos\lambda)/2$ and $\Delta(\lambda) = \sin\lambda$ (see Fig. 5.5b). If we apply this pumping procedure for a Hamiltonian with open boundary condition at half-filling and track the density evolution over a half-cycle, then charge accumulates such that there is a quadrupole configuration, which is displayed in Fig. 5.5c. All corners carry fractional charge, where the sign of fractional charges on diagonally opposite corners is different. In total, there are two fractional charges with positive $+1/2$ and two with negative sign $-1/2$, respectively.

Symmetry transformations. For finding a sum rule of the four Chern numbers associated to each corner, and a characterization of the half-cycle, it is useful to study how Hamiltonian (5.10) transforms under symmetries. Indeed, the arrangement of local density terms in Hamiltonian (5.10) transforms nicely under C_4 symmetry (setting $\theta = 0$), namely,

$$C_4 : \hat{H}^{CPBC}_{\text{diag}}(\lambda) \to \hat{H}^{CPBC}_{\text{diag}}(-\lambda). \tag{5.11}$$

Similarly, it transforms under $\hat{\mathcal{S}}$, which, however, leads to a constant shift,

$$\hat{\mathcal{S}} : \hat{H}^{CPBC}_{\text{diag}}(\lambda) \to \hat{H}^{CPBC}_{\text{diag}}(-\lambda) + \text{const.} \tag{5.12}$$

resulting from $\hat{\mathcal{S}} : \hat{n}_{x,y} \to \mathbb{1}_{x,y} - \hat{n}_{x,y}$.

Horizontal charge transport (non-diagonal pump)

For the second procedure, each column has the same sign of the on-site potentials. The corresponding Hamiltonian reads:

$$\hat{H}^{CPBC}_{i;\text{hor}}(\lambda,\theta) = \hat{H}^{OBC}(\lambda) + \hat{H}^{C}_{i}(\lambda,\theta) - \Delta(\lambda) \sum_{x,y=-D}^{D} (-1)^{(x+D)} \hat{n}_{x,y}. \tag{5.13}$$

The parameters have the same parametrization as previously. However, this time, if we track the density for a system with open boundary conditions over a half-cycle, then the final charge configuration has the form of a dipole, i.e, on the left the two corners carry fractional charge with positive sign $+1/2$, while the corners on the right have a particle missing and, thus, carry a fractional charge with a negative sign $-1/2$.

Symmetry transformations. Likewise to the previous path, this trajectory transforms nicely under $C_2 = C_4^2$ symmetry with $(\theta = 0)$:

$$C_2 : \hat{H}^{CPBC}_{\text{hor}}(\lambda) \to \hat{H}^{CPBC}_{\text{hor}}(-\lambda), \tag{5.14}$$

while for $\hat{\mathcal{S}}$, we again obtain a constant shift,

$$\hat{\mathcal{S}} : \hat{H}^{CPBC}_{\text{hor}}(\lambda) \to \hat{H}^{CPBC}_{\text{hor}}(-\lambda) + \text{const.}. \tag{5.15}$$

5.2.2 Characterization of Thouless pumps

Here, we first argue that the four Chern numbers characterizing the Thouless pump are the winding numbers of the $\mathbb{Z}_2$ higher-order Zak (Berry) phases. Second, we show how charge transport and Chern numbers are related. Using the symmetry properties of the pumping procedures and the $\mathbb{Z}_2$ higher-order Zak (Berry) phases, we relate the fractional corner charge to the $\mathbb{Z}_2$ higher-order Zak (Berry) phase. Lastly, we argue that although the global $\mathbb{Z}_2$ symmetry for softcore bosons, i.e., $U < \infty$ is broken, the $\mathbb{Z}_2$ higher-order Zak (Berry) phase can still be used to characterize the Thouless pumps.

Chern numbers and the $\mathbb{Z}_2$ higher-order Zak (Berry) phases

In seminal works [173–176] Thouless, Niu and others showed that the many-body Chern number for a two parameter dependent wave function, $|\psi(\lambda,\theta)\rangle$, where parameter space defines a torus, $(\lambda,\theta) \in T^2$, can be written as:

$$C_i = \frac{i}{2\pi}\int_0^{2\pi} \mathrm{d}\lambda \int_0^{2\pi} \mathrm{d}\theta \ \left(\langle\partial_\lambda\psi_i(\lambda,\theta)|\partial_\theta\psi_i(\lambda,\theta)\rangle - \langle\partial_\theta\psi_i(\lambda,\theta)|\partial_\lambda\psi_i(\lambda,\theta)\rangle\right) \tag{5.16}$$

where the subscript on the Chern number is explained soon. This integral formula is precisely the flux of the Berry curvature through the surface of a compact manifold [71, 178] and, thus, integer quantized $C \in \mathbb{Z}$. On the other hand, using that $\langle\partial_\theta\psi_i(\lambda,\theta)|\psi(\lambda,\theta)\rangle = -\langle\psi_i(\lambda,\theta)|\partial_\theta\psi(\lambda,\theta)\rangle$, the Chern number reads:

$$C_i = \frac{i}{2\pi}\int_0^{2\pi} \mathrm{d}\lambda\, \partial_\lambda \int_0^{2\pi} \langle\psi_i(\lambda,\theta)|\partial_\theta|\psi_i(\lambda,\theta)\rangle = \frac{1}{2\pi}\int_0^{2\pi} \mathrm{d}\lambda\, \partial_\lambda\gamma_i(\lambda), \tag{5.17}$$

which is nothing else than the winding number of the i-th $\mathbb{Z}_2$ higher-order Zak (Berry) phase. Note that in the definition of the Chern number we could have also used $\gamma_{i;V}$ because the shift, defined in Eq. (5.8), is gauge-invariant and, thus, periodic in $\lambda \to \lambda + 2\pi$.

Sum rule. The sum over all four Chern numbers of the diagonal and horizontal pump is zero, which can be deduced from the symmetry properties of the paths defined in Eq. (5.11) and Eq. (5.14). For example, if we consider the diagonal arrangement, then we obtain (by a similar trick as used in Eq. (5.5)):

$$\begin{aligned} C_i =& \frac{1}{2\pi}\int_0^{2\pi} \mathrm{d}\lambda\, \partial_\lambda\gamma_i(\lambda) \\ \overset{C_4}{=}& \frac{1}{2\pi}\int_0^{2\pi} \mathrm{d}\lambda\, \partial_\lambda\gamma_{i+1}(-\lambda) \\ =& -\frac{1}{2\pi}\int_0^{2\pi} \mathrm{d}\lambda\, \partial_\lambda\gamma_{i+1}(\lambda) \\ =& -C_{i+1}. \end{aligned} \tag{5.18}$$

A similar argument we can use for the horizontal path. There we find that $C_1 = -C_3$ and $C_2 = -C_4$. As we will see in the next section, the sum rule guarantees charge conservation.

Chern number and quantized charge transport

Later, in Sec. 5.3 we will prove that the charge transport is related to the Chern number by extending Resta's argument [45] to higher-order topological systems. A key step in this process is, that the adiabatic flux insertion in Eq. (5.7) can be directly related to a current passing diagonally through a corner, $\hat{J}_i = \partial_\theta \hat{H}_{i;V}(\theta)|_{\theta=0}$ for $i = \{1, ..., 4\}$[8]. Integrating up these currents along an adiabatic path, touching two HOSPTs, gives the total charge pumped during one cycle,

$$\Delta q_{c_i} = -C_i. \tag{5.19}$$

From Eq. (5.17) it follows that this is given by the change of the $\mathbb{Z}_2$ higher-order Zak (Berry) phase over one cycle. Thus, the sum rule of the Chern numbers indeed corresponds to charge conservation along a cycle. Moreover, this shows that we need in total *four* Chern numbers to fully specify the charge flow in HOSPT phases.

Half-Thouless pump cycle

From the density plots of Fig. 5.5c, we conclude that after a half-cycle, charges at the corners pile up. Under assumption of Eq. (5.19), which is proved in Sec. 5.3, we show that after a half-cycle the change in corner charge is given by

$$\Delta q_{c_i}^{\text{half}} = -C_i/2. \tag{5.20}$$

To this end let us consider the following path: For $\lambda \in \{0, \pi\}$ we follow the path introduced above, also shown in Fig. 5.5b, which we denote as $\mathcal{L}_0$. On the second half; however, we use the path $\hat{\mathcal{S}}\mathcal{L}_0$. This path is obtained as follows: From each state of $\mathcal{L}_0$, the state on the second half can be obtained via applying $\hat{\mathcal{S}}$. Thus, the total path reads: $\mathcal{L} = \mathcal{L}_0 \cup \left(-\hat{\mathcal{S}}\mathcal{L}_0\right)$. The minus sign is needed since we have to reverse the orientation of the path to have a closed trajectory. Hence, we obtain:

$$2\pi C_i = \oint_{\mathcal{L}} \mathrm{d}\lambda\, \partial_\lambda \gamma_i(\lambda) = \int_0^\pi \mathrm{d}\lambda\, \partial_\lambda \gamma_i(\lambda) - \int_0^\pi \mathrm{d}\lambda\, \partial_\lambda \gamma_i(-\lambda) \overset{\hat{\mathcal{S}}}{=} 2\int_0^\pi \mathrm{d}\lambda\, \partial_\lambda \gamma_i(\lambda), \tag{5.21}$$

which implies that

$$\Delta q_{c_i}^{\text{half}} = -\frac{C_i}{2} = -\frac{1}{\pi}\int_0^\pi \mathrm{d}\lambda\, \partial_\lambda \gamma_i(\lambda). \tag{5.22}$$

For getting this result, we used the symmetry properties of the pumping procedures, Eq. (5.12) and Eq. (5.15), and of γ_i, defined in Eq. (5.5). Note if we, on the other hand, write:

$$\Delta q_{c_i}^{\text{half}} = -\frac{\gamma_i(\pi) - \gamma_i(0)}{\pi} \bmod 1, \tag{5.23}$$

then this equation defines the corner charge only modulo integer because γ_i is only defined modulo 2π. This happens since we have lost the information about the path (see also Ref. [179]). The previous result clearly shows that after a half-cycle we moved from the trivial to the topological phase, and the emergence of fractional corner charges is directly related to quantized changes of the $\mathbb{Z}_2$ higher-order Zak (Berry) phase.

[8] However, for the evaluation of the Chern number it does not matter which gauge choice we use.

Softcore bosons

If we consider the SL-BHM with finite interactions, then the additional $\mathbb{Z}_2$ symmetry is broken and the remaining symmetries are $U(1) \times C_4$—still distinguishing HOSPTs of the SL-BHM. This clearly implies that our $\mathbb{Z}_2$ higher-order Zak (Berry) phase is no longer quantized in individual HOSPT phases; however, the associated Chern numbers defined as the winding number of these phases are unchanged. Consequently, this particular higher-order Zak (Berry) phase can still be used to characterize Thouless pumps of softcore bosons, *although* its quantizing symmetry is broken. However, if the $\mathbb{Z}_2$ higher-order Zak (Berry) phases loses its quantization, we can no longer use it to characterize the change of the fractional charge during a half-cycle. But, in Sec. 5.4 we show that this relation remains true if we instead consider the C_4 higher-order Zak (Berry) phase.

5.2.3 Numerical evaluation of Thouless pumps and quadrupole operators

Having characterized Thouless pumps in terms of Chern numbers and quantized charge transports, we now numerically evaluate the previously introduced pumping procedures, using exact diagonalization of an 4×4 SL-BHM at half-filling and hardcore bosons with CPBC. To this end, we evaluate the Chern numbers and the $\mathbb{Z}_2$ higher-order Zak (Berry) phase, using the following discretized formulas [149]:

$$\begin{aligned} \gamma_i(\lambda) =& -\prod_{n=1}^{N} \langle \psi_n(\lambda) | \psi_{n+1}(\lambda) \rangle \,, \quad |\psi_n(\lambda)\rangle \equiv |\psi(\lambda, 2\pi \frac{n}{N})\rangle \\ C_i =& \frac{1}{2\pi} \int_0^{2\pi} \mathrm{d}\lambda \; \partial_\lambda \gamma_i(\lambda) = \sum_n \left[\frac{\gamma_i(\lambda_{n+1})}{2\pi} - \frac{\gamma_i(\lambda_n)}{2\pi} \right], \end{aligned} \tag{5.24}$$

with a sufficiently large number of discrete points in the intervals $(\lambda_n, \theta_n) \in [0, 2\pi) \times [0, 2\pi)$.

Diagonal pump: As shown in Fig. 5.6b, the four Chern numbers are extracted from the windings of the $\mathbb{Z}_2$ higher-order Zak (Berry) phases and read $C^{\mathrm{diag}} = (-1, 1, -1, 1)$. Clearly, the total charge is conserved. Moreover, a negative (positive) Chern number means charge transport towards (away from) the corner. Furthermore, as predicted, consecutive Chern numbers have opposite sign.

Horizontal pump: Here, in Fig. 5.6c,d, the four Chern numbers are specified by $C^{\mathrm{hor}} = (-1, -1, 1, 1)$, i.e., charge flows towards (away from) left (right) corner such that a dipole configuration after a half-cycle appears. Furthermore, as stated above, sequential Chern numbers have the same sign.

Quadrupole operator

In Sec. 3.3.1 we already discussed that a quadrupole operator, defined as the generalization of the many-body polarization, is not well-defined for classifying $U(1)$ conserving HOSPT phases without conservation of dipole moments. From the Thouless pumps discussed in this section, Fig. 5.5 and Fig. 5.6, we can also physically understand that a

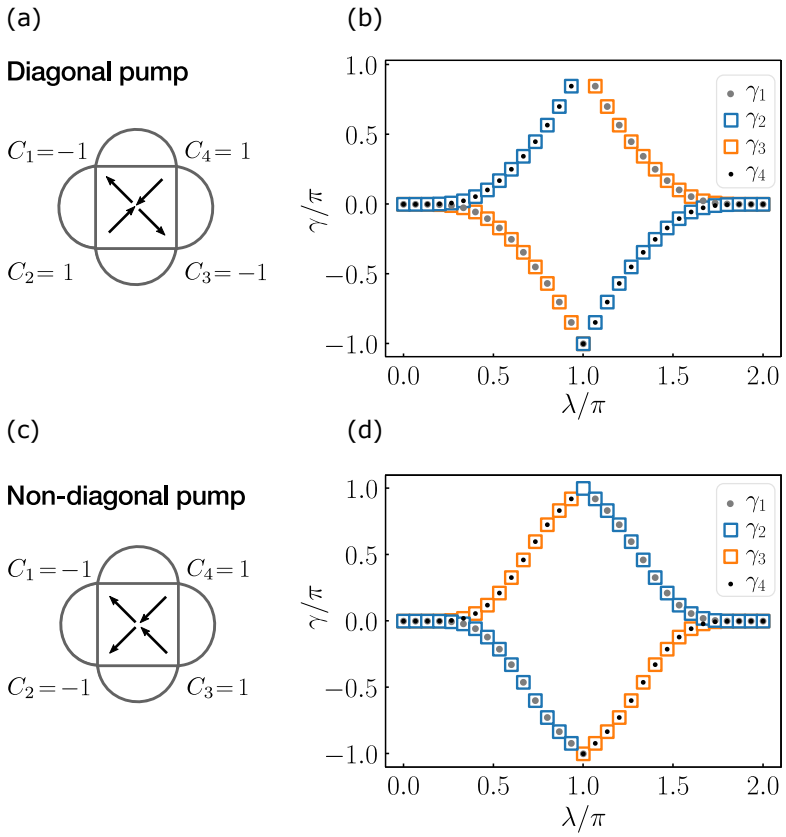

Figure 5.6: **Chern number tuples for diagonal and non-diagonal Thouless pumps.** (b, d) Evolution of the $\mathbb{Z}_2$ higher-order Zak (Berry) phases γ_i along the diagonal (upper panel) and non-diagonal (lower panel) Thouless pumps, Eq. (5.10) and Eq. (5.13), respectively. (a, c) The charge flows towards (away from) a corner are characterized by a negative (positive) Chern number C_i.

quadrupole operator is not sufficient to describe the system because there can be both: a quadrupole and a dipole configuration.

5.3 A bulk-boundary correspondence

A unifying feature of certain topological phases of matter is the correspondence between bulk and edge properties. In this sense, changes of bulk topology are directly related to changes on the edges [21, 22, 29, 71, 74, 75, 177, 178]. This correspondence reflects the fact that, unlike SSB phases, such states of matter are symmetric and, hence, no local order parameter distinguishes them. If we form a spatial interface of two such phases, then there must occur a phase transition, which is locally confined near the interface. Hence, if such interface is between the vacuum (trivial phase) and a topological phase,

there can be, among other things, gapless edge modes. Such interfaces, for instance, can easily be constructed from Chern insulators with different Chern numbers [84, 180].

In this section, we will prove such bulk-boundary correspondence for the 2D SL-BHM with hardcore bosons at half-filling and relate the $\mathbb{Z}_2$ higher-order Zak (Berry) phase to fractional charges sitting at the corner[9]. To this end, we first introduce a lattice Hamiltonian in Sec. 5.3.1 and briefly repeat the discussion on flux insertion. Afterwards, we generalize in Sec. 5.3.2 the Ansatz of Resta [45] to higher-order topological systems, and then in Sec. 5.3.3, we define a current operator as well as consider charge transport. By relating two initially distinct phases factors, we finally arrive at the desired bulk-boundary correspondence (see Sec. 5.3.4).

Before we proceed, let us emphasize that no step in this section requires the limit of hardcore bosons and, thus, remains true for finite U. Thus, whenever necessary, we stick to the general labelling of operators.

5.3.1 Lattice Hamiltonian

For proving a bulk-boundary correspondence, it turns out to be useful to define a lattice Hamiltonian that depends on a parameter $\boldsymbol{\alpha} \in \mathbb{R}^d$, where d is the dimension of parameter space. A given Hamiltonian can be written as follows:

$$\hat{H}^{CPBC}_{\boldsymbol{\alpha}} = \hat{H}^{OBC}_{\boldsymbol{\alpha}_{OBC}} + \hat{H}^{C}_{\boldsymbol{\alpha}_C} \tag{5.25}$$

where $\hat{H}^{OBC}_{\boldsymbol{\alpha}_{OBC}}$ is the Hamiltonian for open boundaries and $\hat{H}^{C}_{\boldsymbol{\alpha}_c}$ includes the links connecting different corners. Note in the definition $\hat{H}^{OBC}_{\boldsymbol{\alpha}_{OBC}}$ we allow for arbitrary on-site chemical potentials $\sim \sum_{x,y} \Delta_{x,y}\hat{n}_{x,y}$ that might break global symmetries of $\hat{H}^{CPBC}_{\boldsymbol{\alpha}}$, while keeping global charge conservation[10]. An example of such Hamiltonian is given in Eq. (5.10).

Flux insertion

Another essential ingredient for the upcoming proof is to introduce phase twists, as discussed in Sec. 5.1.3. To this end, we first apply the gauge transformation $\hat{U}_i(\theta)$, and then subsequently the gauge transformation $\hat{V}_i(\theta)$ to finally arrive at the Hamiltonian

$$\hat{H}^{CPBC}_{\boldsymbol{\alpha},i;V}(\theta) = \hat{V}_i(\theta)\left(\hat{H}^{OBC}_{\boldsymbol{\alpha}_{OBC}} + \hat{U}_i^\dagger(\theta)\hat{H}^{C}_{\boldsymbol{\alpha}_C}\hat{U}_i(\theta)\right)\hat{V}_i^\dagger(\theta), \tag{5.26}$$

which is graphically shown in Fig. 5.4. Recall that this Hamiltonian does not return to its initial form after a 2π shift, namely, $\hat{H}^{CPBC}_{\boldsymbol{\alpha},i;V}(\theta+2\pi) = \hat{V}_i(2\pi)\hat{H}^{CPBC}_{\boldsymbol{\alpha},i;V}(\theta)\hat{V}_i(2\pi)$.

5.3.2 Generalizing Resta's construction

The main ideas of Resta's construction [45] are to use non-degenerate perturbation theory, to relate the generator of the gauge transformation, defined in Eq. (5.6), to

[9] In the presence of this additional symmetry, the modes at the corner are actually gapless.
[10] It is assumed that the overall filling is not changed by adding such terms.

another phase, which is in direct correspondence with the $\mathbb{Z}_2$ higher-order Zak (Berry) phase and, second, to make the parameters time-dependent, to connect changes of this phase to an adiabatic current and charge transport.

A new phase

As a starting point, we assume that the initial lattice Hamiltonian, i.e., with no flux $\hat{H}^{CPBC}_{\boldsymbol{\alpha},i;V}(0) \equiv \hat{H}^{CPBC}_{\boldsymbol{\alpha}}$, has a unique ground state $\hat{H}^{CPBC}_{\boldsymbol{\alpha}} |\Psi^0_{\boldsymbol{\alpha}}\rangle = E^0_{\boldsymbol{\alpha}} |\Psi^0_{\boldsymbol{\alpha}}\rangle$. Hence, if $\theta = 2\pi$ (or equivalently $\Phi = 2\pi$, see Fig. 5.4)[11], then we find that

$$\hat{H}^{CPBC}_{\boldsymbol{\alpha},i;V}(2\pi)\, \hat{V}_i(2\pi)\, |\Psi^0_{\boldsymbol{\alpha}}\rangle = E^0_{\boldsymbol{\alpha}}\, \hat{V}_i(2\pi)\, |\Psi^0_{\boldsymbol{\alpha}}\rangle\,. \tag{5.27}$$

From non-degenerate perturbation theory up to first-order, we obtain ($L \to \infty$):

$$\hat{V}_i(2\pi)\, |\Psi^0_{\boldsymbol{\alpha}}\rangle = e^{i\tilde{\gamma}_i(\boldsymbol{\alpha})} \left(|\Psi^0_{\boldsymbol{\alpha}}\rangle + \frac{2\pi}{L} \sum_{j>0} |\Psi^j_{\boldsymbol{\alpha}}\rangle \frac{\langle \Psi^j_{\boldsymbol{\alpha}}|\, \partial_{\tilde{\theta}} \hat{H}^{CPBC}_{\boldsymbol{\alpha},i;V}(\tilde{\theta})|_{\tilde{\theta}=0}\, |\Psi^0_{\boldsymbol{\alpha}}\rangle}{\left(E^0_{\boldsymbol{\alpha}} - E^j_{\boldsymbol{\alpha}}\right)} \right), \tag{5.28}$$

where the sum runs over all excited states. Moreover, as pointed out by Resta [45], there can in general be a global phase in the expansion denoted by $\tilde{\gamma}_i(\boldsymbol{\alpha})$. Later, we show that the phase $\tilde{\gamma}_i(\boldsymbol{\alpha})$ is related to the $\mathbb{Z}_2$ higher-order Zak (Berry) phase considered previously. To arrive at this result, we used the following expansion:

$$\hat{H}^{CPBC}_{\boldsymbol{\alpha},i;V}(2\pi) = \hat{H}^{CPBC}_{\boldsymbol{\alpha},i;V} + \partial_{\tilde{\theta}} \hat{H}^{CPBC}_{\boldsymbol{\alpha},i;V}(\tilde{\theta})|_{\tilde{\theta}=0} \frac{2\pi}{L}, \tag{5.29}$$

where we introduced the notation $\tilde{\theta} = \theta/L$[12].

Expectation value of $\hat{X}_i$

Due to CPBC, the expectation value of $\langle \hat{X}_i \rangle_{\boldsymbol{\alpha}} = \langle \Psi^0_{\boldsymbol{\alpha}} | \hat{X}_i | \Psi^0_{\boldsymbol{\alpha}} \rangle$ is not well-defined. However, similar to the one dimensional case [45], we can define the expectation value of a many-body operator as:

$$\langle \hat{X}_i \rangle_{\boldsymbol{\alpha}} = \frac{L}{2\pi} \mathrm{Im} \log \langle \Psi^0_{\boldsymbol{\alpha}}|\, e^{\frac{2\pi i}{L} \hat{X}_i}\, |\Psi^0_{\boldsymbol{\alpha}}\rangle \pmod{L}, \tag{5.30}$$

which is well-defined modulo L. Using Eqs. (5.28) and (5.30), we obtain:

$$\boxed{\langle \hat{X}_i \rangle_{\boldsymbol{\alpha}} = \frac{L}{2\pi} \tilde{\gamma}_i(\boldsymbol{\alpha})}. \tag{5.31}$$

[11] Note, compared to Ref. [45], we put the factor $1/L$ in the definition of the gauge transformation $\hat{V}_i(\theta)$.
[12] Since we put the factor $1/L$ in the definition of the gauge transformation, taking the derivative w.r.t θ means we have to make use of the chain rule.

Time dependence and adiabatic change of parameters

Similarly to Ref. [45], we now want to relate Eq. (5.31) to a physical observable. Therefore, we assume an adiabatic change of parameters, i.e., $\boldsymbol{\alpha} \to \boldsymbol{\alpha}(\tau)$ where τ denotes time to not confuse it with the hopping parameter t. Using the corresponding instantaneous eigenstates $|\Psi^j_{\boldsymbol{\alpha}(\tau)}\rangle$ (shorthand we write $|\Psi^j_{\boldsymbol{\alpha}}\rangle$), we can calculate the time derivative of Eq. (5.30)

$$\frac{\mathrm{d}}{\mathrm{d}\tau}\langle \hat{X}_i\rangle_{\boldsymbol{\alpha}} = \frac{L}{2\pi}\mathrm{Im}\left(\frac{\langle\dot{\Psi}^0_{\boldsymbol{\alpha}}|e^{\frac{2\pi i}{L}\hat{X}_i}|\Psi^0_{\boldsymbol{\alpha}}\rangle}{\langle\Psi^0_{\boldsymbol{\alpha}}|e^{\frac{2\pi i}{L}\hat{X}_i}|\Psi^0_{\boldsymbol{\alpha}}\rangle} + \frac{\langle\Psi^0_{\boldsymbol{\alpha}}|e^{\frac{2\pi i}{L}\hat{X}_i}|\dot{\Psi}^0_{\boldsymbol{\alpha}}\rangle}{\langle\Psi^0_{\boldsymbol{\alpha}}|e^{\frac{2\pi i}{L}\hat{X}_i}|\Psi^0_{\boldsymbol{\alpha}}\rangle}\right). \tag{5.32}$$

Inserting the results of Eq. (5.28), and keeping only first-order terms we obtain:

$$\boxed{\frac{\mathrm{d}}{\mathrm{d}\tau}\langle \hat{X}_i\rangle_{\boldsymbol{\alpha}} = \sum_{j>0}\langle\dot{\Psi}^0_{\boldsymbol{\alpha}}|\Psi^j_{\boldsymbol{\alpha}}\rangle\frac{\langle\Psi^j_{\boldsymbol{\alpha}}|(-i)\partial_{\tilde{\theta}}\hat{H}^{CPBC}_{\boldsymbol{\alpha},i;V}(\tilde{\theta})|_{\tilde{\theta}=0}|\Psi^0_{\boldsymbol{\alpha}}\rangle}{E^0_{\boldsymbol{\alpha}} - E^j_{\boldsymbol{\alpha}}} + \text{c.c.}}, \tag{5.33}$$

where c.c. means complex conjugation. Here, similar to Resta [45], we use that $\hat{H}_{\boldsymbol{\alpha}}$ is time reversal symmetric. Since particles are spinless, this is just given by complex conjugation $\hat{\mathcal{T}} = \hat{K}$ with $\hat{\mathcal{T}}^{-1}\hat{a}_{x,y}\hat{\mathcal{T}} = \hat{a}_{x,y}$, $\hat{\mathcal{T}}^{-1}\hat{a}^\dagger_{x,y}\hat{\mathcal{T}} = \hat{a}^\dagger_{x,y}$ and $\hat{\mathcal{T}}^{-1}i\hat{\mathcal{T}} = -i$. This symmetry guarantees that all instantaneous eigenstates can be chosen to be real and that the overlap $\langle\dot{\Psi}^0_{\boldsymbol{\alpha}}|\Psi^0_{\boldsymbol{\alpha}}\rangle = 0$[13]. The imaginary unit "i" appears because the derivative is of the form $\partial_{\tilde{\theta}}\hat{H}^{CPBC}_{\boldsymbol{\alpha},i}(\tilde{\theta})|_{\tilde{\theta}=0} \sim i(\hat{A}^\dagger - \hat{A})$ with $\hat{\mathcal{T}}^{-1}\hat{A}\hat{\mathcal{T}} = \hat{A}$. Thus, taking its imaginary part corresponds to multiplying it with an additional factor of $(-i)$ or i, for the complex conjugate part, respectively.

5.3.3 Adiabatic current and total charge transport

Here, following Ref. [174], we construct an expression for the adiabatic current and connect it to the time derivative in Eq. (5.33). Similar to our previous discussion, we use a shorthand notation, i.e., $\hat{H}^{CPBC}_{\boldsymbol{\alpha}(\tau)} \equiv \hat{H}^{CPBC}_{\boldsymbol{\alpha}}$. As we are at this point only interested in the adiabatic change of parameters, we do not consider a θ dependence here. Moreover, we assume that after one period, $\tau = T$, the Hamiltonian returns to itself $\hat{H}^{CPBC}_{\boldsymbol{\alpha}(\tau+T)} \equiv \hat{H}^{CPBC}_{\boldsymbol{\alpha}(\tau)}$.

Adiabatic approximation

The density matrix associated with the adiabatic evolution is defined as:

$$\hat{\rho}_{\boldsymbol{\alpha}} \equiv \hat{\rho}_{\boldsymbol{\alpha}(\tau)} = \underbrace{|\Psi^0_{\boldsymbol{\alpha}(\tau)}\rangle\langle\Psi^0_{\boldsymbol{\alpha}(\tau)}|}_{=\hat{\rho}^I_{\boldsymbol{\alpha}(\tau)}} + \Delta\hat{\rho}(\tau), \tag{5.34}$$

[13] The argument goes as follows: The ground state can always be chosen to be an eigenstate of $\hat{\mathcal{T}}$ with $\hat{\mathcal{T}}|\Psi^0_{\boldsymbol{\alpha}}\rangle = |\Psi^0_{\boldsymbol{\alpha}}\rangle$. From $\partial_\tau\langle\Psi^0_{\boldsymbol{\alpha}}|\Psi^0_{\boldsymbol{\alpha}}\rangle = 0$ if follows that $\langle\dot{\Psi}^0_{\boldsymbol{\alpha}}|\Psi^0_{\boldsymbol{\alpha}}\rangle$ must be imaginary. However, if $|\Psi^0_{\boldsymbol{\alpha}}\rangle$ is real, then also its time derivative is real. Thus, $\langle\dot{\Psi}^0_{\boldsymbol{\alpha}}|\Psi^0_{\boldsymbol{\alpha}}\rangle = 0$.

where $\hat{\rho}^I_{\boldsymbol{\alpha}(\tau)} \equiv \hat{\rho}^I_{\boldsymbol{\alpha}}$ is the density matrix associated with instantaneous eigenstates. The time evolution of the complete density matrix is governed by,

$$i\partial_\tau \hat{\rho}_{\boldsymbol{\alpha}} = \left[\hat{H}^{CPBC}_{\boldsymbol{\alpha}}, \Delta\hat{\rho}(\tau)\right]. \tag{5.35}$$

Dropping higher-order terms such as $\partial_\tau \Delta\hat{\rho}(\tau)$ [181], we obtain for the instantaneous density matrix:

$$i\partial_\tau \hat{\rho}^I_{\boldsymbol{\alpha}} \approx \left[\hat{H}^{CPBC}_{\boldsymbol{\alpha}}, \Delta\hat{\rho}(\tau)\right]. \tag{5.36}$$

Further, we can write,

$$\begin{aligned}\langle\Psi^0_{\boldsymbol{\alpha}}| i\left(\partial_\tau \hat{\rho}^I_{\boldsymbol{\alpha}}\right)|\Psi^j_{\boldsymbol{\alpha}}\rangle =& i\underbrace{\partial_\tau \langle\Psi^0_{\boldsymbol{\alpha}}|\hat{\rho}^I_{\boldsymbol{\alpha}}|\Psi^j_{\boldsymbol{\alpha}}\rangle}_{=0} - i\underbrace{\langle\dot{\Psi}^0_{\boldsymbol{\alpha}}|\hat{\rho}^I_{\boldsymbol{\alpha}}|\Psi^j_{\boldsymbol{\alpha}}\rangle}_{=0} - i\langle\Psi^0_{\boldsymbol{\alpha}}|\hat{\rho}^I_{\boldsymbol{\alpha}}|\dot{\Psi}^j_{\boldsymbol{\alpha}}\rangle \\ =& i\langle\dot{\Psi}^0_{\boldsymbol{\alpha}}|\Psi^j_{\boldsymbol{\alpha}}\rangle.\end{aligned} \tag{5.37}$$

Here we used the following identities: First, the instantaneous eigenstates are orthogonal $\langle\Psi^0_{\boldsymbol{\alpha}}|\Psi^j_{\boldsymbol{\alpha}}\rangle = \delta_{0j}$. Second, the time derivative of $\partial_\tau \langle\Psi^0_{\boldsymbol{\alpha}}|\Psi^j_{\boldsymbol{\alpha}}\rangle = 0$ vanishes and, thus, $\langle\dot{\Psi}^0_{\boldsymbol{\alpha}}|\Psi^j_{\boldsymbol{\alpha}}\rangle = -\langle\Psi^0_{\boldsymbol{\alpha}}|\dot{\Psi}^j_{\boldsymbol{\alpha}}\rangle$. Moreover, we find that

$$\langle\Psi^0_{\boldsymbol{\alpha}}|\left[\hat{H}^{CPBC}_{\boldsymbol{\alpha}}, \Delta\hat{\rho}(\tau)\right]|\Psi^j_{\boldsymbol{\alpha}}\rangle = \left(E^0_{\boldsymbol{\alpha}} - E^j_{\boldsymbol{\alpha}}\right)\langle\Psi^0_{\boldsymbol{\alpha}}|\Delta\hat{\rho}(\tau)|\Psi^j_{\boldsymbol{\alpha}}\rangle. \tag{5.38}$$

Note that the term proportional to $j = 0$ vanish. Inserting Eq. (5.36) into Eq. (5.38) and, using the result of Eq. (5.37), gives:

$$\boxed{\langle\Psi^0_{\boldsymbol{\alpha}}|\Delta\hat{\rho}(\tau)|\Psi^j_{\boldsymbol{\alpha}}\rangle = i\frac{\langle\dot{\Psi}^0_{\boldsymbol{\alpha}}|\Psi^j_{\boldsymbol{\alpha}}\rangle}{E^0_{\boldsymbol{\alpha}} - E^j_{\boldsymbol{\alpha}}},\ j > 0.} \tag{5.39}$$

Charge transport

The total charge transport over one period T averaged over space[14] is defined as follows:

$$\mathcal{C} = \frac{1}{L}\int_0^T \mathrm{d}\tau\ \mathrm{tr}\left(\hat{\rho}_{\boldsymbol{\alpha}}\hat{J}\right), \tag{5.40}$$

where $\hat{J}$ is the current operator, which at this point is just a general operator and will be defined later. To evaluate the trace, we choose instantaneous eigenstates as our basis and replace $\hat{\rho}_{\boldsymbol{\alpha}}$ by Eq. (5.34). Thus, the total charge transport reads:

$$\begin{aligned}\mathcal{C} =& \frac{1}{L}\int_0^T \mathrm{d}\tau\ \mathrm{tr}\left(\hat{\rho}_{\boldsymbol{\alpha}}\hat{J}\right) \\ =& \frac{1}{L}\int_0^T \mathrm{d}\tau\left[\left(1 + \langle\Delta\hat{\rho}\rangle^{00}_{\boldsymbol{\alpha}}\right)\langle\hat{J}\rangle^{00}_{\boldsymbol{\alpha}} + \sum_{j>0}\langle\Delta\hat{\rho}\rangle^{0j}_{\boldsymbol{\alpha}}\langle\hat{J}\rangle^{j0}_{\boldsymbol{\alpha}} + \langle\Delta\hat{\rho}\rangle^{j0}_{\boldsymbol{\alpha}}\langle\hat{J}\rangle^{0j}_{\boldsymbol{\alpha}}\right].\end{aligned} \tag{5.41}$$

[14] The generator of the gauge transformation is linear in coordinates, which, as we shall see, results in a charge transport along the diagonals, which thus gives rise to the factor $1/L$.

where $\langle\cdot\rangle_{\boldsymbol{\alpha}}^{jj'} \equiv \langle\Psi_{\boldsymbol{\alpha}}^{j}|\cdot|\Psi_{\boldsymbol{\alpha}}^{j'}\rangle$. Moreover, we used that there is no population of higher-energy instantaneous eigenstates, i.e., $\langle\Delta\hat{\rho}\rangle_{jj'} = 0$ for $j > 0$ and $j' > 0$ (adiabatic theorem [181]). Since the current is odd under time reversal symmetry, we have that $\langle\hat{J}\rangle_{00} = -\langle\hat{J}\rangle_{00}$. Because the total charge current per length is real, the first term proportional to $\langle\hat{J}\rangle_{00}$ vanish, and we are left with:

$$\begin{aligned}\mathcal{C} =& \frac{1}{L}\int_0^T \mathrm{d}\tau\ \mathrm{tr}\left(\hat{\rho}_{\boldsymbol{\alpha}}\hat{J}\right)\\ =& \frac{1}{L}\sum_{j>0}\int_0^T \mathrm{d}\tau\ \left(\langle\Delta\hat{\rho}\rangle_{\boldsymbol{\alpha}}^{0j}\langle\hat{J}\rangle_{\boldsymbol{\alpha}}^{j0} + \langle\Delta\hat{\rho}\rangle_{\boldsymbol{\alpha}}^{j0}\langle\hat{J}\rangle_{\boldsymbol{\alpha}}^{0j}\right)\\ \overset{(5.39)}{=}& \frac{1}{L}\sum_{j>0}\int_0^T \mathrm{d}\tau\ \left(i\frac{\langle\dot{\Psi}_{\boldsymbol{\alpha}}^{0}|\Psi_{\boldsymbol{\alpha}}^{j}\rangle}{E_{\boldsymbol{\alpha}}^{0}-E_{\boldsymbol{\alpha}}^{j}}\langle\hat{J}\rangle_{\boldsymbol{\alpha}}^{j0} + \text{c.c.}\right).\end{aligned} \tag{5.42}$$

The expression of the integral looks almost like the expression of Eq. (5.33). Thus, if we replace the current operator with $\hat{J} \to -\partial_{\tilde{\theta}}\hat{H}^{CPBC}_{\boldsymbol{\alpha},i;V}|_{\tilde{\theta}=0}$ and $\mathcal{C} \to \mathcal{C}_i$, we obtain the charge transport associated to corner c_i,

$$\begin{aligned}\boxed{\mathcal{C}_i} =& \frac{1}{L}\sum_{j>0}\int_0^T \mathrm{d}\tau\ \left(\frac{\langle\dot{\Psi}_{\boldsymbol{\alpha}}^{0}|\Psi_{\boldsymbol{\alpha}}^{j}\rangle}{E_{\boldsymbol{\alpha}}^{0}-E_{\boldsymbol{\alpha}}^{j}}\langle(-i)\partial_{\tilde{\theta}}\hat{H}^{CPBC}_{\boldsymbol{\alpha},i;V}|_{\tilde{\theta}=0}\rangle_{\boldsymbol{\alpha}}^{j0} + \text{c.c.}\right)\\ \overset{(5.33)}{=}& \frac{1}{L}\int_0^T \mathrm{d}\tau\ \frac{\mathrm{d}}{\mathrm{d}\tau}\langle\hat{X}_i\rangle_{\boldsymbol{\alpha}}\\ \overset{(5.30)}{=}& \boxed{\frac{\Delta\tilde{\gamma}_i}{2\pi}},\end{aligned} \tag{5.43}$$

which is given by the change $\tilde{\gamma}_i$ over one period, normalized by 2π.

Current operator

Now we need to justify that $\partial_{\tilde{\theta}}\hat{H}^{CPBC}_{\boldsymbol{\alpha},i;V}|_{\tilde{\theta}=0}$ indeed corresponds to a current. Evaluating the derivative[15] for $i = 1$ gives:

$$\begin{aligned}\partial_{\tilde{\theta}}\hat{H}^{CPBC}_{\boldsymbol{\alpha},1}|_{\tilde{\theta}=0} =& i\left[\sum_{y\in\Lambda}\sum_{x\in T_1'} t(x)\left(\hat{a}^\dagger_{x+1,y}\hat{a}_{x,y} - \hat{a}^\dagger_{x,y}\hat{a}_{x+1,y}\right) - \sum_{x\in\Lambda}\sum_{y\in T_1'} t(y)\left(\hat{a}^\dagger_{x,y+1}\hat{a}_{x,y} - \hat{a}^\dagger_{x,y}\hat{a}_{x,y+1}\right)\right]\\ & - it\left[\left(\hat{a}^\dagger_{c_4}\hat{a}_{c_1} - \hat{a}^\dagger_{c_1}\hat{a}_{c_4}\right) - \left(\hat{a}^\dagger_{c_1}\hat{a}_{c_2} - \hat{a}^\dagger_{c_2}\hat{a}_{c_1}\right)\right]\\ =& i\left(\Delta\hat{h}^{x,T_1'} - \Delta\hat{h}^{y,T_1'}\right) + i\left(-\Delta\hat{h}^{x,c_1} + \Delta\hat{h}^{y,c_1}\right)\\ =& i\begin{pmatrix}\Delta\hat{h}^{x,T_1'}\\ \Delta\hat{h}^{y,T_1'}\end{pmatrix}\cdot\begin{pmatrix}1\\-1\end{pmatrix} + i\begin{pmatrix}\Delta\hat{h}^{x,c_1}\\ \Delta\hat{h}^{y,c_1}\end{pmatrix}\cdot\begin{pmatrix}-1\\1\end{pmatrix}\\ =& \hat{J}^{T_1'}(\searrow) + \hat{J}^{c_1}(\nwarrow),\end{aligned} \tag{5.44}$$

[15] Note by applying C_4 symmetry we can generate all other derivatives $\partial_{\tilde{\theta}}\hat{H}^{CPBC}_{\boldsymbol{\alpha},i}|_{\tilde{\theta}=0}$ and currents, respectively.

where Λ is the set of all lattice points, $T_1^{'}$ is defined such that the sums in the above equation do not contain the corner-connecting hopping terms. The operator $\Delta\hat{h}^{x(y),T_1^{'}}$ defines the difference of particles hopping along the $x(y)$-direction in $T_1^{'}$, and the operator $\Delta\hat{h}^{x(y),c_1}$ defines a similar expression for the corner c_1 only. Multiplying those terms with the imaginary unit gives indeed a current. Note that the sign of each term is chosen such that a positive expectation value of $i\Delta h^{\nu,T_1^{'}(c_1)}$ with $\nu \in \{x, y\}$ means a current along $x(y)$. The final result shows that a non-zero expectation value of the derivative $\partial_{\tilde{\theta}}\hat{H}^{CPBC}_{\boldsymbol{\alpha},1}|_{\tilde{\theta}=0}$ is equal to the projection of the current along the diagonal in the triangle T_1. Thus, this expectation value measures the net charge Δq_{c_1} that passes the corner over one period of time T. Hence, using Eq. (5.43), we obtain:

$$\boxed{\Delta q_{c_i} = \frac{\Delta\tilde{\gamma}_i}{2\pi}}. \tag{5.45}$$

5.3.4 The relation to the $\mathbb{Z}_2$ higher-order Zak (Berry) phase

To arrive at the conclusion, we have to find a relation between the $\mathbb{Z}_2$ higher-order Zak (Berry) phase and the phase $\tilde{\gamma}_i(\boldsymbol{\alpha})$, which is done in this last part.

Perturbation theory

To this end, we first evaluate the ground states of $\hat{H}^{CPBC}_{\boldsymbol{\alpha},i;V}(\theta)$ using non-degenerate perturbation theory up to first-order, similar to Eq. (5.28),

$$|\Psi^0_{\boldsymbol{\alpha},i;V}(n\Delta\theta)\rangle = e^{i\phi_n}\left(|\Psi^0_\alpha\rangle + \frac{n\Delta\theta}{L}\sum_{j>0}|\Psi^j_{\boldsymbol{\alpha}}\rangle\frac{\langle\Psi^j_{\boldsymbol{\alpha}}|\,\hat{J}_i\,|\Psi^0_{\boldsymbol{\alpha}}\rangle}{\left(E^0_{\boldsymbol{\alpha}} - E^j_{\boldsymbol{\alpha}}\right)}\right), \tag{5.46}$$

where $n\Delta\theta = n\frac{2\pi}{N}$, $n \leq N$. Moreover, we defined $\hat{J}_i = \partial_{\tilde{\theta}}\hat{H}^{CPBC}_{\boldsymbol{\alpha},i;V}(\tilde{\theta})|_{\tilde{\theta}=0}$. As a next step, we evaluate the overlap of two states differing by $\Delta\theta$:

$$\langle\Psi^0_{\boldsymbol{\alpha},i;V}(n\Delta\theta)|\Psi^0_{\boldsymbol{\alpha},i;V}((n+1)\Delta\theta)\rangle = e^{i\Delta\phi_{n+1,n}}\left(1 + \frac{n(n+1)\Delta\theta^2}{L^2}\sum_j\frac{\left|\langle\Psi^j_{\boldsymbol{\alpha}}|\,\hat{J}_i\,|\Psi^0_{\boldsymbol{\alpha}}\rangle\right|^2}{\left(E^0_{\boldsymbol{\alpha}} - E^j_{\boldsymbol{\alpha}}\right)^2}\right), \tag{5.47}$$

where the term inside the brackets is real. Note if we went to higher-order perturbation theory, then there would also be imaginary terms inside the bracket[16]. However, the first imaginary term is proportional to L^{-3}, which results from the cross term of first-order and second-order perturbation theory.

[16] Note, from time reversal symmetry it follows that the expectation value $\langle\Psi^j_{\boldsymbol{\alpha}}|\,\hat{J}_i\,|\Psi^l_{\boldsymbol{\alpha}}\rangle$ for $j \neq l$ is purely imaginary. Thus, a product of three such terms is also purely imaginary.

Relation of phases and charges

As a next step, we use that in the limit $N \to \infty$ the $\mathbb{Z}_2$ higher-order Zak (Berry) phase, Eq. (5.8), can be written in a discretized form [149] given by[17],

$$\gamma_{i;V}(\boldsymbol{\alpha}) = -\lim_{N\to\infty} \operatorname{Im}\log\big[\langle\Psi_{\boldsymbol{\alpha},i}(0)|\Psi_{\boldsymbol{\alpha},i;V}(\Delta\theta)\rangle\,\langle\Psi_{\boldsymbol{\alpha},i;V}(\Delta\theta)|\Psi_{\boldsymbol{\alpha},i;V}(2\Delta\theta)\rangle \\ \cdots\langle\Psi_{\boldsymbol{\alpha},i;V}(N\Delta\theta)|\hat{V}_i(2\pi)|\Psi_{\boldsymbol{\alpha},i}(0)\rangle\big]\,. \tag{5.48}$$

Since the Hamiltonian $\hat{H}^{CPBC}_{\boldsymbol{\alpha},i;V}(\theta)$ after a 2π flux insertion does not return to itself, the same is true for its ground state. This explains why we need to include the gauge transformation $\hat{V}_i(2\pi)$ in the last step of Eq. (5.48). If we finally insert the result of Eq. (5.47) into the discretized version of the higher-order Zak (Berry) phase, Eq. (5.48), we obtain:

$$\boxed{\gamma_{i;V}(\boldsymbol{\alpha}) \overset{L\to\infty}{=} -\operatorname{Im}\log\langle\Psi^0_{\boldsymbol{\alpha},i}|\hat{V}_i(2\pi)|\Psi^0_{\boldsymbol{\alpha},i}\rangle = -\tilde{\gamma}_i(\boldsymbol{\alpha})}\,. \tag{5.49}$$

Given this result, we can finally confirm Eq. (5.19),

$$\boxed{\Delta q_{c_i} \overset{(5.45)}{=} -\frac{\Delta\gamma_i}{2\pi} \overset{(5.17)}{=} -C_i}\,. \tag{5.50}$$

Hence, we showed that the pumped charge during one cycle is quantized and given by the change of $\mathbb{Z}_2$ higher-order Zak (Berry) phase. From the result of the half-cycle, Eq. (5.20), we also conclude that—in the presence of the $\mathbb{Z}_2$ symmetry—a non-trivial, quantized change of the $\mathbb{Z}_2$ higher-order Zak (Berry) phase corresponds to a non-trivial change of quantized fractional charges at the corners.

5.4 Generalization to the C_4 higher-order Zak (Berry) phase

Up to this point, we have considered the simplified $\mathbb{Z}_2$ higher-order Zak (Berry) phase, from which we obtained a rigorous bulk-boundary correspondence, relating the fractional corner charge and a bulk invariant. Naturally, the question arises to which extent the previous results hold for the higher-order Zak (Berry) phase introduced in Chap. 3. Since we have not answered this in full detail yet, we only outline the most relevant and promising steps.

Flux insertion and Resta's construction

Flux insertion. The starting point of the previous proof was to distribute the phase twists over many links, Fig. 5.4, such that we were able to exploit non-degenerate perturbation theory, starting from a Hamiltonian $\hat{H}^{CPBC}_{i;V}(2\pi)$, Eq. (5.27), that locally has a phase twist $\sim 2\pi/L$. This Ansatz can be straightforwardly generalized to the C_4 higher-order Zak (Berry) phase if the phase twists are at the corner-connecting links. To this end, we use that the gauge choices, Eq. (5.6), distribute only one out of four phases over an

[17] Recall that $|\Psi_{\boldsymbol{\alpha},i;V}(0)\rangle = |\Psi_{\boldsymbol{\alpha},i}(0)\rangle$.

entire region, which implies that the resulting Hamiltonian for $\theta_i = 2\pi$ looks the same as for the $\mathbb{Z}_2$ higher-order Zak (Berry) phase.

Resta's construction. From the previous result, it directly follows that we can again apply perturbation theory up to first-order, to introduce the phase $\tilde{\gamma}_i$ and time dependency, from which we then derive the same adiabatic current and total charge transport.

Relation of phases, bulk-boundary correspondence and half-cycles

Relation of phases. The argument we used to arrive at Eq. (5.49) cannot be straightforwardly generalized, since the perturbative expansion of Eq. (5.46) is not justified in this case. The reason is that not all phase twists are small—meaning that twists contain a factor of $1/L$ once we applied the gauge choice of Eq. (5.6). Moreover, unlike the $\mathbb{Z}_2$ symmetry, which quantizes $\tilde{\gamma}_i$ to $\{0, \pi\}$, upon subtracting the average charge, this is no longer true for the C_4 symmetry. This symmetry only guarantees that $\tilde{\gamma}_1 = ... = \tilde{\gamma}_4$. The reason C_4 symmetry does not lead to a quantization of this phase is that the generator of the gauge choice, Eq. (5.6), is linear in coordinates and acts only on a subregion of the total system.

Bulk-boundary correspondence. However, for proving the bulk-boundary correspondence, it is actually not necessary that the individual phases coincide. It turns out to be sufficient to argue that the loop integrals defining the Chern numbers, up to a sign, match[18]

$$\oint \mathrm{d}\lambda\, \partial_\lambda \gamma_i(\lambda) \overset{!}{=} -\oint \mathrm{d}\lambda\, \partial_\lambda \tilde{\gamma}_i(\lambda). \tag{5.51}$$

Since the dependence on the parameter λ is the same in both integrals (which comes through the ground states of the Thouless pumps) we believe that integrals indeed coincide. To confirm this expectation—at least numerically—we redid the above numerical experiment for the diagonal Thouless pump, Sec. 5.2.3, where we in addition added a $\mathbb{Z}_2$ symmetry breaking term. From Fig. 5.7b, we clearly see that the result of the Thouless pump is unchanged. This means it does not matter which higher-order Zak (Berry) we use to evaluate the charge transport. Furthermore, in the same figure, Fig. 5.7a, we see that loop integrals—as expected—coincide. This clearly underpins the interpretation of the higher-order Zak (Berry) phase as a sensor of charge flow.

Half-cycle. If we consider a half-cycle of the diagonal pump and use the symmetry properties defined in Eq. (5.11), and of the C_4 higher-order Zak (Berry) phase, we obtain:

$$C_i = \frac{1}{2\pi} \oint \mathrm{d}\lambda\, \partial_\lambda \gamma_i(\lambda) \overset{C_4}{=} -\frac{1}{2\pi} \oint \mathrm{d}\lambda\, \partial_\lambda \gamma_{i+1}(\lambda) = -C_{i+1}. \tag{5.52}$$

Second, if we consider the total path to be $\mathcal{L} = \mathcal{L}_0 \cup (-C_4\mathcal{L}_0)$ (similar to Sec. 5.2.2), then the Chern number reads:

$$C_i = \frac{1}{2\pi} \int_0^\pi \mathrm{d}\lambda\, \partial_\lambda \gamma_i(\lambda) - \frac{1}{2\pi} \int_0^\pi \mathrm{d}\lambda\, \partial_\lambda \gamma_i(-\lambda) \overset{C_4}{=} \frac{1}{2\pi} \int_0^\pi \mathrm{d}\lambda\, \left[\partial_\lambda \gamma_i(\lambda) - \partial_\lambda \gamma_{i+1}(\lambda)\right] \tag{5.53}$$

[18] The sign difference can be understood as follows: To obtain $\tilde{\gamma}_i$ we evaluate the overlap of a state at 0 flux with a state containing a 2π flux, while for the C_4 higher-order Zak (Berry) phase it is precisely the opposite case (due to the global minus sign in the definition of γ_i, see Eqs. (5.24, 5.31)).

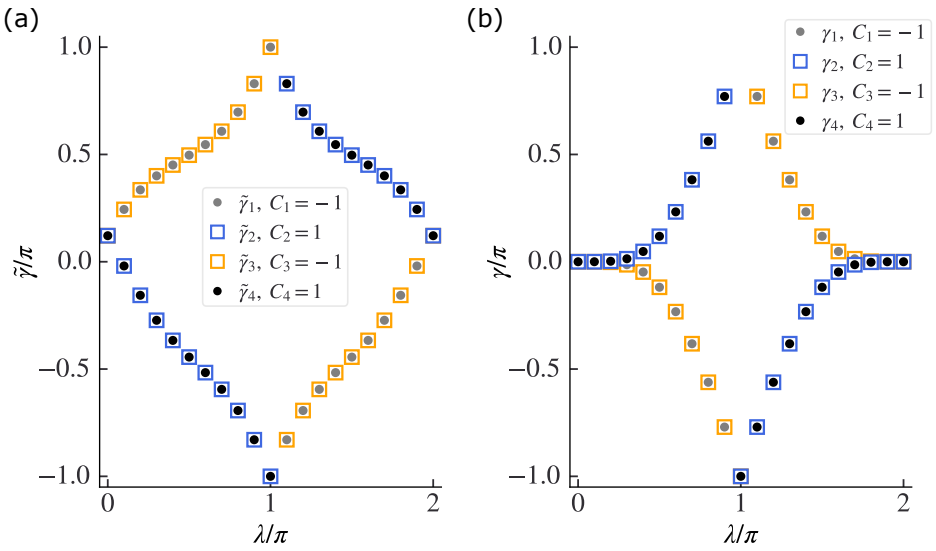

Figure 5.7: **Chern number tuples for diagonal Thouless pumps.** (a) The Chern numbers obtained from evaluating the loop integral corresponding to $\tilde{\gamma}_i$, while (b) shows the Chern numbers using the C_4 higher-order Zak (Berry) phases γ_i. As expected, the loop integrals over both phases are identical, although individual phases differ. (To evaluate $\tilde{\gamma}_i$, we subtracted the average charge.)

Finally, knowing that the sum of overall higher-order Zak (Berry) phases vanishes, we can write:

$$C_i = \frac{2}{2\pi} \int_0^\pi \mathrm{d}\lambda\, \partial_\lambda \gamma_i(\lambda). \tag{5.54}$$

Hence, as stated, $\Delta q_{c_i}^{\text{half}} = -C_i/2$. Similarly, this works for the non-diagonal pump. Consequently, for C_4 symmetry—assuming the identity in Eq. (5.51)—we have shown that a non-trivial, quantized change of the C_4 higher-order Zak (Berry) phase corresponds to a non-trivial, quantized change of the fractional charge at the corner.

Generalizations

The advantage of using the C_4 higher-order Zak (Berry) is that none of the previous results require hardcore bosons. Moreover, this allows us to study Thouless pumps of HOSPT phases with other filling factors. However, the generalization for other fillings is not straightforward: First, we need to find suitable terms that keep edges gapped and, second, we need to find an appropriate path in the enlarged parameter space.

5.5 Summary & Outlook

In summary, starting from a reconsideration of the C_4 higher-order Zak (Berry) phase, we introduced new boundary conditions that render the C_4 higher-order Zak (Berry) phase, as constructed by Ref. [128], as a genuine topological invariant in the thermodynamic limit. From this, we constructed a simplified $\mathbb{Z}_2$ higher-order Zak (Berry) phase that distinguishes HOSPTs of the SL-BHM with hardcore bosons at half-filling and sets the stage to prove a bulk-boundary correspondence. However, before that, we investigated quantized charge transports in terms of two different Thouless pumps, a diagonal and horizontal pump, respectively. We fully characterized these pumps in terms of four Chern numbers linked to the windings of the $\mathbb{Z}_2$ higher-order Zak (Berry) phases associated with the four corners. Thereby, we argued that the latter acts as a direction dependent sensor of charge flow. Moreover, we showed that after a half-cycle, the quantized fractional corner charge is in one-to-one correspondence with a quantized change of this phase. After a numerical case study of the two different Thouless pumps, we explained why a quadrupole operator is not sufficient for the description of this phase, namely, because we saw that after a half-cycle both configurations can appear: a dipole and a quadrupole configuration, respectively. Further, we proved a bulk-boundary correspondence for HOSPTs by extending Resta's earlier work [45] to higher-order topological systems and related changes of the $\mathbb{Z}_2$ higher-order Zak (Berry) phase to the emergence of fractional charges at the corners. Lastly, we discussed a generalization of the bulk-boundary correspondence for the C_4 higher-order Zak (Berry) phase, showed to which extent the former results generalize and provided numerical evidence that the bulk-boundary correspondence remains true. However, this has to be worked out with more details in the future. Moreover, as briefly stated, it is an open question how to construct Thouless pumps for HOSPTs with fillings $n_0 \in \{1/4, 3/4\}$.

Part II

Quotient group symmetry-protected topological phenomena

Chapter 6

Quotient group symmetry-protected topological phenomena in $\mathbb{Z}_n \times \mathbb{Z}_n$ chains

In previous chapters, we extensively discussed classifications and properties of higher-order SPTs along a particular model, the 2D SL-BHM. Here, however, we focus on one-dimensional interacting bosonic SPT phases that have been fully classified in terms of the second cohomology group [50, 64, 93–95]. The elements of such groups label distinct classes of projective representations of a global symmetry, that is—intuitively speaking—how symmetries act on the edges of such systems[1]. To this end, we are particularly interested in quantum phase transitions among distinct classes of SPT phases and want to give partial answers to the following questions: When are there direct transitions between SPT phases, and how fine-tuned are they? How to characterize the corresponding conformal field theory (CFT)? When will the transition itself have certain remnant topological properties?

Some general results are known: Firstly, previous works argued that certain SPT transitions naturally come with (emergent) anomalous symmetries forbidding a flow to an intermediate gapped, symmetric phase[2], i.e., implying a direct (continuous or discontinuous) transition or an intermediate spontaneous-symmetry-breaking phase[3] [18, 82, 91, 108]. This was shown to be the case for SPTs, which cannot be written as the square of another SPT phase [82]. A second insight is that a CFT describing a continuous SPT transition can be enriched by additional symmetries. I.e., in the presence of certain symmetries, a given CFT can form distinct symmetry-enriched versions [183], some of which exhibit protected edge modes at criticality, giving rise to gapless SPT phases [183, 184]. Most examples studied so far have focused on critical points between SSB phases and SPT phases. This is in part due to the focus, thus far, on simple symmetry groups, which do not realize several non-trivial SPT phases, whereas it would be interesting to understand such cases better.

To gain further insight into the above questions and general results, we study the universe of 1D SPT phases protected by $\mathbb{Z}_n \times \mathbb{Z}_n$ symmetry. Certain properties of these models and, in particular, of their transitions are already known [34, 185]. In-

[1] For example, if we consider π rotations, then if the edge has half-integer spin representations, generators anticommute, while for integer representations they commute.

[2] A well-known anomaly is the Lieb-Schultz-Mattis anomaly [182] of the spin-1/2 Heisenberg chain, which can also be interpreted as arising at an SPT transition: explicit dimerization flows to two distinct SPT phases, which are related by single site translations.

[3] In higher dimensions, certain intrinsic topological order is also an option.

deed, Ref. [34] considered transitions between neighboring SPT classes—here we note that the classification $H^2(\mathbb{Z}_n \times \mathbb{Z}_n, U(1)) \cong \mathbb{Z}_n$ gives a natural notion of whether two SPT classes are (non-)neighboring. The authors found that for all $n < 5$ neighboring transitions are direct and continuous, and can be characterized by a CFT with central charge $c \in \{1, 8/5, 2\}$ (corresponds to $n \in \{2, 3, 4\}$). Otherwise, such transitions cross an intermediate gapless phase, which is as well characterized by a CFT with central charge $c = 2$. However, the nature of CFTs, i.e., its topological properties, and transitions between non-neighboring classes have not been studied yet. Instead, the authors expected that transitions between non-neighboring phases generically split into successive transitions between neighboring ones. However, we will show that this is not the case.

Based on previous results, we gain insight into the $\mathbb{Z}_n \times \mathbb{Z}_n$ critical points by asking which degrees of freedom remain gapped at criticality, finding that it is determined by the nature of nearby SPT phases. These gapped degrees of freedom lead to an effective low-energy description of the global symmetry group $G = \mathbb{Z}_n \times \mathbb{Z}_n$ in terms of a quotient group, that is, at low-energy degrees of freedom the action of G is given by G/H, where H is normal subgroup of G[4]. This has the following consequences:
(1) There can be direct, continuous quantum phase transitions between non-neighboring classes of SPTs. In fact, we find that in the presence of certain gapped degrees of freedom, it is impossible to perturb the critical point to certain intermediate SPT phases, thereby stabilizing the direct transition.
(2) The gapped degrees of freedom can be non-trivial, giving rise to symmetry-enriched quantum criticality [183, 184] with edge modes and degenerate entanglement spectra of critical states. Those states, living on the quantum critical point (QCP) of two SPTs or in intermediate gapless phases, form so called gapless SPTs protected by $\mathbb{Z}_n \times \mathbb{Z}_n$ symmetry.
(3) Finally, we find emergent anomalies related to the low-energy symmetry being given by a quotient symmetry group, where we quotient out by the symmetries, which act purely on gapped degrees of freedom.

Aside. This work has not been published yet and is based on [P4]. Moreover, certain parts of this chapter I obtained during my masters, in particular, the observation of direct transitions between non-neighboring classes of SPT phases. Furthermore, the numerical calculations of the central charges as well as parts of the analytical arguments have already been given there. However, for the ease of readability, we included the results in this chapter.

Overview. The remainder of this work is structured in three parts. Sec. 6.1 illustrates the above features in $\mathbb{Z}_4 \times \mathbb{Z}_4$ for ease of reading because this simpler case already exhibits many of these general features. We refer to the introduction of that section for a detailed outline. The second part of this work, Sec. 6.2, generalizes these findings to all $\mathbb{Z}_n \times \mathbb{Z}_n$ cases. In addition to this, we discuss that if one considers an equal-weighted sum of all fixed-point models, that a $\mathbb{Z}_n$ symmetry, that shifts the index of each fixed-point model by one, enhances to a $U(1)$ symmetry (a detailed outline is again found in the introduction of this section). Lastly, in Sec. 6.3 we argue on general grounds that our

[4] A subgroup H is normal if for any $h \in H$ and $g \in G$ the following holds: $ghg^{-1} \in H$.

findings are not particular to this class of models and can be generalized to other classes and dimensions.

6.1 Illustrative case: $\mathbb{Z}_4 \times \mathbb{Z}_4$ SPT transitions

This section studies quantum phase transitions between fixed-point models of $\mathbb{Z}_4 \times \mathbb{Z}_4$ symmetry, also known as (generalized) cluster chains. As necessary background information, we review these fixed-point Hamiltonians in Sec. 6.1.1, and in Sec. 6.1.2 we briefly recap their classifications in terms of projective representations and symmetry fluxes. In Sec. 6.1.3 we then turn to direct interpolations between these cluster chains, showing that all quantum phase transitions are direct, and we specify the CFT and its central charge. This generalizes the findings of Tsui et al. [34], who only considered the interpolation between neighboring SPT classes. For transitions between non-neighboring SPTs, there are additional gapped degrees of freedom at the QCP, such that we effectively obtain a $c = 1$ transition of $\mathbb{Z}_2 \times \mathbb{Z}_2$.

At low energy, the resulting quotient group $\mathbb{Z}_4 \times \mathbb{Z}_4/(\mathbb{Z}_2 \times \mathbb{Z}_2)$ shares an anomaly with the SPT duality transformation, exchanging the two SPTs. In combination with another symmetry, this stabilizes quantum criticality (see Sec. 6.1.4). To verify this, we perturb the QCP with a symmetry preserving perturbation and numerically confirm that the critical line is stable up to a finite value of the perturbation (Sec. 6.1.5). In the penultimate part, Sec. 6.1.6, we show that for certain fixed-point models the SPTs do not require the $\mathbb{Z}_4 \times \mathbb{Z}_4$ symmetry itself to be robust; instead, we find that the embedding of the quotient group in the full Hilbert space can protect the SPTs. Finally, in Sec. 6.1.7 we argue that in the presence of additional gapped degrees of freedom, the CFTs characterizing the QCPs have the same central charge but realize topologically distinct RG fixed-points in the presence of symmetries, some of which protect edge modes.

6.1.1 $\mathbb{Z}_4 \times \mathbb{Z}_4$ fixed-point models

We consider SPTs protected by $\mathbb{Z}_4 \times \mathbb{Z}_4$ symmetry. This symmetry group protects four distinct topological phases, labeled by $d \in \{0, 1, 2, 3\}$ where d characterizes the $\mathbb{Z}_n$ charge (see Eq (6.6)) classifying the SPT phase. The *fixed-point* Hamiltonians, realizing these distinct phases, are defined as follows [34, 185]:

$$\hat{H}_d = -\sum_j \left(\hat{Z}^{\dagger d}_{j-1,B}\hat{X}_{j,A}\hat{Z}^{d}_{j,B} + \text{h.c.}\right) - \sum_j \left(\hat{Z}^{d}_{j,A}\hat{X}_{j,B}\hat{Z}^{\dagger d}_{j+1,A} + \text{h.c.}\right) \tag{6.1}$$

with sublattices A and B, respectively. Here the operators $\hat{X}_{j,\sigma}$ and $\hat{Z}_{j,\sigma}$ are (generalized) Pauli matrices,

$$\hat{Z}^4 = \mathbb{1},\ \hat{X}^4 = \mathbb{1},\ \hat{X}\hat{Z} = -i\hat{Z}\hat{X}. \tag{6.2}$$

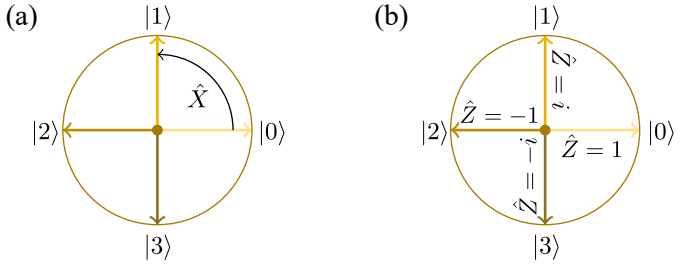

Figure 6.1: **Local Hilbert space.** Graphical representation of basis states of the local $\mathbb{Z}_4$ Hilbert space on the unit circle. The operator $\hat{X}$, panel (a), change among different "time" states, while the operator $\hat{Z}$, panel (b), measures the "time" of a given state.

In the eigenbasis of $\hat{Z}_{j,\sigma}$, the operators read:

$$\hat{X} = \begin{pmatrix} 0 & 0 & 0 & 1 \\ 1 & 0 & 0 & 0 \\ 0 & 1 & 0 & 0 \\ 0 & 0 & 1 & 0 \end{pmatrix}, \quad \hat{Z} = \begin{pmatrix} 1 & 0 & 0 & 0 \\ 0 & i & 0 & 0 \\ 0 & 0 & -1 & 0 \\ 0 & 0 & 0 & -i \end{pmatrix}, \tag{6.3}$$

and the action on local basis states—reminiscent of a $\mathbb{Z}_4$ clock—is graphically illustrated in Fig. 6.1. The $\mathbb{Z}_4 \times \mathbb{Z}_4$ symmetry is generated by two operators,

$$\mathcal{G}_\sigma = \prod_j \hat{X}_{j,\sigma}, \ \sigma \in \{A, B\}, \tag{6.4}$$

acting on disjoint sublattices A and B, respectively. By construction (for details, see Ref. [64]) all four phases can be generated from the trivial phase by successively applying the SPT-Entangler[5] denoted by $\hat{U}$,

$$\hat{H}_0 \xrightarrow{\hat{U}} \hat{H}_1 \xrightarrow{\hat{U}} \hat{H}_2 \xrightarrow{\hat{U}} \hat{H}_3 \xrightarrow{\hat{U}} \hat{H}_0. \tag{6.5}$$

6.1.2 Projective representations and symmetry fluxes of $\mathbb{Z}_4 \times \mathbb{Z}_4$ fixed-point models

Here we recall the classification of SPTs protected by $\mathbb{Z}_4 \times \mathbb{Z}_4$ symmetry, first using projective representations and, second, string operators constructed from symmetry fluxes. Further, we briefly consider how gapped degrees of freedom can be detected using string operators.

Projective representations

As briefly mentioned in the introduction and also in Sec. 2.2.1, one-dimensional interacting bosonic SPT phases are classified in terms of the second cohomology group [64], which

[5] See Eqs. (6.31) and (6.32) for a definition.

for the particular example results in four topological distinct phases $H^2(\mathbb{Z}_4 \times \mathbb{Z}_4, U(1)) = \mathbb{Z}_4$. Each element of this group labels a distinct class of projective representations[6]. These elements, which we in the following call *charges* $q_\sigma^d \in \mathbb{Z}_4$, are related to the anomalous action of symmetry on the boundary if the SPT is considered with edges [85, 86, 88, 94, 95]. Since the bulk of SPT states is symmetric, we say *symmetry fractionalizes* [95] (see also App. C.1) and we can write $\mathcal{G}_\sigma = \mathcal{G}_{L,\sigma}\mathcal{G}_{R,\sigma}$, where $\mathcal{G}_{L(R),\sigma}$ is an operator localized on the left (right) boundary of the system and $\sigma \in \{A, B\}$. These operators form projective representations of the symmetry group and, thus, commute up to a $U(1)$ phase factor[7]

$$\mathcal{G}_{\sigma+1}^{-1}\mathcal{G}_{R,\sigma}\mathcal{G}_{\sigma+1} = q_{\sigma+1}^d \mathcal{G}_{R,\sigma}, \quad q_{\sigma+1}^d \in \mathbb{Z}_4. \tag{6.6}$$

with $A+1 \equiv B$ (and vice versa), and charges given by $q_A^d = \omega_4^d$ and $q_B^d = \bar{\omega}_4^d$. Details on projective representations for the fixed-point models have been evaluated by Geraedts et al. [185].

String order parameters

There is an alternative way of detecting the charges q_σ^d, using so-called *symmetry fluxes* [94, 183]. A symmetry flux associated to $\mathbb{Z}_4 \times \mathbb{Z}_4$ symmetry is a half-infinite string operator, where the string consists of on-site symmetry operators $\hat{X}_{j,\sigma}$,

$$\hat{\mathcal{S}}_{r,A}^d = \prod_{j \le r} \hat{X}_{j,A}\mathcal{O}_{r,B}^d, \quad \hat{\mathcal{S}}_{r,B}^d = \prod_{j \le r} \hat{X}_{j,B}\mathcal{O}_{r+1,A}^d, \tag{6.7}$$

whose end-point is decorated by an operator that has a well-defined charge w.r.t $\mathbb{Z}_4 \times \mathbb{Z}_4$ symmetry defined by,

$$\mathcal{G}_{\sigma+1}^{-1}\hat{\mathcal{S}}_{r,\sigma}^d\mathcal{G}_{\sigma+1} = Q_{\sigma+1}^d\hat{\mathcal{S}}_{r,\sigma}^d, \quad Q_{\sigma+1}^d \in H^2(\mathbb{Z}_4 \times \mathbb{Z}_4, U(1)) = \mathbb{Z}_4. \tag{6.8}$$

For a given SPT phase, the string operator,

$$\langle \hat{\mathcal{S}}_{r-r_0,\sigma}^{\dagger d}\hat{\mathcal{S}}_{r,\sigma}^d \rangle \xrightarrow{r_0 \to \infty} \text{const.} \tag{6.9}$$

has long-range order if we choose the end-point operator appropriately[8]. Indeed, for the correlator not to vanish, the charges q_σ^d and Q_σ^d have to fulfill the following compatibility conditions [94]:

$$q_A^d Q_A^d = 1, \qquad q_B^d Q_B^d = 1. \tag{6.10}$$

For models considered here, the end-point operators read [186]:

$$\mathcal{O}_{r,B}^d = \hat{Z}_{r,B}^d, \quad \mathcal{O}_{r+1,A}^d = \hat{Z}_{r+1,A}^{\dagger d}, \quad d \in \{0, 1, 2, 3\}. \tag{6.11}$$

[6] For Abelian symmetry groups, this simply means that group multiplications are obeyed up to a $U(1)$ phase factor. For example, the on-site operators $\hat{X}_{j,\sigma}^{d'}$ and $\hat{Z}_{j,\sigma}^d$ form a projective representation of $\mathbb{Z}_4 \times \mathbb{Z}_4$ symmetry, $\hat{X}_{j,\sigma}^{d'}\hat{Z}_{j,\sigma}^d = (-i)^{dd'}\hat{Z}_{j,\sigma}^d\hat{X}_{j,\sigma}^{d'}$ with $(d, d') \in \mathbb{Z}_4 \times \mathbb{Z}_4$

[7] Using symmetry fractionalization, we can safely replace $\mathcal{G}_{R,\sigma+1} \to \mathcal{G}_{\sigma+1}$.

[8] Note the "†" in the definition of $\hat{\mathcal{S}}_{r-r_0,\sigma}^{\dagger d}$ means that we replace all operators by its hermitian conjugate, but the string of the symmetry flux still starts at $-\infty$ and ends at $r - r_0$.

String operators and gapped degrees of freedom

For gapped degrees of freedom that are charged under a certain symmetry, a string operator associated to the corresponding symmetry flux has long-range order [183]. This makes symmetry fluxes an appropriate tool to diagnose gapped degrees of freedom on QCPs. For some QCPs of transitions of $\mathbb{Z}_4 \times \mathbb{Z}_4$ symmetric fixed-point models, we will show that there are two topologically distinct (i.e., end-point operators have distinct charges w.r.t to $\mathbb{Z}_4 \times \mathbb{Z}_4$ symmetry) symmetry fluxes associated to the $\mathbb{Z}_2 \times \mathbb{Z}_2$ subgroup such that the resulting string operators have long-range order *even though* the underlying state is critical. The corresponding symmetry fluxes are given by,

$$\hat{\mathrm{s}}^{2,d}_{r,\sigma} = \left(\hat{\mathcal{S}}^{d}_{r,\sigma}\right)^2, \; d \in \mathbb{Z}_4. \tag{6.12}$$

If a string operator built from such symmetry fluxes has long-range order, we say the associated symmetry is *gapped*.

6.1.3 Quantum phase transitions

Quantum phase transitions among different classes of SPTs protected by $\mathbb{Z}_4 \times \mathbb{Z}_4$ symmetry can be described by the following Hamiltonian:

$$\hat{H}_{d\delta}(\lambda) = (1-\lambda)\hat{H}_d + \lambda \hat{H}_{d+\delta}, \quad d \in \{0,1,2,3\}, \quad \delta \in \{1,2\}. \tag{6.13}$$

In Ref. [34] it was shown that any quantum phase transition between adjacent classes ($\delta = 1$) of SPTs, protected by $\mathbb{Z}_4 \times \mathbb{Z}_4$ symmetry, is direct, continuous and its critical point $\lambda_c = 1/2$ is characterized by a CFT with central charge $c = 2$. Quantum phase transitions among non-neighboring classes of SPTs have not been considered so far. Naively, one might expect that, for example, the transition for $(d, \delta) = (0, 2)$ splits into the following sequence of transitions $0 \to 1 \to 2$, where the numbers label different classes of SPTs. However, it turns out that this not the case and for Hamiltonian (6.13) it is actually not possible (see below). Instead, the following scenario applies:

Direct transition. Any quantum phase transition described by Hamiltonian (6.13) is direct and continuous. The QCP is characterized by a CFT with central charge $c = 2$ if $\delta = 1$ and $c = 1$ otherwise (see Fig. 6.2).

To show that models with $(d, \delta = 2)$ have a direct transition, it is sufficient to consider the case $d = 0$[9] for which the Hamiltonian reads:

$$\hat{H}_{02}(\lambda) = -\sum_j \left[(1-\lambda)\hat{X}_j + \lambda \hat{Z}^2_{j-1}\hat{X}_j\hat{Z}^2_{j+1} + \text{h.c.}\right], \tag{6.14}$$

where we used that $\hat{H}_{02}(\lambda)$ is translation symmetric and, thus, there is no need for a sublattice index. The Hamiltonian conserves a local $\mathbb{Z}_2$ symmetry generated by $\hat{X}^2_j$,

$$\left[\hat{H}_{02}(\lambda), \hat{X}^2_j\right] = 0, \; \forall \, j, \lambda, \tag{6.15}$$

[9] Other cases are related by applications of the SPT-Entangler $\hat{U}$.

where all $\hat{X}_j^2 = 1$ in the ground state subspace (gs) (see App. B.3). In this sector, local operators of Hamiltonian (6.14) reduce to Pauli operators $\hat{X}_j := \hat{\mathcal{X}}_j$ and $\hat{Z}_j^2 := \hat{\mathcal{Z}}_j$ and, hence, the effective Hamiltonian is given by,

$$\hat{H}_{02}(\lambda) \overset{gs}{=} -2 \sum_j \left[(1-\lambda)\hat{\mathcal{X}}_j + \lambda \hat{\mathcal{Z}}_{j-1} \hat{\mathcal{X}}_j \hat{\mathcal{Z}}_{j+1} \right], \tag{6.16}$$

describing the interpolation between the $\mathbb{Z}_2 \times \mathbb{Z}_2$ cluster model [61] and a paramagnetic phase. Upon tuning λ, there is a single QCP at $\lambda = 1/2$ characterized by a CFT with central charge $c = 1$ [34]. Since the central charge of a CFT is related to spectral properties of a Hamiltonian [187], unitary transformations cannot change its value. Thus, the quantum phase transition of Hamiltonian $\hat{H}_{12}(\lambda)$—related to $\hat{H}_{02}(\lambda)$ by applying the SPT-Entangler $\hat{U}$ once—has to have the same central charge. (However, this transformation changes the nature of the underlying CFT, see Sec. 6.1.7). Thus, we showed

Figure 6.2: **Phase diagram of $\mathbb{Z}_4 \times \mathbb{Z}_4$ interpolation.** The symmetry group $\mathbb{Z}_4 \times \mathbb{Z}_4$ allows for four distinct SPT phases. Transitions at $\lambda_c = 1/2$, described by Hamiltonian (6.13), are characterized by a central charge $c = 2$ if $\delta = 1$ and central charge $c = 1$ if $\delta = 2$. In fact, for the case $\delta = 2$ we show that the two different choices (i.e., $\hat{H}_0 + \hat{H}_2$ and $\hat{H}_1 + \hat{H}_3$) are distinct symmetry-enriched CFTs, where the latter is topologically non-trivial with exponentially localized edge modes (see Sec. 6.1.7).

that the low-energy theory of $\hat{H}_{02}(\lambda)$ is completely specified in terms of the $\mathbb{Z}_2 \times \mathbb{Z}_2$ fixed point models. As we shall see, this is not fine-tuned and is robust to finite perturbations.

A comment on notation: Whenever a Hamiltonian is equal-weighted, we write $\hat{H}_{02}(\lambda = 1/2) \equiv \hat{H}_{02}$

6.1.4 Stability of quantum criticality

Previously, we showed that $\hat{H}_{02}(\lambda)$ conserves a local $\mathbb{Z}_2$ symmetry. Given that its generator is equal to identity in the ground state subspace, $\hat{X}_j^2 \overset{gs}{=} 1$, $\forall j$, this implies that the string operators associated to symmetry fluxes of the $\mathbb{Z}_2 \times \mathbb{Z}_2$ subgroup have long-range order—even at criticality ($\lambda = 1/2$),

$$\langle \hat{\mathrm{s}}_{l,\sigma}^{\dagger 2,0} \hat{\mathrm{s}}_{l+r_0,\sigma}^{2,0} \rangle = \langle \hat{X}_{l,\sigma}^2 ... \hat{X}_{l+r_0,\sigma}^2 \rangle \xrightarrow{r_0 \to \infty} \text{const.} \tag{6.17}$$

Thus, degrees of freedom charged under this symmetry are massive—meaning excitations associated to these degrees of freedom require a finite amount of energy. On the other hand, the action of the $\mathbb{Z}_2 \times \mathbb{Z}_2$ subgroup on low-energy degrees of freedom is trivial. Hence, in the low-energy subspace the global $\mathbb{Z}_4 \times \mathbb{Z}_4$ symmetry acts as a quotient group,

$$\mathbb{z}_2 \times \mathbb{z}_2 = (\mathbb{Z}_4 \times \mathbb{Z}_4) \,/\, (\mathbb{Z}_2 \times \mathbb{Z}_2)\,, \tag{6.18}$$

for which we used small letters to distinguish it from the gapped $\mathbb{Z}_2 \times \mathbb{Z}_2$ subgroup. (We emphasize that the quotient group $\mathbb{z}_2 \times \mathbb{z}_2$ is *not* a subgroup of $\mathbb{Z}_4 \times \mathbb{Z}_4$.) Note the long-range order of the string operator, Eq. (6.17), has an important consequence. As long as it has long-range order, starting from $d = 0$, it is impossible to enter the SPTs associated to the fixed-point Hamiltonians $\hat{H}_1$ and $\hat{H}_3$.

Intrinsic anomalies

To argue the stability of low-energy properties, let us emphasize that Hamiltonian (6.14) has an additional $\mathbb{Z}_2$ symmetry at the QCP generated by $\hat{U}^2$, which exchanges $\hat{H}_0 \leftrightarrow \hat{H}_2$. Together with the $\mathbb{Z}_4 \times \mathbb{Z}_4$ symmetry, this imposes a powerful constraint on the possible phase diagram:

Absence of gapped, symmetric phases. There is no $\mathbb{Z}_4 \times \mathbb{Z}_4 \times \mathbb{Z}_2$ symmetric perturbation that gaps out the QCP of $\hat{H}_{02}$ towards a gapped, symmetric phase (where the latter $\mathbb{Z}_2$ symmetry is generated by $\hat{U}^2$). Moreover, the effective symmetry group in the low-energy subspace is given by $\mathbb{z}_2 \times \mathbb{z}_2 \times \mathbb{Z}_2$.

To see this, first note that any gapped, symmetric phase must be equivalent[10] to one of the four possible SPTs associated to $\mathbb{Z}_4 \times \mathbb{Z}_4$ symmetry. Thus, according to Sec. 6.1.2, there must exist a pair of symmetry fluxes such that their associated string operators have long-range order. However, no symmetry flux is invariant under the action of $\hat{U}^2$. Consequently, there cannot be a perturbation towards a gapped, symmetric phase. We say the symmetry $\mathbb{Z}_4 \times \mathbb{Z}_4 \times \mathbb{Z}_2$ has a *gauge anomaly* also called an *intrinsic anomaly* [91, 188] (see App. B.4).

Emergent anomalies

In the following we will show that perturbations can non-trivially change the representation of the duality symmetry in a way such that the intrinsic anomaly becomes emergent, and finally can be lifted for sufficiently strong perturbations. To this end, we perturb the criticality of Hamiltonian $\hat{H}_{02}$ with $\hat{H}_1$ resulting in the following Hamiltonian:

$$\hat{H}_{021}(\gamma) = \frac{1-\gamma}{2}\left(\hat{H}_0 + \hat{H}_2\right) + \gamma \hat{H}_1. \tag{6.19}$$

The perturbation preserves the additional $\mathbb{Z}_2$ symmetry, but non-trivially changes its generator

$$\hat{U}^2 \to \hat{S}_{AB}\hat{U}^2, \tag{6.20}$$

where $\hat{S}_{AB}$ denotes a sublattice symmetry exchanging $A \leftrightarrow B$. This new generator still exchanges $\hat{H}_0 \leftrightarrow \hat{H}_2$—but unlike $\hat{U}^2$—it maps $\hat{H}_1$ to itself.
Given this new generator, what does change? Previously, we argued none of the symmetry fluxes is invariant under the duality transformation, but given its new representation,

[10] See Chap. 2 for a definition of equivalence.

this is no longer true. Indeed, since $\hat{H}_1$ is invariant under this symmetry, also its symmetry fluxes are unchanged. However, as long as the string operators defined in Eq. (6.17) have long-range order, no string operator associated to $\hat{H}_1$ can have long-range order. The reason is that charges are not compatible, which can be deduced from symmetry fluxes. To be compatible, such symmetry flux must square to $\hat{\mathrm{s}}^{2,0}_{r,\sigma}$, which is not the case for $\hat{\mathcal{S}}^{1}_{r,\sigma}$.

Emergent anomaly. The QCP of $\hat{H}_{02}$ cannot be symmetrically gapped out by $\hat{H}_1$ as long as the $\mathbb{Z}_2 \times \mathbb{Z}_2 \subset \mathbb{Z}_4 \times \mathbb{Z}_4$ subgroup remains gapped, and the string operators associated to $\hat{\mathrm{s}}^{2,0}_{r,\sigma}$ have long-range order.

For the emergent anomaly to persist, it is crucial that the action of the $\mathbb{Z}_2 \times \mathbb{Z}_2$ subgroup on low-energy degrees of freedom is trivial. This ensures that the global $\mathbb{Z}_4 \times \mathbb{Z}_4$ symmetry acts as a quotient group, which together with the duality symmetry has an anomaly. If the anomaly is lifted, i.e., the long-range order of the string operators, Eq. (6.17), disappears, then the effective symmetry group at low energies is lifted: $\mathbb{z}_2 \times \mathbb{z}_2 \to \mathbb{Z}_4 \times \mathbb{Z}_4$. Mathematically, this is called *symmetry extension*, which is known to be a mechanism of lifting anomalies[11] [39, 188–192]. If the long-range order of the string operators, Eq. (6.17), disappears, nothing forbids the existence of a gapped, symmetric state (see Fig. 6.3).

Field theory. In accordance with the results obtained from the lattice perspective, there is also a field theoretic argument why quantum criticality is stable to finite perturbations of $\hat{H}_1$, which is discussed in detail in App. B.5. The low-energy theory of Hamiltonian (6.16) is described by a Luttinger liquid (LL) and for the particular symmetries, we argue that the LL cannot be gapped out as long as symmetries are preserved, and the $\mathbb{Z}_2 \times \mathbb{Z}_2$ subgroup remains gapped.

6.1.5 Numerical evaluation of the phase diagram and emergent anomaly

Next we show that, upon increasing the coupling of $\hat{H}_1$, the emergent anomaly is robust to a finite value of γ, where the system enters an SSB phase, and then finally arrive in the gapped, symmetric phase of $\hat{H}_1$. To study the stability of the direct transition of $\hat{H}_{02}$ and also its emergent anomaly, we numerically evaluated the phase diagram of the following Hamiltonian using the infinite density matrix renormalization group (iDMRG) [40, 41, 122] Ansatz:

$$\hat{H}_{021}(\alpha, \beta, \gamma) = \alpha \hat{H}_0 + \beta \hat{H}_2 + \gamma \hat{H}_1, \tag{6.21}$$

where $\alpha + \beta + \gamma = 1$. Note, along the line $\alpha = \beta$ the Hamiltonian reduce to $\hat{H}_{021}(\gamma)$ defined in Eq. (6.19). The phase diagram is shown in Fig. 6.3 (for numerical details, see App. B.1). As theoretically predicted, the critical point of $\hat{H}_{02}$ stays stable, upon

[11] On the Hilbert space the global symmetry is always $\mathbb{Z}_4 \times \mathbb{Z}_4$, but its action in the low-energy subspace can be different. In this sense, we say that the low-energy action is lifted upon considering the high-energy degrees of freedom.

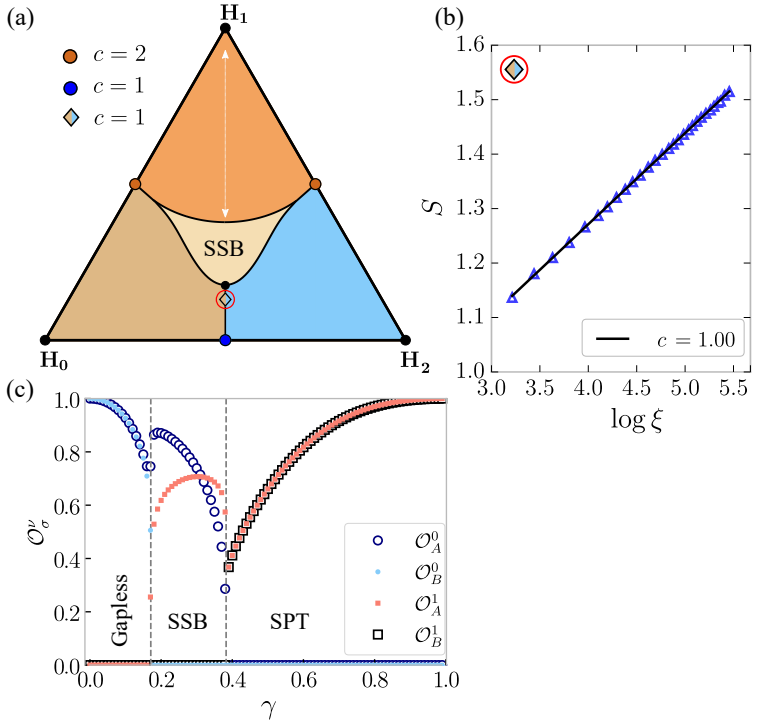

Figure 6.3: **Phase diagram and emergent anomaly of $\hat{H}_{021}(\alpha, \beta, \gamma)$.** (a) There are three topologically distinct phases labeled by $\hat{H}_0$, $\hat{H}_1$ and $\hat{H}_2$, respectively. The phase in the middle is SSB, where one of the $\mathbb{Z}_4$ symmetries and sublattice symmetry are broken spontaneously. (b) The central charge, obtained with iDMRG from $S = \frac{c}{6} \log \xi + \text{const.}$ [193, 194], of the CFT along the direct transition between $\hat{H}_0$ and $\hat{H}_2$ is unchanged even in the presence of $\hat{H}_1$ (data are evaluated at the red encircled point in (a)). Panel (c) shows the string operators $\mathcal{O}^\nu_\sigma$, Eq. (6.22), along the line $\alpha = \beta$, $\gamma \in [0, 1]$ (indicated by the white arrow in (a)) characterizing the emergent anomaly. Note, for the evaluation of the string operator in the SSB phase we explicitly conserved the $\mathbb{Z}_4$ symmetry on the A sublattice.

increasing $\hat{H}_1$ to a finite value of γ. Up to this point, the renormalization group fixed-point, given by the CFT with central charge $c = 1$, is unchanged, see Fig. 6.3b. The SSB phase in the middle spontaneously breaks the sublattice symmetry $\hat{S}_{AB}$, introduced in Eq. (6.20), and one of the global $\mathbb{Z}_4$ symmetries. To measure the emergent anomaly, we evaluated the following four string operators (see also Eq. (6.12)):

$$\mathcal{O}^\nu_\sigma = \lim_{r_0 \to \infty} \left| \langle \hat{\mathrm{s}}^{\dagger 2,\nu}_{l,\sigma} \hat{\mathrm{s}}^{2,\nu}_{l+r_0,\sigma} \rangle \right|, \ \sigma \in \{A, B\}, \ \nu \in \{0, 1\}. \tag{6.22}$$

What behavior do we expect? If there is an emergent anomaly we expect $\mathcal{O}^0_A = \mathcal{O}^0_B \neq 0$ and $\mathcal{O}^1_A = \mathcal{O}^1_B = 0$, while in the symmetric, gapped phase of $\hat{H}_1$ the behavior is exactly opposite. Note, long-range order of the non-charged string operators $\mathcal{O}^0_\sigma$ is forbidden

in any gapped SPT that is neither $\hat{H}_0$ nor $\hat{H}_2$. Given the nature of the SSB phase, we expect all string operators on the symmetry preserving sublattice to be non-zero. The results of the string operators are shown in Fig. 6.3c, which very well agree with the theoretical predictions. As we tune towards the SSB phase, the emergent anomaly is lost since the $\mathbb{Z}_2 \times \mathbb{Z}_2$ subgroup becomes gapless. Indeed, this subgroup is (partly) broken in the SSB phase, which means it cannot remain gapped along the transition.

Note upon relabelling $\hat{H}_i \to \hat{H}_{i+1}$ and $\mathcal{O}^0_{r,\sigma} \leftrightarrow \mathcal{O}^1_{r,\sigma}$ in Fig. 6.3a and Fig. 6.3c, respectively, the phase diagram shows the stability of the QCP of $\hat{H}_{12}$.

6.1.6 The embedding of the quotient group

The Hamiltonian $\hat{H}_{02}(\lambda)$ has a salient feature, namely, the SPTs are stable even if the global $\mathbb{Z}_4 \times \mathbb{Z}_4$ symmetry is broken. Given that the individual Hamiltonians are fixed-point models of this symmetry, this is somewhat surprising. It turns out that if the quotient group is embedded into the full Hilbert space, it becomes an exact symmetry of the Hamiltonian. Formally, this additional $\mathbb{Z}_2 \times \mathbb{Z}_2$ symmetry (which is *not* a subgroup of the above $\mathbb{Z}_4 \times \mathbb{Z}_4$ symmetry) is generated by two operators

$$\hat{\mathcal{Q}}_\sigma = \prod_{j,\sigma} \left(\mathbb{1} \otimes \hat{\mathcal{X}}\right)_{j,\sigma}, \ \sigma \in \{A, B\}, \tag{6.23}$$

which transform local operators as follows (see App. B.2):

$$\hat{\mathcal{Q}}_\sigma : \hat{X}_{j,\sigma} \leftrightarrow \hat{X}^\dagger_{j,\sigma}, \quad \hat{\mathcal{Q}}_\sigma : \hat{Z}^2_{j,\sigma} \leftrightarrow -\hat{Z}^2_{j,\sigma}. \tag{6.24}$$

This clearly shows that both $\hat{H}_0$ and $\hat{H}_2$ are invariant under this transformation. According to Sec. 6.1.2 we can define symmetry fluxes whose end-point operators have a discrete charge w.r.t this symmetry. Given that this a $\mathbb{Z}_2 \times \mathbb{Z}_2$ symmetry, there are two different charges. Since in the low-energy subspace this symmetry is indistinguishable from the quotient symmetry, we know that—depending on λ—a pair of its associated string operators has long-range order. Thus, as long as this symmetry is preserved, the SPTs are well-defined. A possible perturbation that keeps the embedding of the quotient group but breaks the global $\mathbb{Z}_4 \times \mathbb{Z}_4$ symmetry is given by[12],

$$\hat{V} = \sum_{j,\sigma} \left(\hat{\mathcal{Z}} \otimes \mathbb{1}\right)_{j,\sigma} \tag{6.25}$$

for which the ground states of the individual Hamiltonians can be calculated exactly.

6.1.7 Symmetry-enriched quantum criticality

In Sec. 6.1.3 we argued that the CFTs of $\hat{H}_{02}$ and $\hat{H}_{12}$ ($H_{d\delta}$ with $(d, \delta) = (1, 2)$; interpolation between $\hat{H}_1$ and $\hat{H}_3$) have the same central charge. However, as we demonstrate now, their CFTs are topologically distinct—following Ref. [183] we say that the underlying CFT is *symmetry-enriched* by $\mathbb{Z}_4 \times \mathbb{Z}_4$ symmetry. On each of the QCPs, there are

[12] This operator does not commute with the generator of the $\mathbb{Z}_4 \times \mathbb{Z}_4$ symmetry, see App. B.2.

additional gapped degrees of freedom, which is reflected in long-range order of string operators associated to the $\mathbb{Z}_2 \times \mathbb{Z}_2$ subgroup. However, the end-point operators of the symmetry fluxes are oppositely charged w.r.t $\mathbb{Z}_4 \times \mathbb{Z}_4$ symmetry. While symmetry fluxes $\hat{\mathrm{s}}^{2,0}_{r,\sigma}$ are trivially charged, the symmetry fluxes $\hat{\mathrm{s}}^{2,1}_{r,\sigma}$[13], according to which string operators have long-range order at the QCP of $\hat{H}_{12}$, have a non-trivial charge $(Q^1_{r,\sigma+1})^2 = -1$ (see Eq. (6.12)).

Topologically distinct CFTs. In the presence of $\mathbb{Z}_4 \times \mathbb{Z}_4$ symmetry, the CFTs of $\hat{H}_{02} \propto \hat{H}_0 + \hat{H}_2$ and $\hat{H}_{12} \propto \hat{H}_1 + \hat{H}_3$ carry topologically distinct charges $(Q^0_{r,\sigma+1})^2 = 1$ and $(Q^1_{r,\sigma+1})^2 = -1$, respectively, measured by the long-range order of string operators of the gapped $\mathbb{Z}_2 \times \mathbb{Z}_2$ subgroup.

These charges assign the CFTs discrete quantum numbers, which are protected by a finite energy gap associated to the gapped degrees of freedom (see Secs. (6.1.4, 6.1.5)). *What does this imply?* Since symmetry-enriched CFTs carry distinct quantum numbers w.r.t $\mathbb{Z}_4 \times \mathbb{Z}_4$ symmetry, they represent two distinct renormalization group fixed-points that cannot be smoothly connected, i.e., there exists no path connecting the QCPs of $\hat{H}_{02}$ and $\hat{H}_{12}$ along with the central charge is unchanged [183].

Edge modes and a degenerate entanglement spectrum

The non-trivial charges of end-point operators of $\hat{\mathrm{s}}^{2,1}_{r,\sigma}$ further imply that the ground state of $\hat{H}_1 + \hat{H}_3$ has (at least) a two-fold degenerate entanglement spectrum and, moreover, if we consider a half-infinite chain, then there are exponentially localized edge modes [93–95, 183]. For Hamiltonian $\hat{H}_{12}$, this can be shown explicitly: If the system is considered as a half-infinite chain, then $\hat{H}_{12}$ commutes with two locally confined operators $\hat{\epsilon}_1 = \hat{Z}_{1,A}$ and $\hat{\epsilon}_2 = \hat{X}^2_{1,A}\hat{Z}^2_{1,B}$, which themselves anticommute $\{\hat{\epsilon}_1, \hat{\epsilon}_2\} = 0$. This algebra implies a two-fold degeneracy of the ground state manifold[14]. Moreover, as neither of the two operators commutes with the global $\mathbb{Z}_4 \times \mathbb{Z}_4$ symmetry, there is SSB at the edge of the system. The degeneracy of the entanglement spectrum becomes more apparent if a possible ground state is written as Schmidt decomposition,

$$|\Psi_{12}\rangle = \sum_\alpha \Lambda_\alpha \, |\alpha_\mathcal{E}\rangle \, |\alpha_\mathcal{B}\rangle \,, \tag{6.26}$$

where the system is bipartite into an edge region $\mathcal{E}$ and a bulk region $\mathcal{B}$[15]. If $|\Psi_{12}\rangle$ is a common eigenstate of $\hat{H}_{12}$ and $\hat{\epsilon}_1$, then the other ground state is obtained from the action of $\hat{\epsilon}_2$ on this state. Given the spatial confinement of this operator, the Schmidt states in the bulk $\{|\alpha_\mathcal{B}\rangle\}$ are unchanged upon acting with $\hat{\epsilon}_2$. However, as the two

[13] The Hamiltonians $\hat{H}_{02}$ and $\hat{H}_{12}$ are related by the SPT-Entangler $\hat{U} : \hat{H}_{02} \to \hat{H}_{12}$, which maps $\hat{U} : \hat{\mathrm{s}}^{2,0}_{r,\sigma} \to \hat{\mathrm{s}}^{2,1}_{r,\sigma}$.

[14] Actually, the overall spectrum is at least twofold degenerate, which is, however, not relevant here.

[15] The size of the edge region can be determined in terms of the localization length of the edge modes. We then require the edge region to be much larger than the localization length.

ground states are orthogonal, the Schmidt states associated to the edge region $\mathcal{E}$ must be non-trivially transformed. Consequently, to each bulk state there are two edges states having the same Schmidt value $\Rightarrow$ each Schmidt value is at least two-fold degenerate (cf. Sec 2.2.1). Instead of using the operators $\hat{\epsilon}_1$ and $\hat{\epsilon}_2$, we could have used the projective representations of the gapped $\mathbb{Z}_2 \times \mathbb{Z}_2$ subgroup[16]. Thus, as long as the latter is gapped, there are exponentially localized edge modes and an entanglement spectrum that is at least two-fold degenerate.

Gapless SPTs. States characterized by CFTs with symmetry-enriched quantum criticality form gapless SPTs, which similar to their gapped counterparts have edge modes and degeneracies in the entanglement spectrum protected by symmetry. Commonly, gapless SPTs occur on QCPs between SSB and SPT transitions [183, 184], here; however, they appear on QCPs between two SPTs. Their protection requires the global $\mathbb{Z}_4 \times \mathbb{Z}_4$ symmetry and the additional $\mathbb{Z}_2$ symmetry.

6.1.8 Summary

In the first part, we considered quantum phase transitions among fixed-point SPT models with $\mathbb{Z}_4 \times \mathbb{Z}_4$ symmetry. Generalizing a previous work of Tsui et al. [34], we showed that all quantum phase transitions described by Hamiltonian (6.13) have a single QCP classified by a CFT with central $c = 2$ for transitions among neighboring classes and $c = 1$ otherwise. In the latter case, we showed that the Hamiltonian conserves a local $\mathbb{Z}_2$ symmetry, from which we concluded that the effective low-energy theory is described by the transition between the fixed-point models of $\mathbb{Z}_2 \times \mathbb{Z}_2$ symmetry. Indeed, if the $\mathbb{Z}_2 \times \mathbb{Z}_2$ subgroup is gapped, i.e., the string operators associated to the symmetry fluxes, Eq. (6.17), have long-range order, then starting from $d = 0$ it is impossible to enter the SPT phases associated to $\hat{H}_1$ and $\hat{H}_3$. Afterwards, we argued that there is an additional $\mathbb{Z}_2$ symmetry at the QCP which together with the global $\mathbb{Z}_4 \times \mathbb{Z}_4$ symmetry gives rise to an intrinsic or emergent anomaly—depending on the representation of its generator. Nevertheless, we found that the QCP point is stable against perturbations towards a gapped, symmetric phase, and in the case of an intrinsic anomaly, it is even impossible. To numerically validate our findings, we perturbed the QCP of $\hat{H}_{02}$ with $\hat{H}_1$ and evaluated a full phase diagram, Fig. 6.3, where we also explicitly calculated the emergent anomaly using string operators. Although the individual parts of $\hat{H}_{02}(\lambda)$ are fixed-point Hamiltonians of $\mathbb{Z}_4 \times \mathbb{Z}_4$ symmetry, we showed that the SPTs do not require the $\mathbb{Z}_4 \times \mathbb{Z}_4$ symmetry to be protected. Indeed, we argued that the embedding of the quotient group becomes an exact symmetry protecting these phases. Lastly, we discussed that although the CFTs of $\hat{H}_{02}$ and $\hat{H}_{12}$ have the same central charge, the topological nature—in the presence of $\mathbb{Z}_4 \times \mathbb{Z}_4$ symmetry—is distinct. In the latter case, we argued that the gapped degrees of freedom form a non-trivial topological state resulting in exponentially localized edge modes and an entanglement spectrum that is at least two-fold degenerate.

[16] These are exponentially localized near the edge of the system.

6.2 The general case: $\mathbb{Z}_n \times \mathbb{Z}_n$ SPT transitions

Having discussed an illustrative case, we now turn over to redo the previous analysis and consider fixed-point models of $\mathbb{Z}_n \times \mathbb{Z}_n$ symmetry (see Sec. 6.2.1). To this end, in Sec. 6.2.2 we will show that there are many more direct transitions among fixed-point models, as initially expected. Moreover, for the particular choice of paths, we show that there are only three different central charges $c \in \{1, 8/5, 2\}$ characterizing the CFTs. To verify our analytical predictions, Sec. 6.2.2, we numerically evaluated the central charges of several transitions. Afterwards, unlike in the previous section, we demonstrate that for certain classes of SPTs subgroups of $\mathbb{Z}_n \times \mathbb{Z}_n$ symmetry can stabilize the phase. In this context, Sec. 6.2.3, we show that the embedding of the quotient group is an exact symmetry only for two particular classes of Hamiltonians. Subsequently, in Sec. 6.2.4 we will prove that for odd n there are no intrinsic anomalies, and discuss when to expect emergent anomalies. At the end of this section, Sec. 6.2.6, we consider the equal-weighted sum of all fixed-point Hamiltonians and discover an additional $\mathbb{Z}_n$ symmetry that together with $\mathbb{Z}_n \times \mathbb{Z}_n$ symmetry leads to an intrinsic anomaly, and can be enhanced to a global $U(1)$ symmetry.

6.2.1 $\mathbb{Z}_n \times \mathbb{Z}_n$ fixed-point models

The fixed-point models associated to SPT phases protected by $\mathbb{Z}_n \times \mathbb{Z}_n$ symmetry are given by the following Hamiltonian [34, 185]:

$$\hat{H}_d^{(n)} = -\sum_j \left(\hat{Z}_{j-1,B}^{\dagger d}\hat{X}_{j,A}\hat{Z}_{j,B}^{d} + \text{h.c.}\right) - \sum_j \left(\hat{Z}_{j,A}^{d}\hat{X}_{j,B}\hat{Z}_{j+1,A}^{\dagger d} + \text{h.c.}\right), \tag{6.27}$$

with $d \in \mathbb{Z}_n$. In the eigenbasis of $\hat{Z}_{j,\sigma}$, the operators $\hat{X}_{j,\sigma}$ and $\hat{Z}_{j,\sigma}$ can be written as:

$$\hat{Z} = \sum_{l=0}^{n-1} \omega_n^l \left|l\right\rangle\left\langle l\right|, \quad \hat{X} = \sum_{l=0}^{n-1} \left|l+1\right\rangle\left\langle l\right|, \quad \omega_n = e^{2\pi i/n}, \quad \bar{\omega}_n = e^{-2\pi i/n}. \tag{6.28}$$

Moreover, the defining properties of the operators read:

$$\hat{Z}^n = \mathbb{1},\ \hat{X}^n = \mathbb{1},\ \hat{X}\hat{Z} = \bar{\omega}_n \hat{Z}\hat{X}. \tag{6.29}$$

SPT-Entangler

By construction[17], every non-trivial fixed-point model can be constructed from $\hat{H}_0^{(n)}$ via the following sequence,

$$\hat{H}_0^{(n)} \xrightarrow{\hat{U}^{(n)}} \hat{H}_1^{(n)} \xrightarrow{\hat{U}^{(n)}} \ldots \xrightarrow{\hat{U}^{(n)}} \hat{H}_{n-1}^{(n)} \xrightarrow{\hat{U}^{(n)}} \hat{H}_0^{(n)}, \tag{6.30}$$

where the SPT-Entangler is a quantum circuit consisting of two layers of two-qudit gates (see Fig. 6.4):

$$\hat{U}^{(n)} = \hat{U}_{AB}^{(n)}\hat{U}_{BA}^{(n)}, \tag{6.31}$$

[17] This is an inherent property of fixed-point models constructed using the methods given by Ref [64].

with operators $\hat{U}^{(n)}_{AB}$ and $\hat{U}^{(n)}_{BA}$

$$\hat{U}^{(n)}_{AB} = \prod_j C\bar{Z}^{(n)}_{j,AB}, \quad \hat{U}^{(n)}_{BA} = \prod_j CZ^{(n)}_{(j,B),(j+1,A)}. \tag{6.32}$$

The notation $CZ^{(n)}$ refers to the *Controlled-Z* gate, known from quantum information theory. These two-site gates have a rather simple definition[18],

$$CZ = \begin{pmatrix} \hat{Z}^0 & 0 & 0 & 0 \\ 0 & \hat{Z} & 0 & 0 \\ 0 & 0 & \ddots & \vdots \\ 0 & 0 & \cdots & \hat{Z}^{n-1} \end{pmatrix}, \quad C\bar{Z} = (CZ)^*, \tag{6.33}$$

where we suppressed the index. For $n = 2$, this reduces to the two-qubit Controlled-Z gate $CZ = \mathrm{diag}\,(1, 1, 1, -1)$. The SPT-Entangler transforms local operators as follows:

$$\hat{U}^{(n)} : \hat{X}_{j,A} \to \hat{Z}^\dagger_{j-1,B}\hat{X}_{j,A}\hat{Z}_{j,B}, \quad \hat{U}^{(n)} : \hat{X}_{j,B} \to \hat{Z}_{j,A}\hat{X}_{j,B}\hat{Z}^\dagger_{j+1,A}, \tag{6.34}$$

while it commutes with $\hat{Z}_{j,\sigma}$ and $\hat{U}^{(n)}$ acts on the right. The $\mathbb{Z}_n \times \mathbb{Z}_n$ symmetry is

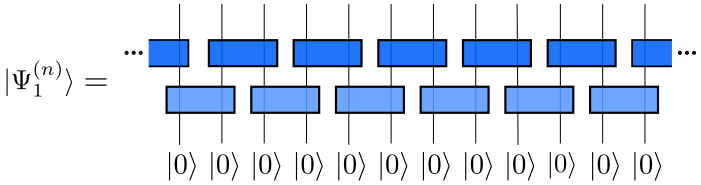

Figure 6.4: **Quantum circuit representation.** To obtain the SPT wave function $|\Psi^{(n)}_1\rangle$, we have to act with inverse circuit $\left(\hat{U}^{(n)}\right)^\dagger$ on the ground state of $\hat{H}^{(n)}_0$.

generated by the operators $(\mathcal{G}_A, \mathcal{G}_B)$ already defined in Eq. (6.4). For more details about these fixed-point models and their properties, we refer to Ref. [185].

Detection and classification of $\mathbb{Z}_n \times \mathbb{Z}_n$ fixed-point models

All information on symmetry fluxes of Sec. 6.1.2 can straightforwardly be generalized to all n. Hence, to each fixed point model, $d \in \{0, ..., (n-1)\}$, we can define a pair of symmetry fluxes,

$$\hat{\mathcal{S}}^d_{r,A} = \prod_{j \le r} \hat{X}_{j,A}\mathcal{O}^d_{r,B}, \quad \hat{\mathcal{S}}^d_{r,B} = \prod_{j \le r} \hat{X}_{j,B}\mathcal{O}^d_{r+1,A} \tag{6.35}$$

with end-point operators

$$\mathcal{O}^d_{r,B} = \hat{Z}^d_{r,B}, \quad \mathcal{O}^d_{r+1,A} = \hat{Z}^{\dagger d}_{r+1,A}, \tag{6.36}$$

[18] For an alternative definition, see Sec. 6.2.6.

that have a well-defined charge w.r.t $\mathbb{Z}_n \times \mathbb{Z}_n$ symmetry defined by:

$$\mathcal{G}_{\sigma+1}^{-1}\hat{\mathcal{S}}_{r,\sigma}^{d}\mathcal{G}_{\sigma+1} = Q_{\sigma+1}^{d}\hat{\mathcal{S}}_{r,\sigma}^{d}, \quad Q_{\sigma+1}^{d} \in \mathbb{Z}_n, \tag{6.37}$$

and $Q_{\sigma+1}^{d} \in H^2(\mathbb{Z}_n \times \mathbb{Z}_n, U(1))$. For a relation of charges q_σ^d and Q_σ^d, see Eq. (6.10). If the end-point operator is chosen appropriately, then for a particular SPT the associated string operators have long-range order[19]

$$\langle \hat{\mathcal{S}}_{r-r_0,\sigma}^{\dagger d}\hat{\mathcal{S}}_{r,\sigma}^{d}\rangle \xrightarrow{r_0\to\infty} \text{const.}. \tag{6.38}$$

In summary, for a given n, there are n distinct possible SPTs classified by charges of $H^2(\mathbb{Z}_n \times \mathbb{Z}_n, U(1)) = \mathbb{Z}_n$.

Gapped degrees of freedom

Symmetry fluxes associated to gapped degrees of freedom are again denoted by,

$$\hat{\mathrm{s}}_{r,\sigma}^{n_\delta,d} = \left(\hat{\mathcal{S}}_{r,\sigma}^{d}\right)^{n_\delta}, \; d \in \mathbb{Z}_n \tag{6.39}$$

with $n_\delta \equiv n/\delta$ integer-valued and δ characterizes the corresponding subgroup $\mathbb{Z}_\delta \times \mathbb{Z}_\delta$ of $\mathbb{Z}_n \times \mathbb{Z}_n$ symmetry.

6.2.2 Direct quantum phase transitions

Having introduced the models and notations, we now turn over to study (direct) quantum phase transitions between distinct classes of SPT phases protected by $\mathbb{Z}_n \times \mathbb{Z}_n$ symmetry. In particular, we are interested in a single parameter interpolation between two fixed-point Hamiltonians $\hat{H}_d^{(n)}$ and $\hat{H}_{d+\delta}^{(n)}$ with $d \in \mathbb{Z}_n$ and $\delta \in \{1, ..., \lfloor n/2 \rfloor\}$[20]. For such interpolations, we find the following result:

Direct transitions. If two $\mathbb{Z}_n \times \mathbb{Z}_n$ fixed-point models $\hat{H}_d^{(n)}$ and $\hat{H}_{d+\delta}^{(n)}$ satisfy $n_\delta := \frac{n}{\delta} \in \{2, 3, 4\}$, then there exists a path $\Gamma_{d\delta}^{(n)}(\lambda, \mu)$, connecting the two fixed-point models, which has a single continuous quantum phase transition and whose QCP is characterized by a CFT with central charge $c = \{1, 8/5, 2\}$, respectively.

A path that realizes such transition is given by (here we set $d = 0$),

$$\boxed{\Gamma_{0\delta}^{(n)}(\lambda, \mu) = (1-\lambda)\hat{H}_0^{(n)} + \lambda\hat{H}_\delta^{(n)} - \mu\sum_{j,\sigma}\left(\hat{X}_{j,\sigma}^{n_\delta} + \text{h.c.}\right)}, \tag{6.40}$$

[19] Note the "†" in the definition of $\hat{\mathcal{S}}_{r-r_0,\sigma}^{\dagger d}$ means that we replace all operators by its hermitian conjugate, but the string of the symmetry flux still starts at $-\infty$ and ends at $r - r_0$.

[20] The floor function $\lfloor x \rfloor$ gives the closest integer, which is smaller or equal to x. For example, take $x = 3/2$, then $\lfloor 3/2 \rfloor = 1$.

with $n_\delta = n/\delta$ integer-valued and positive μ. Given this, the claim is as follows: If we choose μ sufficiently large (which does not affect the ground state of the gapped SPT phases), then the path has a direct, continuous quantum phase transition if $n_\delta \in \{2, 3, 4\}$. This is equivalent to say that the change of the charges characterizing the projective representations of the SPTs, Eq. (6.6), is given as follows:

$$\Delta q := q_B^d q_B^{-(d+\delta)} = \bar{q}_B^\delta \in \{-1, \omega_3, i\}, \tag{6.41}$$

where q_B^d is the charge associated to the fixed-point model $\hat{H}_d^{(n)}$ and $q_B = \bar{\omega}_n$[21]. Before we discuss the construction of this path, let us emphasize two important aspects:

- First, knowing a path for $d = 0$ is sufficient, since all other cases can be obtained via application of the SPT-Entangler $\hat{U}^{(n)}$, which for certain cases non-trivially transform the term $\sim \mu$, see Eq. (6.34).
- Second, if $n_\delta \in \{2, 3, 4\}$, then the path $\Gamma_{d\delta}^{(n)}(\lambda, \mu)$ realizes a direct transition of symmetry groups $\mathbb{Z}_{n'} \times \mathbb{Z}_{n'}$ with $2 \leq n' \leq 4$ (as we will now explain).

Construction of the path

The construction of the path hinges on the fact that Hamiltonians given in the definition of Eq. (6.40) conserve a local $\mathbb{Z}_\delta$ symmetry, which is generated by $\hat{X}_{j,\sigma}^{n_\delta}$. To see this, it is sufficient to consider the following commutator (which follows from the definition of the fixed-point models in Eq. (7.1)):

$$n_\delta \in \mathbb{N} \Rightarrow \hat{X}_{j,\sigma}^{n_\delta} \hat{Z}_{j,\sigma}^{\delta} = \hat{Z}_{j,\sigma}^{\delta} \hat{X}_{j,\sigma}^{n_\delta}. \tag{6.42}$$

For the fixed-point models, we can evaluate the ground states exactly and find that it has all $\hat{X}_{j,\sigma}^{n_\delta} = 1$. In this sector, the Hamiltonian $\hat{H}_\delta^{(n)}$ reduces to:

$$\hat{H}_\delta^{(n)} \overset{gs}{=} \hat{H}_1^{(n_\delta)}, \ \delta \in \left\{1, ..., \left\lfloor \frac{n}{2} \right\rfloor\right\}, \tag{6.43}$$

(see App. B.2 and Fig. 6.5). Models with $\delta > \lfloor \frac{n}{2} \rfloor$ can be obtained via complex conjugation. Although at the beginning and end of the path, the ground state is found in the sector with all $\hat{X}_{j,\sigma}^{n_\delta} = 1$, we cannot prove this in general for every λ, and thus need to add the additional term $\sim \mu$. Moreover, if $n_\delta \leq 4$, then the path given in Eq. (6.40) realizes a direct, continuous phase transition of symmetry groups $\mathbb{Z}_{n'} \times \mathbb{Z}_{n'}$ with $2 \leq n' \leq 4$.

As stated previously, all other paths can be obtained by applying the SPT-Entangler,

$$\Gamma_{d\delta}^{(n)}(\lambda, \mu) = \left(\hat{U}^{(n)}\right)^{\dagger d} \Gamma_{0\delta}^{(n)}(\lambda, \mu) \left(\hat{U}^{(n)}\right)^{d}, \tag{6.44}$$

which generically non-trivially affect the representation of the local $\mathbb{Z}_\delta$ symmetry. Note, the reduction scheme is not limited to particular models and also works for $n_\delta > 4$; however, according to Ref. [34], we do not expect a direct quantum phase transition for such paths.

[21] Knowing the charge on the B sublattice is sufficient, since the charge on the A sublattice can be obtained via complex conjugation, see Sec. 6.1.2.

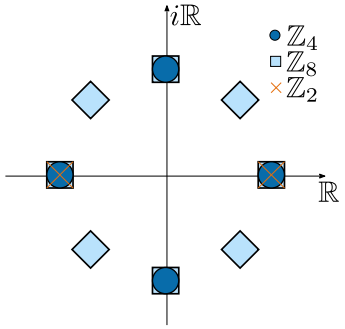

Figure 6.5: **Reduction scheme.** Here we plot charges q_σ^d (as defined in Eq. (6.6)) characterizing projective representations, which classify fixed-point models of different symmetry groups. Thereby, all charges are on the unit circle, plotted in the complex plane. From this figure, we can read off whenever the ground state of a fixed-point model of a higher-dimensional symmetry group reduce to the ground state of a lower-dimensional fixed-point model. For example, the ground states of cetain fixed-point models for $\mathbb{Z}_8 \times \mathbb{Z}_8$ reduce to ground states of fixed-point models for $\mathbb{Z}_4 \times \mathbb{Z}_4$, which even further reduce to ground states for the fixed model of $\mathbb{Z}_2 \times \mathbb{Z}_2$ if the corresponding charges coincide. This is the case if symbols associated to different symmetry groups match.

A related path and numerics

Although at first sight this path looks rather fine-tuned, it turns out that the very natural choice of a single parameter interpolation (i.e., setting $\mu = 0$),

$$\Gamma_{0\delta}^{(n)}(\lambda, 0) = \hat{H}_{0\delta}^{(n)}(\lambda) = (1-\lambda)\hat{H}_0^{(n)} + \lambda \hat{H}_\delta^{(n)} \tag{6.45}$$

follows the path of $\hat{H}_{01}^{(n_\delta)}(\lambda)$, which we can prove—assuming certain symmetries—for many cases (see App. B.3). To confirm our analytical results, we numerically evaluated the central charges for path (6.45). The analytically expected values are listed in Tab. 6.1 and the numerically obtained values are shown in Fig. 6.6. Indeed, the central charges obtained by iDMRG calculations agree very well with the predicted values.

6.2.3 Protecting symmetry groups

In Sec. 6.1 we showed that the embedding of the quotient group can stabilize SPTs, while the subgroup cannot. If $n > 4$, there are cases where subgroups can stabilize the SPTs.

Embedding of the quotient group

There are only two fixed-point Hamiltonians for which the embedding of the quotient group can protect the SPT:

$\hat{H}^{(n)}_{0\delta}$	Δq	Central charge c
$\hat{H}^{(4)}_{02}$	-1	1
$\hat{H}^{(6)}_{02}$	ω_3	8/5
$\hat{H}^{(6)}_{03}$	-1	1
$\hat{H}^{(8)}_{02}$	i	2
$\hat{H}^{(8)}_{04}$	-1	1

Table 6.1: **Central charges.** Central charges for direct quantum phase transitions of Hamiltonian (6.45).

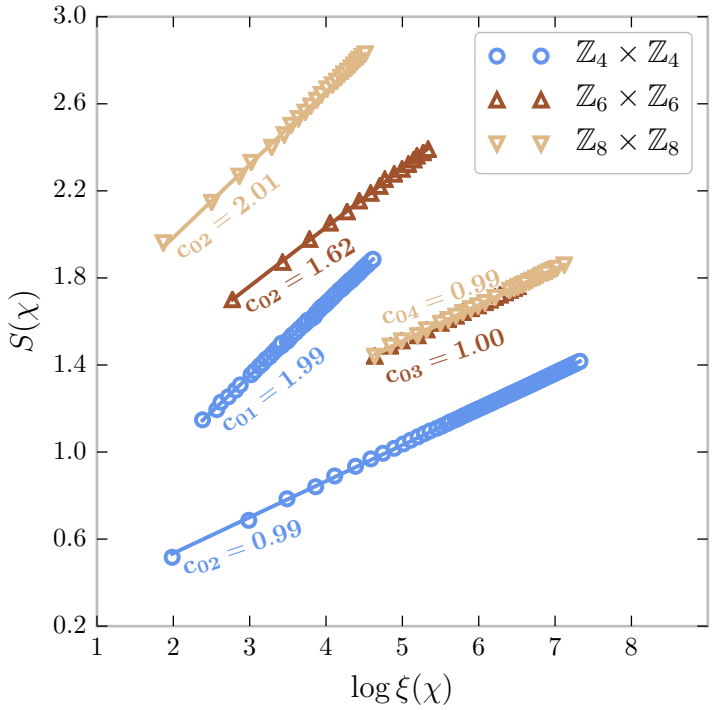

Figure 6.6: **Central charges.** Central charges $c_{0\delta}$ characterizing the CFT of the critical point of quantum phase transitions $(n, 0\delta) \in \{(4, 02), (6, 02), (6, 03), (8, 02), (8, 04)\}$. The central charge is obtained from the scaling of the half-infinite chain entanglement entropy $S(\chi) = c/6 \log \xi(\chi) + \text{const.}$, where χ is the bond dimension of the corresponding MPS [193, 194].

Quotient group protection. The embedding of the quotient group is an exact symmetry of $\hat{H}_0^{(n)}$ and $\hat{H}_{n/2}^{(n)}$, i.e., $n = 2\delta$.

For these cases, there exists a unitary operator $\hat{\mathcal{W}}$ such that the embedding of the quotient group

$$\hat{\mathcal{Q}}_\sigma = \prod_{j,\sigma} \left(\hat{\mathcal{W}} \otimes \hat{\mathcal{X}}\right)_{j,\sigma}, \ \sigma \in \{A, B\}, \tag{6.46}$$

transforms local operators as follows:

$$\hat{\mathcal{Q}}_\sigma : \hat{X}_{j,\sigma} \leftrightarrow \hat{X}_{j,\sigma}^\dagger, \quad \hat{\mathcal{Q}}_\sigma : \hat{Z}_{j,\sigma}^{\frac{n}{2}} \leftrightarrow -\hat{Z}_{j,\sigma}^{\frac{n}{2}}, \tag{6.47}$$

where $\hat{\mathcal{X}}$ denotes the Pauli matrix along x (see App. B.2). Since this symmetry becomes indistinguishable from the quotient symmetry at low-energies, this implies that the embedding of the quotient group keeps SPTs non-trivial, even if the global $\mathbb{Z}_n \times \mathbb{Z}_n$ symmetry is explicitly broken.

Subgroups

For a fixed-point model $\hat{H}_d^{(n)}$, with $d \in \mathbb{Z}_n$, the charge associated to a subgroup $\mathbb{Z}_{n_m} \times \mathbb{Z}_{n_m}$[22] of $\mathbb{Z}_n \times \mathbb{Z}_n$ symmetry, according to Eq. (6.6), is given by,

$$\mathcal{G}_{\sigma+1}^{-m} \mathcal{G}_{R,\sigma}^m \mathcal{G}_{\sigma+1}^m = q_{\sigma+1}^{m^2 d} \mathcal{G}_{R,\sigma}^m. \tag{6.48}$$

Subgroup protection. A subgroup $\mathbb{Z}_{n_m} \times \mathbb{Z}_{n_m}$ can protect the SPT of a fixed-point model $\hat{H}_d^{(n)}$ if the following equation, for a given triple (n, d, m), can be solved by an integer p_0,

$$dm^2 = p_0 n + d, \ p_0 \in \mathbb{N}. \tag{6.49}$$

If this is the case, then the classifying charge reduce to $q_{\sigma+1}^{m^2 d} = q_{\sigma+1}^d$. A necessary condition for a subgroup being able to protect an SPT is that its dimension is equal or larger than the number of edge modes $n_m \geq N_{\mathcal{E}}(d)$[23]. For a given fixed-point model $\hat{H}_d^{(n)}$, the number of protected edge modes $N_{\mathcal{E}}$ is defined as the smallest integer such that the classifying charge, Eq. (6.6), fulfills:

$$\left(q_\sigma^d\right)^{N_{\mathcal{E}}} = 1. \tag{6.50}$$

[22] Here we again defined $n/m \equiv n_m$.

[23] The number of edge modes is determined by the dimension of the irreducible projective representation of $\mathbb{Z}_{n_m} \times \mathbb{Z}_{n_m}$. For this symmetry, the maximal dimension is given by n_m. If two matrices U, V commute up to a phase factor ω_n^m, $UVU^{-1}V^{-1} = \omega_n^m$, then their dimension must be at least n_m. This follows from the determinant of $UVU^{-1}V^{-1}$, $\det\left(UVU^{-1}V^{-1}\right) = 1$.

For example, if we consider the triple $(6, d, m)$, then there are two subgroups with $n_m \in \{2, 3\}$. For the $\mathbb{Z}_2 \times \mathbb{Z}_2$ subgroup, the only relevant fixed-point model is $d = 3$ because here $N_{\mathcal{E}} = n_m$. Inserting the numbers in Eq. (6.49), we see that this can be solved by an integer $p_0 = 4$ and, consequently, this subgroup protects the phase. For the other subgroup, there are two possible cases $d \in \{2, 4\}$ for which $N_{\mathcal{E}} = n_m$. Here, Eq. (6.49) can again be solved by integers $p_0 \in \{1, 2\}$, which implies that subgroups can stabilize the phases as well. For the triple $(8, 2, 2)$, however, there is no integer solution to this equation. An explicit calculation shows that the resulting charge is trivial and, hence, the subgroup cannot protect any SPT. We conclude, if Eq. (6.49) cannot be fulfilled by any integer, then the ground state is either trivial or realize another class of an SPT.

6.2.4 Anomalies of $\mathbb{Z}_n \times \mathbb{Z}_n$ chains

To study anomalies of Hamiltonians $\Gamma^{(n)}_{d\delta}(\lambda, 0)$, denoted by,

$$\hat{H}^{(n)}_{d\delta} = (1-\lambda)\hat{H}^{(n)}_{d} + \lambda \hat{H}^{(n)}_{d+\delta}, \tag{6.51}$$

we first introduce two duality transformations, which become an additional symmetry at $\lambda = 1/2$. Since it is already known that there exists an antiunitary transformation [82], generating an additional $\mathbb{Z}_2^T$ symmetry at the equal-weighted point[24], we will consider the yet unknown unitary representation of the duality transformation, which, however, leads to the same conclusions.

Intrinsic anomalies

The unitary representation of the duality symmetry is given by,

$$\hat{D}^{(n)}_{d\delta;\sigma} = \hat{W}_\sigma \left(\hat{U}^{(n)}\right)^{2d+\delta}, \quad \hat{W}_\sigma = \prod_j \hat{W}_{j,\sigma}, \tag{6.52}$$

where $\hat{W}_\sigma$[25] is defined through the action on local operators:

$$\hat{W}_\sigma : \hat{X}_{j,\sigma} \leftrightarrow \hat{X}^\dagger_{j,\sigma}, \quad \hat{W}_\sigma : \hat{Z}_{j,\sigma} \leftrightarrow \hat{Z}^\dagger_{j,\sigma}. \tag{6.53}$$

Under this transformation, Hamiltonian (6.51) changes as follows:

$$\left(\hat{D}^{(n)}_{d\delta;\sigma}\right)^\dagger \hat{H}^{(n)}_{d\delta}(\lambda)\hat{D}^{(n)}_{d\delta;\sigma} = \hat{H}^{(n)}_{d\delta}(1-\lambda). \tag{6.54}$$

At $\lambda = 1/2$ this duality mapping together with the global $\mathbb{Z}_n \times \mathbb{Z}_n$ symmetry forms a $\mathbb{Z}_n \times \mathbb{Z}_n \rtimes (\mathbb{Z}_2 \times \mathbb{Z}_2)$ symmetry. The semi-direct product results, since $\hat{W}_\sigma$ does not commute

[24] The antiunitary representation of the duality transformation is given by,

$$\hat{D}^{(n)}_{d\delta;T} = K \left(\hat{U}^{(n)}\right)^{2d+\delta},$$

where K is the operator of complex conjugation and T denotes the antiunitary representation.

[25] Locally, in the eigenbasis of $\hat{Z}$ the operator reads: $\hat{W} = \sum_{l=0}^{n-1} |n-l\rangle\langle l|$.

with the generators of $\mathbb{Z}_n \times \mathbb{Z}_n$ symmetry. Because paths with different parameters d are unitarily related, it is sufficient to consider only cases with $d = 0$.

Intrinsic anomaly. For any (n, δ) with n even and δ odd, there exists no gapped ground state that is symmetric under $\mathbb{Z}_n \times \mathbb{Z}_n \rtimes (\mathbb{Z}_2 \times \mathbb{Z}_2)$ symmetry.

If a gapped, symmetric state exists, there must be a pair of symmetry fluxes associated to $\mathbb{Z}_n \times \mathbb{Z}_n$ symmetry, Eq. (6.35), such that corresponding string operators, Eq. (6.38), have long-range order. These symmetry fluxes must be invariant under the duality transformation, which gives the following constraint:

$$d' = \frac{\delta}{2} \vee d' = \frac{n+\delta}{2}, \tag{6.55}$$

where d' labels a possible gapped, symmetric SPT. Possible scenarios are:

- For odd n, this equation has always a solution[26],
  $\Rightarrow$ *no intrinsic anomaly if n is odd.*
- For even n, this equation has only a solution if δ is even,
  $\Rightarrow$ *no intrinsic anomaly if both (n, δ) even.*

The condition in Eq. (6.55) is equivalent to the non-double stacking condition of Ref. [82], which says that the charge difference, Eq. (6.41), cannot be written as a square of another $\mathbb{Z}_n$ charge. In App. B.4 we explicitly show that this symmetry has a gauge anomaly for cases mentioned in the golden box above.

Emergent anomalies

Given the interpolation described by the path $\Gamma_{0\delta}^{(n)}(\lambda, \mu)$[27], *when do we expect to have an emergent anomaly at* $\lambda = 1/2$?

Emergent anomaly. For any (n, δ) with n_δ integer-valued and even, there is no gapped state that is symmetric under $\mathbb{Z}_n \times \mathbb{Z}_n \rtimes (\mathbb{Z}_2 \times \mathbb{Z}_2)$ as long as the $\mathbb{Z}_\delta \times \mathbb{Z}_\delta$ subgroup is gapped.

Recall that for the reduction to work we need that n_δ is integer-valued, see Eq. (6.43). If n_δ is even, then at low-energies the effective Hamiltonian is given by $\hat{H}_{01}^{(n_\delta)}$, which according to the previous golden box has an intrinsic anomaly[28]. Upon adding symmetric perturbations, the anomaly persists as long as the $\mathbb{Z}_\delta \times \mathbb{Z}_\delta$ subgroup is gapped $\Rightarrow$ *emergent anomaly.*

[26] If n is odd it can be written as $n = 2l + 1$, this, however, implies that δ is odd as well. Since the sum of two odd numbers is even, $d' = (n + \delta)/2$ is always integer.

[27] Here we assume μ to be sufficiently large such that we are in the correct sector.

[28] We used again the shorthand notation $\hat{H}_{01}^{(n_\delta)} \equiv \hat{H}_{01}^{(n_\delta)}(\lambda = 1/2)$. Moreover, the previous discussed model $\hat{H}_{02}^{(4)}$ is an example of such case.

6.2.5 Symmetry-enriched quantum criticality

If the SPT-Entangler $\hat{U}^{(n)}$ acts with arbitrary powers on the path described by $\Gamma^{(n)}_{0\delta}(\lambda,\mu)$, then, although the central charge of the CFT is unchanged, the CFT itself is non-trivially transformed. We say the *CFT is symmetry-enriched by* $\mathbb{Z}_n \times \mathbb{Z}_n$ *symmetry* [183]. To characterize different CFTs, we assign to each symmetry flux of the gapped $\mathbb{Z}_\delta \times \mathbb{Z}_\delta$ subgroup an end-point operator that has a well-defined charge w.r.t $\mathbb{Z}_n \times \mathbb{Z}_n$ symmetry (see Eq. (6.37) and Eq. (6.39)),

$$\hat{\mathrm{s}}^{n_\delta,d}_{r,\sigma} = \left(\hat{\mathcal{S}}^{d}_{r,\sigma}\right)^{n_\delta},\ d \in \mathbb{Z}_n, \quad \left(Q^{d}_{r,\sigma+1}\right)^{n_\delta} \in \mathbb{Z}_\delta. \tag{6.56}$$

Symmetry-enriched CFTs. For a given (n,δ), with n_δ integer-valued, there are δ distinct CFTs characterized by symmetry fluxes $\hat{\mathrm{s}}^{n_\delta,d}_{r,\sigma}$, $d \in \mathbb{Z}_n$ whose end-point operators are charged under $\mathbb{Z}_n \times \mathbb{Z}_n$ symmetry.

Entanglement spectrum and edge modes

In Sec. 6.1.7 we discussed the case $(n,\delta) = (4,2)$, which gave rise to two topologically distinct CFTs. By similar arguments as given there, we can explicitly show that if the charges are non-trivial, there is a degeneracy in the entanglement spectrum. Moreover, if the system is considered with a single edge, there are edge modes. To this end, we again define two locally confined operators $\hat{\epsilon}_1$ and $\hat{\epsilon}_2$, which are given by,

$$\hat{\epsilon}_1 = \hat{Z}_{1,A}, \quad \hat{\epsilon}_2 = \hat{X}^{n_\delta}_{1,A}\hat{Z}^{n_\delta d}_{1,B}, \quad \hat{\epsilon}_1\hat{\epsilon}_2\hat{\epsilon}_1^{-1}\hat{\epsilon}_2^{-1} = \omega_\delta, \quad d > 0 \tag{6.57}$$

that commute with the Hamiltonian, defined by $\Gamma^{(n)}_{d\delta}(\lambda,\mu)$ in Eq. (6.44), and itself up to a phase factor ω_δ—resulting in δ degenerate ground states. This implies, equivalently to Sec. 6.1.7, that there is SSB at the edge and edge modes for a system with a single edge[29]. Furthermore, the bulk entanglement spectrum is at least δ-fold degenerate.

Gapless SPTs. Similar to the illustrative case, there are also gapless SPTs for models with $\mathbb{Z}_n \times \mathbb{Z}_n$ symmetry. Aside from examples with direct transitions, there are gapless SPTs that do not require the duality symmetry in addition to be well-defined. Indeed, in Ref. [34] it was shown that for transitions with $n > 4$, where the change of the charge $\Delta q \notin \{-1, \omega_3, i\}$, Eq. (6.41), the interpolation crosses an intermediate gapless phase characterized by a CFT with central charge $c = 2$. From the previous discussion, we conclude that such phases—in the presence of gapped degrees of freedom—form gapless SPTs if associated string operators are non-trivially charged[30].

[29] Note that the edge modes are perfectly localized, which, under symmetry preserving perturbations, turns over to an exponential decay into the bulk with $\xi_{loc} < \infty$.

[30] An example of such phase is given by the interpolation between $\hat{H}^{10}_1$ and $\hat{H}^{10}_3$, which is obtained from $\hat{H}^{10}_{02}(\lambda)$ by applying the SPT-Entangler once. The latter transition effectively reduces to an interpolation between $\hat{H}^{5}_0$ and $\hat{H}^{5}_1$ crossing an intermediate gapless phase with central charge $c = 2$.

6.2.6 Spontaneous-symmetry-breaking and $U(1)$ symmetry

In Sec. 6.1.4 we have seen that, upon increasing the perturbation with $\hat{H}_1$, the system enters an SSB phase, where the emergent anomaly is no longer well-defined. This phase is characterized by SSB of a single $\mathbb{Z}_4$ and sublattice symmetry. However, such a phase can also arise for cases that do not have an emergent anomaly, which is the case for odd n. To see this, let us emphasize that all fixed-point models can be obtained from the trivial phase via successive applications of the SPT-Entangler, which is shown in Eq. (6.30). Thus, the following Hamiltonian:

$$\hat{H}^{(n)} = \sum_{d=0}^{n-1} \hat{H}_d^{(n)} \tag{6.58}$$

has an additional $\mathbb{Z}_n$ symmetry generated by the SPT-Entangler $\hat{U}^{(n)}$. Such a Hamiltonian cannot have a gapped, symmetric ground state that is invariant under the global $\mathbb{Z}_n \times \mathbb{Z}_n \times \mathbb{Z}_n$ symmetry[31]. This follows from the fact that no symmetry flux is invariant under the action of the SPT-Entangler $\Rightarrow$ *the ground state must be gapless or SSB.* Thus, irrespective of n, the given representation of the $\mathbb{Z}_n \times \mathbb{Z}_n \times \mathbb{Z}_n$ symmetry has a gauge anomaly (see App. B.4).

A concrete case: $\mathbb{Z}_3 \times \mathbb{Z}_3$ fixed-point models

To verify the previous predictions, we evaluated the phase diagram of fixed-point models of $\mathbb{Z}_3 \times \mathbb{Z}_3$ symmetry, shown in Fig. 6.7, where the SSB phase is characterized by spontaneously breaking one of the $\mathbb{Z}_3$ symmetries and sublattice symmetry $\hat{S}_{AB}$. Although Hamiltonian (6.58) is only realized at the center of mass of the triangular, the SSB phase extends over a large region in parameter space[32].

Enhanced $U(1)$ symmetry

It turns out that the additional $\mathbb{Z}_n$ symmetry of Hamiltonian (6.58) can be enhanced to a global $U(1)$ symmetry. However, it is important to note that the overall symmetry is not $\mathbb{Z}_n \times \mathbb{Z}_n \times U(1)$, since the $U(1)$ symmetry does not commute with generators of $\mathbb{Z}_n \times \mathbb{Z}_n$.

Definition. To see this enhancement, we first have to rewrite the SPT-Entangler differently. Therefore, we define an operator $\hat{\mathcal{F}}_{j,\sigma}$[33] that measures the $\mathbb{Z}_N$ charge $l_{j,\sigma}$ of a local basis state $|l\rangle_{j,\sigma}$,

$$\hat{\mathcal{F}}_{j,\sigma} = \sum_{l=0}^{n-1} l_{j,\sigma} \left(|l\rangle \langle l|\right)_{j,\sigma} \Rightarrow \hat{Z}_{j,\sigma} = \omega_n^{\mathcal{F}_{j,\sigma}}. \tag{6.59}$$

[31] Here we assume the system to have no boundaries, otherwise the generators of the $\mathbb{Z}_n \times \mathbb{Z}_n$ symmetry do not commute with the SPT-Entangler $\hat{U}^{(n)}$ generating the other $\mathbb{Z}_n$ symmetry

[32] Note a similar phase diagram was obtained for a two-dimensional system with SPT phases protected by $\mathbb{Z}_3$ symmetry [195].

[33] In terms of total spin S, this operator for a given n can be written as $\hat{\mathcal{F}}^{(n)} = S \cdot \mathbb{1} + \hat{S}^z$. Thus, all odd n correspond to integer spin and all even n to half-integer spin representations, respectively.

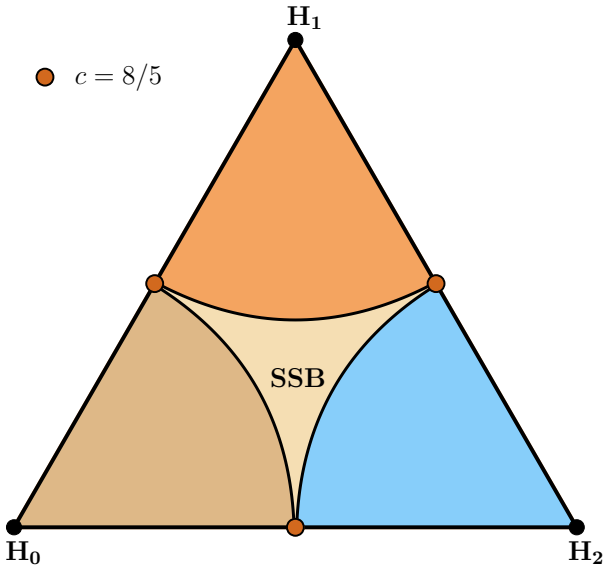

Figure 6.7: **Phase diagram of $\hat{H}^{(3)}_{021}(\alpha, \beta, \gamma)$.** There are three topologically distinct phases labeled by $\hat{H}_0$, $\hat{H}_1$ and $\hat{H}_2$ respectively. The phase in the middle is SSB, where one of the $\mathbb{Z}_3$ symmetries and sublattice symmetry are broken spontaneously. The critical point is immediately gapped out by perturbing it with $\hat{H}^{(3)}_1$. In the center of mass, the Hamiltonian takes the form given by Eq. (6.58).

Using this, the SPT-Entangler can be written as follows:

$$\hat{U}^{(n)}_{AB} = \prod_j \bar{\omega}_n^{\hat{\mathcal{F}}_{j,A}\hat{\mathcal{F}}_{j,B}}, \quad \hat{U}^{(n)}_{AB} = \prod_j \omega_n^{\hat{\mathcal{F}}_{j,B}\hat{\mathcal{F}}_{j+1,A}} \tag{6.60}$$

and, thus, the overall $U(1)$ symmetry is generated by,

$$\hat{U}^{(n)}_{\phi} = \bar{\omega}_n^{\phi\sum_j(\hat{\mathcal{F}}_{j,A}\hat{\mathcal{F}}_{j,B} - \hat{\mathcal{F}}_{j,B}\hat{\mathcal{F}}_{j+1,A})}, \ \phi \in \mathbb{R}. \tag{6.61}$$

For a given basis state $|l\rangle_{1,A} \ldots |l\rangle_{L,B}$, the generator of the $U(1)$ symmetry measures the following charge difference:

$$\Delta Q = \sum_j (l_{j,A}l_{j,B} - l_{j-1,B}l_{j,A}) = Q_{AB} - Q_{BA}. \tag{6.62}$$

Commutation relation. To show that the generator of the $U(1)$ symmetry and the Hamiltonian (6.58) commute, we prove that the action of the Hamiltonian on an arbitrary basis state does not change its charge difference ΔQ. To this end, we use that the Hamiltonian (6.58), on each sublattice, can be written as follows:

$$\hat{H}^{(n)}_A = -n\sum_j \left(\hat{X}_{j,A} + \hat{X}^{\dagger}_{j,A}\right)\hat{P}_{j,B}, \quad \hat{H}^{(n)}_B = -n\sum_j \left(\hat{X}_{j,B} + \hat{X}^{\dagger}_{j,B}\right)\hat{P}_{j+1,A}, \tag{6.63}$$

where we defined the projection operators

$$\hat{P}_{j,B} = \frac{1}{n}\sum_{d=0}^{n-1} \hat{Z}^{\dagger d}_{j-1,B}\hat{Z}^{d}_{j,B}, \quad \hat{P}_{j,A} = \frac{1}{n}\sum_{d=0}^{n-1} \hat{Z}^{d}_{j-1,A}\hat{Z}^{\dagger d}_{j,A}. \tag{6.64}$$

These projection operators ensure that the local charge $l_{j,\sigma}$ can only change if neighboring charges are equal. For example, the charge $l_{j,A}$ can only change if $l_{j-1,B} = l_{j,B}$. The local operator $\hat{X}_{j,A}$ changes the charges Q_{AB} and Q_{BA} of an arbitrary basis state as follows: $Q_{AB} \to Q_{AB} + l_{j,B}$ and $Q_{BA} \to Q_{BA} + l_{j-1,B}$, which results in:

$$\Delta Q' = \Delta Q + l_{j,B} - l_{j-1,B} \tag{6.65}$$

However, such a process is only possible if $l_{j-1,B} = l_{j,B}$, which implies $\Delta Q' = \Delta Q$. A similar consideration holds for complex conjugate terms and for the other sublattice. Thus, no term of the Hamiltonian changes the global charge of any basis state and, hence, the Hamiltonian is charge conserving. Given the particular form of the SPT-Entangler, we explicitly checked[34] if the ground state, in the center of Fig. 6.7, is symmetric under this $U(1)$ symmetry, which is indeed the case.

Let us emphasize that such an enhancement is not special to this class of models. It is very common that different classes of SPT phases can be mapped to each other via duality transformations[35], which—for a half way interpolation between two distinct classes—generates an additional symmetry. Occasionally, this symmetry enhances to a $U(1)$ symmetry. In a recent work by Tantivasadakarn et al. [197], a sufficient condition was provided, when a $\mathbb{Z}_2$ symmetry enhances to a global $U(1)$ symmetry.

6.3 Generalizations to other symmetry groups and dimensions

Thus far, we have studied the criticality of $\mathbb{Z}_n \times \mathbb{Z}_n$ chains in great detail. In this last section, we emphasize that certain key insights generalize to other symmetry groups and dimensions. In particular, an essential ingredient in many of the above discussions was the idea that at an SPT transition, a certain symmetry (sub)group could remain gapped—with a variety of consequences—which we further explore here.

One-dimensional SPTs

Let us first still consider 1D SPT phases, but for a more general symmetry group G. As mentioned in the introduction, the SPT phases are classified by projective representations, or equivalently, $H^2(G, U(1))$. Suppose we have two distinct SPT classes $\alpha, \beta \in H^2(G, U(1))$ and would like to gain insight into possible quantum criticality arising between them. Our above work suggests that it is paramount to find the largest normal subgroup $N \subset G$ where both SPT classes are compatible. (We will discuss in a moment how to characterize this compatibility condition.) In that case, we argue that N

[34] This can be easily done using the ITEBD algoritm [196].
[35] This naturally occurs for fixed-point models constructed by the method of Ref. [64].

can remain gapped when tuning between the two classes, with the effective low-energy criticality looking like a transition for $\tilde{G}$-SPT phases, where $\tilde{G} = G/N$ is the quotient group. This way, we can reduce the study of the SPT criticality to a smaller symmetry group, where remaining degrees of freedom can help in stabilizing criticality. The simplest example we found is where $G = \mathbb{Z}_4 \times \mathbb{Z}_4$ and $\tilde{G} = \mathbb{Z}_2 \times \mathbb{Z}_2$, with the effective low-energy transition looking like the usual cluster chain transition with central charge $c = 1$.

Compatibility condition. What does it mean for two SPT phases with a symmetry group G to have a compatible normal subgroup N? In the simplest case, such as an Abelian group G, it simply means that all symmetry fluxes for N have the same charge in both phases. I.e., their string order parameters are compatible. Indeed, if they agree, there is a priori no *need* for them to go critical, and they can remain gapped at criticality, whereas fluxes with different charges need to lose long-range order at criticality. However, for non-Abelian groups G it is known that string orders do not necessarily give a full characterization of the SPT phase [95]. In such a case, however, we can consider symmetry fractionalization of each symmetry $g \in G$: for each on-site symmetry $U^g = \prod_n U_n^g$, symmetry fractionalization tells us that when acting with U^g on a large but finite segment, the ground state only transforms near the boundary of that segment, i.e., $U^g = U_L^g U_R^g$ for some "fractionalized" $U_{L,R}^g$. Then U_R^g gives a *projective* representation of G, with different classes leading to different SPT phases labeled by $H^2(G, U(1))$. We say two SPT phases have a compatible normal subgroup N if all the fractionalized operators U_R^h (for $h \in N$) have consistent symmetry transformations when conjugating by elements in $g \in G$. Note that in the Abelian case, this coincides with checking the charges of string order parameters, since $ghg^{-1} = h$, such that conjugation always preserves the symmetry string.

Topological properties. The remaining gapped degrees of freedom can endow the critical point with a topological twist. The gapped symmetries have long-range order for their symmetry flux, and if the latter carries a non-trivial charge under some symmetries, it implies that the system has exponentially localized edge modes with open boundaries. This is consistent with one of the known mechanisms for gapless SPT phases [183, 184] and it agrees with the above examples we found (such as the $\hat{H}_1^{(4)}$ to $\hat{H}_3^{(4)}$ SPT transition for $\mathbb{Z}_4 \times \mathbb{Z}_4$-symmetric chains).

Higher dimensions

Lastly, let us note that this discussion naturally generalizes to higher dimensions. Instead of using string order parameters, one can say that two SPT phases (for a symmetry group G) in d dimensions have a consistent or compatible normal subgroup $N \subset G$ if all symmetry twists [64, 80, 81, 85, 164, 198–204] with respect to elements $h \in G$ have the same transformation properties in both phases. The simplest example in 2+1D is for $G = \mathbb{Z}_4$. Since $H^3(\mathbb{Z}_4, U(1)) \cong \mathbb{Z}_4$, there are four distinct phases (including the trivial phase). The middle SPT class has the same properties as the trivial phase for symmetry twists with respect to the normal subgroup $\mathbb{Z}_2 \subset \mathbb{Z}_4$. Hence, this subgroup can remain gapped at the transition between these two, such that at low energies it will

effectively look like an $\mathbb{Z}_2 \cong \mathbb{Z}_4/\mathbb{Z}_2$ SPT transition. A similar statement holds for the transition between class one and class three in $H^3(\mathbb{Z}_4, U(1))$; however, in this case the gapped $\mathbb{Z}_2$ subgroup is itself topologically non-trivial and will protect edge modes at criticality. (While a continuous $\mathbb{Z}_2$ SPT criticality is difficult to find in 2+1D, we note that it has recently been suggested that such a continuous transition can be found for $\mathbb{Z}_2^3$ [197, 205], and by the above this can arise as an effective low-energy description for $\mathbb{Z}_4^3$ SPT transitions.)

6.4 Summary & Outlook

In this chapter, we showed that the fixed-point models of one-dimensional SPTs protected by $\mathbb{Z}_n \times \mathbb{Z}_n$ symmetry have much more direct quantum phase transitions as initially expected [34]. Moreover, for paths considered here, we showed that if a single unique QCP exists, the CFT is characterized by a central charge $c \in \{1, 8/5, 2\}$, which we numerically demonstrated for several examples using iDMRG calculations (see Fig. 6.6). We argued that the direct transitions are a consequence of additional gapped degrees of freedom, that is, starting from the trivial phase $d = 0$ not all SPTs of $\mathbb{Z}_n \times \mathbb{Z}_n$ symmetry can be reached if particular subgroups remain gapped along the interpolation.

Aside from this, we discussed the topological nature of the underlying CFTs and showed that CFTs having the same central charge not necessarily represent the same RG fixed-points. If the topological nature of a CFT was non-trivial, we argued that if such a critical system is considered with boundary that there are exponentially localized edge modes and degeneracies in the entanglement spectrum. These properties and, in particular, the topological distinction is another feature resulting from additional gapped degrees of freedom at quantum criticality. These together with the critical bulk form gapless SPTs on the QCP of two gapped SPTs, or in intermediate, gapless phases characterized by a CFT. Most examples of such phases have been so far considered on transitions between SPTs and SSB phases (see Refs. [183, 184] and references therein).

Moreover, we showed that the action of the global $\mathbb{Z}_n \times \mathbb{Z}_n$ symmetry on low-energy degrees of freedom is given by a quotient group, which together with a duality mapping can lead to an emergent anomaly, and in particular cases, $\mathbb{Z}_4 \times \mathbb{Z}_4$, together with sublattice symmetry forbids a gapped state; thus stabilizing quantum criticality. To study this and the former mentioned features, we numerically evaluated the phase diagram of fixed-point models protected by $\mathbb{Z}_4 \times \mathbb{Z}_4$ (see Fig. 6.3). In the context of anomalies, we proved that emergent anomalies appearing in higher-dimensional symmetry groups, $\mathbb{Z}_n \times \mathbb{Z}_n$, emerge from an effective Hamiltonian that has an intrinsic anomaly and describes the interpolation in a lower-dimensional symmetry group $\mathbb{Z}_{n/\delta} \times \mathbb{Z}_{n/\delta}$, where δ specifies the distance of two fixed-point Hamiltonians in $\mathbb{Z}_n \times \mathbb{Z}_n$.

We also briefly discussed the protection of SPT phases realized by fixed-point Hamiltonians of $\mathbb{Z}_n \times \mathbb{Z}_n$ symmetry and showed that not all of them require the global $\mathbb{Z}_n \times \mathbb{Z}_n$ symmetry to realize a non-trivial state. For special cases, we argued that the embedding of the quotient group or subgroups can protect the SPT.

Penultimately, we proved that if we consider a Hamiltonian consisting of an equal-

weighted sum of all fixed-point models, that the $\mathbb{Z}_n$ symmetry together with the global $\mathbb{Z}_n \times \mathbb{Z}_n$ symmetry has a gauge anomaly as it forbids a gapped, symmetric ground state. To demonstrate this, we evaluated the phase diagram of a Hamiltonian consisting of all fixed-point models of $\mathbb{Z}_3 \times \mathbb{Z}_3$ symmetry and found that the ground state—for a certain parameter regime—is spontaneous-symmetry-breaking. Moreover, we explicitly showed that the $\mathbb{Z}_n$ symmetry due to the SPT-Entangler can be enhanced to a $U(1)$ symmetry.

Finally, in Sec. 6.3 we generalized our findings to other symmetry groups and higher dimensions, in particular, when to expect gapped degrees of freedom and topological properties at quantum criticality.

Outlook. So far, we have studied how gapped degrees of freedom can enrich quantum criticality. Moreover, we saw that the presence of such degrees of freedom results in an effective low-energy description of the global symmetry group in terms of a quotient group, which together with a duality symmetry can lead to an emergent anomaly stabilizing criticality. In this overall work, the global symmetry group itself has been able to protect non-trivial SPTs, i.e., $H^2(\mathbb{Z}_n \times \mathbb{Z}_n, U(1)) = \mathbb{Z}_n$. Since low-energy properties were completely determined by the quotient group, naturally the question arises what happens if the global symmetry group G does not allow for non-trivial SPTs, i.e., $H^2(G, U(1)) = 0$, but if at low-energies the effective symmetry group G/H[36] does. Exactly, this is the question that is answered in the next chapter, where we study a descendant of the Hubbard model.

[36] Where H denotes a normal subgroup.

Chapter 7

Quotient group symmetry-protected topological phases in the bond-alternating ionic Hubbard chain

In the previous chapter we have seen that for certain quantum phase transitions among SPT phases the action of the global symmetry G on low-energy degrees of freedom is given is by its quotient group G/H, where H is a normal subgroup. Moreover, we saw that this low-energy representation can have an emergent anomaly, which can be lifted upon tuning some parameter of the Hamiltonian. In all foregoing cases, however, the lifting of the emergent anomaly resulted in a gapped, symmetric SPT state. A necessary condition for this to happen is that G itself can protect non-trivial SPTs, i.e., $H^2(G, U(1)) \neq 0$. In this chapter, we will explore a different scenario, namely, where G *cannot* protect non-trivial SPTs, but its quotient group G/H can.

To this end we consider a descendant of the Hubbard model, a bond-alternating ionic Hubbard model (BIHM) [206–219] where constituents have charge and spin degrees of freedom. If on-site interactions dominate, charges are immobile and the effective description is in terms of spin degrees of freedom. The resulting model is given by the bond-alternating spin-1/2 Heisenberg chain [35, 206], $\hat{H} = \sum_j (1 + (-1)^j \delta) \hat{\boldsymbol{S}}_j \cdot \hat{\boldsymbol{S}}_{j+1}$. Depending on the dimerization, this model is a representative of the Haldane phase, an SPT protected, among others, by spin-rotation symmetry $SO(3)$. For the bond-alternating Heisenberg model, the unit cell consists of two sites; thus, two spin-1/2 degrees of freedom form an integer representation of $SO(3)$. If lattice sites start at $j = 1$, then $\delta > 0$ is the topological Haldane phase, with a zero-energy spin-1/2 degree of freedom at each edge. Note, no gapped, spin-rotation symmetric Hamiltonian can adiabatically connect the two $\delta < 0$ and $\delta > 0$ regimes.

In recent times, it has been realized that the anomalous action of the global symmetry on the boundary of SPT phases is its Achilles' heel [18, 50, 64, 86, 93, 95, 220]. Unlike SSB phases, any SPT phase can be trivialized by extending its symmetry group [39, 189–192]. For instance, the non-trivial topological phase of the formerly introduced low-energy description of the BIHM—the Haldane phase of the bond-alternating spin-1/2 Heisenberg chain—is trivialized by extending $SO(3)$ into $SU(2)$. This corresponds to introducing degrees of freedom (here charges) on which the -1 element of $SU(2)$ acts as an operator, rather than a number (such that it remains $SU(2)$ even after blocking sites into unit cells). In the presence of charges this can be achieved by driving the spin

chain away from its Mott limit, such that 2π-rotations equal the fermion parity operator, rather than a classical number. Such paths—connecting the Haldane phase to a trivial phase via fluctuating charges—were explicitly constructed in Refs. [36, 37] for related fermionic models.

However, so far, the following questions have not been addressed: *How immediate is this trivialization?* Are topological characteristics—such as edge modes—immediately gapped out by some exponentially small energy scale? Or do edge modes remain *exact* zero-energy edge modes over some finite region of parameter space?

In this chapter, we show that—remarkably—the latter option is realized. When an SPT phase is—strictly speaking—trivialized by introducing new degrees of freedom on which the symmetry group acts in an extended way, we argue that while certain features such as string orders are known to immediately lose their meaning [36], other salient features, such as edge modes, degeneracies of the low-lying entanglement spectrum and bulk phase transitions are stable over a finite region in parameter space. We identify quantized invariants, which characterize this stability. Hence, the original symmetry group—which is now a quotient group of the extended symmetry group—can still protect certain topological phenomena; we refer to these as *quotient group symmetry-protected topological (QSPT)* phenomena.

Overview. This chapter is based on [P5]. In the first section, Sec. 7.1, we introduce the Hamiltonian describing the BIHM and discuss its symmetries and, in particular, the subtlety of π-rotations in the fermionic Hilbert space. Then, we provide a full phase diagram of the BIHM for a particular value of ionicity. Thereby, we briefly give a historical review on the ionic Hubbard model, shortly consider different regimes of the on-site repulsion and demonstrate that there is a gapped, symmetric path along which the Haldane phase is trivialized.

In the second part, Sec. 7.2, we elaborate on the quotient group symmetry-protected topological signatures of the BIHM and explicitly verify that edges modes and degeneracies in the low-lying entanglement spectrum are parametrically stable as we lower U. Thereby, we argue that these features can only disappear if the edge has a gap closing. Moreover, we will explain the robustness of the critical line, Fig. 7.1, which has so far mainly addressed using field theory or numerical tools. Here we will show that it is due to an emergent anomaly of the quotient group and a duality symmetry exchanging the dimerization pattern.

Lastly, in Sec. 7.3 we give a more general understanding of QSPTs starting from the one-dimensional case, and then briefly, consider a possible generalization to a two-dimensional case.

7.1 Introduction of the bond-alternating ionic Hubbard model

Here we first introduce the Hamiltonian describing the BIHM and its symmetries, then we show the phase diagram obtained using iDMRG for a particular value of the ionicity and discuss different parameter regimes in the phase diagram. Finally, we argue how the Haldane phase of the effective spin description is trivialized by introducing charge

degrees of freedom.

7.1.1 The Hamiltonian of the BIHM

The bond-alternating ionic Hubbard model of spinful fermions consists of three terms:

$$\hat{H} = -\sum_{j,s}\left[t_j(\delta)\hat{c}^\dagger_{j+1,s}\hat{c}_{j,s} + \text{h.c.}\right] + \frac{\Delta}{2}\sum_{j,s}(-1)^j\hat{n}_{j,s} + U\sum_j\left(\hat{n}_{j,\uparrow} - \frac{1}{2}\right)\left(\hat{n}_{j,\downarrow} - \frac{1}{2}\right) \quad (7.1)$$

with $t_j(\delta) = (1 + (-1)^j\delta)$. The interactions among the fermions are controlled by the parameter U, while Δ ($\equiv$ ionicity) is a local chemical potential that has different signs on the two sublattices. From the bond-alternating hopping and the local chemical potential, it follows that each unit cell consists of two sites. The operator $\hat{c}^\dagger_{j,s}(\hat{c}_{j,s})$ creates (annihilates) a fermion with spin $s \in \{\uparrow,\downarrow\}$ on site j and the particle number operator is given by $\hat{n}_{j,s} = \hat{c}^\dagger_{j,s}\hat{c}_{j,s}$ with $\hat{n}^2_{j,s} = \hat{n}_{j,s}$.

7.1.2 Symmetries of the BIHM

Hamiltonian (7.1) conserves the total particle number and, thus, has a global $U(1)$ symmetry. Aside from global charge conservation, the Hamiltonian is symmetric with respect to a global $SU(2)$ spin-rotation symmetry generated by,

$$\hat{S}^+ = \sum_j \hat{c}^\dagger_{j,\uparrow}\hat{c}_{j,\downarrow}, \quad \hat{S}^- = \sum_j \hat{c}^\dagger_{j,\downarrow}\hat{c}_{j,\uparrow}, \quad \hat{S}^z = \frac{1}{2}\sum_j\left(\hat{n}_{j,\uparrow} - \hat{n}_{j,\downarrow}\right), \quad (7.2)$$

where x, y components are defined as follows:

$$\hat{S}^x = \frac{1}{2}\left(\hat{S}^+ + \hat{S}^-\right), \quad \hat{S}^y = \frac{1}{2i}\left(\hat{S}^+ - \hat{S}^-\right). \quad (7.3)$$

The two symmetry groups $U(1)$ and $SU(2)$ are not independent (see also Ref. [35]). Since $\hat{S}^z$ and $\hat{N}$ commute among each other and with the Hamiltonian, associated quantum numbers are conserved. Thus, we find:

$$\hat{S}^z + \frac{\hat{N}}{2} = \frac{1}{2}\left(N_\uparrow - N_\downarrow\right) + \frac{1}{2}\left(N_\uparrow + N_\downarrow\right) = N_\uparrow \in \mathbb{Z}. \quad (7.4)$$

Since the right side is integer-valued both terms on the left must take either integer or half-integer values, which implies that not all representation of $U(1)\times SU(2)$ are allowed. Hence, the resulting symmetry group is $U(2) = \left(U(1)\times SU(2)\right)/\mathbb{Z}_2$[1] [221].

[1] There is an alternative way of seeing this: Both symmetry groups share a common element, given by fermion parity. Indeed, we find that $\hat{P} = e^{i\pi\hat{N}} = e^{i2\pi\hat{S}^\gamma}$. Since the generators of $U(1)$ and $SU(2)$ commute, the representation of $U(1)\times SU(2)$ is given by $\hat{V}(\phi,\boldsymbol{\theta}) = e^{i\phi\hat{N}}e^{i\boldsymbol{\theta}\hat{\boldsymbol{S}}}$. However, from this, we see that two different elements in $U(1)$ and $SU(2)$ denoted by $\hat{V}'(\phi) = \hat{P}\hat{V}(\phi)$ and $\hat{V}'(\boldsymbol{\theta}) = \hat{P}\hat{V}(\boldsymbol{\theta})$ map to the same element under $\hat{V}'(\phi,\boldsymbol{\theta}) = \hat{V}(\phi,\boldsymbol{\theta})$. Hence, two elements of $U(1)\times SU(2)$ differing by fermion parity need to be considered as equivalent, or said differently, the kernel of this map is given by $\mathbb{Z}_2 = \{(\mathbb{1},\mathbb{1}),(\hat{P},\hat{P})\}$ and from the first isomorphism theorem it follows that the resulting symmetry group is $\left(U(1)\times SU(2)\right)/\mathbb{Z}_2$.

Fermion parity and π-rotations

A key aspect—which we will often return to—is that 2π rotations, defined by,

$$\hat{P} = \exp\left(2\pi i \hat{S}^{\gamma}\right), \quad \gamma \in \{x, y, z\}, \quad \hat{P}^2 = \mathbb{1}, \tag{7.5}$$

equal the fermion parity *operator* $\hat{P}$ rather than a classical *number* ± 1, as in spin chains. This has an important consequence, namely, even after blocking sites into unit cells, the symmetry remains $SU(2)$ instead of becoming $SO(3)$[2]. A similar result we find for π-rotations, which in the spin chain limit generates a $\mathbb{Z}_2 \times \mathbb{Z}_2$ symmetry; however, in the fermionic Hilbert space correspond to a group isomorphic to quaternions $\mathbb{Q}_8 \subset SU(2)$. The group representation of this symmetry is given by,

$$\mathbb{Q}_8 = \langle \hat{R}^x, \hat{R}^y, \hat{R}^z, \hat{P} | \hat{P}^2 = \mathbb{1}, \left(\hat{R}^x\right)^2 = \left(\hat{R}^y\right)^2 = \left(\hat{R}^z\right)^2 = \hat{R}^x \hat{R}^y \hat{R}^z = \hat{P} \rangle, \tag{7.6}$$

where $\hat{R}^{\gamma} = e^{i\pi \hat{S}^{\gamma}}$. It is important to note that none of the symmetries introduced here can stabilize a non-trivial SPT phase, i.e., they do not admit any non-trivial projective representations, or in terms of group cohomology: $H^2(SU(2), U(1)) = H^2(\mathbb{Q}_8, U(1)) = 0$.

Particle-hole transformations and bond-centered inversion symmetry

In the absence of ionicity Δ, Hamiltonian (7.1) is invariant under particle-hole transformations $\hat{c}_{j,s} \to (-1)^j \hat{c}^{\dagger}_{j,s}$ as well as bond-centered inversion symmetry $\hat{c}_{j,s} \to \hat{c}_{-j-1,s}$ (similarly for complex conjugate terms). For the latter to be well-defined and compatible with Hamiltonian (7.1), the underlying lattice must consist of $2L$ sites with L even and labeling of sites as follows: $j \in \{-L, ..., L-1\}$.

In the presence of ionicity Δ, neither particle-hole transformations nor bond-centered inversion symmetry are symmetries of the Hamiltonian; however, their combined action is preserved. Thus, if the BIHM has a unique ground state—given this symmetry—it is naturally at half-filling.

Duality symmetry

Our model has a useful duality symmetry $(U, \Delta, \delta) \to (U, \Delta, -\delta)$, given by the modified (unitary) translation operator[3],

$$\hat{\mathcal{D}} \hat{c}_{j,s} \hat{\mathcal{D}}^{\dagger} = (-1)^j \hat{c}^{\dagger}_{j+1,s}. \tag{7.7}$$

Consequently, a single direct transition can thus only occur at $\delta = 0$. In the spin chain limit, $\hat{\mathcal{D}}$ acts as a single-site translation symmetry and an on-site unitary transforming spin operators as follows:

$$\hat{\mathcal{D}} \hat{S}^{\gamma}_j \hat{\mathcal{D}}^{\dagger} = \hat{R}_y \hat{S}^{\gamma}_{j+1} \hat{R}^{\dagger}_y. \tag{7.8}$$

[2] For a spin-1/2 chain, this is different. If a unit cell consist of two spin-1/2 degrees of freedom, the symmetry is $SO(3)$ rather than $SU(2)$.

[3] This requires a lattice with PBC or infinite extension.

7.1.3 Quantum phases: An overview

In this part, we study Hamiltonian (7.1) at half-filling with finite ionicity and different values of dimerization $\delta \in [-1, 1]$ and obtain a phase diagram of this model using iDMRG (for details on this, we refer to App. C.2.1). We start the discussion with a brief historical review, and then briefly discuss limiting cases. Lastly, we consider how we can trivialize the Haldane phase using charge fluctuations.

Historical review

The ionic Hubbard model has been extensively studied before at $\delta = 0$ and the nature of transitions along this line has been under debate for almost forty years [206–219]. In the $U \to +\infty$ limit, it reduces to the gapless spin-1/2 Heisenberg chain. Although $\Delta \neq 0$ breaks translation symmetry, the effective spin chain is translation-invariant at all orders in U [206]. Remarkably, criticality persists far beyond this perturbative regime (see Fig. 7.1). To highlight this, we denote the point (U_{pert}) where perturbation theory for the translation invariant Hubbard model ($\delta = \Delta = 0$) in $1/U$ diverges [35]. Along the line $\delta = 0$, the model shows two quantum phase transitions: first, a BKT-transition (U_{c_2}) into a spontaneously dimerized insulator (SDI) phase, and afterwards, an Ising transition (U_{c_1}) into a bond insulator (BI) phase. Note the exact values of the critical points shifts as a function of Δ [217]. Most of previous studies have been mainly field-theoretic or numerical, we, however, will explain the persistence of this critical line as being a quotient group symmetry-protected topological phenomenon.

Mott limit

In the Mott limit $U \to \infty$, the ground state has exactly one particle per site. At low energy, the effective description is a spin-1/2 bond-alternating Heisenberg chain. Hence, fermion parity becomes a classical number: $P = -1$ per site, or $P = 1$ for a two-site unit cell. The symmetry group per unit cell is the quotient group[4] $SO(3) = SU(2)/\mathbb{Z}_2^f$, which is well-known to protect a non-trivial SPT phase, i.e., $H^2(SO(3), U(1)) = \mathbb{Z}_2$. Indeed, in the introduction we saw how $\delta > 0$ ($\delta < 0$) is a topological (trivial) phase. Similarly, $\mathbb{Z}_2 \times \mathbb{Z}_2 = \mathbb{Q}_8/\mathbb{Z}_2^f$ also protects the Haldane phase.

Finite interactions

Although in the limit of large $U \to \infty$ the ionicity $\Delta \neq 0$ is not relevant, it becomes relevant as U is lowered because it explicitly breaks bond-centered inversion [17], $SO(4)$[5][38] and antiunitary particle-hole symmetry [38, 222], which would otherwise still distinguish two SPT phases for arbitrary values of U. Since there is no symmetry distinguishing different SPTs, we expect to have a single phase realized by Hamiltonian (7.1), which

[4] If H is a normal subgroup of G, the quotient group G/H is defined by identifying every element of H with the identity element. Note $\mathbb{Z}_2^f$ is generated by fermion parity.

[5] For the Hubbard model, i.e., $\Delta = 0$, there is another $SU(2)$ symmetry formed by charge degrees of freedom that together with the spinful $SU(2)$ symmetry forms this symmetry group [35].

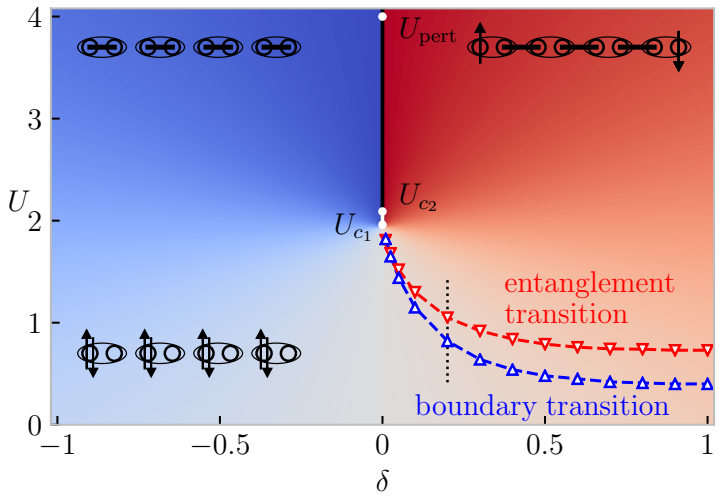

Figure 7.1: **Emergent Haldane phase in the ionic Hubbard chain with $\Delta = 0.4$.** The Mott limit $U \to \infty$ recovers two topologically distinct spin chains which are connected by the small-U regime. The solid black (white) line is a second (first) order phase transition. The transition line ends in Ising criticality at U_{c_1}. The edge mode of the (emergent) Haldane phase is stable until it gaps out at small U (blue dashed line) without a bulk phase transition. The red dashed line indicates where degeneracy of the lowest entanglement level is lost.

indeed coincides with the results shown in Fig. 7.1. Note, similar results have been obtained by Refs. [36, 37] in related models.

Zero interactions

At $U = 0$, the Hamiltonian reduce to two decoupled SSH chains, which—in the presence of ionicity Δ—realize a single phase. There are two reasons: First, all symmetries that can distinguish the two topologically distinct phases of the half-filled SSH model are broken, and second, the bulk gap of the half-filled SSH chain at momentum $k = \pi \sim |\Delta|$ is finite for all values of the dimerization. Note, for vanishing ionicity and dimerization, the bulk gap of the SSH model at half-filling closes at $k = \pi$ [180].

Trivializing the Haldane phase

From Fig. 7.1 we find that the Haldane SPT phase, for small U, is adiabatically connected to the trivial phase. This can even be done analytically by choosing $\delta = 1$, then tune U down to 0 and finally use that the two-decoupled SSH model have a finite gap as δ is changed. Group-theoretically, the Haldane phase is thus trivialized by including fluctuating charges (i.e., finite U). This has been explored before [36, 37] and is a particular instance of how extending a symmetry group (here, extending $SO(3)$ by fermion

parity into $SU(2)$) can trivialize any SPT phase [39, 189–192]. The question of interest, further explored in this chapter, is to which extent the topological features such as edge modes or degeneracies in the entanglement spectrum immediately disappear, i.e., are they fine-tuned or not?

7.2 Quotient group symmetry-protected topological phenomena of the BIHM

Previously, we argued that in the limit of large $U \to \infty$ the BIHM has an effective description in terms of a bond-alternating spin-1/2 Heisenberg chain, which, depending on the dimerization, realizes two topologically distinct SPTs. Thereby, we argued that the effective symmetry group protecting these phases is given by the quotient symmetry $SO(3) = SU(2)/\mathbb{Z}_2^f$. Clearly, as long as perturbation theory applies and the low-energy description is given in terms of spin chains, we expect that topological signatures such as edge modes and degeneracies in the entanglement spectrum remain. This is not overly surprising because if we use the effective Hamiltonian derived from perturbation theory [206], charge degrees of freedom are completely frozen and only spin degrees of freedom remain. Thus, the effective local state space contains only two states $\{|\uparrow\rangle, |\downarrow\rangle\}$ and, consequently, the global symmetry—in this Hilbert space—is given by $SO(3)$. Note, this is precisely what we have in mind if we study models only containing spin degrees of freedom. In practice, however, spin degrees of freedom are inherently coupled to electrons (or atoms) and, thus, pure spin models do not exist!

This naturally leads to the question of what happens to the topological signatures if we consider the bond-alternating ionic Hubbard model in the full fermionic Hilbert space. Do these features immediately disappear or remain robust to a certain extent? Interestingly, from the numerical results shown in Fig. 7.1, we see that the critical line along $\delta = 0$ persists way beyond the value of U, where perturbation theory for $\delta = \Delta = 0$ diverge. Although we do not know how this point changes as $\Delta > 0$ becomes finite, we, nevertheless, believe that for the choice we made, $\Delta = 0.4$, it still diverges much before U_{c_2}. Indeed, for Δ to become relevant it must be of the same order as U[6], and given that $U_{c_2} \approx 5 \cdot \Delta$, this assumption seems reasonable.

It turns out that a fundamental ingredient for QSPTs to exist is a separation of energy scales. This is rather similar to cases we discussed in the previous chapter, Chap. 6, where, however, the global symmetry group itself protected non-trivial SPTs. For the one-dimensional Hubbard model, it is known that along the gapless line, $\delta = 0$, charge and spin degrees of freedom separate [35]. Moreover, along this line spin degrees of freedom are gapless, while charges remain gapped. We will explicitly demonstrate this using symmetry fluxes and associated string operators. Consequently, along this line we naturally have a separation of energy scales and, consequently, the effective action of the global symmetry is $SO(3)$ rather than $SU(2)$. Note, by the reasoning above, this holds way beyond the limit of perturbation theory.

[6] For example, edges modes at $\delta = 1$ disappear if $U = \Delta$.

In the Mott limit $U \to \infty$, it is known that spin-rotation symmetry and duality symmetry forbid a gapped, symmetric ground state (Lieb-Schultz-Mattis anomaly). In the fermionic Hilbert space, this anomaly can be lifted and, thus, is only emergent. However, as long as it forbids a gapped, symmetric state—to enter a gapped QSPT—we have to explicitly break duality symmetry by slightly tuning δ away from 0. Clearly, near the critical line the separation of energy scales remains true and, hence, also the effective action of the global symmetry on low-energy degrees of freedom. Depending on how we dimerize the system, we expect to see topological signatures such as edge modes and degeneracies of low-lying eigenvalues of the entanglement spectrum[7]. Up to which point such separation and, hence, topological signatures remain, depends on details of the model.

In the following two subsections, we discuss the stability of the topological signatures using DMRG and investigate their robustness upon lowering the on-site interaction U. First, we study the stability of edge modes and the degeneracy of the entanglement spectrum. Thereby, we explicitly demonstrate that the fermion parity gap for a system with open boundary conditions closes and show that a similar scenario applies for the entanglement spectrum. Second, we explain the robustness of the critical line by showing that at low-energies the quotient group and the duality symmetry have an emergent (Lieb-Schultz-Mattis) anomaly, which can be detected using symmetry fluxes associated to fermion parity.

7.2.1 Stability of edge modes and degeneracies in the entanglement spectrum

Here, we show that the zero-energy edge modes of the Haldane phase are stable until the fermion parity gap closes for open boundary conditions. Since gaps are parametrically stable, this implies that the topological edge modes exist over a finite region of parameter space, i.e., they do not vanish as soon as U is finite.
Per the usual arguments of symmetry fractionalization (see App. C.1), an on-site unitary symmetry $\hat{U}$ acts on a symmetric, gapped chain with edges as $\hat{U} = \hat{U}^L\hat{U}^R$ [95, 220]. Here, $\hat{U}^{L,R}$ are exponentially localized on the boundaries. As discussed above, a fermionic chain with $SU(2)$ symmetry cannot host a non-trivial SPT phase; hence, these fractionalized symmetries must obey the same group properties as the bulk symmetry, in particular: $\hat{R}_x^L\hat{R}_y^L = \hat{P}^L\hat{R}_y^L\hat{R}_x^L$. In the Mott limit $U \to \infty$ for $\delta > 0$, we know that the edge hosts a spin-1/2, i.e., $P^L = -1$ such that $\hat{R}_x^L\hat{R}_y^L = -\hat{R}_y^L\hat{R}_x^L$ implies a twofold degeneracy. An eigenvalue of $\hat{P}^L$ cannot immediately jump such that its associated twofold degeneracy is parametrically stable. The only way P^L can change is if we make U sufficiently small such that another (non-degenerate) level with $P^L = +1$ crosses it in energy.

To illustrate this boundary transition, consider the case $\delta = 1$ where the decoupled edge is a single-site problem. The edge mode is stable until $U = \Delta$, where the energy

[7] Eigenvalues at higher energies must keep track of charge fluctuations destroying SPT order and, consequently, will generically not show degeneracies.

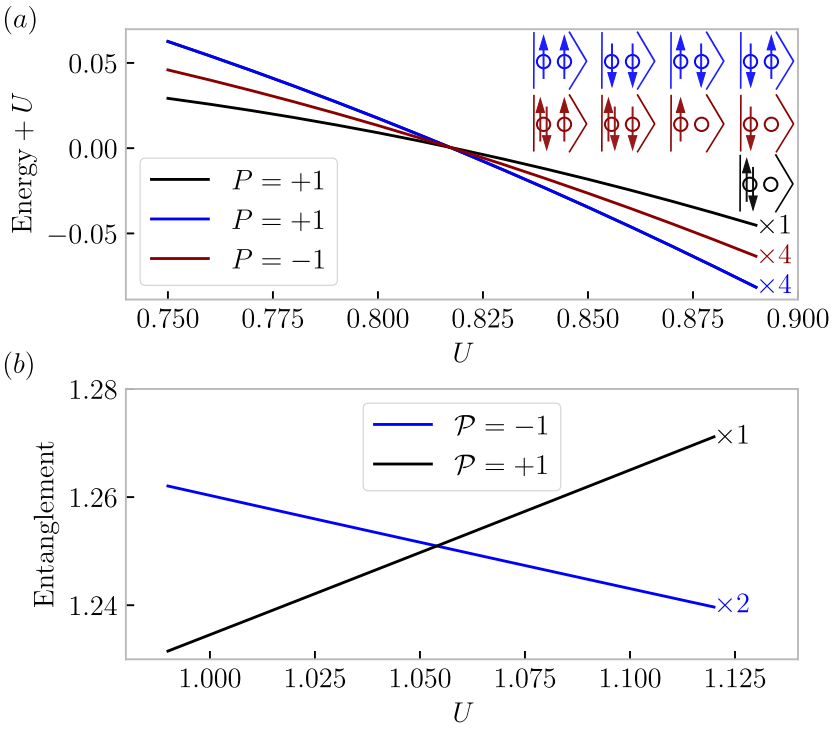

Figure 7.2: **QSPT edge phenomena.** We evaluate parity quantum numbers for a vertical slice $\delta = 0.2$ (dotted line in Fig. 7.1). (a) The ground state degeneracy and parity quantum numbers (P) for a system with open boundaries. We observe a boundary phase transition where the parity gap closes below (above) which the ground state is unique (degenerate). (b) The three lowest entanglement levels and the quantum numbers of $\hat{\mathcal{P}} = \hat{\mathcal{U}}_x\hat{\mathcal{U}}_y\hat{\mathcal{U}}_x^\dagger\hat{\mathcal{U}}_y^\dagger$ where $\hat{\mathcal{U}}_\gamma$ is the action of $\hat{R}_\gamma$ on the space of dominant eigenstates of the reduced density matrix for a bipartition of an infinitely-long chain [93].

levels of a doubly occupied ($P^L = 1$) and a singly occupied ($P^L = -1$) site cross (for a detailed discussion, see App. C.2). Away from this exactly solvable limit, we numerically determine this boundary transition as shown in Fig. 7.1. In the many-body system, we cannot directly read off the eigenvalue of $\hat{P}^L$; instead, we focus on $\hat{P} = \hat{P}^L\hat{P}^R$. The ground state always satisfies $P = +1$ (since both edges happen to undergo the boundary transition at the same time); nevertheless, the above reasoning shows that the gap for this global parity does close with open boundary conditions (since it must close at each edge), which we verify in Fig. 7.2a. Note, this gap closing does not exist if the system is considered with PBC. If it did, then we would have an actual bulk gap closing.

Entanglement spectrum

The above arguments can be repeated for a virtual bipartition of an infinite system, with the degenerate low-lying entanglement spectrum being stabilized by the parity quantum numbers of the dominant eigenstates of the reduced density matrix, confirmed in Fig. 7.2b. To demonstrate this, we first similar to Eq. (4.38) use that fermion parity is on-site and, thus, we can write the reduced density matrix as follows:

$$\hat{\rho}_L = \sum_\alpha \Lambda_\alpha \hat{P}|\alpha\rangle_{LL}\langle\alpha|\hat{P} = \hat{P}\hat{\rho}_L\hat{P}. \tag{7.9}$$

This implies that $\hat{P}$ commutes with the reduced density matrix $\hat{\rho}_L$ and the Schmidt spectrum is block diagonal with blocks labelled by the symmetry eigenvalues. To obtain the associated parity quantum numbers, we need to measure the symmetry eigenvalue of corresponding Schmidt states. The way we technically do this, is to obtain effective action of symmetry operators $\hat{R}_\gamma$ on the dominant Schmidt states (following Refs. [93, 94]), denoted by $\hat{\mathcal{U}}_\gamma$, and then use that fermion parity is given by,

$$\hat{\mathcal{P}} = \hat{\mathcal{U}}_x\hat{\mathcal{U}}_y\hat{\mathcal{U}}_x^\dagger\hat{\mathcal{U}}_y^\dagger. \tag{7.10}$$

The advantage of evaluating fermion parity this way is that $\hat{\mathcal{P}}$ only contains ± 1 entries[8] for corresponding blocks of the reduced density matrix since the expression remains invariant under rephasing $\hat{\mathcal{U}}_\gamma \to e^{i\Omega}\hat{\mathcal{U}}_\gamma$. If we used directly $\hat{P}$ to obtain $\hat{\mathcal{P}}$, then the eigenvalues of individual blocks could, in general, be decorated with an arbitrary phase factor (see also App C.2).

7.2.2 Stability of SPT transition

Here, we explain why the phase transition between a trivial and SPT phase does not immediately gap out after extending the symmetry group. Consequently, the critical line in Fig. 7.1 is a generic QSPT phenomenon.

Lieb-Schultz-Mattis anomaly

It is well-known that in spin chain limit the duality symmetry, Eq. (7.7), in combination with spin-rotation symmetry implies a Lieb-Schultz-Mattis (LSM) anomaly, disallowing a gapped, symmetric ground state [182, 188, 223–227]: in the absence of symmetry breaking this stabilizes a direct phase transition. The standard proofs for the LSM anomaly hinge on the fact that, on a single site, $\hat{R}_x$ and $\hat{R}_y$ anticommute. This no longer holds when charges fluctuate: $\hat{R}_x\hat{R}_y\hat{R}_x^{-1}\hat{R}_y^{-1} = \hat{P}$ (and indeed, in Fig. 7.1 we see that small U admits a gapped phase). Nevertheless, we show that there is an *emergent Lieb-Schultz-Mattis theorem* for large U, enforcing the parametric stability of the phase transition.

[8] To this end note that we explicitly conserve the particle number in our calculations. Thus, each Schmidt state has a well-defined particle number and, hence, a well-defined eigenvalue with respect to fermion parity.

Gapped degrees of freedom and quantized invariant

Above, we understood the parametric stability of edge modes in terms of parity quantum numbers. To characterize the bulk, we instead identify a quantized invariant associated to a parity *string*. As long as charge degrees of freedom remain gapped, the fermion parity string generically has long-range order[9]. Moreover, at $\delta = 0$, this must have a well-defined momentum θ under the duality/translation symmetry $\hat{\mathcal{D}}$ such that $(m < n)$

$$\langle \hat{P}_m \hat{P}_{m+1} \cdots \hat{P}_{n-1} \hat{P}_n \rangle \sim \text{constant} \times e^{i\theta(n-m)}. \tag{7.11}$$

Using symmetry fractionalization we can rigorously derive the result above. For a parity string, which is much longer than the fermionic correlation length[10], we can write (using symmetry fractionalization)

$$\hat{\mathcal{P}}_{m,n} := \prod_{m \leq k \leq n} \hat{P}_k = \hat{P}^L_m \hat{P}^R_n. \tag{7.12}$$

From $\hat{\mathcal{D}} \hat{\mathcal{P}}_{m,n} \hat{\mathcal{D}}^\dagger = \hat{\mathcal{P}}_{m+1,n+1}$, we obtain $\left(\hat{\mathcal{D}} \hat{P}^L_m \hat{\mathcal{D}}^\dagger\right) \left(\hat{\mathcal{D}} \hat{P}^R_n \hat{\mathcal{D}}^\dagger\right) = \hat{P}^L_{m+1} \hat{P}^R_{n+1}$ and, hence,

$$\hat{\mathcal{D}} \hat{P}^L_m \hat{\mathcal{D}}^\dagger = \alpha_{m,n} \hat{P}^L_{m+1} \wedge \hat{\mathcal{D}} \hat{P}^R_n \hat{\mathcal{D}}^\dagger = \bar{\alpha}_{m,n} \hat{P}^R_{n+1}, \tag{7.13}$$

where $\alpha_{m,n}$ is some proportionality factor. Note that the first (second) equation tells us that it cannot depend on n (m). I.e., the proportionality factor is a genuine constant. Let us denote it as $\alpha_{n,m} = e^{i\theta}$. Since $\langle \hat{\mathcal{P}}_{m,n} \rangle = \langle \hat{P}^L_m \rangle \langle \hat{P}^R_n \rangle$ (due to locality and the spatial separation between the fractionalized symmetries $\hat{P}^{L,R}$) and the fact that $\hat{\mathcal{D}}$ is a symmetry, i.e.,

$$\langle \hat{P}^L_m \rangle = \langle \hat{\mathcal{D}} \hat{P}^L_m \hat{\mathcal{D}}^\dagger \rangle = e^{i\theta} \langle \hat{P}^L_{m+1} \rangle = e^{i\theta k} \langle \hat{P}^L_{m+k} \rangle, \tag{7.14}$$

we derive Eq. (7.11):

$$\langle \hat{P}_m \hat{P}_{m+1} \cdots \hat{P}_{n-1} \hat{P}_n \rangle = \langle \hat{\mathcal{P}}_{m,n} \rangle = \langle \hat{P}^L_m \rangle \langle \hat{P}^R_n \rangle = e^{i\theta(n-m)} \langle \hat{P}^L_{n_0} \rangle \langle \hat{P}^R_{n_0} \rangle, \tag{7.15}$$

where n_0 is some reference site that does neither depend on n nor m. Finally, the quantization of θ follows from $\hat{\mathcal{P}}^2_{m,n} = 1$ since then $(\hat{P}^R_n)^2 \propto 1$ such that $e^{2i\theta} = 1$ from which we obtain a $\mathbb{Z}_2$-valued invariant $\theta = \{0, \pi\}$. As an illustration, note that in the spin chain limit, $P^R_n = (-1)^n$, which implies $\theta = \pi$. Hence, $\theta = \pi$ intuitively formalizes the idea of being close to a Mott limit, where fermion parity coincides with the parity of the number of sites.

[9] Following Ref. [183] the claim is that there exist some end-point operator such that a string consisting of fermion parity has long-range order as long as fermionic degrees of freedom are gapped.

[10] This length scale can be defined from correlation functions of fermionic operators, that is, operators that are charged with respect to fermion parity. An example of such correlation function is given by $\langle \hat{c}^\dagger_{j,s} \hat{c}_{j+l,s} \rangle$, where individual operators are charged with respect to fermion parity. Since charge degrees of freedom remain gapped, we expect such correlations to decay exponentially with a length scale set by the fermionic correlation length.

Emergent anomaly

We claim that if $\theta = \pi$, then there is an emergent (Lieb-Schultz-Mattis) anomaly that forbids a gapped, symmetric ground state. To show this, we first have to find a relation of spin-rotation symmetry and the quantized invariant θ introduced earlier. To this end, let us define a composite symmetry $\hat{\mathcal{I}} = \hat{R}_y \hat{\mathcal{D}} \hat{R}_y^\dagger \hat{\mathcal{D}}^\dagger$. Since $\hat{\mathcal{D}}$ and $\hat{R}_y$ commute, we find that $\hat{\mathcal{I}} = \mathbb{1}$. As a next step we will show, upon using this symmetry, that

$$\hat{\mathcal{I}} \hat{R}_x^L \hat{\mathcal{I}}^\dagger = e^{i\theta} \hat{R}_x^L. \tag{7.16}$$

This straightforwardly follows from symmetry fractionalization. We will need what we derived above: $\hat{\mathcal{D}} \hat{P}_n^L \hat{\mathcal{D}}^\dagger = e^{i\theta} \hat{P}_{n+1}^L$. Similarly, there is a phase factor $e^{i\kappa}$ such that $\hat{\mathcal{D}} [\hat{R}_x^L]_n \hat{\mathcal{D}}^\dagger = e^{i\kappa} [\hat{R}_x^L]_{n+1}$. Lastly, since group relations are always obeyed up to a phase factor, there is another phase factor $e^{i\mu}$ such that[11]

$$\hat{R}_y^\dagger [\hat{R}_x^L]_n \hat{R}_y = [\hat{R}_y^L]_n^\dagger [\hat{R}_x^L]_n [\hat{R}_y^L]_n = e^{i\mu} \hat{P}_n^L [\hat{R}_x^L]_n. \tag{7.17}$$

Note that this also implies $\hat{R}_y \hat{P}_n^L [\hat{R}_x^L]_n \hat{R}_y^\dagger = e^{-i\mu} [\hat{R}_x^L]_n$. Plugging in these identities, we obtain:

$$\begin{aligned}
\boxed{\hat{\mathcal{I}} [\hat{R}_x^L]_n \hat{\mathcal{I}}^\dagger} &= \hat{R}_y \hat{\mathcal{D}} \hat{R}_y^\dagger (\hat{\mathcal{D}}^\dagger [\hat{R}_x^L]_n \hat{\mathcal{D}}) \hat{R}_y \hat{\mathcal{D}}^\dagger R_y^\dagger \\
&= e^{-i\kappa} \hat{R}_y \hat{\mathcal{D}} (\hat{R}_y^\dagger [\hat{R}_x^L]_{n-1} \hat{R}_y) \hat{\mathcal{D}}^\dagger R_y^\dagger \\
&= e^{i\mu} e^{-i\kappa} \hat{R}_y \hat{\mathcal{D}} \hat{P}_{n-1}^L [\hat{R}_x^L]_{n-1} \hat{\mathcal{D}}^\dagger R_y^\dagger \\
&= e^{i\mu} e^{-i\kappa} \hat{R}_y (\hat{\mathcal{D}} \hat{P}_{n-1}^L \hat{\mathcal{D}}^\dagger) (\hat{\mathcal{D}} [\hat{R}_x^L]_{n-1} \hat{\mathcal{D}}^\dagger) R_y^\dagger \\
&= e^{i\mu} e^{-i\kappa} e^{i\theta} e^{i\kappa} \hat{R}_y \hat{P}_n^L [\hat{R}_x^L]_n R_y^\dagger \\
&= e^{i\mu} e^{-i\kappa} e^{i\theta} e^{i\kappa} e^{-i\mu} [\hat{R}_x^L]_n \\
&= \boxed{e^{i\theta} [\hat{R}_x^L]_n}.
\end{aligned} \tag{7.18, 7.19}$$

Let us emphasize again that for the last identity to hold, we need to make use of symmetry fractionalization, which requires a gapped, symmetric state. Indeed, this is precisely the key for proving the emergent anomaly.

Proof. Suppose there is a gapped, symmetric ground state, then using the previous result and that $\hat{\mathcal{I}} = \mathbb{1}$, we deduce:

$$[\hat{R}_x^L]_n = \hat{\mathcal{I}} [\hat{R}_x^L]_n \hat{\mathcal{I}}^\dagger = e^{i\theta} [\hat{R}_x^L]_n, \tag{7.20}$$

which implies that $\theta = 0$. Thus, if $\theta = \pi$ the assumption of a gapped, symmetric ground state must be wrong $\Rightarrow$ emergent anomaly.

[11] Here we use that $\hat{P}_n^L = [\hat{R}_x^L]_n^\dagger [\hat{R}_y^L]_n^\dagger [\hat{R}_x^L]_n [\hat{R}_y^L]$ and $[\hat{R}_x^L]_n \hat{P}_n^L = e^{i\mu} \hat{P}_n^L [\hat{R}_x^L]_n$. The last equation follows from the fact that fermion parity commutes with any element of $SU(2)$, which, for fractionalized operator means, that group relations are obeyed up to a phase.

Note as long as the Hamiltonian conserves global spin-rotation symmetry and the ground state is symmetric with respect to duality symmetry, the emergent anomaly implies gaplessness, which follows from the Mermin-Wagner-Hohenberg-Coleman theorem stating that *continuous* symmetries cannot be broken spontaneously for one-dimensional systems—independent of temperature [228–230] (see also Ref. [53]).

Mott limit. In the Mott limit we have $\theta = \pi$ such that we rederive the known LSM anomaly. However, since θ is a robust quantized invariant, we know that the transition is parametrically stable to finite U. The only way θ can change is:

(*i*) by closing the fermion parity gap (such that the parity string does not have long-range order),

(*ii*) or by spontaneously breaking the duality symmetry $\hat{\mathcal{D}}$, such that the charge $e^{i\theta}$ is no longer well-defined[12].

This particular model, Eq. (7.1), opts for the second option, as we see in Fig. 7.1 (the white line corresponds to the SDI phase).

Numerical results

To confirm this interpretation of the phase diagram, we measure θ by plotting

$$\mathcal{O}^{\pm} := \lim_{|n-m|\to\infty} |\langle \hat{\mathcal{S}}^{\pm}_m \hat{\mathcal{S}}^{\pm}_n \rangle| \text{ with } \hat{\mathcal{S}}^{\pm}_n := \prod_{k<n} \hat{P}_k \left(\hat{P}_n \pm 1 \right), \tag{7.21}$$

which we obtain using iDMRG, see App. C.2.4. It is easy to see that $\mathcal{O}^{\pm} \propto |1 \pm e^{i\theta}|$, which is nonzero if $e^{i\theta} = \pm 1$. From Fig. 7.3, we conclude that the gapless MI ($U > U_{c_2}$) has $\theta = \pi$, the BI ($U < U_{c_1}$) has $\theta = 0$, and the SDI phase has no well-defined θ since $\hat{\mathcal{D}}$ is broken spontaneously.

7.3 General emergent anomalies

The arguments for the parametric stability of edge modes and phase transitions readily extend to other symmetry groups and dimensions. Edge modes of 1D SPT phases are characterized by a non-trivial projective representation of a symmetry group $\tilde{G}$ [50, 93, 95, 96, 220] labeled by the second cohomology group $H^2(\tilde{G}, U(1))$. One can always extend the symmetry group by H[13] into a bigger symmetry group G (where $\tilde{G} = G/H$) such that the lifted representation becomes linear[14], thereby trivializing the SPT phase [39, 189–192]. However, focusing on a single edge, the quantum numbers of the additional symmetry group H still label these distinct representations[15]. Since quantum numbers

[12] Recall by the MWHC theorem the $SU(2)$ symmetry cannot be broken spontaneously.

[13] Here we assume H to be a finite group.

[14] Note this does not require that G itself cannot host non-trivial SPTs. The only requirement is that a non-trivial cocycle of $H^2(\tilde{G}, U(1))$ becomes a trivial element in $H^2(G, U(1))$ [39].

[15] For example, for fermion parity we found that the eigenvalue of $\hat{P}^L$ changed as a function of U from -1 to $+1$ and, thus, $\hat{P}^L = \hat{R}^L_x \hat{R}^L_y \left[\hat{R}^L_x\right]^\dagger \left[\hat{R}^L_y\right]^\dagger$ turns over to a linear representation.

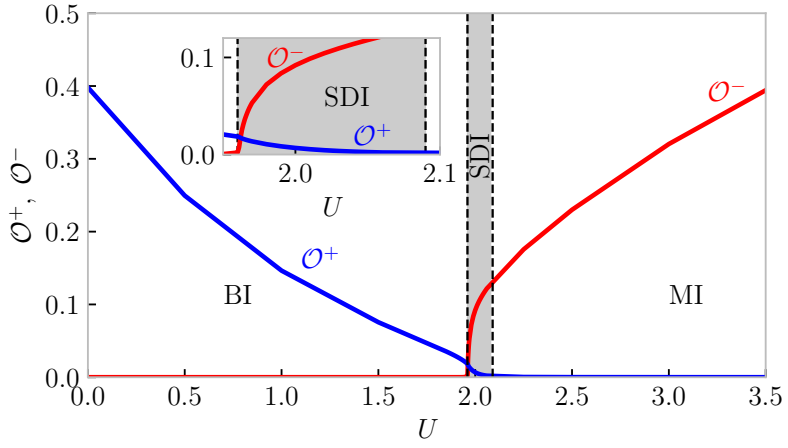

Figure 7.3: **QSPT transition and emergent anomaly along the self-dual line $\delta = 0$ (with ionicity $\Delta = 0.4$).** The observable $\mathcal{O}^{\pm}$ captures whether the fermion parity string oscillates or not: it measures the $\mathbb{Z}_2$ invariant $\theta = 0, \pi$ in Eq. (7.11). If $\theta = \pi$ (i.e., $\mathcal{O}^- \neq 0$ and $\mathcal{O}^+ = 0$), there is an emergent Lieb-Schultz-Mattis anomaly, preventing a symmetric, gapped state. Inset: the intermediate phase spontaneously breaks the duality symmetry $\hat{\mathcal{D}}$ such that both $\mathcal{O}^{\pm}$ are nonzero. Note to have $\mathcal{O}^+(U = 0) \approx \mathcal{O}^-(U \to \infty)$ we rescaled the operator $\mathcal{O}^-$ by a factor of 5.

are discrete, they can only change if the boundary undergoes a phase transition, which implies that edge modes remain stable until the gap to excitations, charged under H, close[16]. In the above example (where $\tilde{G} = SO(3)$, $H = \mathbb{Z}_2^f$ and $G = SU(2)$), we had to close the fermion parity gap at the boundary to destroy the edge mode.

Emergent anomalies

SPT transitions are stabilized by the mutual anomaly between the protecting symmetry group $\tilde{G}$ and the duality symmetry at the transition (e.g., the Lieb-Schultz-Mattis anomaly of the Heisenberg chain, as discussed above) [82, 91, 231]. This anomaly is lifted when we extend $\tilde{G}$ by H, but we propose that there is always an *emergent anomaly* encoded in the symmetry properties of the string orders associated to the symmetry group H (such as the fermion parity string in Eq. (7.11) being odd under $\hat{\mathcal{D}}$). It is interesting to observe that since a QSPT transition involves the whole 1D bulk, the emergent anomaly is characterized by a 1D object. In contrast, an edge mode is a zero-dimensional QSPT phenomenon, and correspondingly its parametric stability is encoded in a 0D charge.

[16] To change from half-integer to integer representation on a single edge, we have to create (annihilate) a fermion. Such operation clearly changes fermion parity and, thus, is charged with respect to $H = \mathbb{Z}_2^f$.

Higher dimensions

Note that the same mechanism of emergent anomalies in 1D SPT transitions applies to the 1D edge modes of 2D SPT phases.

For instance, if one trivializes an $\mathbb{Z}_2$-SPT in 2D by extending by a second $\mathbb{Z}_2$ symmetry $\hat{P}$ into $\mathbb{Z}_4$, then we expect that the string order of $\hat{P}$ will have a non-trivial charge under $\mathbb{Z}_4$—encoding the emergent anomaly. For example, the $\mathbb{Z}_2$ bosonic SPT can be trivialized by introducing fermions, similar to what we considered here [232]. In the simplest case, where the (now non-anomalous) edge mode is written as a 1D system, this string order can be directly computed and its non-trivial charge is a mechanism for the recently discovered intrinsically gapless SPT phases [233][17]. In the full 2D model, it can be challenging to access this string order directly (similar to access P_L directly in Fig. 7.2), but a clear-cut implication is that the edge mode has an emergent anomaly that can only disappear by spontaneously breaking the symmetry or by driving a boundary phase transition where the gap associated to the extending symmetry $\hat{P}$ must close. This situation is analogous to what we saw for the SPT transition in the ionic Hubbard chain.

7.4 Summary & Outlook

It is commonly known that SPT phases can be trivialized by symmetry breaking. However, this way all topological signatures immediately disappear. In this chapter, we studied an alternative way of trivializing SPTs by extending the symmetry group, which, in contrast to symmetry breaking, leaves various topological phenomena intact over a finite region of the phase diagram. For the concrete case study of the BIHM, we characterized this stability in terms of discrete invariants: a parity quantum number $\hat{P}^L = \pm 1$ labeling distinct representations of π-rotations and an $\mathbb{Z}_2$ invariant, whose non-trivial element signals an emergent anomaly of the quotient group and duality symmetry. Thereby, we argued that different representations on the edges can only change if the fermion parity gap closes, and the emergent anomaly disappears if fermions become gapless or there is spontaneous-symmetry breaking. Similar signatures we have found for the low-lying eigenvalues of the entanglement spectrum. A key observation made in this overall discussion was that there is a separation of energy scales. We argued that charge degrees of freedom along the gapless line are gapped, while spin degrees of freedom are gapless, which was reflected in the long-range order of the fermion parity string. Thus, the $\mathbb{Z}_2$ invariant associated to a fermion parity string is protected by a finite gap, which explains its parametric stability. On the other hand, if the emergent anomaly is gapped out by explicitly breaking duality symmetry in a way that the resulting state is a non-trivial QSPT, then edge modes are parametrically stable as long as the separation of energy scales remains intact.

The results obtained in this chapter are of particular relevance to physical implementations of SPT phases, where the protecting symmetry group is often a low-energy effective

[17] Such phase has no gapped analogue—meaning the symmetry group, here $\mathbb{Z}_4$, has a trivial second cohomology group $H^2(\mathbb{Z}_4, U(1)) = 0$.

quotient group. For instance, the spin-rotation symmetry protecting the Haldane phase in a spin chain is typically derived from a fermion symmetry of an underlying Hubbard model. The results in this work thus show that the experimental realization of such bosonic SPT phases is meaningful, since many of their topological phenomena are stable even when the bulk is—strictly speaking—not in a true SPT phase. As an aside, we note that string observables as in Eq. (7.11) are measurable in cold-atom systems [234–237].

Outlook. In the above lattice model, we saw a (parametrically) stable transition and edge mode. It is an open question how closely these are linked: it is tempting to think that the emergent edge mode cannot disappear before the emergent phase transition gaps out. Indeed, in Fig. 7.1 both features terminate at U_{c1}. This is intuitive given the interpretation of edge modes as being spatially localized phase transitions [238–241], but it would be interesting to make this correspondence more exact.

Chapter 8

Conclusion & Outlook

In this thesis, we studied two different branches of bosonic symmetry-protected topological phases. In the first three chapters, we considered higher-order topology in the 2D super-lattice Bose-Hubbard model. Thereby, we discussed various aspects of higher-order topology, and found an experimentally accessible, strongly-interacting lattice model. In the second half, we focused on quotient group symmetry-protected topological phenomena in one-dimensional $\mathbb{Z}_n \times \mathbb{Z}_n$-symmetric chains and the ionic Hubbard model, where we found that additional gapped degrees of freedom can endow the quantum critical point between distinct SPTs (protected by $\mathbb{Z}_n \times \mathbb{Z}_n$ symmetry) with additional topological properties, or protect topological signatures of the Haldane phase even though the bulk is strictly speaking in a trivial phase. These phenomena are based on the fact that the global symmetry acts as quotient group at low-energies.

Although at first glance the aforementioned topics seem to be unrelated, that is actually not the case. In fact, those two topics can be considered from a common standpoint: From a very general point of view, we studied the interplay of SPTs[1] with additional symmetries. In the first part, when discussing HOSPT phases, we saw that internal symmetries are not sufficient to protect the non-trivial topology and, thus, we had to require additional spatial symmetries. Together, these symmetries have been able to differentiate distinct phases of matter. On the other hand, in the second part, we learned that enlarging the symmetry group can trivialize the topology of the underlying state *without* a bulk phase transition and can change quantum criticality between two distinct classes of SPTs. Hence, while one side (additional) symmetries can increase the number of phases, it can on the other side also decrease the number of distinct states, which, however, depends strongly on the global symmetry group and models of interest. In summary, we can say that (additional) symmetries can be "foes" and "friends" of SPTs.

Below we provide a brief summary of the most important results we obtained in this thesis, and give an outlook.

[1] Note in the presence of symmetries even a trivial disordered state is a SPT, it is a trivial one.

Part I: Higher-order symmetry-protected topological phenomena

Chapter 3

In Chap. 3 we considered the 2D Bose-Hubbard model on a super-lattice and showed that this model—at half-filling—realizes two robust higher-order SPT phases protected by $U(1) \times C_4$ symmetry. In the limit of hardcore bosons, there is an additional $\mathbb{Z}_2$ symmetry that together with $U(1)$ gives rise to exact zero-energy modes at the corners. In this limit, the 2D SL-BHM fits into the classification of HOSPT phases discussed in Sec. 2.2.3. To argue non-trivial topology of the two distinct phases realized by this model, we considered the higher-order Zak (Berry) phase introduced by Araki et al. [128] for which we found two distinct quantized values in individual phases. Moreover, we introduced fractional corner charges and argued that these serve as a genuine topological invariant. Since at the beginning of this thesis, one of the main questions was to provide an experimentally accessible model, we evaluated full-counting statistics for the one-dimensional and two-dimensional SL-BHM to which experimentalists can compare to. While in 1D the distribution is sharply peaked (for large enough systems), in 2D we are limited by our numerical technique to consider systems sizes beyond 10×10. Nevertheless, we find reasonable data centered around the expected values of the fractional corner charge. Moreover, we argued that for the parameters we used, the model is accessible in the lab. Thus, we have shown that the 2D SL-BHM at half-filling realizes two distinct and robust higher-order topological phases that can be detected in experiments and paved the way to verify theoretically predicted higher-order topology.

Chapter 4

So far, we demonstrated that the 2D SL-BHM realizes a gapped, symmetric phase at half-filling, here, however, we showed that this also the case for commensurate bulk fillings $\{1/4, 3/4\}$, which we numerically verified using iDMRG. Moreover, we also identified a many-body invariant relating bulk topology to fractional corner charges. To this end, we showed that the higher-order Zak (Berry) phase, introduced previously, measures the C_4 eigenvalue of the underlying state after a 2π flux insertion into the central plaquette. From this observation, we constructed a many-body invariant, a $U(1)$ flux insertion operator, that inserts non-trivial flux into the central plaquette—causing a non-trivial shift of angular momentum. This non-trivial shift is directly related to binding of fractional charges at disclinations, a topological lattice defect that in a continuum approximation of crystals is related to non-trivial curvature of space. This interplay of gravitational and electromagnetic degrees of freedom we characterized using the discrete Wen-Zee response, which distinguishes different HOSPT phases of the 2D SL-BHM, and is related to non-trivial fractional corner charges. To substantiate our analytical results, we numerically evaluated the many-body invariants for several bulk fillings of the 2D SL-BHM.

In the second half of this chapter, we asked whether we can deduce non-trivial topology

of the state by investigating the entanglement spectrum. Indeed, we found that in the case of exact zero-energy modes (hardcore bosons), i.e., projective presentations at the corners, the entanglement spectrum of the reduced density matrix at the corner is degenerate with even multiplicities. For finite interactions among the bosons, there are no zero-energy modes anymore, but still fractional charges at the corners. Upon a C_4-symmetric bipartition, we showed that for the quarter-filled cases the degeneracy remains, while for the half-filled case we found both; degenerate and non-degenerate eigenvalues. However, we demonstrated that the entanglement spectrum becomes fully degenerate if we further bipartite non-degenerate Schmidt states, which we denoted as higher-order entanglement—a unique feature of HOSPT phases.

Chapter 5

In this chapter, we showed that the fractional corner charge and a variant of the higher-order Zak (Berry) phase—for the half-filled case—are in one-to-one correspondence, that is, a non-trivial, quantized change of the latter implies a quantized change of the former. To this end, we showed that conventional periodic boundary conditions for studying HOSPT phases are not the optimal choice, and introduced corner periodic boundary conditions. As a consequence, the separation of edges and bulk remains intact. This has the advantage that we can move the symmetry twist—to evaluate the formerly introduced higher-order Zak (Berry) phase—of the central plaquette to the boundary plaquette and, thus, avoid non-trivial flux insertion in the bulk, which might cause a gap closing in the thermodynamic limit. From this, we constructed a new variant of a higher-order Zak (Berry) phase, which, however, is only quantized in the limit of hardcore bosons and half-filling.

By explicitly constructing two distinct Thouless pumps, we numerically demonstrated that a non-trivial, quantized change of this new higher-order Zak (Berry) phase serves a sensor of charge flow, and measured at each corner, gives us the quantized change of the fractional corner charge. Afterwards, we explicitly proved that a change of the higher-order Zak (Berry) phase is directly related to a quantized charge transport. For this, we generalized Resta's construction of the many-body polarization to higher-order systems, and used an adiabatic approximation. This gives rise to a strict bulk-boundary correspondence in higher-order topological systems. Importantly, although the higher-order Zak (Berry) phase introduced here is only a well-defined quantized invariant in the limit of hardcore bosons, we argued that the bulk-boundary correspondence remains intact even if the on-site repulsion becomes finite, since the change of this phase—during one Thouless pump cycle—remains quantized.

Although we were unable to prove the bulk-boundary correspondence for the higher-order Zak (Berry) phase introduced by Araki et al. [128], we, nevertheless, argued it numerically. Moreover, we showed that the proof hinge on the fact to prove that the loop integrals in parameter space[2] of the higher-order Zak (Berry) phase and the phase introduced by Resta's construction must coincide.

[2]This parameter space characterizes different Thouless pumps.

In the first three chapters we have characterized higher-order topological phases in the 2D SL-BHM from many points of view, and demonstrated that this model is the optimal choice for comparing theoretical results to experiments, which is essential, then one major task of theoretical physicists is to provide predictions that can be either verified or falsified by experimentalists. A theory, without experimental probes, remains what is—a theory. Even though we already characterized many aspects of this model, there are still a few open questions: First, up to this point, we have not been able to prove a strict bulk-boundary correspondence for the higher-order Zak (Berry) phase discussed in Chap. 3, albeit we already sketched a possible solution. Moreover, the Thouless pumps considered here were only for a particular filling. In the future, it would be worthwhile to study Thouless pumps of the quarter-filled cases, although this might be more challenging because we have to ensure gapped edges if we use corner periodic boundary conditions.

Part II: Quotient group symmetry-protected topological phenomena

Chapter 6

Here we studied fixed-point models of bosonic SPTs in one-dimensional $\mathbb{Z}_n \times \mathbb{Z}_n$ symmetric quantum chains, and analyzed their transitions. Thereby, we first generalized previous results and found that for $n < 4$ any single parameter interpolation between two-fixed point models crosses a single, unique QCP. Moreover, we uncovered that direct transitions of lower dimensional symmetry groups, $n \leq 4$, reappear in higher-dimensional symmetry groups and, consequently, are embedded into a higher-dimensional Hilbert space. This naturally leads to additional gapped degrees of freedom at quantum criticality, which also occur for transitions with an intermediate gapless phase. As a consequence, we found that the action of the global symmetry on low-energy degrees of freedom is given by the quotient group. This had a number of consequences: First, we found that in the presence of additional gapped degrees of freedom, not all SPT transition are allowed. Starting from the trivial phase, we can only enter those classes for which certain compatibility conditions are satisfied. For example, projective representations of gapped symmetries (subgroups acting on high-energy degrees of freedom) must be trivial. Second, the QCP or intermediate gapless phases ($n > 5$) can be endowed with additional topological properties, such as edge modes and degeneracy of the entanglement spectrum and, thus, form so-called gapless SPTs. Hence, in the presence of symmetries, we can further specify the nature of the underlying CFTs and distinguish them even if they have the same central charge. Third, for certain transitions the low-energy representation of the global symmetry together with a duality mapping, which gets a symmetry if both Hamiltonians have equal weight, has an emergent anomaly—forbidding a gapped, symmetric state. This makes criticality parametrically robust to perturbations to a gapped, symmetric phase. We explicitly demonstrated this by studying a phase diagram of the $\mathbb{Z}_4 \times \mathbb{Z}_4$ case, where we indeed found a stable gapless line that ends in a non-trivial SPT. The results we obtained from the study of these models naturally generalize to other

SPT transitions. Namely, if certain compatibility conditions are fulfilled and a normal subgroup[3] remains gapped throughout the interpolation, then the low-energy theory is governed by the quotient group.

By evaluating a second phase diagram of $\mathbb{Z}_3 \times \mathbb{Z}_3$ fixed-point models, we showed that the equal-weighted sum of all fixed-point models cannot have a gapped, symmetric ground state. At this fine-tuned point, there is an additional $\mathbb{Z}_n$ symmetry, which together with the global symmetry has an anomaly. Intriguingly, we discovered that this additional symmetry enhances to a global $U(1)$ symmetry, but the global symmetry is not $\mathbb{Z}_n \times \mathbb{Z}_n \times U(1)$. What the precise form of this symmetry is, has not been answered yet, and we leave it to future research.

Chapter 7

In the former case of quotient group symmetry-protected topological phenomena, we saw that, by lifting the emergent anomaly, quantum criticality can be gapped out towards a non-trivial SPT. This was possible because the global symmetry group can protect non-trivial SPTs, here, however, this is not possible. For the bond-alternating ionic Hubbard model, studied in this chapter, the global symmetry of interest is spinful $SU(2)$ symmetry, which cannot protect non-trivial SPTs. Indeed, we found here that the quotient symmetry, $SO(3)$, together with modified translations has an emergent anomaly, that is parametrically stable and is gapped out towards a trivial, disordered phase. In fact, this line, in the limit of strong on-site repulsion among fermions, separates the Haldane phase from its trivial counterpart, both realized as the low-energy description of the bond-alternating ionic Hubbard model. Along this line charge degrees of freedom remain gapped, which was reflected in long-range order of fermion parity and, thus, the global symmetry—at low-energy—is given by $SU(2)/\mathbb{Z}_2^f = SO(3)$.

An important observation made in both chapters is a separation of energy scales. Upon breaking the duality symmetry, unnecessary quantum criticality (in the bond-alternating ionic Hubbard model) is gapped out towards a trivial or non-trivial SPT, and as long as the separation of energy scales remains intact, topological signatures such as edge modes and degeneracies—at least for low-lying levels—persist, and are symmetry-protected. Unlike conventional SPTs, we demonstrated that QSPTs do not require a bulk phase transition to be trivialized; however, if considered with boundaries, there is a parity gap closing on the edge, where the parity quantum number along the edge can change. In more formal language, we say projective representations at the boundary have been lifted to a linear one.

By numerically evaluating a two-parameter phase diagram, we showed that topological signatures are stable over a large parameter regime, and that the Haldane phase, appearing as a low-energy phase in the bond-alternating ionic Hubbard model, is trivialized by fluctuating charges. Since the underlying mechanism here is not model specific, we dubbed those phases QSPTs and argued that they can appear in higher-dimensions as well.

[3] A subgroup H is normal if for any $h \in H$ and $g \in G$ the following holds: $ghg^{-1} \in H$.

In summary, we have shown that quotient group symmetry-protected topological phenomena go hand in hand with a separation of energy scales and, consequently, the low-energy representation of the global symmetry is a quotient group. Moreover, the presence of additional gapped degrees of freedom can endow quantum criticality with non-trivial topological properties, and, in particular, keeps it parametrically stable against symmetry preserving perturbations. Depending on the overall symmetry group, we showed that quantum criticality can be gapped out either to non-trivial SPTs or to trivial, disordered phases. In the latter case, this opens up a new door for experimentalists to realize "SPT" phases without breaking global symmetries nor ramping trough critical points.

The topological signatures of the Haldane phase have been remarkably stable; however, we do not know how generic this is. Thus, it would be interesting to study another model that realizes such phase in certain limits, maybe even in 2D because here we expect the full one-dimensional edge to go critical, which, unlike the 0D case, is a true quantum phase transition.

Appendix A

Finding gapped phases of the 2D SL-BHM at half-filling

A.1 Bulk correlation length

In Fig. A.1 we show the bulk correlation length ξ of the 2D SL-BHM, which we evaluated using iDMRG on an infinite cylinder with circumference $L_y = 6$. To obtain the phase diagram, we calculated ξ starting from the trivial phase up to $t = 0.5$. The reason is that for such geometry there is a duality transformation that exchanges the hopping amplitudes $t \leftrightarrow 1 - t$ and, hence, both phases of the 2D SL-BHM. Consequently, the phase diagram is symmetric around $t = 0.5$. Thus, to obtain the full phase diagram, we mirrored the results with respect to the axis defined by $t = 0.5$. The duality transformation is given by single-site translation along x and y, respectively.

From the results shown in Fig. A.1, we clearly see that as the bond dimension increases, the bulk correlation length ξ in the gapped phases saturates, while in the intermediate superfluid phase increases as a function of bond dimension. For a gapless phase, the scaling of the correlation length and MPS bond dimension is given as follows [194]:

$$\xi \sim \chi^{\kappa}, \quad \kappa > 0. \tag{A.1}$$

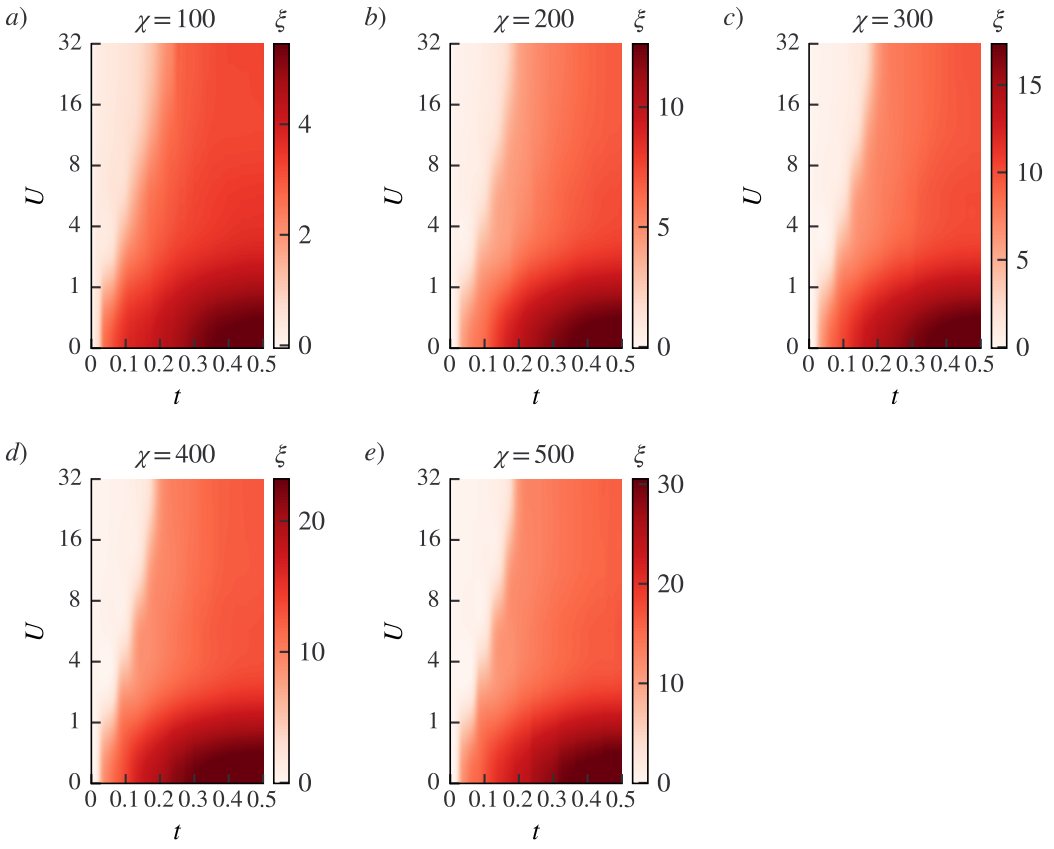

Figure A.1: **Bulk correlation length.** From the ground state at different bond dimensions χ, we obtain the bulk correlation length ξ. In regions where ξ saturates, the 2D SL-BHM has extended gapped phases, while in other regions ξ grows indefinitely, signaling a superfluid phase. Moreover, there is a duality transformation for the 2D SL-BHM on such geometry and, hence, the phase diagram is symmetric with respect to $t = 0.5$. For the simulation, we truncated the local Hilbert space, i.e., we allowed for maximal four bosons per site.

Appendix B

Add-ons to quotient group symmetry-protected topological phenomena in $\mathbb{Z}_n \times \mathbb{Z}_n$ chains

B.1 Details of numerical calculations

Here we shortly explain how we obtained the phase diagrams shown in Figs. 6.3 and 6.7, and, moreover, give details of how we evaluated the central charges for Figs. 6.3 and 6.6. In addition, we provide information about the calculation of string operators in Fig 6.3c. All numerical data have been obtained using iDMRG with open boundary conditions, where, most of the time, we explicitly conserved the global $\mathbb{Z}_n \times \mathbb{Z}_n$ symmetry.

B.1.1 Calculations of phase diagrams

To obtain the ternary plots, we first evaluated the phase diagram of

$$\hat{H}^{(n)}_{021}(\lambda,\mu) = (1-\lambda)\hat{H}^{(n)}_0 + \lambda\hat{H}^{(n)}_2 + \mu\hat{H}^{(n)}_1, \tag{B.1}$$

with $(\lambda,\mu) \in [0,1]\times[0,1]$ and $n \in \{3,4\}$. To this end, we evaluated the ground states using iDMRG with a maximal bond dimension of $\chi = 700$ and a resolution $\Delta\lambda = \Delta\mu = 0.01$. The phase boundaries are set at those points, where (η,ξ)—the second-largest eigenvalue of the MPS transfer matrix and correlation length [98]—fulfill the condition: $\eta = e^{-1/\xi} > 0.99$. For the ternary diagram, we need to normalize the couplings by rescaling the Hamiltonian $\hat{H}^{(n)}_{021}(\lambda,\mu) \to (1+\mu)^{-1}\hat{H}^{(n)}_{021}(\lambda,\mu)$. Thus, as shown in the main text, the couplings add up to one

$$\underbrace{\frac{1-\lambda}{1+\mu}}_{\equiv\alpha} + \underbrace{\frac{\lambda}{1+\mu}}_{\equiv\beta} + \underbrace{\frac{\mu}{1+\mu}}_{\equiv\gamma} = 1. \tag{B.2}$$

Finally, we need to map the ternary coordinates to Cartesian coordinates [242]

$$x = \frac{\lambda}{1+\mu} + \frac{\mu}{2(1+\mu)}, \quad y = \frac{\sqrt{3}}{2}\frac{\mu}{1+\mu}, \tag{B.3}$$

with $(x,y) \in [0,1]\times[0,\sqrt{3}/2]$, from which we obtained the phase diagrams shown in Figs. 6.3 and 6.7.

B.1.2 Calculations of central charges

To obtain the central charges of Figs. 6.3b and 6.6, we evaluated the ground states using iDMRG and evaluated the half-infinite chain entanglement entropy S for different MPS bond dimensions χ. The central charge is then obtained via the formula [193, 194]:

$$S(\chi) = \frac{c}{6} \log \xi(\chi) + \text{const.}. \tag{B.4}$$

For Fig. 6.3b, the central charge was evaluated for Hamiltonian (B.1) at $(n, \lambda, \mu) = (4, 0.5, 0.15)$. The iDMRG calculation stopped if, for a given bond dimension, the relative change in energy and half-infinite chain entanglement entropy among two successive sweeps was below $\Delta E < 10^{-8}$ and $\Delta S < 10^{-6}$, respectively.

B.1.3 Calculations of string operators

For obtaining the string operators, shown in Fig. 6.3c, we evaluated the ground state for Hamiltonian

$$\hat{H}^{(4)}_{021}(\gamma) = \frac{1-\gamma}{2}\left(\hat{H}^{(4)}_0 + \hat{H}^{(4)}_2\right) + \gamma \hat{H}^{(4)}_1, \quad \gamma \in [0,1]. \tag{B.5}$$

In the SSB phase and the SPT phases, we evaluated the ground states for bond dimensions up to $\chi \in \{100, 200, ..., 1000\}$ and obtained the string operators for different numbers of unit cells $r_0 \in \{100, 200, ..., 1000\}$, and then checked convergence in χ as well as in distance. For iDMRG calculations in the SSB phase, we conserved only one of the $\mathbb{Z}_n$ symmetries. The data in Fig. 6.3c are shown for $\chi = 1000$ and $r_0 = 1000$. Along the gapless line, the situation is different. Here we conserved the full $\mathbb{Z}_4 \times \mathbb{Z}_4$ symmetry in our calculations. The string operators with trivial end-points are quickly converged as a function of (χ, r_0), while this is not the case for the string operators with non-trivial end-points. There string operators act on both, gapped and gapless degrees of freedom. In the unperturbed case, the string, consisting of the generators of $\mathbb{Z}_2 \times \mathbb{Z}_2$ subgroup, can be ignored as $\hat{X}^2_{j,\sigma} = 1$ for all sites, and it remains to evaluate the correlation function $\langle \hat{Z}_{l,\sigma} \hat{Z}_{l+r_0,\sigma} \rangle$. According to App. B.2, Eq. (B.13), these operators have a non-trivial action on gapless degrees of freedom. As a consequence, these string operators decay algebraically (see Fig. B.1.) For a critical state, the MPS approximates true correlations only up to the MPS correlation length. Thus, for each bond dimension, the length of the string is set by the MPS correlation length. Afterwards we can do an extrapolation to obtain the infinite length value of the string operator, which in this case is zero[1].

[1] From the analytical side—given the discrete charges of end-point operators—we know that if the ground state is $\mathbb{Z}_4 \times \mathbb{Z}_4$ symmetric and the trivially charged string operator has long-range order, the other string operator must vanish.

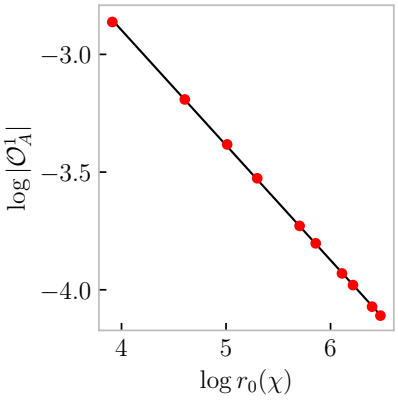

Figure B.1: **Algebraic decay.** Algebraic decay of non-trivially charged string operators along the gapless line, explicitly shown for $\mathcal{O}_A^1$ ($\gamma = 0.02$) as a function of distance, which is fixed by the MPS correlation length depending on $\chi \in \{100, ..., 1000\}$.

B.2 Operator identities, quotient symmetry and effective Hamiltonians

In this section we discuss how the quotient symmetry, the effective Hamiltonian and the embedding of the quotient symmetry in the full Hilbert space arise if a local $\mathbb{Z}_\delta$ symmetry is conserved. To this end, we first discuss an alternative representation of the local operator $\hat{X}_{j,\sigma}$ from which we then derive the representation of local operators in the ground state subspace.

B.2.1 A new representation and a projection operator

As a first step, we prove that the generator of $\mathbb{Z}_n$ can be written as:

$$\hat{X}_{j,\sigma} = \mathbb{1}_{j,\sigma_1} \otimes \hat{X}_{j,\sigma_2} + \left(\hat{X}_{j,\sigma_1} - \mathbb{1}_{j,\sigma_1}\right) \otimes \Sigma^+_{j,\sigma_2}, \tag{B.6}$$

where we decomposed the local Hilbert space as follows:

$$\mathcal{H}_{j,\sigma} = \mathcal{H}_{j,\sigma_1} \otimes \mathcal{H}_{j,\sigma_2}, \quad \dim\left(\mathcal{H}_{j,\sigma_i}\right) = D_i, \quad D_1 \times D_2 = n. \tag{B.7}$$

The operator $\hat{X}_{j,\sigma_i}$ is the generator of the $\mathbb{Z}_{D_i}$ symmetry, defined in Eq. (6.28), and the operator Σ^+_{j,σ_2} has a single entry given by $\Sigma^+_{j,\sigma_2} = (|0\rangle \langle D_2 - 1|)_{j,\sigma_2}$. The basis states of $\mathcal{H}_{j,\sigma}$ can be identified with basis states of $\mathcal{H}_{j,\sigma_1} \otimes \mathcal{H}_{j,\sigma_2}$ in the following way:

$$\left\{|l\rangle_{j,\sigma}\right\} = \bigcup_{l_1=0}^{D_1-1} \bigcup_{l_2=0}^{D_2-1} \left\{|l_1\rangle_{j,\sigma_1} |l_2\rangle_{j,\sigma_2}\right\}. \tag{B.8}$$

For example, if we take $n = 4, D_i = 2$, then

$$\begin{aligned} |0\rangle_{j,\sigma} &= |0\rangle_{j,\sigma_1} |0\rangle_{j,\sigma_2}\,, \quad |1\rangle_{j,\sigma} = |0\rangle_{j,\sigma_1} |1\rangle_{j,\sigma_2} \\ |2\rangle_{j,\sigma} &= |1\rangle_{j,\sigma_1} |0\rangle_{j,\sigma_2}\,, \quad |3\rangle_{j,\sigma} = |1\rangle_{j,\sigma_1} |1\rangle_{j,\sigma_2}\,. \end{aligned} \tag{B.9}$$

To prove the operator identities, we need to show that both operators act in the same way on local basis states. From Eq. (6.28) we recall that

$$\hat{X}_{j,\sigma} |l\rangle_{j,\sigma} = |l + 1 \bmod n\rangle_{j,\sigma}\,. \tag{B.10}$$

On the other hand, if the operator, defined in Eq. (B.6), is applied on a local basis state such as $|l_1\rangle_{j,\sigma_1} |l_2\rangle_{j,\sigma_2}$ we obtain:

$$\hat{X}_{j,\sigma} |l_1\rangle_{j,\sigma_1} |l_2\rangle_{j,\sigma_2} = \begin{cases} |l_1\rangle_{j,\sigma_1} |l_2 + 1\rangle_{j,\sigma_2} & ,\ l_2 \neq D_2 - 1 \\ |l_1 + 1\rangle_{j,\sigma_1} |0\rangle_{j,\sigma_2} & ,\ l_2 = D_2 - 1. \end{cases} \tag{B.11}$$

From Eqs. (B.8, B.9) we see that there are D_1 blocks of size D_2. Inside each block, the state $|l_1\rangle_{j,\sigma_1}$ is unchanged, while the state $|l_2\rangle_{j,\sigma_2}$ is shifted:

$$|l_2\rangle_{j,\sigma_2} \to |l_2 + 1\rangle_{j,\sigma_2}\,.$$

On the other hand, if a basis state $|l\rangle_{j,\sigma}$ is transferred from one block to another, then the state $|l_1\rangle_{j,\sigma_1}$ is shifted:

$$|l_1\rangle_{j,\sigma_1} \to |l_1 + 1\rangle_{j,\sigma_1}\,,$$

while the state $|l_2\rangle_{j,\sigma_2}$ jumps back to zero $|l_2\rangle_{j,\sigma_2} \to |0\rangle_{j,\sigma_2}$. This is exactly what the operator defined in Eq. (B.6) does, see also Eq. (B.11). For example, if we set $D_1 = \delta$ and $D_2 = n_\delta$ ($n_\delta \equiv n/\delta$), then the operator $\hat{X}^{n_\delta}_{j,\sigma}$ is given by,

$$\hat{X}^{n_\delta}_{j,\sigma} = \hat{X}_{j,\sigma_1} \otimes \mathbb{1}_{j,\sigma_2}. \tag{B.12}$$

To see this, note that for this operator any local basis state $|l\rangle_{j,\sigma}$ is always shifted by n_δ:

$$|l\rangle_{j,\sigma} \to |l + n_\delta\rangle_{j,\sigma}\,,$$

and since $D_2 = n_\delta$, this implies that each time $\hat{X}^{n_\delta}_{j,\sigma}$ is applied, $|l_1\rangle_{j,\sigma_1}$ is shifted $|l_1\rangle_{j,\sigma_1} \to |l_1 + 1\rangle_{j,\sigma_1}$.

Projection operator

If we now project, with a projector given by,

$$\hat{P}^{(n)}_{j,\sigma} = \left(|\omega^0\rangle \langle\omega^0|\right)_{j,\sigma_1} \otimes \mathbb{1}_{j,\sigma_2}, \quad \hat{X}_{j,\sigma_1} |\omega^0\rangle_{\sigma_1} = |\omega^0\rangle_{j,\sigma_1}\,, \tag{B.13}$$

into the n_δ-fold degenerate eigenspace with eigenvalue one—$e(\hat{X}^{n_\delta}_{j,\sigma}) = 1$—then the operator $\hat{X}_{j,\sigma}$, in this subspace, reduce to

$$\hat{X}_{j,\sigma} \xrightarrow{e(\hat{X}^{n_\delta}_{j,\sigma})=1} \hat{X}_{j,\sigma_2}. \tag{B.14}$$

If $n_\delta = 2$, then the operator $\hat{X}_{j,\sigma_2}$ reduce to the Pauli operator $\hat{\mathcal{X}}_{j,\sigma_2}$. Similarly, given the decomposition of the basis states, Eq. (B.8), it is easily verified that

$$\hat{Z}^\delta_{j,\sigma} = \mathbb{1}_{j,\sigma_1} \otimes \hat{Z}_{j,\sigma_2} \xrightarrow{e(\hat{X}^{n_\delta}_{j,\sigma})=1} \hat{Z}_{j,\sigma_2}, \tag{B.15}$$

is up to dimensional reduction, unchanged under projections. Moreover, if $n_\delta = 2$, then $\hat{Z}^\delta_{j,\sigma}$ reduce to the Pauli operator $\hat{\mathcal{Z}}_{j,\sigma_2}$

B.2.2 Quotient symmetry group

If the generators of the global $\mathbb{Z}_n \times \mathbb{Z}_n$ symmetry are projected into the ground state subspace, then the global symmetry reduce to its quotient group given by $\mathbb{Z}_{n_\delta} \times \mathbb{Z}_{n_\delta}$. This can be seen as follows: In the low-energy subspace the identity element and the generators of $\mathbb{Z}_\delta \times \mathbb{Z}_\delta$ are mapped to the same element, namely:

$$\mathbb{1}_{j,\sigma} \xrightarrow{e(\hat{X}^{n_\delta}_{j,\sigma})=1} \mathbb{1}_{j,\sigma_2}, \quad \hat{X}^{n_\delta}_{j,\sigma} \xrightarrow{e(\hat{X}^{n_\delta}_{j,\sigma})=1} \mathbb{1}_{j,\sigma_2}. \tag{B.16}$$

Hence, two elements of $\mathbb{Z}_n \times \mathbb{Z}_n$ symmetry that differ by an element of $\mathbb{Z}_\delta \times \mathbb{Z}_\delta$ belong to the same element in the low-energy subspace. This is precisely the definition of a quotient group[2]. Thus, at low-energies the symmetry group acts indeed as a quotient group

$$\mathbb{Z}_{n_\delta} \times \mathbb{Z}_{n_\delta} = (\mathbb{Z}_n \times \mathbb{Z}_n) \,/\, (\mathbb{Z}_\delta \times \mathbb{Z}_\delta)\,. \tag{B.17}$$

B.2.3 Embedding of the quotient symmetry

In the main text, we argued that the embedding of the quotient group becomes an exact symmetry of $\hat{H}^{(n)}_0$ and $\hat{H}^{(n)}_{n/2}$. To see this, we set $D_2 = 2$[3], then according to Eq. (B.6) we can write[4]

$$\hat{X}_{j,\sigma} = \hat{\mathcal{X}}_{j,\sigma_2} + \frac{1}{2}\left(\hat{X}_{j,\sigma_1} - \mathbb{1}_{j,\sigma_1}\right)\left(\hat{\mathcal{X}}_{j,\sigma_2} + i\hat{\mathcal{Y}}_{j,\sigma_2}\right), \tag{B.18}$$

where we used that—Σ^+_{j,σ_2}—reduce to the raising operator of spin-1/2 degrees of freedom. Similarly, we find that $\hat{Z}^{n/2}_{j,\sigma} = \hat{\mathcal{Z}}_{j,\sigma_2}$. Now let us define the embedding of the quotient symmetry as follows:

$$\hat{\mathcal{Q}}_\sigma = \prod_j \hat{W}_{j,\sigma_1} \otimes \hat{\mathcal{X}}_{j,\sigma_2}, \tag{B.19}$$

where we identified $\hat{\mathcal{W}}$ from the main text, Eq. (6.46), with $\hat{W}_{j,\sigma_1}$, which itself is defined through:

$$\hat{W}_{j,\sigma_1} : \hat{X}_{j,\sigma_1} \leftrightarrow \hat{X}^\dagger_{j,\sigma_1}, \quad \hat{W}_{j,\sigma_1} : \hat{Z}_{j,\sigma_1} \leftrightarrow \hat{Z}^\dagger_{j,\sigma_1}. \tag{B.20}$$

[2] Aside from the condition that the subgroup H of G must be normal, i.e., for each $h \in H$ and $g \in G$ we have that $ghg^{-1} \in H$, which is clearly the case here.

[3] For $\hat{H}^{(n)}_0$ the dimensions of how we decompose the local Hilbert space can be chosen arbitrarily.

[4] Recall that for two-dimensional subspaces we use a different notation for the Pauli operators.

In the eigenbasis of $\hat{Z}_{j,\sigma_1}$, it can be written as:

$$\hat{W}_{j,\sigma_1} = \sum_{l_1=0}^{\frac{n}{2}-1} \left(|\frac{n}{2} - l_1\rangle \langle l_1| \right)_{j,\sigma_1} . \tag{B.21}$$

This indeed shows that under the embedding of the quotient symmetry, local operators, with $\hat{X}_{j,\sigma}$ given in Eq. (B.18), transform as follows:

$$\hat{\mathcal{Q}}_\sigma : \hat{X}_{j,\sigma} \leftrightarrow \hat{X}^\dagger_{j,\sigma}, \quad \hat{\mathcal{Q}}_\sigma : \hat{Z}^{\frac{n}{2}}_{j,\sigma} \leftrightarrow -\hat{Z}^{\frac{n}{2}}_{j,\sigma} \tag{B.22}$$

from which we conclude that the embedding of the quotient group becomes an additional $\mathbb{Z}_2 \times \mathbb{Z}_2$ symmetry of $\hat{H}^{(n)}_0$ and $\hat{H}^{(n)}_{n/2}$.

B.2.4 Effective Hamiltonian

Given the local projection operator, Eq. (B.13), we immediately see that the effective Hamiltonian of $\hat{H}^{(n)}_\delta$—with n_δ integer-valued—is indeed given by $\hat{H}^{(n_\delta)}_1$,

$$\hat{H}^{(n)}_\delta \xrightarrow{e(\hat{X}^{n_\delta}_{j,\sigma})=1} \hat{H}^{(n_\delta)}_1, \tag{B.23}$$

where $\hat{H}^{(n_\delta)}_1$ acts solely on $\{\sigma_2\}$ degrees of freedom. The remaining degrees of freedom, $\{\sigma_1\}$, form a trivial product state,

$$|\Psi^{(n)}_\delta\rangle = \underbrace{|\omega^0\rangle}_{\sigma_1} \underbrace{|\Psi^{(n_\delta)}_1\rangle}_{\sigma_2}, \quad |\omega^0\rangle = \prod_{j,\sigma_1} |\omega^0\rangle_{j,\sigma_1}, \quad \hat{X}_{j,\sigma_1} |\omega^0\rangle_{j,\sigma_1} = |\omega^0\rangle_{j,\sigma_1} . \tag{B.24}$$

Thus, the path $\Gamma^{(n)}_{0\delta}(\lambda,\mu)$, defined in Eq. (6.45), reduce for sufficiently large $\mu \in \mathbb{R}^+_0$ to the interpolation of $\hat{H}^{n_\delta}_{01}(\lambda)$—up to a constant shift. Note if the representation of the local $\mathbb{Z}_\delta$ symmetry changes after applying powers of the SPT-Entangler on $\Gamma^{(n)}_{0\delta}(\lambda,\mu)$, to arrive at $\Gamma^{(n)}_{d\delta}(\lambda,\mu)$, the ground state cannot be longer factorized as in Eq. (B.24).

B.3 Ground state sector

In this section, we prove that if certain global symmetries are preserved that the interpolation $\Gamma^{(n)}_{0\delta}(\lambda,0) = \hat{H}^{(n)}_{0\delta}(\lambda)$[5], Eq. (6.45)—with $n_\delta \equiv n/\delta$ integer-valued—indeed reduce to the path $\hat{H}^{(n_\delta)}_{01}(\lambda)$. To this end, we first summarize for which cases we are able to prove the equivalence of paths:

> ***Main result.*** If the ground state is symmetric under the product of sublattice symmetry and $\hat{W}_\sigma$, $\hat{S}_{AB}\hat{W}_\sigma$, with $\sigma \in \{A,B\}$ and two-site translations, then the interpolation $\Gamma^{(n)}_{0\delta}(\lambda,0) = \hat{H}^{(n)}_{0\delta}(\lambda)$ reduce to the path $\hat{H}^{(n_\delta)}_{01}(\lambda)$ if δ is odd or if $n_\delta = 2$.

[5]Note since all paths are unitarily related, it is sufficient to discuss this for $d = 0$.

Symmetry transformation

Under the first symmetry, $\hat{S}_{AB}\hat{W}_\sigma$, any fixed-point model is mapped to itself. First, the operator $\hat{W}_\sigma$, defined in Eq. (6.53), maps the local operators $\hat{X}_{j,\sigma}$ and $\hat{Z}_{j,\sigma}$ to their complex conjugates and, thus, exchanges a pair of complex conjugate fixed-point Hamiltonians

$$\hat{W}_\sigma : \hat{H}_d^{(n)} \leftrightarrow \hat{H}_{-d}^{(n)}.$$

Second, sublattice symmetry, by definition exchanges, $A \leftrightarrow B$, which results in

$$\hat{S}_{AB} : \hat{H}_d^{(n)} \leftrightarrow \hat{H}_{-d}^{(n)}.$$

Hence, both symmetries together leave a fixed-point model unchanged. Clearly, by construction, any fixed-point model is invariant under two-site translations.

Validity of results

Although we cannot prove the above result (golden box) for all cases, we, nevertheless, believe that it is true for all (n, δ) with n_δ integer-valued. To substantiate this, recall that we have already considered two examples of such scenarios in the main text, which are given by $(n, \delta) \in \{(6, 2), (8, 2)\}$ (see Fig. 6.6). Here the path followed the effective description.

B.3.1 Proof of effective paths

For all interpolations, with $n_\delta \in \mathbb{N}$, the Hamiltonian conserves a local $\mathbb{Z}_\delta$ symmetry generated by $\hat{X}_{j,\sigma}^{n_\delta}$, see Eq. (6.42). By Elitzur's theorem [243] we guaranteed that local symmetries are not spontaneously broken and, thus, the ground state is always a common eigenstate of the Hamiltonian and these operators. Hence, for such basis, we can replace the operators by their corresponding quantum numbers. From the previous section, we know that if we can argue that all these local quantum numbers are equal to one, then we have shown that the interpolation $\hat{H}_{0\delta}^{(n)}(\lambda)$ reduce to $\hat{H}_{01}^{(n_\delta)}(\lambda)$ (see Eq. (B.23)).

Fixing the local subspace

As a first step, using the additional symmetry, we show that all local quantum numbers associated to $\hat{X}_{j,\sigma}^{n_\delta}$ must be real and equal for all sites. To this end, assuming a symmetric ground state, we obtain the following two conditions[6]:

$$(i) : \langle \hat{X}_{j,A}^{n_\delta} \rangle = \langle \hat{X}_{j,B}^{\dagger n_\delta} \rangle , \quad (ii) : \langle \hat{X}_{j,A}^{n_\delta} \rangle = \langle \hat{X}_{j,B}^{n_\delta} \rangle , \tag{B.25}$$

where in (i) we applied $\hat{S}_{AB}\hat{W}_B$, while in (ii) we acted with $\hat{S}_{AB}\hat{W}_A$. This implies that possible local eigenspaces are: $e(\hat{X}_{j,\sigma}^{n_\delta}) = 1$ or $e(\hat{X}_{j,\sigma}^{n_\delta}) = -1$ for all sites[7] within a unit cell. Together with two-site translation symmetry, this must hold for all sites in the lattice.

[6] Note that $\hat{S}_{AB}\hat{W}_\sigma$ acts on the right.

[7] Recall here $e(\hat{X}_{j,\sigma}^{n_\delta})$ denotes the eigenspace characterized by its eigenvalue.

Models with $\delta \in 2\mathbb{N}+1$

For these cases, the generator of the local $\mathbb{Z}_\delta$ symmetry has exactly one eigenspace, which is characterized by a real eigenvalue, namely, $e(\hat{X}_{j,\sigma}^{n_\delta}) = 1$. Thus, for odd δ we have shown that the interpolation of $\hat{H}_{0\delta}^{(n)}(\lambda)$ reduce to the path $\hat{H}_{01}^{(n_\delta)}(\lambda)$—if the symmetry generated by $\hat{S}_{AB}\hat{W}_\sigma$, with $\sigma \in \{A, B\}$, is not spontaneously broken. Note, since there is no other real eigenspace, we do not need two-site translations for these cases.

Models with $\delta \in 2\mathbb{N}$

On the other hand, if $\delta \in 2\mathbb{N}$, then there are two possible eigenspaces characterized by real quantum numbers $e(\hat{X}_{j,\sigma}^{n_\delta}) = \pm 1$. For these cases, we can prove, given that the ratio $n_\delta = 2$, that the ground state must be in the sector with all local quantum numbers equal to one.

If $n_\delta = 2$ and the Hamiltonian is projected into the eigenspace where all local eigenspaces are characterized by the negative quantum number, i.e., $e(\hat{X}_{j,\sigma}^{n_\delta}) = -1$, then the resulting Hamiltonian vanishes, which can be seen as follows: For $n_\delta = 2$, the operator $\hat{X}_{j,\sigma}$ in this subspace, Eq. (B.18), reduce to

$$\hat{X}_{j,\sigma} \xrightarrow{e(\hat{X}_{j,\sigma}^{n_\delta})=-1} -i\hat{\mathcal{Y}}_{j,\sigma_2}, \tag{B.26}$$

where $\hat{\mathcal{Y}}_{j,\sigma_2}$ is the Pauli operator along y. Hence, in this subspace complex conjugate terms add up to zero

$$\hat{X}_{j,\sigma} + \hat{X}_{j,\sigma}^\dagger = 0, \tag{B.27}$$

and similarly for terms of $\hat{H}_{n/2}^{(n)}$.

Variational principle. Second, using the variation principle, we can prove that the ground state energy of the Hamiltonian $\hat{H}_{0n/2}^{(n)}(\lambda)$ must be negative,

$$E_G \leq \langle \Psi_0^{(n)} | \hat{H}_{0n/2}^{(n)}(\lambda) | \Psi_0^{(n)} \rangle = -4(1-\lambda)L \tag{B.28}$$

where E_G denotes the ground state energy, $|\Psi_0^{(n)}\rangle$ the ground state of $\hat{H}_0^{(n)}$ and L is the number of unit cells. Moreover, we used that the expectation value,

$$\langle \Psi_0^{(n)} | \hat{H}_{n/2}^{(n)} | \Psi_0^{(n)} \rangle = 0,$$

vanishes. If $\lambda = 1$, then the expression on the right of Eq. (B.28) vanishes, but at this point, the Hamiltonian $\hat{H}_{0n/2}^{(n)}(\lambda = 1)$ reduce to $\hat{H}_{n/2}^{(n)}$, for which we know that the ground state energy is negative. In conclusion, if $n_\delta = 2$ and there is no SSB of $\hat{S}_{AB}\hat{W}_\sigma$ with $\sigma \in \{A, B\}$ and two-site translation symmetry, then the ground state is found in the sector with all local eigenvalues equal to one. For instance, for the Hamiltonian $\hat{H}_{02}^{(4)}$ discussed in Sec. 6.1 this is the case.

B.4 Gauge anomalies

In Secs. 6.1.4 and 6.2.4 we saw that if the duality mapping becomes an additional symmetry that it together with the global $\mathbb{Z}_n \times \mathbb{Z}_n$ symmetry forbids a gapped, symmetric ground state. In Sec. 6.2.6 we observed a similar scenario, where we considered the equal-weighted sum of all fixed-point Hamiltonians and found that—in addition to the global $\mathbb{Z}_n \times \mathbb{Z}_n$ symmetry—the SPT-Entangler generates an additional $\mathbb{Z}_n$ symmetry such that the representation of the symmetry group, $\mathbb{Z}_n \times \mathbb{Z}_n \times \mathbb{Z}_n$, forbids a gapped, symmetric ground state. To this end, we first give a brief definition of gauge anomalies and discuss the link to group cohomology and 2D interacting bosonic SPTs. Second, we introduce the ansatz of Ref. [85] that allows for an explicit calculation of elements of group cohomology, which we then use for cases mentioned above.

Definition of gauge anomalies

If a representation of a symmetry is anomalous, there cannot be a gapped, symmetric ground state [18, 86, 88, 91, 108][8]. We say such symmetry has a *gauge anomaly*—also known as 't Hooft anomaly [244], which is an obstruction to being able to gauge a global symmetry [86, 89, 244, 245]. For lattice systems, this means that we cannot promote a global symmetry to a local one by introducing additional degrees of freedom (cf. $\mathbb{Z}_2$ lattice gauge theory [246]). Moreover, if a representation of a symmetry is anomalous, it does not allow for an on-site representation [86]. Formally, a representation of a symmetry group G is on-site if the representation $U(g)$, $g \in G$ can be written as a product $U(g) = \prod_i U_i(g)$ of terms acting on disjoint regions [18, 86, 88].

Note, certain authors [91] consider it as a definition of an anomalous symmetry if a particular representation of a symmetry group forbids a gapped, symmetric ground state. We follow this convention, but as pointed out by the authors of this reference, a more fundamental understanding of anomalies can be obtained if its link to group cohomology is considered. This also allows for a connection of 1D gauge anomalies and 2D interacting bosonic SPTs [86].

B.4.1 Connection to group cohomology

Previously, we defined gauge anomalies as representations of symmetries that forbid gapped, symmetric ground states. For one-dimensional systems, with a global symmetry G and a representation $U(g)$, it was shown that there cannot be a gapped, symmetric ground state if a given representation belongs to a non-trivial 3-cocycle, which form the elements of the third cohomology group $H^3(G, U(1))$ [18, 108]. Indeed, gauge anomalies for one-dimensional systems have been classified by the third cohomology group $H^3(G, U(1))$ [86, 88, 91]. Such groups also label distinct classes of interacting bosonic SPTs in two dimensions [64]. This naturally leads to the question: *How are one-dimensional gauge anomalies and 2D SPTs are related?* The answer to this has

[8] Here we mainly focus on 1+1D systems. In higher dimensions there can be gapped, symmetric states which, however, are topologically ordered.

been, among others, given by Ref. [85], where the authors showed that 2D interacting bosonic SPTs protected by on-site symmetries are fully characterized by the anomalous action of its protecting symmetry on its one-dimensional boundary[9]. Moreover, the boundary theory of such two-dimensional SPT can be considered as a model—in one dimension lower—on its own right [82, 85]. Upon explicit symmetry-breaking, this gives rise to non-trivial SPTs in one dimension lower [82].

Gauge anomaly of $\mathbb{Z}_n \times \mathbb{Z}_n \times \mathbb{Z}_2^T$ symmetry

Why is the previous relationship important? When discussing gauge anomalies, Sec. 6.2.4, we argued that there exists an antiunitary representation of the duality mapping, which in combination with $\mathbb{Z}_n \times \mathbb{Z}_n$ symmetry can forbid a gapped, symmetric ground state. This happens if the relative charge along the transition cannot be written as a square of another $\mathbb{Z}_n$ charge, i.e., $\Delta q \neq q'^2$ with $q' \in \mathbb{Z}_n$. Indeed, in Ref. [82] it was shown, that given this condition, the one-dimensional system with $\mathbb{Z}_n \times \mathbb{Z}_n \times \mathbb{Z}_2^T$ symmetry can be considered as the low-energy boundary theory of a non-trivial two-dimensional SPT protected by this symmetry. Hence, the representation of this symmetry amounts to a non-trivial 3-cocycle of $H^3(\mathbb{Z}_n \times \mathbb{Z}_n \times \mathbb{Z}_2^T, U(1))$ and, thus, according to the definition, has a gauge anomaly.

B.4.2 The idea of dimensional reductions

To evaluate the 3-cocycles of $H^3(G, U(1))$, the authors of Ref. [85] made use of dimensional reduction. For example, the 2-cocycle of $H^2(G, U(1))$ classifying one-dimensional SPTs is obtained on how the symmetry acts on the zero-dimensional boundary. To obtain the 3-cocycle of a two-dimensional SPT, the symmetry action is first restricted to the one-dimensional boundary of the system. As a boundary itself has no boundary, the action of the symmetry on the one-dimensional subsystem is further restricted to a finite segment M. Finally, the 3-cocycle is obtained from how the symmetry acts on the zero-dimensional boundary of M (see Fig B.2).

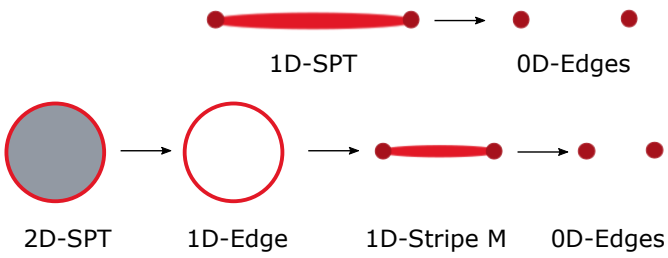

Figure B.2: **Dimensional reduction.** To obtain the 2-cocycles and 3-cocycles classifying one- and two-dimensional SPTs, respectively, the action of the global symmetry on a 0-dimensional boundary is considered.

[9] For detailed examples, see Refs. [18, 80] and also Sec. 2.2.2

B.4.3 The details of dimensional reductions

For what follows, we assume that the global symmetry, on the one-dimensional boundary, can be represented by a finite-depth quantum circuit[10]. Then, there is a clear notion of what is meant to restrict the symmetry action further to a finite strip M. A representation $U_M(g)$, with $g \in G$, is called a *restriction* of $U(g)$ on M if deep inside the strip it is indistinguishable from the global representation $U(g)$. However, this immediately implies that the restriction is not unique, and only well-defined up to local unitary transformations residing near the boundary ∂M. If $U(g)$, with $g \in G$, is a faithful representation of the symmetry group on the one-dimensional submanifold, then given the ambiguity of restrictions, the group multiplication law for $U_M(g)$ holds up to a local unitary $\Omega(g_1, g_2)$, which is localized near the boundary of ∂M, i.e.,

$$U_M(g_1)U_M(g_2) = \Omega(g_1, g_2)U_M(g_1 g_2), \tag{B.29}$$

which we will see soon for a concrete example. From the associative property of groups, it follows that:

$$\Omega(g_1, g_2)\Omega(g_{12}, g_3) = {}^{U_M(g_1)}\,\Omega(g_2, g_3)\Omega(g_1, g_{23}) \tag{B.30}$$

where we followed Ref. [85] in using the conjugation notation ${}^y x = yxy^{-1}$ and defined $g_{ij} \equiv g_i g_j$.

Fractionalization and 3-cocycles

Since the boundary of a one-dimensional strip consists of two points, (l, r), and $\Omega(g_1, g_2)$ is a local unitary acting near the boundaries, we can write:

$$\Omega(g_1, g_2) = \Omega_l(g_1, g_2)\Omega_r(g_1, g_2). \tag{B.31}$$

In Ref. [85] it was proven that for the restriction $\Omega(g_1, g_2) \to \Omega_r(g_1, g_2)$, Eq. (B.30) is fulfilled up to a $U(1)$ phase factor:

$$\begin{aligned}\Omega_r(g_1, g_2)\Omega_r(g_{12}, g_3) =& \omega(g_1, g_2, g_3)^{U_M(g_1)}\Omega_r(g_2, g_3)\\ & \Omega_r(g_1, g_{23})\end{aligned} \tag{B.32}$$

where $\omega(g_1, g_2, g_3) \in H^3(G, U(1))$ is a 3-cocycle. However, note that the 3-cocycle itself is only well-defined modulo a gauge transformation, which can be seen from Eq. (B.31). If we simultaneously replace

$$\Omega_l(g_1, g_2) \to \bar{\beta}(g_1, g_2)\Omega_l(g_1, g_2) \quad \wedge \quad \Omega_r(g_1, g_2) \to \beta(g_1, g_2)\Omega_r(g_1, g_2),$$

where $\beta(g_1, g_2) \in U(1)$, then we obtain after insertion into Eq. (B.30):

$$\omega'(g_1, g_2, g_3) = \omega(g_1, g_2, g_3)\frac{\beta(g_1, g_2)\beta(g_{12}, g_3)}{\beta(g_2, g_3)\beta(g_1, g_{23})}, \tag{B.33}$$

[10] This naturally occurs on the boundary of a 2+1D gapped, symmetric system with an on-site symmetry.

which shows that $\omega(g_1, g_2, g_3)$ is not uniquely defined and any other $\omega'(g_1, g_2, g_3)$, related through Eq. (B.33), needs to be considered as equivalent[11]. Given this degree of freedom, it is important to construct an invariant that is unchanged—upon rephasing the 3-cocycle—since finding the invariant to be non-trivial then implies a non-trivial anomaly! As we shall see, such an invariant can be built from a product of several 3-cocycles.

Inheritance of gauge anomalies

Before we explicitly calculate the gauge anomalies, let us emphasize an important point: To prove that a given representation of a symmetry group G has a gauge anomaly, it is sufficient to evaluate the gauge anomaly of a subgroup $\tilde{G} \subset G$. If a symmetry G is anomaly-free, then the same holds for all of its subgroups. Conversely, an anomalous subgroup implies that G itself is anomalous.

B.4.4 Gauge anomaly of $\mathbb{Z}_n \times \mathbb{Z}_n \rtimes (\mathbb{Z}_2 \times \mathbb{Z}_2)$ symmetry

For demonstrating the gauge anomaly of this symmetry, it is sufficient to consider a subgroup $\tilde{G} = \mathbb{Z}_2$ consisting of two elements $\mathbb{Z}_2 = \{\underline{1}, P\}$. Since the third cohomology group is given by $H^3(\mathbb{Z}_2, U(1)) = \mathbb{Z}_2$ [64], a non-trivial anomaly corresponds to the (unique) nonzero element of this. From the group properties, it follows that the product of two 3-cocycles is again a 3-cocycle. According to Eq. (B.33), the following product is gauge-invariant:

$$\omega'(P,P,P)\omega'(P,\underline{1},P) = \omega(P,P,P)\omega(P,\underline{1},P), \tag{B.34}$$

and since it is another 3-cocycle of $H^3(\mathbb{Z}_2, U(1)) = \mathbb{Z}_2$, it must square to one

$$\omega(P,P,P)^2\omega(P,\underline{1},P)^2 = 1. \tag{B.35}$$

Consequently, we obtain $\omega(P,P,P)\omega(P,\underline{1},P) = \pm 1$. Thus, if we find $+1$, the symmetry is non-anomalous, whereas -1 implies an anomaly.

Construction of an observable

If we denote the representation of the elements by $U(P)$ and $U(\underline{1})$, respectively, then as we will see for the relevant $\mathbb{Z}_2$ symmetry, Eq. (B.38), the following property holds:

$$U_M(P) = U_M(P)U_M(\underline{1}) \quad \wedge \quad U_M(P) = U_M(\underline{1})U_M(P), \tag{B.36}$$

which implies that $\Omega(g,\underline{1}) = \Omega(\underline{1},g) = \mathbb{1}$, defined in Eq. (B.29), for any $g \in \mathbb{Z}_2$. Thus, $\Omega_r(\underline{1},g)$ and $\Omega_r(g,\underline{1})$ can be at most a $U(1)$ phase factor. Inserting the 3-cocycles—defined through Eq. (B.32)—into the gauge-invariant expression, $\omega(P,P,P)\omega(P,\underline{1},P)$, shows that its sign can be obtained from:

$$\boxed{U(P)U^2_{M,r}(P)U^{-1}(P) = \pm U^2_{M,r}(P)}, \tag{B.37}$$

[11] Note this property, beside the cocycle condition, defines the third cohomology group $H^3(G, U(1))$.

where we used that a single end-point is sufficient and, thus, send the left end-point of M to $-\infty$, which makes $U^2_{M,r}(P)$ a semi-infinite string with end-point at site r. Moreover, without changing the final result, we replaced the restriction of $U_M(P)$ by its global representation. If the sign on the right is non-trivial, then the representation has a gauge anomaly.

Explicit calculation of the 3-cocycle

On the operator level the $\mathbb{Z}_2$ subgroup is given by,

$$\mathbb{Z}_2 = \left\{ \mathbb{1}, \mathcal{G}_A \mathcal{G}_B^{n/2} \hat{D}^{(n)}_{d\delta;A} \right\}, \quad U(\underline{1}) = \mathbb{1}, \quad U(P) = \mathcal{G}_A \mathcal{G}_B^{n/2} \hat{D}^{(n)}_{d\delta;A} \tag{B.38}$$

where $\mathcal{G}_\sigma$, with $\sigma \in \{A, B\}$, generates the $\mathbb{Z}_n \times \mathbb{Z}_n$ symmetry, and $\hat{D}^{(n)}_{d\delta;A}$ is the duality transformation defined in Eq. (6.52). As a first step, we need to evaluate the semi-infinite circuit $U^2_{M,r,B}(P)$ terminating at site (r, B). This results in[12],

$$\begin{aligned} U^2_{M,r,B}(P) \sim \Bigg[& \prod_{j \leq r} \hat{X}_{j,A} \prod_{j \leq r} \hat{X}^{n/2}_{j,B} \prod_{j \leq r} \hat{W}_{j,A} \\ & \prod_{j<r} \left(C \bar{Z}^{(n)} \right)^{2d+\delta}_{j,AB} \left(C Z^{(n)} \right)^{2d+\delta}_{(j,B),(j+1,A)} \\ & \cdot \left(C \bar{Z}^{(n)} \right)^{2d+\delta}_{r,AB} \Bigg]^2 \\ & \sim \hat{Z}^{\dagger(2d+\delta)}_{r,B}, \end{aligned} \tag{B.39}$$

which becomes a local operator. Here we used Eq. (6.34) and the fact that any operator $\hat{X}_{j,\sigma}$ is only affected by nearby gates (see also Fig. B.3)

$$\begin{aligned} C \bar{Z}^{(n)}_{j,AB} \hat{X}_{j,A} &= \hat{X}_{j,A} \hat{Z}^\dagger_{j,B} C \bar{Z}^{(n)}_{j,AB} \\ C Z^{(n)}_{(j-1,B),(j,A)} \hat{X}_{j,A} &= \hat{Z}_{j-1,B} \hat{X}_{j,A} C Z^{(n)}_{(j-1,B),(j,A)}, \end{aligned} \tag{B.40}$$

and similarly for $\hat{X}_{j,B}$. The half-infinite string of $\hat{W}_{M,r,A}$ has no relevant effect, it just sends $\hat{W}_{M,r,A} : \mathcal{G}_{M,r,A} \to \mathcal{G}^\dagger_{M,r,A}$.

From Fig. B.3 we see that in Eq. (B.39) the semi-infinite string of $\mathcal{G}^{n/2}_{M,r,B}$ commutes with the SPT-Entangler and the non-trivial end-point operator arises from the half-infinite string of $\mathcal{G}^\dagger_{M,r,A}$, where the complex conjugate appears due to the semi-infinite string of $\hat{W}_{M,r,A}$. Inserting Eq. (B.39) into Eq. (B.37) gives

$$U(P) \hat{Z}^{\dagger(2d+\delta)}_{r,B} U^{-1}(P) = \omega_2^{-\delta} \hat{Z}^{\dagger(2d+\delta)}_{r,B}, \tag{B.41}$$

where we used that $\omega_2^{2d+\delta} = \omega_2^\delta$. As stated in the main text, there is an intrinsic anomaly if n is even and δ is odd. Note, this results holds for all $n \in 2\mathbb{N}$. In particular, if $n = 2$,

[12] Since we consider only a single end-point, the final result is well-defined up to phase factor, which, however, is not relevant for evaluating the gauge anomaly.

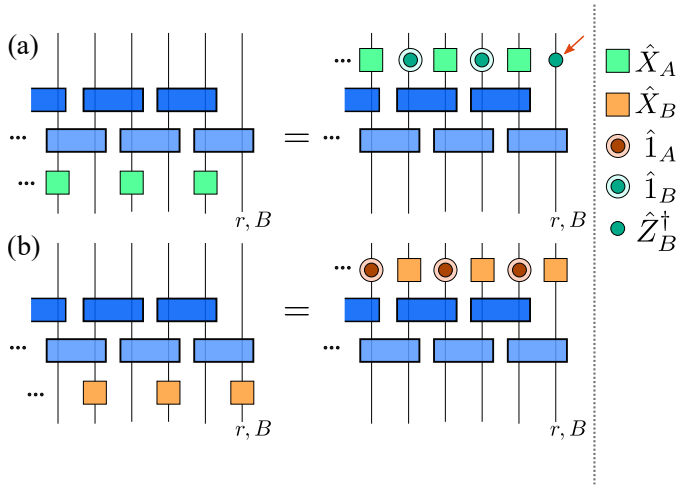

Figure B.3: **Commutation relations.** Graphical representation of the commutation relations of the semi-infinite strings $\mathcal{G}_{M,r,A}$, panel (a), and $\mathcal{G}_{M,r;B}$, panel (b), with the SPT-Entangler $\hat{U}^{(n)}_{M,r,B}$. The red arrow denotes the remaining operator once the half-infinite symmetry generator $\mathcal{G}_{M,r,A}$ is pulled through the half-infinite circuit.

then $\hat{W}_A = \mathbb{1}$ and $\mathcal{G}_A \mathcal{G}_B^{n/2} = \mathcal{G}_{AB}$ such that we obtain the $\mathbb{Z}_2$ gauge anomaly of $\hat{H}^{(2)}_{01}$, which was, among others, shown in the CZX model [18, 108] and reviewed in Sec. 2.2.2.

B.4.5 Gauge anomaly of $\mathbb{Z}_4 \times \mathbb{Z}_4 \times \mathbb{Z}_2$ symmetry

In Sec. 6.1.4 we showed that the combination of $\mathbb{Z}_4 \times \mathbb{Z}_4$ symmetry together with the $\mathbb{Z}_2$ symmetry generated by $\left(\hat{U}^{(4)}\right)^2 \equiv \hat{U}^2$ forbids a gapped, symmetric ground state. Unlike previously, any $\mathbb{Z}_2$ subgroup of $\mathbb{Z}_4 \times \mathbb{Z}_4 \times \mathbb{Z}_2$ is anomaly-free since their generators are explicitly on-site. Consequently, we cannot use the foregoing approach to evaluate the corresponding 3-cocycle.

Slant product

However, there is another way of detecting the gauge anomaly of this symmetry, using a slant product. Following Refs. [107, 198] a slant product maps a 3-cocycle of $H^3(G, U(1))$ to a 2-cocycle of $H^2(G, U(1))$. Such map is defined as follows:

$$\chi_g(h,k) = \frac{\omega(g,h,k)\omega(h,k,g)}{\omega(h,g,k)}, \quad g,h,k \in G, \tag{B.42}$$

where $\chi_g(h,k)$ is the corresponding 2-cocycle. As cocycles are not gauge-invariant, Eq. (B.42) changes by a 2-coboundary if we change ω by a 3-coboundary according to Eq. (B.33). However, from Sec. 2.2.1 we remember that for Abelian symmetry groups

the quotient of two 2-cocycles remains invariant under such transformations,

$$q_g(h,k) = \frac{\chi_g(h,k)}{\chi_g(k,h)}. \tag{B.43}$$

Thus, if $q_g(h,k)$ is non-trivial, then the associated representation of a symmetry group has a gauge anomaly.

Evaluation of $q_g(h,k)$

To evaluate the gauge invariant expression, we first have to find an expression for $\omega(g,h,k)$ considering the full symmetry group $\mathbb{Z}_4 \times \mathbb{Z}_4 \times \mathbb{Z}_2$. To simplify notation, we introduce a shorthand writing: $\boldsymbol{g} \equiv (g_1, g_2, g_3)$. Thus, representations of the symmetry group are defined as follows:

$$U(\boldsymbol{g}) = \mathcal{G}_A^{g_1} \mathcal{G}_B^{g_2} [\hat{U}^2]^{g_3}, \quad \boldsymbol{g} \in \mathbb{Z}_4 \times \mathbb{Z}_4 \times \mathbb{Z}_2. \tag{B.44}$$

Note for finding $\omega(\boldsymbol{g},\boldsymbol{h},\boldsymbol{k})$ it is sufficient to consider a single end-point. Therefore, similar to the previous case, we define semi-infinite strings,

$$U_{M,r}(\boldsymbol{g}) = \left(\prod_{j\leq r} \hat{X}_{j,A}\right)^{g_1} \left(\prod_{j\leq r} \hat{X}_{j,B}\right)^{g_2} \left(\prod_{j<r} C\bar{Z}_{j,AB} CZ_{(j,B),(j+1,A)} C\bar{Z}_{r,AB}\right)^{g_3}, \tag{B.45}$$

where gates are given by Eq. (6.33). Using Eq. (B.29), we obtain $\Omega_r(\boldsymbol{g},\boldsymbol{h})$ (up to a phase)

$$U_{M,r}(\boldsymbol{g}) U_{M,r}(\boldsymbol{h}) \sim \Omega_r(\boldsymbol{g},\boldsymbol{h}) U_{M,r}(\boldsymbol{g}+\boldsymbol{h}) \tag{B.46}$$

where addition of group elements is defined modulo four for (g_1, g_2) and modulo two for g_3. Inserting the representation, Eq. (B.45), into this formula, we find[13]:

$$\Omega_r(\boldsymbol{g},\boldsymbol{h}) \sim \hat{Z}_{r,B}^{2g_3h_1}. \tag{B.47}$$

To obtain an expression for $\omega(\boldsymbol{g},\boldsymbol{h},\boldsymbol{k})$, we need to plug in this result into Eq. (B.32) from which we get:

$$\omega(\boldsymbol{g},\boldsymbol{h},\boldsymbol{k}) = (-1)^{g_2h_3k_1} \tag{B.48}$$

and, thus, using Eq. (B.43) we finally arrive at,

$$q_{\boldsymbol{g}}(\boldsymbol{h},\boldsymbol{k}) = (-1)^{k_1(g_2h_3-h_2g_3)} (-1)^{h_1(k_2g_3-g_2k_3)} (-1)^{g_1(h_2k_3-k_2h_3)}. \tag{B.49}$$

For example, if we choose $\boldsymbol{g} = (1,0,0)$, $\boldsymbol{h} = (0,1,0)$ and $\boldsymbol{k} = (0,0,1)$, then $q_{\boldsymbol{g}}(\boldsymbol{h},\boldsymbol{k})$ is non-trivial,

$$q_{\boldsymbol{g}}(\boldsymbol{h},\boldsymbol{k}) = -1. \tag{B.50}$$

Consequently, the representation of $\mathbb{Z}_4 \times \mathbb{Z}_4 \times \mathbb{Z}_2$ has a gauge anomaly.

[13] Note, the calculation is rather similar to the foregoing case, see also Fig. B.3.

B.5 Robustness and field theory

Here we show from a field theory standpoint that the transition of $\hat{H}_{02}(\lambda = 1/2)$, discussed in Sec. 6.1.4, is robust to finite perturbations with $\hat{H}_1$. If the perturbation is zero, then the Hamiltonian $\hat{H}_{02}(\lambda)$ in the ground state subspace, upon a unitary transformation, reduce the spin-1/2 quantum XY chain. The corresponding transformation is given by,

$$\hat{U}_{XY} = \prod_j \hat{u}_{j,AB}\hat{u}_{(j,B),(j+1,A)} \prod_{j,\sigma} e^{-i\frac{\pi}{4}\hat{\mathcal{X}}_{j,\sigma}}, \tag{B.51}$$

where $\hat{\mathcal{X}}_{j,\sigma}$ is a Pauli operator and the two-site gates taken from Ref. [34] read:

$$\hat{u}_{j,AB} = \frac{1}{\sqrt{2}} \begin{pmatrix} 1 & 1 & 0 & 0 \\ 1 & -1 & 0 & 0 \\ 0 & 0 & 1 & 1 \\ 0 & 0 & -1 & 1 \end{pmatrix}_{j,AB}, \tag{B.52}$$

and the same for $\hat{u}_{(j,B),(j+1,A)}$. Using this transformation, we obtain:

$$\hat{U}_{XY}^{\dagger}\hat{H}_{01}^{(2)}(\lambda = 1/2)\hat{U}_{XY} = 2\hat{H}_{XY}, \tag{B.53}$$

where $\hat{H}_{01}^{(2)}$, defined in Eq. (6.16), denotes the effective Hamiltonian of $\hat{H}_{02}(\lambda = 1/2)$ in the ground state subspace.

Luttinger liquid

Mapping this model to free-fermions allows for a straight-forward continuum limit of the lattice model. The derivation of the low-energy field theory of the quantum XY chain is explicitly shown in Ref. [247], here, however, we use the conventions of Ref. [197],

$$H_{LL} = \frac{1}{2\pi}\int \mathrm{d}x \left[K\left(\partial_x\varphi(x)\right)^2 + \frac{1}{4K}\left(\partial_x\theta(x)\right)^2\right]. \tag{B.54}$$

The parameter K is the Luttinger liquid parameter characterizing a one-parameter family of compact bosons CFTs, where the compactification radius $r_c = \sqrt{K}$ [248]. The two conjugate, 2π-periodic fields are denoted by $\theta(x)$ and $\varphi(x)$. These fields fulfil the following commutation relation: $[\partial_x\theta(x), \varphi(x')] = 2\pi i\delta(x - x')$. The free-fermion point, Eq. (B.53), is characterized by a Luttinger parameter $K = 1/4$. From the *vertex operators* $\mathcal{V}_r(x) = e^{ir\varphi}$ and $\mathcal{V}_s(x) = e^{is\theta}$ we can construct local perturbations given that $r, s \in \mathbb{Z}$, which keeps the invariance of the theory under a 2π shift of the fields. For example, adding a perturbation such as $\mathcal{V}_1 + \mathcal{V}_{-1} = 2\cos(\varphi)$ to the Hamiltonian results in a model reminiscent of the sine-Gordon model [246, 249]. The vertex operators have the following scaling dimensions: $[\mathcal{V}_r(x)] = \frac{r^2}{4K}$ and $[\mathcal{V}_s(x)] = s^2K$. In 1D, the scaling dimensions of relevant operators must be less than 2 [246], which for $K = 1/4$ and

$r, s \in \mathbb{Z}$ implies: $r \in \{\pm 1\}$ and $s \in \{\pm 1, \pm 2\}$[14]. Hence, possible relevant perturbations can be constructed from:

$$\begin{aligned} \varphi\ , r &:= \{\cos\varphi,\ \sin\varphi\} \\ \theta,\ s &:= \{\cos\theta,\ \sin\theta,\ \cos 2\theta,\ \sin 2\theta\}\,. \end{aligned} \tag{B.55}$$

Symmetries and constraints

Finally, we argue that a particular combination of symmetries at low-energies forbids adding perturbations—listed in Eq. (B.55)—to the field theory. In the main text, we showed that if $\hat{H}_1$ is added, neither $\hat{U}^2$ nor sublattice transformation $\hat{S}_{AB}$ are symmetries of the resulting Hamiltonian. Only the combined action is preserved (see Eq. (6.20)). However, as we will show soon, the combined action is not sufficient. Fortunately, there is an additional on-site unitary that acts trivially on low-energy degrees of freedom, and, moreover, keeps sublattice symmetry and the duality symmetry separate. In the full Hilbert space each symmetry operation must be multiplied with $\hat{W}_\sigma$ defined by $\hat{W}_\sigma : \hat{X}_{j,\sigma} \leftrightarrow \hat{X}^\dagger_{j,\sigma}$ and $\hat{W}_\sigma : \hat{Z}_{j,\sigma} \leftrightarrow \hat{Z}^\dagger_{j,\sigma}$ (see also Eq. (B.20)). This ensures that $\hat{H}_1$, under the action of these symmetries, is mapped to itself, while $\hat{H}_{02}$ stays unchanged (see Sec. B.3). If one starts from the unperturbed case, then the trivial action of $\hat{W}_\sigma$ at low-energies can be inferred from the projector defined in Eq. (B.13). The symmetry groups generated by $\hat{U}^2\hat{W}_\sigma$ and $\hat{S}_{AB}\hat{W}_\sigma$ are given as follows:

$$\mathbb{Z}_2 = \{\mathbb{1}, \hat{U}^2\hat{W}_\sigma\}, \quad \mathbb{Z}_4 = \{\mathbb{1}, \hat{S}_{AB}\hat{W}_A, \hat{W}_A\hat{W}_B, \hat{S}_{AB}\hat{W}_B\}. \tag{B.56}$$

Again, from the unperturbed case, upon using Eq. (B.13), we find that both symmetry groups act as an effective $\mathbb{Z}_2$ symmetry at low-energy degrees of freedom. This enables us to find the constraints on the fields imposed by symmetry, which has, among others, partly answered[15] in Ref. [197],

$$\begin{aligned} \hat{\mathcal{G}}_A :&\ \varphi \to -\varphi, \quad \theta \to \pi - \theta \\ \hat{\mathcal{G}}_B :&\ \varphi \to -\varphi, \quad \theta \to -\theta \\ \hat{U}^2\hat{W}_\sigma :&\ \varphi \to \varphi + \pi, \theta \to \theta \\ \hat{S}_{AB}\hat{W}_\sigma :&\ \varphi \to -\varphi, \quad \theta \to \frac{\pi}{2} - \theta. \end{aligned} \tag{B.57}$$

It is easily verified that none of the perturbations, listed in Eq. (B.55), is invariant under the above constraints $\Rightarrow$ there exist no local perturbation that can be added to the Hamiltonian (B.54). There are two important comments: First, if we only conserved the product $\hat{U}^2\hat{S}_{AB}$, then a perturbation $\sim \sin(\varphi)$ would be allowed and since it is relevant, it would drive the theory to a new RG fixed-point. Second, the absence of any perturbation remains true as long as the $\mathbb{Z}_2 \times \mathbb{Z}_2$ subgroup is gapped, i.e, its associated string operators

[14] For $K = 1/4$ there is no marginal operator, i.e., operators that have scaling dimension equal to 2.

[15] In Ref. [197] the authors considered single-site translations instead of sublattice symmetry, but since both symmetries act in the same way on local operators, namely, exchanging sublattices—their action on the fields is the same.

have long-range order and the presence of $\hat{H}_1$ keeps the Luttinger parameter above $K > 1/8$. If it changes to $K = 1/8$, then there is a marginal, symmetry allowed term $\sim \cos 4\theta$ that can be added to the field theory. In summary, the previous results explain the robustness of the critical line observed in Fig. 6.3

Appendix C

Symmetry fractionalization and numerical details of the bond-alternating ionic Hubbard model

C.1 Symmetry fractionalization

For discussing symmetry fractionalization, we follow closely Ref. [95] and focus on 1D systems for concreteness.

If $|\psi\rangle$ is the ground state of a gapped, local Hamiltonian, it has a finite correlation length ξ [121]. For any block of N sites with size $\gg \xi$, we can consider the Schmidt decomposition,

$$|\psi\rangle = \sum_{\alpha} \Lambda_{\alpha} |\psi_{\alpha}^{\text{in}}\rangle \otimes |\psi_{\alpha}^{\text{out}}\rangle, \tag{C.1}$$

where $|\psi_{\alpha}^{\text{in}}\rangle$ are quantum states defined purely within the block of N sites. Due to there being a finite correlation length, all the Schmidt states $|\psi_{\alpha}^{\text{in}}\rangle$ are indistinguishable deep within the block (i.e., they simply look like $|\psi\rangle$). To see this, let us consider a correlation function of two operators $\mathcal{O}_{\text{out}}$ and $\mathcal{O}_{\text{in}}$ that have support only in the outer and inner region, respectively. Such correlation function can be written as follows:

$$\mathcal{C}(l) = \langle \mathcal{O}_{\text{out}} \mathcal{O}_{\text{in}} \rangle_{\psi} \,. \tag{C.2}$$

Now suppose that $\mathcal{O}_{\text{in}}$ has only support far way from the edges of the subsystem and that the distance l is much larger than the bulk correlation length $l \gg \xi$, then correlations factorize (plus exponential corrections)

$$\mathcal{C}(l) \xrightarrow{l \gg \xi} \langle \mathcal{O}_{\text{out}} \rangle_{\psi} \langle \mathcal{O}_{\text{in}} \rangle_{\psi} \,. \tag{C.3}$$

If we initially chose the operator $\mathcal{O}_{\text{out}}$ to be a projector on a particular Schmidt state say, $|\psi_{\beta}^{\text{out}}\rangle$, then using the previous result, we see that dominant Schmidt states[1] must be indistinguishable from the ground state deep inside the block.

[1] For area law states, such as ground states of one-dimensional gapped, local Hamiltonians only a few Schmidt values contribute and others decay exponentially [97, 98].

Fractionalization

Moreover, due to locality, the two edges of the block are effectively independent (up to exponentially small errors). We can thus presume that α can be interpreted as a super-index, which is equivalent to two smaller indices α_L, α_R such that $|\psi^{\text{in}}_{\alpha}\rangle = |\psi^{\text{in}}_{\alpha_L,\alpha_R}\rangle$ where the value of α_L (α_R) only affects correlation functions on the left (right) end of the block.

Let $\hat{U} = \prod_n \hat{U}_n$ be a unitary on-site symmetry. If we act with $\hat{U}$ only within this block, it leaves states $|\psi^{\text{out}}_{\alpha}\rangle$ unaffected. Since the states in a Schmidt decomposition form a complete basis, we can write

$$\hat{U}|\psi^{\text{in}}_{\alpha}\rangle = \sum_{\beta} U_{\beta;\alpha}|\psi^{\text{in}}_{\beta}\rangle = \sum_{\beta_L,\beta_R} U_{\beta_L,\beta_R;\alpha_L,\alpha_R}|\psi^{\text{in}}_{\beta_L,\beta_R}\rangle. \tag{C.4}$$

Moreover, as $\hat{U}$ is an on-site operator, it will preserve locality, i.e., α_L and β_R in $U_{\beta_L,\beta_R;\alpha_L,\alpha_R}$ will be uncorrelated. More precisely, we can write (using a shorthand notation)

$$U_{\beta_L,\beta_R;\alpha_L,\alpha_R} = U^L_{\beta_L;\alpha_L} U^R_{\beta_R;\alpha_R} \;\Rightarrow\; \prod_{n=1}^{L} \hat{U}_n|\psi\rangle = \hat{U}^L\hat{U}^R|\psi\rangle, \tag{C.5}$$

where $\hat{U}^{L,R}$ are exponentially localized near the edges of the block of N sites. The explicit formula in terms of Schmidt states implies that if $\prod_{i=1}^{L} \hat{U}_i|\psi\rangle = \hat{U}^L\hat{U}^R|\psi\rangle$ and $\prod_{i=1}^{L} \hat{V}_i|\psi\rangle = \hat{V}^L\hat{V}^R|\psi\rangle$ (for a second symmetry $\hat{V}$), then we also have that

$$\prod_{i=1}^{L} \hat{V}_i \prod_{i=1}^{L} \hat{U}_i|\psi\rangle = \hat{V}^L\hat{V}^R\hat{U}^L\hat{U}^R|\psi\rangle. \tag{C.6}$$

Group relations

The fractionalized symmetries obey the same group relations as the original symmetries up to potential phase factors (≡ projective representations). For instance, let us suppose $\hat{U}$ and $\hat{V}$ commute. Let us also assume that $\hat{U}^{L,R}$ are bosonic operators (such that $\hat{U}^L$ commutes with $\hat{V}^R$). Then

$$1 = \hat{U}\hat{V}\hat{U}^{-1}\hat{V}^{-1} = \hat{U}^L\hat{V}^L(\hat{U}^L)^{-1}(\hat{V}^L)^{-1} \times \hat{U}^R\hat{V}^R(\hat{U}^R)^{-1}(\hat{V}^R)^{-1}. \tag{C.7}$$

Since the two factors on the right-hand side act on disjoint regions, yet they multiply to identity, each of the two factors has to be proportional to a phase:

$$\hat{U}^L\hat{V}^L(\hat{U}^L)^{-1}(\hat{V}^L)^{-1} = e^{i\alpha}. \tag{C.8}$$

Moreover, using similar manipulations, one can show that if $\hat{U}^2 = 1$, then $e^{i\alpha} = \pm 1$. More generally, the fractionalized symmetries will form a projective representation of the original symmetry group, which are classified by the second cohomology group $H^2(G, U(1))$ [64]. Non-trivial projective representations correspond to non-trivial SPT phases and imply edge modes in the energy spectrum with open boundary conditions, or degeneracies in the entanglement spectrum for virtual bipartitions (since any projective representation acting on a 1D vector space is trivial), see also Sec. 2.2.1.

C.2 Details about numerical calculations and edge gap

To obtain the numerical results, we used DMRG based on the TeNPy library version (0.3.0) [122]. For all calculations, we conserved the total particle number and the total magnetization.

C.2.1 Phase diagram of the bond-alternating ionic Hubbard chain

To obtain the critical line for $\delta = 0$, shown in Fig. 7.1, we used a combination of finite and infinite DMRG with open boundary conditions. To obtain U_{c_1}, we used the infinite DMRG approach and calculated the correlation length $\xi_\chi(U)$ for various values of U and bond dimensions χ. Near the quantum critical point (QCP) we chose $\mathrm{d}U = 0.001$ and the maximal bond dimension was set to $\chi_{max} = 1000$. The number of sweeps was unbounded and the calculations stopped, when the relative error in the energy per unit cell $\Delta E < 10^{-9}$ and the relative error in the half-infinite chain entanglement entropy $\Delta S < 10^{-5}$. In this way, the largest energy truncation error was below 10^{-6}. The critical point $U_{c_1} \approx 1.96$ was found by the maximum value of the correlation length $\xi_\chi(U)$, as shown in Fig. C.1a. Since this is a continuous phase transition, the half-infinite chain entanglement entropy diverges at the QCP as well; from Fig. C.1b we see that the maximum, for the given bond dimension, is at U_{c_1}. For completeness, we also show the dimerization order parameter. In the spontaneously dimerized insulator (SDI) phase, the ground state spontaneously breaks the duality symmetry $\hat{\mathcal{D}}$. As a result, the dimerization order parameter (and also its density) $D = \langle \hat{D} \rangle / L$

$$\hat{D} = \sum_{n,\sigma} (-1)^n \left(\hat{c}^\dagger_{n,\sigma} \hat{c}_{n,\sigma} + \mathrm{h.c} \right) \tag{C.9}$$

gain a non-zero value (see Fig. C.1c).

BKT-transition

Since the second phase transition along this line is a BKT-transition [207], the previous approach to estimate the location of U_{c_2} failed. The reason is that the correlation length for such a transition diverges exponentially as we approach this QCP [250, 251]. To tackle this problem, we used finite DMRG calculations to detect this BKT-transition. In Ref. [252] it was demonstrated that such a QCP can be very precisely located by looking at bipartite fluctuations. The bipartite fluctuations of a subsystem A are defined by,

$$\mathcal{F}_A = \left\langle \left(\sum_{j \in A} \hat{O}_j \right)^2 \right\rangle - \left\langle \sum_{j \in A} \hat{O}_j^2 \right\rangle, \tag{C.10}$$

where for our particular case we chose $\hat{O}_j = \hat{S}^z_j$ because here the BKT-transition into the gapless phase is associated to spin degrees of freedom, i.e., the spin gap closes [207]. For our calculation, we fixed the subsystem A to be the half of the finite chain with total

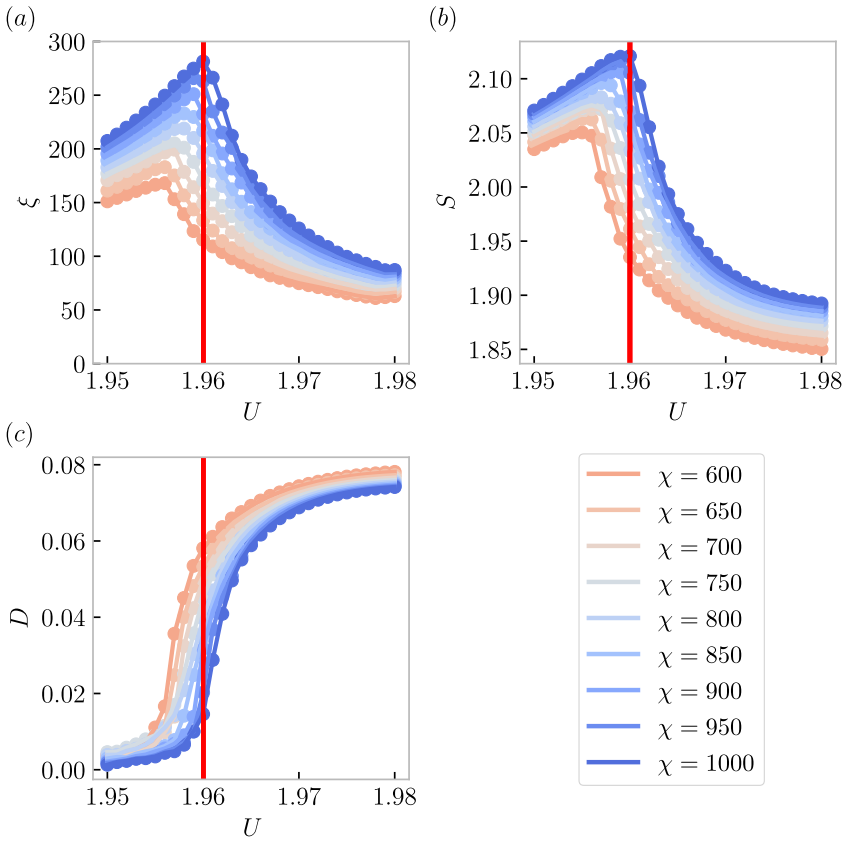

Figure C.1: **Second-order phase transition.** Panel (a) shows the correlation length $\xi_\chi(U)$, panel (b) the half-infinite chain entanglement entropy $S_\chi(U)$ and figure (c) the density of the dimerization order parameter $D_\chi(U)$ for various values of U and χ. The QCP $U_{c_1} = 1.96$ is determined by the maximum value of $\xi_\chi(U)$.

length $L \in \{100, 160, 200, 250\}$. For a gapless system, it is known that the bipartite fluctuations scale logarithmically with system size,

$$\mathcal{F}(L) = \frac{K}{\pi^2} \log L + \text{const.}, \tag{C.11}$$

where the constant pre-factor is given by the Luttinger parameter K. The BKT-transition into the gapless phase is characterized by a Luttinger parameter $K = 1/2$ (its value being pinned by spin-rotation symmetry), which then characterizes the Tomonaga-Luttinger liquid for low-energy degrees of freedom. Numerically, the transition can be detected if $K = 1/2$ because above $U > U_{c_2}$ marginally irrelevant operators lead to logarithmic corrections if K is calculated for finite size systems. The results for different values of U are shown in Fig. C.2 from which we extracted $U_{c_2} \approx 2.09$. To obtain the ground

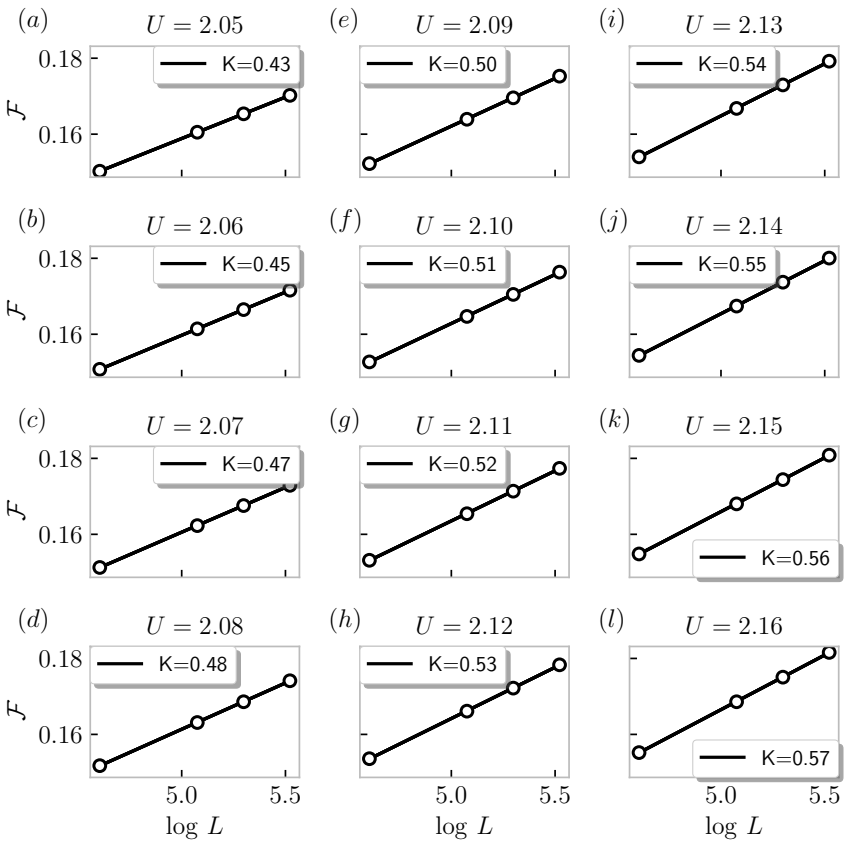

Figure C.2: **BKT-transition.** Panel $(a) - (l)$ show the bipartite fluctuations $\mathcal{F}_{A=L/2}$ for $L \in \{100, 160, 200, 250\}$.

states for different system sizes, the bond dimension was set to $\chi \in \{800, 800, 1000, 1200\}$ resulting in an energy truncation error below 10^{-7} for all system sizes.

C.2.2 Edge and entanglement gap closing

Here we first consider the exactly solvable case $\delta = 1$, where we can explicitly calculate the edge gap closing. Moreover, we numerically demonstrate that the phase boundary, where edge modes disappear, can be extracted from two different approaches: First, using ground states of different spin sectors but same parity sector and, second, using ground states of different parity sectors. Finally, we consider the level crossing in the entanglement spectrum and show that, upon lowering U, the degeneracy of the lowest eigenvalue changes.

Edge gap

To understand why there is an edge gap closing as we tune U, it is very instructive to discuss the limit $\delta = 1$, where the boundary consists of two single sites. The Hamiltonian for these two sites is given by,

$$\hat{H} = -\frac{\Delta}{2}\hat{N}_1 + \frac{\Delta}{2}\hat{N}_2 + U\left(\hat{n}_{1,\uparrow} - \frac{1}{2}\right)\left(\hat{n}_{1,\downarrow} - \frac{1}{2}\right) + U\left(\hat{n}_{2,\uparrow} - \frac{1}{2}\right)\left(\hat{n}_{2,\downarrow} - \frac{1}{2}\right), \quad \text{(C.12)}$$

where $\hat{N}_i = \sum_\sigma \hat{n}_{i,\sigma}$. The relevant eigenstates are summarized in Tab. C.1. For

State	Energy E_0	Parity	S^z_{tot}
$\|\uparrow\ 0\rangle$	$-\frac{\Delta}{2}$	-1	1/2
$\|\downarrow\ 0\rangle$	$-\frac{\Delta}{2}$	-1	-1/2
$\|\uparrow\downarrow\ \downarrow\rangle$	$-\frac{\Delta}{2}$	-1	-1/2
$\|\uparrow\downarrow\ \uparrow\rangle$	$-\frac{\Delta}{2}$	-1	1/2
$\|0\ \uparrow\downarrow\rangle$	$\frac{U}{2} - \Delta$	1	0
$\|\downarrow\ \downarrow\rangle$	$-\frac{U}{2}$	1	-1
$\|\uparrow\ \uparrow\rangle$	$-\frac{U}{2}$	1	1
$\|\downarrow\ \uparrow\rangle$	$-\frac{U}{2}$	1	0
$\|\uparrow\ \downarrow\rangle$	$-\frac{U}{2}$	1	0

Table C.1: **Eigenstates, energy levels and quantum numbers.** Eigenstates of Hamiltonian (C.12) with energy levels, parity eigenvalues and total spin S^z_{tot}. For $U = \Delta$, all states are degenerate.

$U/\Delta \gg 1$, each edge carries a half-integer spin and the overall ground state is fourfold degenerate and in the opposite limit, $U/\Delta \ll 1$, there is a unique ground state with an empty edge on the right and a doubly filled edge on the left. Except for a single point, the ground state is always in the even parity sector, but if $U/\Delta \gg 1$ there can be states in different $S^z_{tot} \in \{-1, 0, 1\}$ sectors. Since spin degrees of freedom are inherently related to fermions, this means that once the spin on the edge changes from integer to half-integer,

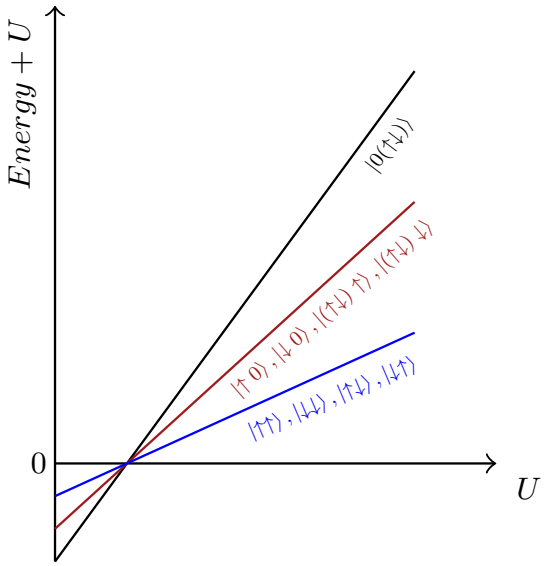

Figure C.3: **Energies.** Energies of the Hamiltonian (C.12) with $\Delta = 0.4$ and $U \in [0, 2]$. The level crossing happens at $U = \Delta$. In this plot, as well as in Fig. 7.2, we plotted the following: $E_0 + U + |E_0(U = U_{c,edge})| - U_{c,edge}$, where E_0 is the ground state energy in the corresponding sector.

the gap between different parity sectors has to close as well. From Tab. C.1, we observe that for $U = \Delta$ states of different parity and spin sectors become degenerate. Note, while states of different spin sectors cross each other at $U = \Delta$, states of different parity sectors only touch each other (see Fig. C.3). As we tune away from this exactly soluble limit, bulk and edge do not decouple anymore, and edge modes penetrate exponentially into the bulk. Nevertheless, the universal features are still present, which we have demonstrated in Fig. 7.2, which looks similar to Fig. C.3.

Numerics. To numerically detect the vanishing of the edge gap for $\delta < 1$, we first estimated from the previous calculation, where we expect the edge gap to vanish. Afterwards, we calculated the ground states in two different $S^z_{tot} = \{0, 1\}$ sectors (blue and black states of Tab. C.1) for ten values of U below our estimation. For each value of U, we calculated the edge gap as a function of system size,

$$\begin{aligned} |\Delta_{edge}(L, U)| =& |E_0\left(N = L, S^z_{tot} = 0, L, U\right) - E_0\left(N = L, S^z_{tot} = 1, L, U\right)| \\ &\sim \Delta_{0,edge}(U, L \to \infty) + e^{-\xi_{loc}(U)/L}, \end{aligned} \tag{C.13}$$

from which we could deduce $\Delta_{0,edge}(U, L \to \infty)$. Lastly, we plotted these constant terms as function of U and extrapolated to $\Delta_{0,edge}(U_{c,edge}, L \to \infty) = 0$ from which we obtained $U_{c,edge}$. For $\delta \geq 0.1$, we chose system sizes up to $L = 76$ sites with a maximal bond dimension $\chi = 400$ to perform our finite DMRG calculations. This results in an energy truncation error below 10^{-9}. For $\delta \leq 0.1$, we had to increase the system size up to $L = 380$ sites with a maximal bond dimension $\chi = 600$, which results in an energy

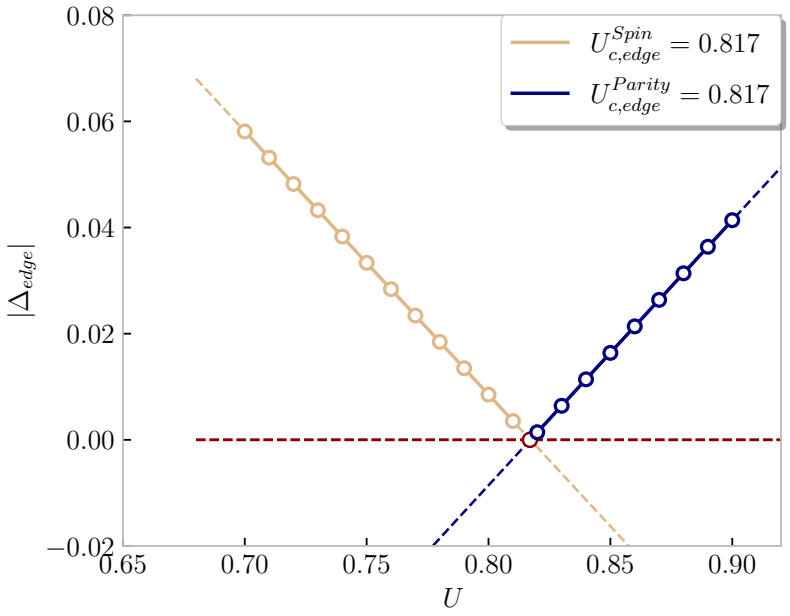

Figure C.4: **Edge gap.** The beige line is obtained for $U \in \{0.70, ..., 0.80\}$ and the blue line for $U \in \{0.82, ..., 0.90\}$. From the extrapolation of both lines, we find that $U_{c,edge}^{Spin} = U_{c,edge}^{Parity} = 0.817$.

truncation error below 10^{-7}. However, we have to admit that the data close to the QCP are much less accurate.

To illustrate that the gap between different parity and spin sectors—aside from the exactly soluble limit—close for open boundaries exactly at the same point, we calculated both gaps for $\delta = 0.2$. From Fig. C.4, we clearly see that both approaches give indeed the same result. To obtain the gap associated to different parity sectors, we calculated the difference $|E_0(N = L, S_{tot}^z = 0) - E_0(N = L + 1, S_{tot}^z = 1/2)|$.

Entanglement gap

To obtain the blue line in Fig. 7.1, we chose a similar approach, except this time we used iDMRG. The level crossing is obtained from the three lowest eigenvalues (two of them are degenerate) of the reduced density matrix of a half-infinite chain. The entanglement eigenvalues are calculated for the same values of $\delta \in \{0.01, 0.05, 0.1, 0.2, ..., 1\}$. For the simulation, we used a maximal bond dimension $\chi = 300$ for $\delta \geq 0.1$ and a maximal bond dimension $\chi = 700$ for $\delta \leq 0.1$. The calculation stopped if the relative change in energy per unit cell and entanglement entropy were below $\Delta E < 10^{-10}$ and $\Delta S < 10^{-6}$, respectively. This way, the energy truncation error is below 10^{-8}.

C.2.3 QSPT edge phenomena

Parity quantum numbers for a system with OBC

To obtain Fig. 7.2a, we evaluated the ground states for $\delta = 0.2$ in various spin and parity sectors. This is similar to what we did for the exactly soluble case shown in Fig C.3. For the calculation, we chose a system with $L = 68$ and a bond dimension $\chi = 400$, which results in an energy truncation error below 10^{-9}. The ground states have been calculated for various values of $U \in \{0.75, 0.76, ..., 0.90\}$. From Fig. C.4 we know that the gap between different parity and spin sectors has to close at $U_{c,edge} = 0.817$ for open boundaries.

Parity quantum number of the entanglement spectrum

Since spin rotations commute with the reduced density matrix of a half-infinite chain, the different blocks of the entanglement spectrum can be labelled by the parity quantum number, which is defined by $\hat{P} = \hat{R}_x \hat{R}_y \hat{R}_x^\dagger \hat{R}_y^\dagger$. The spin rotations acting on the dominant eigenstates of the reduced density matrix have a different representation, which we thus called $\mathcal{U}_\gamma$ with $\gamma \in \{y, z\}$. Hence, the action of fermion parity on these states is given by $\mathcal{P} = \mathcal{U}_x \mathcal{U}_y \mathcal{U}_x^\dagger \mathcal{U}_y^\dagger$. The reason we chose this particular definition of fermion parity is that our algorithm can find these unitary operators $\mathcal{U}_\gamma$ only up a to $U(1)$ phase factor. Given our definition, this phase factor drops out, and we can directly match the eigenvalues with the corresponding parity eigenvalue [93, 94]. To obtain the entanglement spectrum and the corresponding parity eigenvalues, we used iDMRG and calculated the ground state for $U \in \{0.94, 0.95, ..., 1.12\}$ with $U_{c,ent} = 1.054$ for a bond dimension $\chi = 200$. The calculation stopped if the relative change of energy per unit cell was below $\Delta E < 10^{-10}$ and the relative change in the half-infinite chain entanglement entropy below $\Delta S < 10^{-6}$, which gives an overall energy truncation error below 10^{-9}.

C.2.4 QSPT transition and emergent anomaly along the self-dual line $\delta = 0$ (with ionicity $\Delta = 0.4$)

To measure the string operator defined in Eq. (7.11), we evaluated the ground state for several values of U shown in Fig. C.5. The ground state itself was calculated using iDMRG with a maximal bond dimension of $\chi = 1000$. The calculation stopped if the relative change of energy per unit cell was below $\Delta E < 10^{-10}$ and the relative change in the half-infinite chain entanglement entropy below $\Delta S < 10^{-6}$, which gives an energy truncation error below 10^{-6} for all values of U. Clearly, for states in the gapped phases, the energy truncation error is even smaller. To maximize visibility of both operators, we rescaled the operator $\mathcal{O}^-$ by a factor of 5. The maximal values of the operators in the limiting cases are given by,

$$\lim_{U\to\infty} \mathcal{O}^- = 4, \quad \lim_{U\to 0} \mathcal{O}^+ \approx 0.4. \tag{C.14}$$

The former limit is easily obtained because there fermion parity becomes simply the identity operator $\hat{P}_n \xrightarrow{U\to\infty} \hat{\mathbb{1}}_n$, while for the latter limit we used iDMRG to obtain the

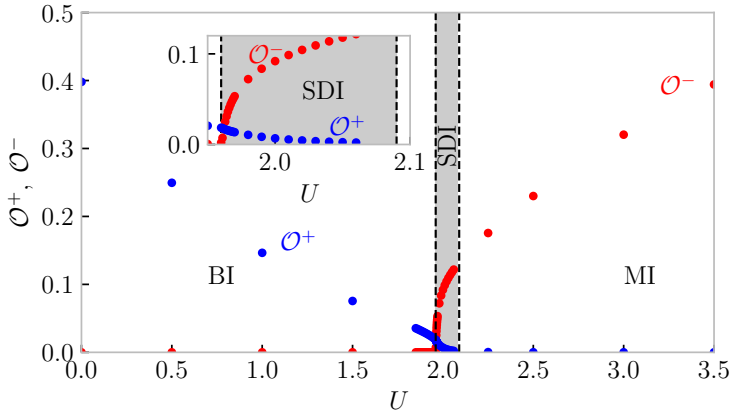

Figure C.5: **Data points for the string order operator.** The data points for which we calculated the string order operators $\mathcal{O}^{\pm}$ defined in the main text.

result (although it could only be obtained using free-fermion calculations).

Bibliography

[1] A. P. W., Science **177**, 393 (1972).

[2] S. Sachdev, *Quantum Phase Transitions*, 2nd ed. (Cambridge University Press, 2011).

[3] L. D. Landau, Phys. Z. Sowjet. **11**, 26 (1937).

[4] X.-G. Wen, Rev. Mod. Phys. **89**, 041004 (2017), arXiv:1610.03911 .

[5] K. v. Klitzing, G. Dorda, and M. Pepper, Phys. Rev. Lett. **45**, 494 (1980).

[6] D. C. Tsui, H. L. Stormer, and A. C. Gossard, Phys. Rev. Lett. **48**, 1559 (1982).

[7] R. B. Laughlin, Phys. Rev. Lett. **50**, 1395 (1983).

[8] F. Wilczek, Physics World **4**, 40 (1991).

[9] C. L. Kane and E. J. Mele, Phys. Rev. Lett. **95**, 226801 (2005).

[10] C. L. Kane and E. J. Mele, Phys. Rev. Lett. **95**, 146802 (2005).

[11] B. A. Bernevig and S.-C. Zhang, Phys. Rev. Lett. **96**, 106802 (2006).

[12] K. Markus, W. Steffen, B. Christoph, R. Andreas, B. Hartmut, M. L. W., Q. Xiao-Liang, and Z. Shou-Cheng, Science **318**, 766 (2007).

[13] F. D. M. Haldane, Phys. Lett. A **93**, 464 (1983).

[14] F. D. M. Haldane, Phys. Rev. Lett. **50**, 1153 (1983).

[15] I. Affleck, T. Kennedy, E. H. Lieb, and H. Tasaki, Comm. Math. Phys. **115**, 477 (1988).

[16] Z.-C. Gu and X.-G. Wen, Phys. Rev. B Condens. Matter **80**, 155131 (2009).

[17] F. Pollmann, E. Berg, A. M. Turner, and M. Oshikawa, Phys. Rev. B **85**, 075125 (2012).

[18] X. Chen, Z.-X. Liu, and X.-G. Wen, Physical Review B **84**, 235141 (2011).

[19] H. Song, S.-J. Huang, L. Fu, and M. Hermele, Phys. Rev. X **7**, 011020 (2017).

[20] Y. You, T. Devakul, F. J. Burnell, and T. Neupert, Phys. Rev. B **98**, 235102 (2018).

[21] W. A. Benalcazar, B. A. Bernevig, and T. L. Hughes, Phys. Rev. B **96**, 245115 (2017).

[22] W. A. Benalcazar, B. A. Bernevig, and T. L. Hughes, Science **357**, 61 (2017).

[23] F. Schindler, A. M. Cook, M. G. Vergniory, Z. Wang, S. S. P. Parkin, B. A. Bernevig, and T. Neupert, Science Advances **4**, eaat0346 (2018).

[24] F. Schindler, M. Brzezińska, W. A. Benalcazar, M. Iraola, A. Bouhon, S. S. Tsirkin, M. G. Vergniory, and T. Neupert, Phys. Rev. Research **1**, 033074 (2019).

[25] O. Dubinkin and T. L. Hughes, Phys. Rev. B **99**, 235132 (2019).

[26] A. Rasmussen and Y.-M. Lu, Phys. Rev. B **101**, 085137 (2020).

[27] W. A. Benalcazar, T. Li, and T. L. Hughes, Phys. Rev. B **99**, 245151 (2019).

[28] W. P. Su, J. R. Schrieffer, and A. J. Heeger, Phys. Rev. Lett. **42**, 1698 (1979).

[29] M. Lohse, C. Schweizer, O. Zilberberg, M. Aidelsburger, and I. Bloch, Nature Physics **12**, 350 (2016).

[30] I. Bloch, J. Dalibard, and W. Zwerger, Rev. Mod. Phys. **80**, 885 (2008).

[31] J. F. Sherson, C. Weitenberg, M. Endres, M. Cheneau, I. Bloch, and S. Kuhr, Nature **467**, 68 (2010).

[32] W. S. Bakr, J. I. Gillen, A. Peng, S. Fölling, and M. Greiner, Nature **462**, 74 (2009).

[33] F. Grusdt, M. Höning, and M. Fleischhauer, Phys. Rev. Lett. **110**, 260405 (2013).

[34] L. Tsui, Y. T. Huang, H. C. Jiang, and D. H. Lee, Nuclear Physics B **919**, 470 (2017).

[35] F. H. L. Essler, H. Frahm, F. Göhmann, A. Klümper, and V. E. Korepin, *The One-Dimensional Hubbard Model* (Cambridge University Press, 2005).

[36] F. Anfuso and A. Rosch, Phys. Rev. B **75**, 144420 (2007).

[37] S. Moudgalya and F. Pollmann, Phys. Rev. B **91**, 155128 (2015).

[38] R. Verresen, R. Moessner, and F. Pollmann, Phys. Rev. B **96**, 165124 (2017).

[39] J. Wang, X.-G. Wen, and E. Witten, Phys. Rev. X **8**, 031048 (2018).

[40] S. R. White, Phys. Rev. Lett. **69**, 2863 (1992).

[41] S. R. White, Phys. Rev. B **48**, 10345 (1993).

[42] Y. Simeng, H. D. A., and W. S. R., Science **332**, 1173 (2011).

[43] X. G. Wen and A. Zee, Phys. Rev. Lett. **69**, 953 (1992).

[44] B. Han, H. Wang, and P. Ye, Physical Review B **99**, 205120 (2019).

[45] R. Resta, Physical Review Letters **80**, 1800 (1998).

[46] F. Schwabl and W. Brewer, *Statistical Mechanics*, Advanced Texts in Physics (Springer Berlin Heidelberg, 2006).

[47] P. Chaikin and T. Lubensky, *Principles of Condensed Matter Physics* (Cambridge University Press, 2000).

[48] S.-J. GU, International Journal of Modern Physics B **24**, 4371 (2010).

[49] X. Chen, Z.-C. Gu, and X.-G. Wen, Phys. Rev. B **82**, 155138 (2010).

[50] N. Schuch, D. Pérez-García, and I. Cirac, Phys. Rev. B **84**, 165139 (2011).

[51] R. B. Laughlin, Phys. Rev. B **23**, 5632 (1981).

[52] B. Zeng, X. Chen, D.-L. Zhou, and X.-G. Wen, Local transformations and long-range entanglement, in *Quantum Information Meets Quantum Matter: From Quantum Entanglement to Topological Phases of Many-Body Systems*, Quantum Science and Technology (Springer New York, New York, NY, 2019) pp. 191–229.

[53] A. J. Beekman, L. Rademaker, and J. van Wezel, SciPost Phys. Lect. Notes , 11 (2019).

[54] G. B. Mbeng, A. Russomanno, and G. E. Santoro, The quantum ising chain for beginners (2020).

[55] D. C. Tsui, H. L. Stormer, and A. C. Gossard, Phys. Rev. Lett. **48**, 1559 (1982).

[56] H. L. Stormer, Rev. Mod. Phys. **71**, 875 (1999).

[57] A. Kitaev, Annals of Physics **303**, 2 (2003).

[58] Z.-C. Gu, Z. Wang, and X.-G. Wen, Phys. Rev. B **91**, 125149 (2015).

[59] J. Sakurai and J. Napolitano, *Modern Quantum Mechanics* (Cambridge University Press, 2017).

[60] M. Suzuki, Physics Letters A **146**, 319 (1990).

[61] R. Raussendorf and H. J. Briegel, Phys. Rev. Lett. **86**, 5188 (2001).

[62] S. Bravyi, M. B. Hastings, and F. Verstraete, Phys. Rev. Lett. **97**, 050401 (2006).

[63] L. D. Landau and V. L. Ginzburg, Zh. Eksp. Teor. Fiz. **20**, 1064 (1950).

[64] X. Chen, Z.-C. Gu, Z.-X. Liu, and X.-G. Wen, Phys. Rev. B **87**, 155114 (2013).

[65] R. Thorngren and D. V. Else, Physical Review X **8**, 011040 (2018).

[66] S. Jiang and Y. Ran, Phys. Rev. B **95**, 125107 (2017).

[67] C. J. Pethick and H. Smith, *Bose–Einstein Condensation in Dilute Gases*, 2nd ed. (Cambridge University Press, 2008).

[68] F. Schwabl, R. Hilton, and A. Lahee, *Advanced Quantum Mechanics*, 2008 Springer E-Books (Springer Berlin Heidelberg, 2008).

[69] L. Fidkowski and A. Kitaev, Phys. Rev. B **81**, 134509 (2010).

[70] S. Ryu, Physica Scripta **T164**, 014009 (2015).

[71] M. Z. Hasan and C. L. Kane, Rev. Mod. Phys. **82**, 3045 (2010).

[72] X.-L. Qi and S.-C. Zhang, Rev. Mod. Phys. **83**, 1057 (2011).

[73] S. Ryu, A. P. Schnyder, A. Furusaki, and A. W. W. Ludwig, New Journal of Physics **12**, 065010 (2010).

[74] A. P. Schnyder, S. Ryu, A. Furusaki, and A. W. W. Ludwig, AIP Conference Proceedings **1134**, 10 (2009).

[75] C.-K. Chiu, J. C. Y. Teo, A. P. Schnyder, and S. Ryu, Rev. Mod. Phys. **88**, 035005 (2016).

[76] B. I. Halperin, Phys. Rev. Lett. **52**, 1583 (1984).

[77] A. Stern, Annals of Physics **323**, 204 (2008).

[78] S. Rao, Introduction to abelian and non-abelian anyons (2016).

[79] X. G. Wen, Phys. Rev. Lett. **66**, 802 (1991).

[80] M. Levin and Z.-C. Gu, Phys. Rev. B **86**, 115109 (2012).

[81] C. Wang and M. Levin, Phys. Rev. B **91**, 165119 (2015).

[82] L. Tsui, H.-C. Jiang, Y.-M. Lu, and D.-H. Lee, Nuclear Physics B **896**, 330 (2015), arXiv:1503.06794 .

[83] S. Shen, *Topological Insulators: Dirac Equation in Condensed Matter*, Springer Series in Solid-State Sciences (Springer Singapore, 2017).

[84] R. Shankar, Topological insulators – a review (2018).

[85] D. V. Else and C. Nayak, Phys. Rev. B **90**, 235137 (2014).

[86] X.-G. Wen, Phys. Rev. D **88**, 045013 (2013).

[87] F. J. Burnell, X. Chen, L. Fidkowski, and A. Vishwanath, Phys. Rev. B **90**, 245122 (2014).

[88] J. C. Wang, L. H. Santos, and X.-G. Wen, Phys. Rev. B **91**, 195134 (2015).

[89] A. Kapustin and R. Thorngren, Phys. Rev. Lett. **112**, 231602 (2014).

[90] A. Kapustin and R. Thorngren, Anomalies of discrete symmetries in various dimensions and group cohomology (2014).

[91] N. Bultinck, Phys. Rev. B **100**, 165132 (2019).

[92] I. Affleck, T. Kennedy, E. H. Lieb, and H. Tasaki, Phys. Rev. Lett. **59**, 799 (1987).

[93] F. Pollmann, A. M. Turner, E. Berg, and M. Oshikawa, Phys. Rev. B **81**, 064439 (2010).

[94] F. Pollmann and A. M. Turner, Phys. Rev. B **86**, 125441 (2012).

[95] A. M. Turner, F. Pollmann, and E. Berg, Phys. Rev. B **83**, 075102 (2011).

[96] X. Chen, Z.-C. Gu, and X.-G. Wen, Phys. Rev. B **84**, 235128 (2011).

[97] M. B. Hastings, Journal of Statistical Mechanics: Theory and Experiment **2007**, P08024 (2007).

[98] U. Schollwöck, Annals of Physics **326**, 96 (2011).

[99] J. I. Cirac, D. Pérez-García, N. Schuch, and F. Verstraete, Rev. Mod. Phys. **93**, 045003 (2021).

[100] M. V. Berry, Proceedings of the Royal Society of London Series A-mathematical Physical and Engineering Sciences **392**, 45 (1984).

[101] D. Vanderbilt, *Berry Phases in Electronic Structure Theory: Electric Polarization, Orbital Magnetization and Topological Insulators* (Cambridge University Press, 2018).

[102] J. Zak, Phys. Rev. Lett. **62**, 2747 (1989).

[103] Y. Hatsugai, Journal of the Physical Society of Japan **75**, 123601 (2006).

[104] R. Peierls, Zeitschrift für Physik **80**, 763 (1933).

[105] A. Kapustin, Bosonic topological insulators and paramagnets: a view from cobordisms (2014).

[106] C. Xu and Y.-Z. You, Phys. Rev. B **91**, 054406 (2015).

[107] D. J. Williamson, N. Bultinck, M. Mariën, M. B. Şahinoğlu, J. Haegeman, and F. Verstraete, Phys. Rev. B **94**, 205150 (2016).

[108] J. C. Bridgeman and D. J. Williamson, Phys. Rev. B **96**, 125104 (2017).

[109] J. Langbehn, Y. Peng, L. Trifunovic, F. von Oppen, and P. W. Brouwer, Phys. Rev. Lett. **119**, 246401 (2017).

[110] M. B. de Paz, M. G. Vergniory, D. Bercioux, A. García-Etxarri, and B. Bradlyn, Phys. Rev. Research **1**, 032005 (2019).

[111] A. Bouhon, A. M. Black-Schaffer, and R.-J. Slager, Phys. Rev. B **100**, 195135 (2019).

[112] H. C. Po, H. Watanabe, and A. Vishwanath, Physical review letters **121**, 126402 (2018).

[113] J. Cano, B. Bradlyn, Z. Wang, L. Elcoro, M. G. Vergniory, C. Felser, M. I. Aroyo, and B. A. Bernevig, Phys. Rev. Lett. **120**, 266401 (2018).

[114] D. V. Else, H. C. Po, and H. Watanabe, Physical Review B **99**, 125122 (2019).

[115] H. Isobe and L. Fu, Physical Review B **92**, 081304 (2015).

[116] X.-Y. Song and A. P. Schnyder, Phys. Rev. B **95**, 195108 (2017).

[117] D. V. Else and R. Thorngren, Physical Review B **99**, 115116 (2019).

[118] Y. You, Higher-order topological phase without crystalline symmetry (2019).

[119] A. Auerbach, *Interacting Electrons and Quantum Magnetism*, Graduate Texts in Contemporary Physics (Springer New York, 2012).

[120] T. Neupert and F. Schindler, Topological crystalline insulators, in *Topological Matter: Lectures from the Topological Matter School 2017*, edited by D. Bercioux, J. Cayssol, M. G. Vergniory, and M. Reyes Calvo (Springer International Publishing, Cham, 2018) pp. 31–61.

[121] M. B. Hastings and T. Koma, Communications in Mathematical Physics **265**, 781–804 (2006).

[122] J. Hauschild and F. Pollmann, SciPost Phys. Lect. Notes **5**, 5 (2018), code available from `https://github.com/tenpy/tenpy`.

[123] M. Fannes, B. Nachtergaele, and R. F. Werner, Communications in Mathematical Physics **144**, 443 (1992).

[124] J. Eisert, Entanglement and tensor network states (2013).

[125] E. M. Stoudenmire and S. R. White, Annual Review of Condensed Matter Physics **3**, 111 (2012).

[126] S. Liang and H. Pang, Phys. Rev. B **49**, 9214 (1994).

[127] I. P. McCulloch, arXiv:0804.2509 (2008).

[128] H. Araki, T. Mizoguchi, and Y. Hatsugai, Phys. Rev. Research **2**, 012009 (2020).

[129] B. Kang, K. Shiozaki, and G. Y. Cho, Phys. Rev. B **100**, 245134 (2019).

[130] W. A. Wheeler, L. K. Wagner, and T. L. Hughes, Phys. Rev. B **100**, 245135 (2019).

[131] S. Ono, L. Trifunovic, and H. Watanabe, Phys. Rev. B **100**, 245133 (2019).

[132] O. Dubinkin, J. May-Mann, and T. L. Hughes, Phys. Rev. B **103**, 125129 (2021).

[133] W. Kohn, Phys. Rev. **133**, A171 (1964).

[134] D. Vanderbilt and R. D. King-Smith, Phys. Rev. B **48**, 4442 (1993).

[135] N. C. Murphy, R. Wortis, and W. A. Atkinson, Phys. Rev. B **83**, 184206 (2011).

[136] A. J. Ferris and G. Vidal, Phys. Rev. B **85**, 165146 (2012).

[137] H.-N. Dai, B. Yang, A. Reingruber, H. Sun, X.-F. Xu, Y.-A. Chen, Z.-S. Yuan, and J.-W. Pan, Nature Physics **13**, 1195 (2017).

[138] H. Li and F. D. M. Haldane, Phys. Rev. Lett. **101**, 010504 (2008).

[139] I. Peschel and V. Eisler, Journal of Physics A: Mathematical and Theoretical **42**, 504003 (2009).

[140] A. Alexandradinata, T. L. Hughes, and B. A. Bernevig, Phys. Rev. B **84**, 195103 (2011).

[141] E. Prodan, T. L. Hughes, and B. A. Bernevig, Phys. Rev. Lett. **105**, 115501 (2010).

[142] L. Fidkowski, Phys. Rev. Lett. **104**, 130502 (2010).

[143] A. Chandran, V. Khemani, and S. L. Sondhi, Phys. Rev. Lett. **113**, 060501 (2014).

[144] M. P. Zaletel, R. S. K. Mong, and F. Pollmann, Phys. Rev. Lett. **110**, 236801 (2013).

[145] S. Liu, A. Vishwanath, and E. Khalaf, Phys. Rev. X **9**, 031003 (2019).

[146] D. V. Else and R. Thorngren, Phys. Rev. B **101**, 224437 (2020).

[147] A. Rasmussen and Y.-M. Lu, Intrinsically interacting topological crystalline insulators and superconductors (2018).

[148] A. Tiwari, M.-H. Li, B. A. Bernevig, T. Neupert, and S. A. Parameswaran, Phys. Rev. Lett. **124**, 046801 (2020).

[149] R. Resta and D. Vanderbilt, Theory of polarization: A modern approach, in *Physics of Ferroelectrics: A Modern Perspective* (Springer Berlin Heidelberg, Berlin, Heidelberg, 2007) pp. 31–68.

[150] T. Li, P. Zhu, W. A. Benalcazar, and T. L. Hughes, Phys. Rev. B **101**, 115115 (2020).

[151] M. Geier, I. C. Fulga, and A. Lau, SciPost Phys. **10**, 92 (2021).

[152] M. Katanaev and I. Volovich, Annals of Physics **216**, 1 (1992).

[153] H. Kleinert, *Gauge Fields in Condensed Matter* (WORLD SCIENTIFIC, 1989).

[154] J. Fröhlich and U. M. Studer, Rev. Mod. Phys. **65**, 733 (1993).

[155] W. A. Benalcazar, J. C. Teo, and T. L. Hughes, Physical Review B **89**, 224503 (2014).

[156] H. Kleinert, in *Gauge Fields in Condensed Matter*, Chap. METRIC-AFFINE SPACES, pp. 1335–1384.

[157] M. J. Bowick and L. Giomi, Advances in Physics **58**, 449 (2009).

[158] K. Warnick, R. Selfridge, and D. Arnold, IEEE Transactions on Education **40**, 53 (1997).

[159] A. Zee, in *Field Theory, Topology and Condensed Matter Physics*, edited by H. B. Geyer (Springer Berlin Heidelberg, Berlin, Heidelberg, 1995) pp. 99–153.

[160] D. Tong, Lectures on the quantum hall effect (2016).

[161] A. G. Abanov and A. Gromov, Phys. Rev. B **90**, 014435 (2014).

[162] A. Cappelli and E. Randellini, Journal of High Energy Physics **2016**, 105 (2016).

[163] C. Hoyos and D. T. Son, Phys. Rev. Lett. **108**, 066805 (2012).

[164] J. C. Wang, Z.-C. Gu, and X.-G. Wen, Phys. Rev. Lett. **114**, 031601 (2015).

[165] E. Andreas, Y. Jinlong, Z. Guanyu, H. Mohammad, P. Frank, Z. Peter, and V. Benoît, Science Advances **6**, eaaz3666 (2022).

[166] S. J. van Enk and C. W. J. Beenakker, Phys. Rev. Lett. **108**, 110503 (2012).

[167] A. Elben, B. Vermersch, M. Dalmonte, J. I. Cirac, and P. Zoller, Phys. Rev. Lett. **120**, 050406 (2018).

[168] L. Amico, R. Fazio, A. Osterloh, and V. Vedral, Rev. Mod. Phys. **80**, 517 (2008).

[169] P. Zhu, K. Loehr, and T. L. Hughes, Phys. Rev. B **101**, 115140 (2020).

[170] I. Peschel, Journal of Physics A: Mathematical and General **36**, L205 (2003).

[171] R. D. King-Smith and D. Vanderbilt, Phys. Rev. B **47**, 1651 (1993).

[172] M. Atala, M. Aidelsburger, J. T. Barreiro, D. Abanin, T. Kitagawa, E. Demler, and I. Bloch, Nature Physics **9**, 795 (2013).

[173] D. J. Thouless, Physical Review B **27**, 6083 (1983).

[174] Q. Niu and D. J. Thouless, Journal of Physics A: Mathematical and General **17**, 2453 (1984).

[175] D. J. Thouless, M. Kohmoto, M. P. Nightingale, and M. den Nijs, Phys. Rev. Lett. **49**, 405 (1982).

[176] Q. Niu, D. J. Thouless, and Y.-S. Wu, Phys. Rev. B **31**, 3372 (1985).

[177] A. Hayward, C. Schweizer, M. Lohse, M. Aidelsburger, and F. Heidrich-Meisner, Phys. Rev. B **98**, 245148 (2018).

[178] N. R. Cooper, J. Dalibard, and I. B. Spielman, Rev. Mod. Phys. **91**, 015005 (2019).

[179] G. Ortiz and R. M. Martin, Phys. Rev. B **49**, 14202 (1994).

[180] J. Asbóth, L. Oroszlány, and A. Pályi, *A Short Course on Topological Insulators: Band Structure and Edge States in One and Two Dimensions*, Lecture Notes in Physics (Springer International Publishing, 2016).

[181] T. Kato, Journal of the Physical Society of Japan **5**, 435 (1950).

[182] E. Lieb, T. Schultz, and D. Mattis, Annals of Physics **16**, 407 (1961).

[183] R. Verresen, R. Thorngren, N. G. Jones, and F. Pollmann, Phys. Rev. X **11**, 041059 (2021).

[184] T. Scaffidi, D. E. Parker, and R. Vasseur, Phys. Rev. X **7**, 041048 (2017).

[185] S. D. Geraedts and O. I. Motrunich, Exact models for symmetry-protected topological phases in one dimension (2014).

[186] K. Duivenvoorden and T. Quella, Phys. Rev. B **88**, 125115 (2013).

[187] P. Di Francesco, P. Mathieu, and D. Sénéchal, *Conformal Field Theory*, Graduate texts in contemporary physics (Island Press, 1996).

[188] M. A. Metlitski and R. Thorngren, Phys. Rev. B **98**, 085140 (2018).

[189] A. Prakash, J. Wang, and T.-C. Wei, Phys. Rev. B **98**, 125108 (2018).

[190] Y. Tachikawa, SciPost Phys. **8**, 15 (2020).

[191] R. Thorngren, Phys. Rev. B **101**, 245160 (2020).

[192] A. Prakash and J. Wang, Phys. Rev. B **103**, 085130 (2021).

[193] P. Calabrese and J. Cardy, Journal of Statistical Mechanics: Theory and Experiment **2004**, P06002 (2004).

[194] F. Pollmann, S. Mukerjee, A. M. Turner, and J. E. Moore, Phys. Rev. Lett. **102**, 255701 (2009).

[195] C.-Y. Huang and T.-C. Wei, Phys. Rev. B **93**, 155163 (2016).

[196] G. Vidal, Phys. Rev. Lett. **98**, 070201 (2007).

[197] N. Tantivasadakarn, R. Thorngren, A. Vishwanath, and R. Verresen, Pivot hamiltonians as generators of symmetry and entanglement (2021).

[198] M. P. Zaletel, Phys. Rev. B **90**, 235113 (2014).

[199] M. Barkeshli, C.-M. Jian, and X.-L. Qi, Phys. Rev. B **88**, 235103 (2013).

[200] X.-G. Wen, Phys. Rev. B **89**, 035147 (2014).

[201] M. Cheng and Z.-C. Gu, Phys. Rev. Lett. **112**, 141602 (2014).

[202] J. C. Y. Teo, A. Roy, and X. Chen, Phys. Rev. B **90**, 115118 (2014).

[203] N. Tarantino, N. H. Lindner, and L. Fidkowski, New Journal of Physics **18**, 035006 (2016).

[204] A. Tiwari, X. Chen, K. Shiozaki, and S. Ryu, Phys. Rev. B **97**, 245133 (2018).

[205] N. Tantivasadakarn, R. Thorngren, A. Vishwanath, and R. Verresen, Building models of topological quantum criticality from pivot hamiltonians.

[206] N. Nagaosa and J.-i. Takimoto, Journal of the Physical Society of Japan **55**, 2735 (1986).

[207] M. Fabrizio, A. O. Gogolin, and A. A. Nersesyan, Phys. Rev. Lett. **83**, 2014 (1999).

[208] M. E. Torio, A. A. Aligia, and H. A. Ceccatto, Phys. Rev. B **64**, 121105 (2001).

[209] P. Brune and A. P. Kampf, in *High Performance Computing in Science and Engineering '01*, edited by E. Krause and W. Jäger (Springer Berlin Heidelberg, Berlin, Heidelberg, 2002) pp. 167–177.

[210] A. P. Kampf, M. Sekania, G. I. Japaridze, and P. Brune, Journal of Physics: Condensed Matter **15**, 5895 (2003).

[211] S. R. Manmana, V. Meden, R. M. Noack, and K. Schönhammer, Phys. Rev. B **70**, 155115 (2004).

[212] C. D. Batista and A. A. Aligia, Phys. Rev. Lett. **92**, 246405 (2004).

[213] H. Otsuka and M. Nakamura, Phys. Rev. B **71**, 155105 (2005).

[214] M. E. Torio, A. A. Aligia, G. I. Japaridze, and B. Normand, Phys. Rev. B **73**, 115109 (2006).

[215] A. Garg, H. R. Krishnamurthy, and M. Randeria, Phys. Rev. Lett. **97**, 046403 (2006).

[216] L. Craco, P. Lombardo, R. Hayn, G. I. Japaridze, and E. Müller-Hartmann, Phys. Rev. B **78**, 075121 (2008).

[217] L. Tincani, R. M. Noack, and D. Baeriswyl, Phys. Rev. B **79**, 165109 (2009).

[218] A. Go and G. S. Jeon, Phys. Rev. B **84**, 195102 (2011).

[219] M. Hafez Torbati, N. A. Drescher, and G. S. Uhrig, Phys. Rev. B **89**, 245126 (2014).

[220] L. Fidkowski and A. Kitaev, Phys. Rev. B **83**, 075103 (2011).

[221] C. Teleman, Representation theory (2005).

[222] M. R. Zirnbauer, Journal of Mathematical Physics **62**, 021101 (2021).

[223] X. Chen, Z.-C. Gu, and X.-G. Wen, Phys. Rev. B **83**, 035107 (2011).

[224] M. Cheng, M. Zaletel, M. Barkeshli, A. Vishwanath, and P. Bonderson, Phys. Rev. X **6**, 041068 (2016).

[225] G. Y. Cho, C.-T. Hsieh, and S. Ryu, Phys. Rev. B **96**, 195105 (2017).

[226] X. Yang, S. Jiang, A. Vishwanath, and Y. Ran, Phys. Rev. B **98**, 125120 (2018).

[227] C.-M. Jian, Z. Bi, and C. Xu, Phys. Rev. B **97**, 054412 (2018).

[228] N. D. Mermin and H. Wagner, Phys. Rev. Lett. **17**, 1133 (1966).

[229] P. C. Hohenberg, Phys. Rev. **158**, 383 (1967).

[230] S. Coleman, Communications in Mathematical Physics **31**, 259 (1973).

[231] L. Tsui, Y.-T. Huang, and D.-H. Lee, Nuclear Physics B **949**, 114799 (2019).

[232] C. Wang, Phys. Rev. B **94**, 085130 (2016).

[233] R. Thorngren, A. Vishwanath, and R. Verresen, Phys. Rev. B **104**, 075132 (2021).

[234] M. Endres, M. Cheneau, T. Fukuhara, C. Weitenberg, P. Schauß, C. Gross, L. Mazza, M. C. Bañuls, L. Pollet, I. Bloch, and S. Kuhr, Science **334**, 200 (2011).

[235] T. A. Hilker, G. Salomon, F. Grusdt, A. Omran, M. Boll, E. Demler, I. Bloch, and C. Gross, Science **357**, 484 (2017).

[236] S. de Léséleuc, V. Lienhard, P. Scholl, D. Barredo, S. Weber, N. Lang, H. P. Büchler, T. Lahaye, and A. Browaeys, Science **365**, 775 (2019).

[237] P. Sompet, S. Hirthe, D. Bourgund, T. Chalopin, J. Bibo, J. Koepsell, P. Bojović, R. Verresen, F. Pollmann, G. Salomon, C. Gross, T. A. Hilker, and I. Bloch, Nature **606**, 484 (2022).

[238] R. Jackiw and C. Rebbi, Phys. Rev. D **13**, 3398 (1976).

[239] J. C. Y. Teo and C. L. Kane, Phys. Rev. B **82**, 115120 (2010).

[240] T. Fukui, K. Shiozaki, T. Fujiwara, and S. Fujimoto, Journal of the Physical Society of Japan **81**, 114602 (2012).

[241] R. Verresen, Topology and edge states survive quantum criticality between topological insulators (2020).

[242] C. Stover, Ternary diagram.

[243] S. Elitzur, Phys. Rev. D **12**, 3978 (1975).

[244] G. Hooft, Naturalness, chiral symmetry, and spontaneous chiral symmetry breaking, in *Recent Developments in Gauge Theories*, edited by G. Hooft, C. Itzykson, A. Jaffe, H. Lehmann, P. K. Mitter, I. M. Singer, and R. Stora (Springer US, Boston, MA, 1980) pp. 135–157.

[245] R. Thorngren and C. von Keyserlingk, Higher spt's and a generalization of anomaly in-flow (2015).

[246] E. Fradkin, *Field Theories of Condensed Matter Physics*, 2nd ed. (Cambridge University Press, 2013).

[247] T. Giamarchi, *Quantum Physics in One Dimension*, International Series of Monographs on Physics (Oxford University Press, Oxford, 2003).

[248] P. H. Ginsparg, Applied conformal field theory (1988), arXiv:hep-th/9108028 [hep-th] .

[249] E. Fradkin, *Quantum Field Theory: An Integrated Approach* (Princeton University Press, 2021).

[250] J. M. Kosterlitz and D. J. Thouless, Journal of Physics C: Solid State Physics **6**, 1181 (1973).

[251] V. L. Berezinskii, Journal of Experimental and Theoretical Physics **34**, 610 (1972).

[252] S. Rachel, N. Laflorencie, H. F. Song, and K. Le Hur, Phys. Rev. Lett. **108**, 116401 (2012).

Acknowledgements

First and foremost, I am deeply indebted to my supervisor, Frank Pollmann, for his constant support during the last five years. In particular, I am thankful that he brought me into the absolutely exciting field of topological phases of matter, and shared his fascination with me. Moreover, he learned me the importance of numerical methods for understanding such states. From my point of view, Frank was the optimal supervisor for me because both of us follow the same strategy to tackle new problems and, second, more importantly, his door was always open, regardless of which nature my problems have been. That is definitely not self-evident, and without that, I would have never been at this stage. Thank you!

However, without two other persons, this thesis had never been possible. Thank you, Ruben Verresen and Fabian Grusdt, for your constant assistance during the last five years. I do know that patience is not something I was born with, and if I wanted to know something, I am out of the sudden jumped into your offices and asked you about my problem, but none of you have ever been annoyed, au contraire, you always took time to discuss with me about physics.

Ruben, you did not only talk to me about physics, you also shared your advice during a difficult time that I had during my PhD, that is something I will never forget!

There have been many other people, without whom I could have never managed this thesis, and, in particular, the results obtained during the PhD. To this end, I need to say thank you to: Johannes Hauschild, Izabella Lovas, Bernhard Jobst, Sheng-Hsuan Lin (although we never published something), Julian Wienand, Friederike Horn, Nick Jones, Josef Willsher, Adam Smith, Yizhi You, Monika Aidelsburger and many others.

Moreover, all the research would not be possible if there was not the administrative staff. Claudine, thank you very much for your help throughout the last years. Regardless how often people dropped by, you were always willing to help us to fill out forms or to answer any other question we had.

Clearly, I thank all my friends and family that supported me during this time, and always forgave me, when I was again unable to better schedule my time. Thank you, Lukas, for the last five years and the daily lunches we had together. In particular, I am deeply indebted to Artöm, who helped me through a very difficult time and offered me his place, whenever I needed it. Moreover, he made it possible that I had a few hours, where I did not think about some physics, which is usually very difficult because I am very passionate about it. For achieving this, he brought me into downhill biking, where we enjoyed a few, very dangerous and funny days with our bikes.

Friends come and go, but family always stays with you. Thank you mum and dad for your constant support throughout my whole life. You gave me the freedom to go my own way, and you always allowed me to do whatever I wanted, especially in the beginning

of my school career, where we together decided not to follow the advice of the teachers; instead, you helped me to successfully proceed with the secondary school. Without that decision, I certainly would have never been at this stage!

Finally, without the great support of my girlfriend Sandrina my whole studies would have been impossible. You did not only give me my lovely and beautiful daughter, Giuliana, you also played the most important part in achieving these results. Although there have been difficult times for both of us, you never complained, and without batting an eye you supported me with the daily business.